Naval Research Laboratory
Washington, DC 20375-5320

NRL/MR/6180--04-8745

Verification and Validation Final Report for Fire and Smoke Spread Modeling and Simulation Support of T-AKE Test and Evaluation

PATRICIA A. TATEM
Global Paperless Solutions
Alexandria, VA

EDWARD K. BUDNICK
SEAN P. HUNT
JAVIER TRELLES
JOSEPH L. SCHEFFEY
DEREK A. WHITE
Hughes Associates, Inc.
Baltimore, MD

JEAN BAILEY
JOHN HOOVER
FREDERICK W. WILLIAMS
Navy Technology Center for Safety and Survivability
Chemistry Division

January 30, 2004

REPORT DOCUMENTATION PAGE

Form Approved
OMB No. 0704-0188

1. REPORT DATE *(DD-MM-YYYY)*	2. REPORT TYPE	3. DATES COVERED *(From - To)*
January 30, 2004	Memorandum	August 2003-December 2003

4. TITLE AND SUBTITLE

Verification and Validation Final Report for Fire and Smoke Spread Modeling and Simulation Support of T-AKE Test and Evaluation

5a. CONTRACT NUMBER

5b. GRANT NUMBER

5c. PROGRAM ELEMENT NUMBER
61-5245-0-4-5

5d. PROJECT NUMBER

5e. TASK NUMBER

5f. WORK UNIT NUMBER

6. AUTHOR(S)

Patricia A. Tatem,* Edward K. Budnick,† Sean P. Hunt,† Javier Trelles,† Joseph L. Scheffey,† Derek A. White,† Jean Bailey, John Hoover, and Frederick W. Williams

7. PERFORMING ORGANIZATION NAME(S) AND ADDRESS(ES)

Naval Research Laboratory, Code 6180
4555 Overlook Avenue, SW
Washington, DC 20375-5320

8. PERFORMING ORGANIZATION REPORT NUMBER

NRL/MR/6180--04-8745

9. SPONSORING / MONITORING AGENCY NAME(S) AND ADDRESS(ES)

Naval Surface Warfare Center/Carderock Division
9500 MacArthur Boulevard
West Bethesda, MD 20817

10. SPONSOR / MONITOR'S ACRONYM(S)

11. SPONSOR / MONITOR'S REPORT NUMBER(S)

12. DISTRIBUTION / AVAILABILITY STATEMENT

Approved for public release; distribution is unlimited.

13. SUPPLEMENTARY NOTES

*Global Paperless Solutions, Alexandria, VA
†Hughes Associates, Inc., Baltimore, MD

14. ABSTRACT

The current approach for the characterization of secondary damage associated with a weapon hit has evolved over several Total Ship Survivability (TSS) and Battle Damage Repair Assessment (BDRA) evaluations. The genesis of the current methodology was rudimentary fire spread times, developed by the Naval Research Laboratory (NRL) and Hughes Associates, Inc., based on USS *Stark* incident data and testing. This information was implemented in a TSS model developed by the Naval Surface Warfare Center, Carderock Division (NSWC/CD). The fire spread methodology was subsequently improved and the framework was expanded to allow for smoke spread during the evaluation performed for the LPD-17 VAR 2. Most recently, the methodology was further refined during the CVNX assessment. This report reflects the most current methodology used for the VAR 3 process for the LPD-17 platform detailed design. This approach is proposed to be adopted for T-AKE.

15. SUBJECT TERMS

Model; Fire; Damage control; Smoke spread; Fire spread

16. SECURITY CLASSIFICATION OF:			17. LIMITATION OF ABSTRACT	18. NUMBER OF PAGES	19a. NAME OF RESPONSIBLE PERSON
a. REPORT	b. ABSTRACT	c. THIS PAGE			Frederick W. Williams
Unclassified	Unclassified	Unclassified	UL	183	19b. TELEPHONE NUMBER *(include area code)* (202) 767-2476

CONTENTS

VERIFICATION AND VALIDATION FINAL REPORT FOR FIRE AND SMOKE SPREAD MODELING AND SIMULATION SUPPORT OF T-AKE TEST AND EVALUATION

1.0 PURPOSE

The Operational Requirements Document (ORD) for the Auxiliary Dry Cargo Carrier, T-AKE, designates survivability as one of the key performance parameters for the ship. The objective requirements linked to this parameter are multi-fold, and include the following:

- Built-in redundancy so that a single equipment failure or loss will not degrade system capability. Redundant system functions will be provided and will be separated so as to avoid the possibility of total system loss due to a single casualty.
- Low expansion fire fighting foam for fire protection of the helicopter deck and hangar and machinery space bilges.
- Water-mist or other USCG approved total flooding fire suppression system for machinery spaces.
- Seawater fire sprinkler systems (wet firemain/dry sprinklers) for cargo ordnance holds.

These requirements are carried into the System Specification, which states that the ship shall meet the above firefighting requirements under all loading conditions. It is the intention of the T-AKE Program to use modeling and simulation (M&S) to certify that the ship meets these requirements. The specific methodology (tool) that will be used in this effort consists of a combination of computer fire modeling using the "Consolidated Model of Fire Growth and Smoke Transport (CFAST), Version 3.1.7" (Peacock, et al., January 2000a; Peacock, et al., January 2000b) and prescriptive rules for fire spread determined with the finite difference heat conduction model –HEATING Version 7.3 (Back, et al., March 2003). The objective of this document is to demonstrate that the methodology, including supporting models, provide reasonable and conservative results in the context of using for T-AKE Vulnerability Assessment Report.

2.0 TOOLS SUMMARY

2.1 Tool/Model: Fire Spread Methodology

Describing the methodology for predicting fire and smoke spread requires an understanding of the shipboard damage zones. The zones are categorized in three ways:

Primary Damage Area (PDA(F)) compartments: PDA(F) compartments are those that incur significant damage from the weapon hit (e.g., failed deck/bulkhead and shock holing). From the standpoint of fire and smoke spread, the vent-connected spaces are included. This is due to the

Manuscript approved January 5, 2004.

fact that the vents provide a means for spreading fire and smoke directly as well as supplying additional oxygen for the fires.

Adjacent to Primary Damage Area (APDA(F)) compartments: These compartments share a common boundary (bulkhead, overhead or deck) with a PDA(F) compartment. The recommended definition for fire and smoke spread for adjacent compartments, APDA(F), excludes any compartments that have vent openings to the PDA(F).

Beyond Adjacent to Primary Damage Area (BAPDA(F)) compartments: These compartments border APDA(F) spaces. They can be otherwise described as "twice removed" from the PDA(F). These spaces may be a concern due to potential fire spread later into the event. It is typically assumed that there are no communicable openings (i.e., vents, ducts, open doors or open hatches) between BAPDA(F) and APDA(F) spaces. This is based on the assumption that the ship is at general quarters prior to the weapon detonation.

The Methodology for predicting fire and smoke spread in a naval platform follows the steps listed below. Steps (3) – (5) are described in further detail in the Appendices, as they constitute the phenomenology that is included in the tools being verified and validated.

1. Establish the primary damage;
2. Review the primary damage information;
3. Characterize the secondary damage (fire and smoke spread) in the PDA(F);
4. Characterize the secondary damage to PDA(F) spaces;
5. Characterize the secondary damage to APDA(F) and BAPDA(F) compartments; and
6. Document the time dependent secondary damage estimates in snapshot format.

Steps 3 and 4 involve characterizing the secondary damage in the PDA(F) by two different approaches—CFAST fire model and prescriptive rules. For conservative estimates, the predicted tenability and fire/smoke spread are dictated by the approach that estimates the shorter time scale (i.e., more conservative) for progressive damage.

2.2 Overview

The current approach for the characterization of secondary damage associated with a weapon hit has evolved over several Total Ship Survivability (TSS) and Battle Damage Repair Assessment (BDRA) evaluations. The genesis of the current Methodology was rudimentary fire spread times, developed by the Naval Research Laboratory (NRL) and Hughes Associates, Inc. based on USS *Stark* incident data and testing (Scheffey, et al., April 1992). This information was implemented in a TSS model developed by the Naval Surface Warfare Center, Carderock Division (NSWC/CD). The fire spread methodology was subsequently improved and the framework was expanded to allow for smoke spread during the evaluation performed for the LPD-17 VAR 2 (White, et al., September 1997). Most recently, the methodology was further refined during the CVNX assessment (Back, et al., April 2002). This report reflects the most

current methodology used for the CVNX assessment and for the VAR 3 process for the LPD-17 platform detailed design. This approach is proposed to be adopted for T-AKE.

2.3 Intended Purpose

The vulnerability assessment process that uses this methodology includes the simulation of weapon damage, characterization of secondary damage (e.g., fire and smoke), and description of the battle damage repair activities and effectiveness. These activities are generally referred to as a TSS and Battle Damage Repair Assessment BDRA. The overall objective of the TSS/BDRA is to identify specific weaknesses and/or shortcomings as well as high payoff research and development efforts that might increase the survivability of the particular ship platform. The current TSS/BDRA process involves consideration of various weapon hits. For each specific weapon threat scenario (shot line), the initial damage is identified by utilizing a blast damage model. Secondary damage, such as fire and smoke spread that results from the blast damage, must also be characterized. The Methodology described in this document concentrates on the fire and smoke spread methodology only. A framework is outlined by which a conservative estimate of the secondary fire and smoke damage can be determined, supported by supplemental fire test data from current and previous tests.

2.4 Tool/Model Accediting Organization.

PEO Ships, PMS 325B (TAKE Program Office) 80 M Street, Suite 610 Washington, DC 20003.

2.5 CFAST

2.5.1 Required Operating Environment

CFAST will run on a 386 or later IBM compatible PC with at least 4 MB free extended memory, at least VGA compatible video card and a 100% MS-MS compatible mouse.

2.5.2 Existing/Published Documentation

An extensive list of references is provided at the end of this document (Section 9.0 - References) and is reviewed in detail in Appendix A.

2.6 Heuristics and HEATING

2.6.1 Required Operating Environment

The minimal environment for running HEATING is a computer system with a FORTRAN 90 compiler and a text editor. This suffices to create the executables and the input files. HEATING has two main formats for data output: an ASCII file for results at user-specified nodes and a binary file for field data. The most expedient environment for post-processing the subsequent results would be any system that runs Tecplot, a commercial scientific plotting tool sold by Amtec, Inc. However, the h7tec FORTRAN code that comes with HEATING can be used on any system with a FORTRAN 90 compiler, a text editor, and a scientific plotter to visualize the results. The process entails employing h7tec to extract data from HEATING's binary data file and then editing the resulting ASCII file(s) to match a specific graphing program's requirements. HEATING 7.3 comes with Windows-compatible executables of the main simulation plus all the supporting programs (such as h7tec). Again, the resultant data is best plotted with Tecplot but it is also possible to use h7tec to extract the field data and Wordpad to edit it so that another Windows-based plotter could be utilized. Node data can be easily plotted with Excel. The operating environments used for the present verification are detailed in Appendix C. The heuristics derived from test data do not require a model shell or computer framework per se.

2.6.2 Existing/Published Documentation

An extensive list of references is provided at the end of this document (Section 9.0 - References). The derivation of the fire spread rules (heuristics) is described in Section 4.0 and Appendix B. A review of HEATING is provided in Appendices C and D.

2.7 Take Ship Data Set

The TAKE General Arrangement and Ventilation drawings will be used for the Ship data set when the accreditation for the Vulnerability Assessment is accomplished. For this Validation experimental data from the Ex-USS Shadwell was used to validate volumetric data.

3.0 RISK ANALYSIS AND ASSESSMENT SUMMARY

3.1 Methodology

The Methodology described in this report outlines the framework through which a conservative estimate of the secondary fire and smoke damage can be established. Fire may spread to compartments within the PDA(F) via either hot gases passing through an open vent or heating of an intact boundary (bulkhead or deck). In this situation, fires resulting from the

weapon detonation in the immediate vicinity of the burst point would spread to other compartments within the PDA(F). Both modes of fire spread are examined when evaluating fire spread to these PDA(F) compartments to determine which mode results in a faster (more conservative) fire spread time.

3.2 CFAST

In the first mode of spread, the temperature(s) of hot gases are determined using CFAST. Based on the review of several potential ignition scenarios, it is conservatively assumed that ignition via hot gases will occur in a PDA(F) compartment when the accumulated fire gas temperatures reach 230°C (446°F) in that adjacent space (Back, et al., February 2000; Naval Ships' Technical Manual, Dec 2001; Setchkin, 1949; Darwin, et al., 1994; Drysdale, 1999).

CFAST was designed to execute very quickly (in real-time, or quicker) on affordable desktop computers. In addition, it was intended to be relatively simple to use, which makes the model accessible to users (such as ship architects and shipboard damage control personnel) who are not experienced fire modelers. In order to meet these requirements, the CFAST developers made certain simplifying assumptions (in addition to those which are inherent in zone models) regarding the range of phenomena and the types of scenarios that could be modeled. In turn, these assumptions led to limitations on the scope of the problems which can be modeled, the ease with which they can be modeled and the accuracy of the results. These limitations can be characterized as inherent (things which CFAST is not capable of doing), or practical (things which require *a priori* knowledge which is not likely to be available or which require too much time and effort to be feasible). Inherent limitations include inability of objects to self-heat based on heat transfer and spontaneously ignite. Practical limitations include inability to predict phenomena such as time-dependent solid phase combustion of Class A fuels.

The limitations in Table 1 were identified in Hoover et al., June 2000, using CFAST Version 3.1.4 (with improved radiation, vertical vent flow and vertical heat transport algorithms). One of the most restrictive limitations of CFAST is the requirement that "intelligent" input parameters be used to run the model. This imposes restrictions on what can be modeled and what approximations must sometimes be made to circumvent those limits.

3.3 HEATING

In the second mode of evaluation for fire spread, the prescriptive rules used in conjunction with the finite element model HEATING are not plagued with the numerous limitations inherent in computer models. Hence, this part of the analysis provides for conservative estimates of fire spread to APDA(F) spaces and BAPDA(F) spaces, which moderates the variability that can occur in the results from the use of computer modeling only (particularly for CFAST). The use of these prescriptive rules is conservative since it is assumed that there is an unlimited amount of fuel and air available in each compartment. In the event that there is a small amount of fuel in the compartment or the compartment is closed, fire spread may be delayed or may not occur at

all. The combination of the computer fire model and prescriptive rules provides an inherent safety factor in the Methodology.

Table 1 - Identified Limitations Of CFAST

Limitation	Effects
Only one internal ambient state is permitted.	May lead to minor errors in predictions if there are large initial temperature differences among the compartments.
Compartments must be rectilinear.	Heat transfer via conduction and radiation will not be correct for surfaces which are not rectangular. Approximation methods that minimize this limitation are provided in Hoover et al., 2000.
Ceiling, floor and walls are each limited to a single set of thermo-physical properties.	Approximations must be made if the ceiling, floor or walls are composed of multiple regions having different properties.
Compartments have only one wrap-around wall, not individual surfaces.	May lead to significant errors if there are large differences in the properties of walls. Work-around methods have been devised in Hoover et al., 2000.
User-specified fire histories are required.	The user must know (or be able to accurately estimate), in advance, the development of the fire.
CFAST does not account for the variability of fire chemistry with pyrolysis and combustion conditions.	Good subject matter experts should estimate user-specified heat release rates so reasonable pyrolysis and combustion product concentrations will be predicted.

4.0 SUMMARY OF PREVIOUS DEVELOPMENTS AND APPLICATIONS

The Methodology described in this report has been successfully used in other Navy damage control/fire protection applications. Additionally, elements of the Methodology, in particular CFAST, have been used to analyze unique Navy situations. Specifically, the techniques have been used for a broad range of problems encountered in Fire Hazard Analyses (FHAs). This section briefly describes these applications.

4.1 Methodology Use in Platform Vulnerability Assessment Reports (VARs)

The genesis of the rules-based aspect of the Methodology was the USS STARK fire dynamics testing at the NRL Chesapeake Beach Detachment (Back et al., 1991) and ex-USS SHADWELL (Scheffey et al., 1999) fire test facilities. The heat transfer data from these tests was summarized and published in the scientific literature (Darwin et al., 1994). Developers of the Ship Vulnerability Model (SVM) at NSWCCD desired a relatively simple method to integrate fire and smoke spread characteristics into their battle damage model. The STARK test data were combined with hand calculation techniques to develop general rules for fire and smoke spread for large, post-flashover fires on Navy ships. These rules, published in 1992 (Scheffey et al., 1992) were the precursor to the Methodology described in this report. These heuristics continue to be adequate for many applications, particularly where there is significant variability in potential fire growth/spread scenarios.

4.1.1 LPD 17 VAR

The Methodology was first developed and applied in the LPD 17 VAR 3 (bid design). It was recognized that a strictly rules-based approach could lead to over-conservative predictions (i.e., very rapid fire and smoke spread). Modeling of the near-field area of the Primary Damage Area (PDA) was included to assess the fire spread in vent-connected areas in the PDA. Fire spread heuristics and a library of space-specific fire growth curves were then used in ADPA spaces. The LPD 17 VAR 3 fire and smoke spread analysis was subsequently documented (White et al., September 1997) and approved by Office of the Secretary of Defense, Live Fire Test and Evaluation (OSD LFT&E). The Methodology is currently being used in the LPD 17 VAR 4 (detailed design).

4.1.2 CVN(X) VAR

A revised Methodology was applied to the CVN(X) VAR 2. The primary improvement was a modified fire growth algorithm for very large spaces. A criticism of the previous Methodology approach was the very rapid fire development in all spaces, independent of size. It was perceived that fire development (i.e., time from ignition to flashover) would be longer in larger spaces compared to small spaces.

The Methodology as applied to CVN(X) (now designated CVN 21) is documented (Back et al., April 2002); the VAR is in the final approval stages. It is anticipated that the Methodology will be used for the CVN 21 VAR 3 now being initiated.

A non-classified version of the Methodology was published for general use (Back et al., March 2003). This document forms the primary technical basis of this report as described in Appendix B. It was during the CVNX VAR 2 and subsequent documentation of the general Methodology that the PDA(F) and ADPA(F) definitions were adopted which clarify the

differences in the treatment of these areas by the blast damage and fire communities (See Appendix B).

4.2 Use in WET Predictions

4.2.1 Ex-USS CARON

The basic Methodology was used to predict unabated fire and smoke spread in weapons effects testing (WET) of the ex-USS CARON sponsored by PMS 500. The results are documented in stand-alone segments which were incorporated in the ex-USS CARON WET pre-hit and post-hit reports (Back et al., January 2002, Back et al, July 2003).

4.2.2 Ex-USS PETERSON

The basic Methodology is being used in pre-hit predictions for the DD(X) industry-sponsored ex-USS PETERSON WET. A fire suppression algorithm has been added to the Methodology since a water mist system designed to prevent fire spread will be installed on the ship. The water mist suppression algorithm is based on a steady-state suppression model documented in the peer-reviewed scientific literature (Back et al., November 2000). Documentation of this prediction is in preparation. The ex-USS PETERSON will also be assessed using a network fire and smoke spread model. This model is being adopted by the DD(X) Recoverability Team and will be used as a replacement/improvement to the Methodology for DD(X) VAR 1. The ex-USS PETERSON test data will be used as part of the V&V of the network model. Floyd et al., 2003, briefly describes this new modeling approach.

4.3 CFAST Modeling for Navy Shipboard FHAs

CFAST has been used in a number of Navy ship platforms to model unique or hazardous situations. This modeling usually is incorporated into a Fire Hazard Analysis. An FHA is used to: inventory the fuel loading; assess ignition sources; quantify the hazard resulting from likely fire scenarios; determine the impact on personnel, equipment, and the ship; and develop appropriate mitigation strategies. CFAST has been an important tool for quantifying fire hazards on ships. Table 2 outlines Navy shipboard FHAs where CFAST has been used to quantify the hazard. The wide-ranging application of CFAST in these situations demonstrates the breath and scope of the use of this model for Navy fire hazard assessment.

5.0 COMMENTS AND TROUBLE REPORTS

The methodology documented in this report reflects the latest approach to characterize fire and smoke spread in the VAR 3 process for the LPD 17 platform detailed design and

CVNX VAR. Comments and trouble reports received from users and technologists relying on the methodology results have been limited to the conservative nature of the approach. This criticism has been addressed by the development of a network fire model (Floyd et al., 2003). The network fire model would provide a physics-based model that could quickly assess fire and smoke spread for ship platforms. Plans also include accounting for fire detection and suppression effects. This type of model would provide better far field secondary damage characterization capabilities. It is unclear if the network fire model will replace the current methodology or if it will be used in conjunction with the methodology or portions of the methodology described in this report.

Table 2 - Use of CFAST in Navy Shipboard Fire Hazard and Modeling Applications

Client/Platform	Task	Reference
LPD 17	Analysis of smoke and heat spread for well deck fire fighting	White et al., 2001
ONR/DC-ARM	Modeling of the probability of compartment flashover resulting from a missile hit scenario (geometry and vent dependent)	Back et al., October 1998
NSWC/OHIO and VIRGINIA Class Submarines	Fire modeling/risk assessment of plastic waste storage/disposal	Back et al., December 2000
LPD 17	Composite mast fire hazard analysis	White et al., 2000
NSWC/DD	USS RADFORD AEMS composite mast fire hazard analysis	White et al., 1996
PMS 400/DDG	Fire hazard analysis of pipe insulation	Beitel et al., 1996
PMS 378/CVN 21	Fire hazard analysis of hangar bay	Parker et al., 2003
Submerged vessel	Fire hazard analysis of dry deck shelter	White et al., November 1997

6.0 ALGORITHM REVIEW

6.1 Methodology

The Methodology is summarized in the flowchart in Figure 1. The process involves modeling PDA(F) compartments with the multi-compartment zone fire model CFAST. The use of CFAST allows for a more complete characterization of these compartments. The output from

CFAST is used to predict fire spread times. Fire spread beyond these compartments to APDA(F) and BAPDA(F) compartments is also predicted using a conservative set of prescriptive rules.

6.2 CFAST

6.2.1 History

HAZARD 1 Version 1.0 was the prototype fire hazard assessment model developed by the National Institutes of Standards and Technology (NIST) that integrated fire dynamics with biology, toxicology and human behavior (Jones, 1985; Jones, 1983). FAST version 18.3 was implemented in HAZARD 1.0 in 1988 and provided the user with a method to simulate the important time-dependent phenomena involved in residential and commercial building fires. In 1990 FAST Version 18.5 was integrated with Consolidated Compartment Fire Model (CCFM) to develop CFAST 1.0 that was functionally equivalent to FAST but more modular like CCFM. The current versions of CFAST available on the web are Version 5.0 (5/7/03) and Version 3.1.7 (11/8/01) that use the Graphical User Interface (GUI)—FAST.

In the case of buildings, the assumptions made by CFAST have proven to be reasonably good and the limitations have not been unduly restrictive (See Table 1). However, naval fire protection problems differ in many critical respects from those found in the civilian world and it was not clear how the limits of CFAST may impact the utility of the model for naval applications.

The US Navy became involved in development of CFAST under its Office of Naval Research (ONR) program conducted through the Science and Technology (S&T) Damage Control (DC) Project at NRL. The emphasis in this program was to evaluate and, where necessary, improve the capabilities of CFAST in predicting fire and smoke transport in naval platforms. Specifically, the Navy's funding has been directed toward making CFAST more useful for simulation of shipboard fires by adding capabilities for modeling phenomena that are absent from, or of little significance to, building fires. In particular, these phenomena have included mass transport via vertical gas flow through horizontal vents (represented by hatches and scuttles)(Bailey, 1994); energy transport via conduction through decks (vertical heat transfer) (Bailey, et al., 1998; Bailey and Tatem, 1995); an improved radiation transport sub-model (Hoover et al., 1996; Hoover et al., 1997; Hoover, 1995; Hoover and Bailey, 2000); and, algorithms for heat conduction through bulkheads as well as smoke movement along a long passageway (Bailey et al., 2002; Bailey and Tatem, 1998).

Although initial joint efforts between NIST and NRL were targeted toward improved algorithm development, later NRL work focused on how CFAST's limits may impact the utility of the model for naval applications. That particular research has identified CFAST's limitations determined their effects on shipboard fire modeling and developed methods for circumventing

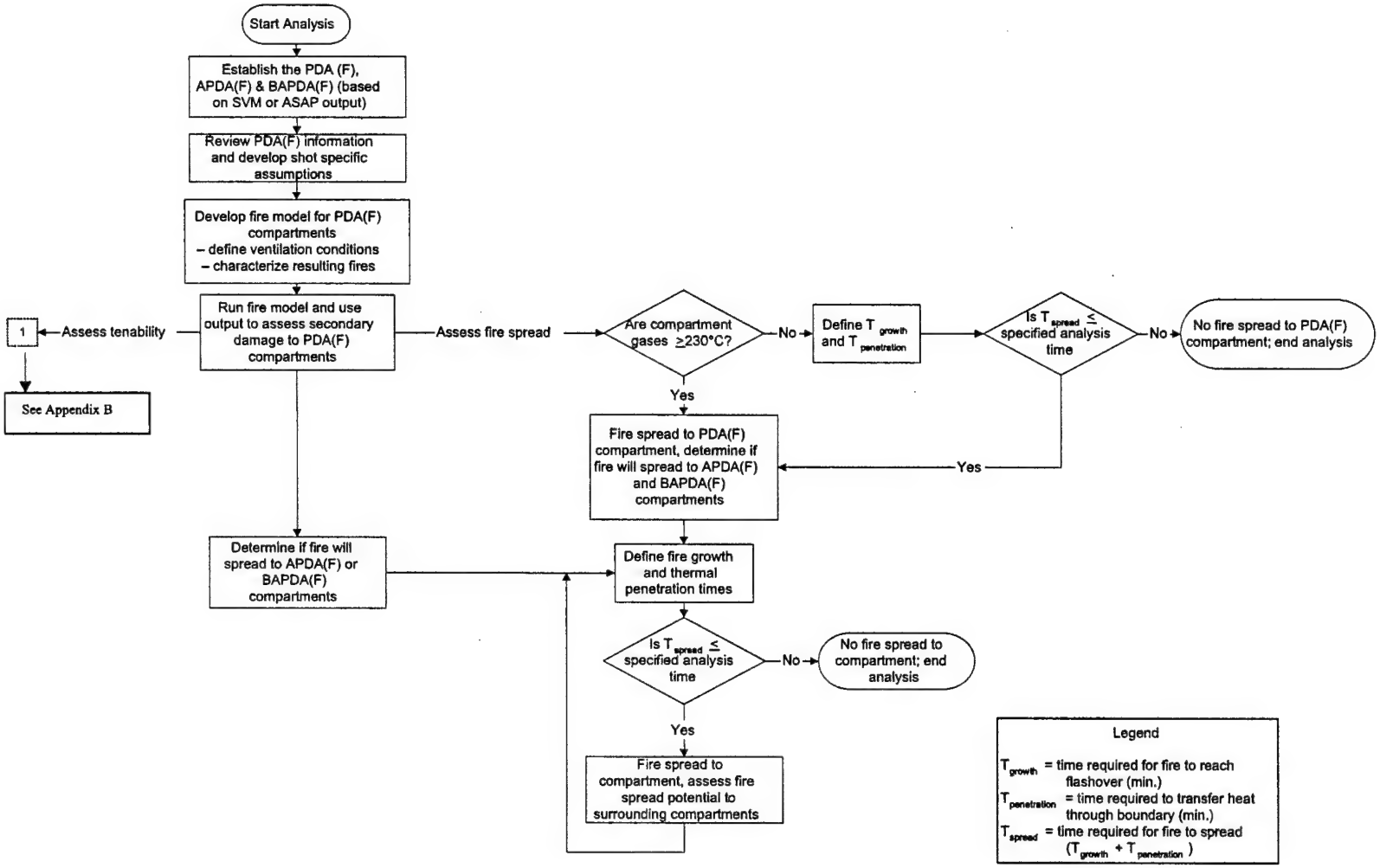

Fig. 1 - Flowchart for fire and smoke spread methodology

those problems that have significant adverse effects (Hoover and Tatem, June 2000; Hoover and Tatem, December 2000) (See Table 1).

6.2.2 Validation of New Phenomena

Vertical Vent Flow – was developed to handle vertical gas flow through horizontal vents (i.e., scuttles and hatches) as opposed to doors and windows. This phenomenon has importance in naval platforms but not necessarily in buildings.

Vertical (and Horizontal) Heat Transport – was developed to correctly account for conductive heat transfer in the vertical (and horizontal) direction through metal decks in naval platforms. The addition of this phenomenon in shipboard environments is necessary since rising temperatures in adjacent steel compartments as a result of fire can cause materials to reach ignition levels even though no breach has occurred in the initial fire compartment.

Single Zone (SHAFT) – When this option is invoked, CFAST uses a single set of parameters (i.e., temperature and gas concentrations) to represent the entire compartment volume, rather than two sets (one for each layer).

Natural and Forced Ventilation – was developed to simulate the presence of heating, ventilation and air conditioning (HVAC) systems and their use to control smoke movement. Both of these concepts are important phenomena that must be accounted for in naval platforms.

Radiation Transport – was developed to permit the use of growing combustion gas concentrations to calculate the absorbance or radiative effect of the fire environment. In the two-zone CFAST model the absorbance of each layer is then calculated as a function of carbon dioxide, water vapor and soot.

Corridor Flow – was developed to predict the flow of a ceiling jet (hot or smoke layer) down the corridor with time. Prior to the addition of this phenomenon, CFAST assumed an isothermal upper layer would immediately cover the entire ceiling area along the entire length of the corridor and the only transient change in the corridor was the smoke layer depth.

6.2.3 CFAST as Fire Model for PDA(F)

CFAST is the multi-compartment zone fire model used to characterize the environment in PDA(F) spaces for each hit scenario. In developing the input for CFAST, the ventilation conditions must be defined. These conditions include those provided by natural and forced ventilation. Natural ventilation may be provided by holes in the skin of the ship (resulting from the weapon hit) and openings between PDA(F) compartments. At a minimum, oxygen for combustion is provided naturally through any openings to weather that result from the weapon hit. Forced ventilation may be provided in vital spaces where ventilation is not secured under materiel condition ZEBRA.

For the initial CFAST run, only the fuel load in PDA(F) compartments is considered. It is assumed that fires ignite in all PDA(F) compartments that are intimate with the compartment containing the burst point and have available fuel at the time of the weapon detonation. This is a very aggressive assumption. Since specific details about the fuel loading are not usually available, fire growth rates associated with the type of materials expected in the spaces are used for these typical materials. More specifically, it is assumed that the fires follow "t-squared" fire growth curves.

6.3 HEATING

The amount of time required to spread fire through an intact boundary is determined by identifying the fire growth time and the thermal penetration time. The fire growth time is a function of type of compartment (PDA(F) as compared to APDA(F)) or BAPDA(F) and/or compartment size. The thermal penetration time is a function of the bulkhead or deck thickness. The thermal penetration time is determined using the finite difference heat conduction model – HEATING (Version 7.3) (Wickstrom, 1999), which has been previously Verified and Validated (Trelles et al, NRL Report in preparation; Hunt, et al., NRL Report in preparation). Fire spread from APDA(F) spaces and BAPDA(F) spaces occurs via heat transfer through intact bulkheads and decks. This mode of fire spread is the most predominant since these spaces normally do not have vent connections to the spaces with fires.

7.0 VERIFICATION AND VALIDATION DESCRIPTION AND RESULTS

7.1 Verification

7.1.1 Methodology

As previously stated, the Methodology is a combination of CFAST and prescriptive rules that invoke HEATING. Its verification is a composite of the verifications of these two components that are described briefly below.

7.1.2 CFAST

CFAST is based on solving a set of equations that predict state variables (pressure, temperature and others) based on the enthalpy and mass flux over small increments of time. These equations are derived from the conservation equations for energy, mass, and momentum, and the ideal gas law. The conservation equations are always correct, everywhere. Thus any errors made by the model cannot come from these equations, but rather come from simplifying assumptions or from processes having been omitted. Examples of sources of errors and omissions have been highlighted in Section 3.0, Table 1.

7.1.3 HEATING

The thermal penetration time ($t_{penetration}$) was determined using the finite difference heat conduction model – HEATING Version 7.3. In the verification process for "HEATING" (Appendix C), a series of eight benchmark reference cases were proposed by Wickström and Pålsson (1999) for use in verifying two-dimensional heat conduction computer programs (Wickström *et al.*, 1999; Pålsson *et al.*, 2000). These entailed thermal calculations of increasing complexity. The reference cases were developed to address the following aspects of a numerical heat transfer calculation:

- Convergence;
- Variable convective and radiative boundary conditions;
- Variable thermal material properties;
- Multiple materials;
- Phase change of material constituents; and
- Radiation and convection in voids.

Results from the Verification Process showed that HEATING compared successfully with Reference Cases 1 through 8 of the benchmark proposed by the developer (Wickström *et al.*, 1999). It was found that for cases 1 through 6, 64 cells are sufficient for satisfactory convergence with either the analytical solution or with the results calculated by the computer code "Temperature Analysis of Structures Exposed to Fire" (TASEF). For Reference Case 7, two bottom cells suffice to yield excellent results for the one-dimensional transfer case (7a). For the two dimensional case (7b), 8 bottom cells result in differences smaller than 3.2%. For the more complex geometry of Reference Case 8, the results for the most refined mesh are in excellent agreement with TASEF when only radiative transfer is occurring in the cavities. When convective heat transfer was added to the cavities, HEATING yielded moderately lower temperatures than TASEF.

7.2 Validation

7.2.1 Methodology

As with "Verification", the "Validation" for the Methodology is a composite of the "Validations" for CFAST and HEATING that are described briefly below.

7.2.2 CFAST

Before the Navy's involvement (circa.1989), V&V work on CFAST dealt with earlier versions of CFAST (1.x or earlier). The modifications to CFAST through Navy involvement are

contained in versions 16.4, 2.x, 3.x, 4.0.1 and 5.0.1. Versions 3.1.4 and 4.0.1 have undergone the most extensive validations, using experimental data documented in various programs conducted aboard ex-USS SHADWELL (Williams, et al, 2001) in Mobile AL. However, the most current publicly available version of CFAST is 5.0.1, for which no validations have been completed to date. The inherent difficulty in using any version of the model is that phenomena implemented and validated in earlier versions are not re-verified after "fixes" have been made in later versions. On the other hand, it is very possible that some of the problems encountered by researchers using earlier versions of CFAST may have been fixed in the latest version(s). The V&V requirements, therefore, consist of demonstrating that these tools, although validated over a number of versions of the methodology, still produce acceptable results and that the results are applicable to a full-size ship, since SHADWELL represents a retired naval platform. For these reasons (and others documented later in this Section) CFAST Version 3.1.7 is the fire model recommended for assessment in the PDA(F) for T-AKE Test and Evaluation.

The Methodology invokes the new phenomena of vertical vent flow, single zone (SHAFT) and improved gas absorbance coefficient in CFAST Version 3.1.7. The validation for vertical vent flow using SHADWELL experimental data from the Smoke Ejection System tests (Appendix A) showed consistent trends in compartment temperatures between CFAST predictions and SHADWELL experiments. The absolute temperature comparison showed an under-prediction by the model attributable to over-prediction of gas flow through the vent. In the fire compartment over a 90-minute period, the experimental temperature range was 150 deg C to 400 deg C. The predicted model temperature in that compartment ranged from 100 deg C to 300 deg C. In the vent-connected compartment, the experimental temperature range was 200 deg C to 700 deg C and the model-predicted temperature range was 200 deg C to 400 deg C. Vertical vent flow phenomenon was the first to be added to enhance the performance of CFAST. Some factors that may have contributed to the only fair comparison were added in later modifications of CFAST, e.g., vertical and horizontal heat transfer and long corridor effects.

CFAST Version 3.1.7 also invokes the improved gas absorbance coefficient and the single zone, or SHAFT, option. One of the assumptions originally made by CFAST was the use of constant (rather than time-variant) extinction coefficients in the upper and lower layers to calculate the absorbance or radiation effect of the combustion gases. In order to address this deficiency, CFAST was modified to permit the absorbance of each layer to be calculated as a function of the time-variant concentration of carbon dioxide, water vapor and soot. With the new algorithm, the total absorbance is calculated analytically from the gas absorbance and various soot parameters and the gas absorbance is estimated by interpolation of values stored in lookup tables.

The SHAFT option was used in the validation of the gas absorbance algorithm. When this option is invoked on a particular compartment, the model uses a single set of parameters (i.e., temperature and gas concentration) to represent the entire compartment volume, rather than two sets (one for each layer). This is appropriate whenever the compartment gases are well mixed and may therefore be represented by a single zone. With the SHAFT option in effect, the temperature at the top of a compartment is affected by heat conducted from the compartment below; therefore, vertical energy transfer is handled correctly. With this in mind, users must be aware that the original, hard-coded extinction value used for the upper layer in any version of CFAST before Version 3.0 is inappropriate for compartments which accumulate little, if any,

combustion products; for example, those compartments far from the fire. If the SHAFT option is used for one of these compartments, the upper layer extinction will be applied to the entire compartment and the results for the whole compartment will be in error. This problem will, of course, be moot if CFAST 3.0 or later versions are used because, in that case, the extinction calculation will be transient.

Complete validation of the horizontal heat conduction algorithm requires comparison with additional experimental data. In the Methodology used for the CVNX VAR (and subsequently to be used for T-AKE), the inclusion of vertical/horizontal heat transfer in CFAST is not as significant as other discussed phenomena since the Methodology invoked to spread fires through intact bulkheads, decks and overheads is via the finite difference heat conduction model HEATING Version 7.3. These give the additional reasons referred to earlier as to why CFAST Version 3.1.7 is the recommended version for use in the T-AKE Test and Evaluation.

The results from the fire modeling are used to predict the temperatures, interface heights (demarcation between smoke and relatively smoke-free zones) and smoke concentrations in the PDA(F) compartments. The temperature data are used to determine when or if fire will spread within these compartments as well as to other spaces. The interface height and smoke density data, in addition to the temperature data, are used to determine how tenable these compartments would be for protected and unprotected personnel. (The criteria used for tenability are not part of this documentation). This information is the most basic output provided by the fire model. The temperature data have been validated and verified extensively and the results of this V& V are contained in Appendix A.

7.2.3 HEATING

HEATING has compared successfully with eight validation cases of increasing complexity. Validation cases were selected based on the availability of test data and material properties for the configurations tested. The validation basis varied from case to case depending on the particular test available, and included fire resistance ratings, temperatures at fixed locations at fixed times, and transient temperatures at fixed locations. Convergence was demonstrated in each case by increasing the number of nodes, reducing the time step, reducing the tolerance, and using alternative solution methods.

The sensitivity of each validation case to the input parameters was also investigated because of the inherent uncertainty in the specific material properties, especially at elevated temperatures, and as well as the boundary condition parameters. An uncertainty of plus or minus 25 percent was assumed where applicable. It was found that the validation cases generally separated into three categories: those sensitive to boundary condition parameters, namely the effective emissivity of the exposed surface; those sensitive to the material properties, in particular the thermal conductivity of the dominant material, and those that were insensitive to uncertainty in either parameter group.

8.0 VERIFICATION AND VALIDATION ADEQUACY

The methodology described in this report is intended to identify specific weaknesses and/or shortcoming that might decrease ship survivability. The methodology is summarized in the flowchart in Figure 1 (Section 6). The process involves modeling PDA(F) compartments with the multi-compartment zone fire model CFAST. The use of CFAST allows for a more complete characterization of these compartments. The output from CFAST is used to predict fire spread time. Fire spread beyond the PDA(F) compartments to APDA(F) and BAPDA(F) compartments is predicted using a conservative set of prescriptive rules in conjunction with the finite element model HEATING to evaluate thermal penetration times.

The software that constitutes CFAST is a collection of data and computer programs that are used to simulate the important time-dependent phenomena involved in fires. The major functions provided include calculation of:

- The buoyancy-driven as well as forced transport of this energy and mass through a series of specified compartments and connections (e.g., doors, windows, cracks, ducts, hatches, scuttles),
- The resulting temperatures, smoke optical densities, and gas concentrations after accounting for heat transfer to surfaces and dilution by mixing with clean air.

As can be seen from this list, fire modeling involves an interdisciplinary consideration of physics, chemistry, fluid mechanics, and heat transfer. In some areas, fundamental laws (conservation of mass, energy, and momentum) can be used, whereas in others empirical correlations or even "educated guesses" must be employed to bridge gaps in existing knowledge. The necessary approximations required by operational practicality result in the introduction of uncertainties in the results. The user should understand the inherent assumptions and limitations of the programs, and use these programs judiciously – including sensitivity analyses for the ranges of values for key parameters – in order to make estimates of these uncertainties.

CFAST has been validated extensively by NIST, NRL and others. Although differences between the model and the experiments were evident in the studies, they are typically explained by limitations and assumptions of the model and of the experiments. Like all predictive models, the best predictions come with a clear understanding of the limitations of the model and of the inputs provided to the calculations.

The use of heuristics for far-field predictions provides conservative/generic guidelines for fire and smoke spread outside of the PDA(F). These prescriptive rules assume that an unlimited amount of fuel and air is available in each compartment so predictions are worst case. In the event that there is a small amount of fuel in the compartment or the compartment is closed, fire spread may be delayed or may not occur at all. The finite difference heat conduction model – HEATING –provides excellent predictions for thermal penetration time through a bulkhead or deck. The limitations imposed by CFAST are tempered by the use of worst-case scenarios in conjunction with the HEATING model to make the overall Methodology approach a conservative estimate of the secondary fire and smoke damage.

9.0 REFERENCES

Back, G.G., Darwin, R.L., Scheffey, J.L., Williams, F.W., and Farley, J.P. (July 8, 2003), "Spruance Class Weapons Effects Tests - Fire Spread Evaluation: Final Report," NRL Ltr Rpt Ser 6180/0263.

Back, G.G, Mack, E.C., Peatross, M.J., Scheffey, J.L., White, D.A., Satterfield, David, Farley, J.P., and Williams, F.W., (March 31, 2003), "A Methodology for Predicting Fire and Smoke Spread Following a Weapon Hit", NRL Ltr Rpt 6180/0014.

Back, G.G., Scheffey, J.L., Darwin, R.L., and Williams, F.W., (January 31, 2002), "Spruance Class Weapons Effects Test (Wet) for Validation of Fire/Smoke Spread," NRL Ltr Rpt Ser 6180/0048.

Back, G.G., Hunt, S.P., White, D.A., Tatem, P.A., and Williams, F.W., (December 28, 2000), "Revised Fire Hazard Assessment of the Storage of Processed Plastic Waste on Ohio Class (SSBN726) and Virginia Class (SSN774) Submarines," NRL Ltr Rpt Ser 6180/0513.

Back, G.G., Darwin, R.L., Hopkins, D., Mack, E.C., Scheffey, J.L., White, D.A., Tatem, P.A., Williams, F.W., and Hunstad, M., "CVNX1 Vulnerability Report (2) and Battle Damage Repair Assessment: Fire and Smoke Spread Evaluation (U)," NRL report in preparation, 18 March 2002 (Secret).

Back, G.G., Beyler, C.L., and Hansen, R., (November 2000), "A Quasi Steady State Model for Predicting Fire Suppression in Spaces Protected by Water Mist Systems," Fire Safety Journal, **35** (4), pp. 327-362.

Back, G.G., Darwin, R.L., and Beyler, C.L., (February 10, 2000), "An Evaluation of the Cooling Capabilities of Water Spray Systems in Cargo Holds," Hughes Associates Report.

Back, G.G., Iqbal, N., Williams, F.W., and Scheffey, J.L., (October 27, 1998), "Potential Compartment Fire Growth Curves Resulting From a Missile Hit," NRL Ltr Rpt Ser 6180/0526.

Back, G.G., Leonard, J.T., Fulper, C.R., Darwin, R.L., Scheffey, J.L., Willard, R.L., DiNenno, P.J., Steel, J.S., Ouellette, R.J., and Beyler, C.L., (September 3, 1991), "Post-Flashover Fires in Simulated Shipboard Compartments: Phase I-Small Scale Studies," NRL Memorandum Rpt 6886.

Bailey, J.L., Forney, G.P., Tatem, P.A., & Jones, W.W., (August 2002), "Development and Validation of Corridor Flow Sub-model for CFAST." Journal of Fire Protection Eng., Vol.12, pp.139-161.

Bailey, J.L., and Tatem, P.A., (October 9, 1998), "Validation of Hybrid Smoke Movement Sub-model Using Shadwell/688 Experiment," NRL Letter Report 6180/0515.

Bailey, J.L., Jones, W.W., Tatem, P.A., Forney, G.P., (May/June 1998), "Development of an Algorithm to Predict Vertical Heat Transfer Through Ceiling/Floor Conduction, Fire Technology, Vol 34, No. 2, 139-155.

Bailey, J.L., and Tatem, P.A., (September 30, 1995), "Validation of Fire/Smoke Spread Model (CFAST) Using ex-USS Shadwell Internal Ship Conflagration Control (ISCC) Fire Tests." NRL/MR/6180-95-7781.

Bailey, J.L., (January 1994), "Validation of Fire/Smoke Spread Model (CFAST) using ex-USS SHADWELL Smoke Ejection System Fire Tests," NRL Letter Report 6180-0007.2.

Beard, A., (1992), "Evaluation of Fire Models: Part I – Introduction," Fire Safety J. 19, 295-306.

Beard, A., (1990), "Evaluation of Fire Models: Overview," Unit of Fire Safety Engineering, University of Edinburgh, Edinburgh, UK.

Beitel, J.J., Beyler, C.L., Sincaglia, P.E., Hill, S.A., Scheffey, J.L., White, D.A., Iqbal, N., Hamer, A.J., Leonard, J.T., and Brown, R., (June 28, 1996), "Fire Performance of Pipe Insulation Materials," NRL Ltr Rpt Ser 6180/0378.

Bukowski, R.W., (1995), "Modeling a Backdraft: The Fire at 62 Watts Street, NFPA Journal", Vol. 89, No. 6, pp. 85-89.

Bukowski, R. W., (1992), "Analysis of the Happyland Social Club Fire With HAZARD I," Fire and Arson Investigator, Vol. 42, No 3, pp. 36-47.

Bukowski, R.W., (June 5-6 1990), "Reconstruction of a Fatal Residential Fire at Ft. Hood, Texas," First HAZARD I Users' Conference, National Institute of Standards and Technology, Gaithersburg, MD.

Collier, P.C.R., (August/September, 1995), "Fire in a Residential Building: Comparisons Between Experimental Data and a Fire Zone Model", Fire Technology, 32:3, pp. 195-218.

Chow, W.K., (July/August 1996), "Prediction of Fire Environment in Apartment Using a Zone Model," Journal of Fire Sciences, 14:4, 263-312.

Darwin, R.L., Leonard, J.T., and Scheffey, J.L., (May 1994), "Fire Spread by Heat Transmission through Steel Bulkheads and Decks," Proceedings of IMAS Conference on Fire Safety on Ship, Institute of Marine Engineers, London, England.

Deal, S., (October 21-24, 1990), "A Review of Four Compartment Fires with Four Compartment Fire Models," Fire Safety Developments and Testing, Proceedings of the Annual Meeting of the Fire Retardant Chemicals Association, Ponte Verde Beach, Florida, pp. 33-51).

Dembsey, N.A., Pagni, P.J., and Williamson R.B., (1995), "Compartment Fire Experiments: Comparison with Models," Fire Safety Journal 25, pp.187-227.

Department of the Navy, (December 2001), "Naval Ships' Technical Manual Chapter 555 – Volume 1, Surface Ship firefighting," S9086-S3-STM-010/CH-555V1R9.

Drysdale, D., (1999), An Introduction to Fire Dynamics, Second Edition, John Wiley & Sons, Chichester.

Duong, D.Q., (1990), "The Accuracy of Computer Fire Models: Some comparisons with Experimental Data from Australia," Fire Safety J., 16(6), 415,431.

Floyd, Jason, Scheffey, J.L., Haupt, T., Habbash, H., Hodge, B., Norton, O., Williams, F.W., Tatem, P.A., (January 23, 2003),"Requirements and Development Plan for A Shipboard Network Fire Model", NRL Ltr Rpt Ser 6180/0469.

He, Y., Fernando, A. and Luo, M., (1998), "Determination of Interface Height from Measured Parameter Profile in Enclosure Fire Experiment", Fire Safety Journal 31:1, pp. 19-38.

Hoover, J.B., & Tatem, P.A., (December 29, 2000),"Application of CFAST to Shipboard Fire Modeling II Specification of Complex Geometry", NRL/MR 6180-00-8489.

Hoover, J.B., & Tatem, P.A., (June 26, 2000),"Application of CFAST to Shipboard Fire Modeling I. Development of the Fire Specification," NRL/MR/6180-00-8466.

Hoover, J.B., & Bailey, J.L., (February 2000), "Appendix G: A Note on Total Gas Layer Absorption, " in "A Technical Reference for CFAST: An Engineering Tool for Estimating Fire and Smoke Transport," Jones, W.W., Forney, G.P., Peacock, R.D., and Reneke, P.A., National Institute of Standards and Technology, Technical Note 1431.

Hoover, J.B., Bailey, J.L., & Tatem, P.A., (1997), "An Improved Radiation Transport Sub-model for CFAST." Combustion Science and Technology 127, 213-229.

Hoover, J.B., Bailey, J.L., & Tatem, P.A., (March 8, 1996), "Validation of Gas Phase Absorbance Algorithm in the Consolidated Fire Growth and Smoke Transport (CFAST) Model," NRL Letter Rpt 6180/0020.

Hoover, J.B., (August 7, 1995), "Addition of Gas Phase Absorbance Calculation Algorithm to the Consolidated Fire and Smoke Transport (CFAST) Model," NRL Letter Report 6180/0438.

Hunt, S.P., Trelles, J. and Williams, F.W., "HEATING 7.3 Validation for Fire Resistive Applications", NRL Report in preparation.

Jones, W.W., Forney, G.P., Peacock, R.D., and Reneke, P.A., (March 2000), "A Technical Reference for CFAST: An Engineering Tool for Estimating Fire and Smoke Transport", NIST TN 1431, National Institute of Standards and Technology, Gaithersburg MD.

Jones, W.W., (1985), "A Multi-Compartment Model for the Spread of Fire, Smoke and Toxic Gases, Fire Safety Journal 9, 55.

Jones, W.W., (1983), "A Review of Compartment Fire Models," National Bureau Standards (U.S.), NBSIR 83-2684, 41 p.

Luo, M., (May/June, 1997), "One Zone or Two Zones in the Room of Fire Origin During Fires? The Effects of the Air-Handling System," Journal of Fire Sciences, 15:3, pp. 240-260.

Nelson, H.E. (1989), "An Engineering View of the Fire of May 4, 1988 in the First Interstate Bank Building, Los Angeles, California," Natl. Inst. Stand. Techno. NISTIR 89-4061, 39 p.

Parker, A.J., Fay, T.S., Floyd, J.E., Darwin, R.L., Scheffey, J.L., Williams, F.W., and Hunstad, M.P., (draft, April 11, 2003), "NIMITZ Class Aircraft Carrier Hangar Bay Fire Hazard Analysis," NRL Memorandum Report.

Peacock, R.D., Reneke, P.A., Jones, W.W., Bukowski, R.W., and Forney, G.P., (January 2000a), "A User's Guide for FAST: Engineering Tools for Estimating Fire Spread and Smoke Transport," Special Publication 921, 2000 Edition, National Institute of Standards and Technology, Gaithersburg, MD.

Peacock, R.D., Forney, G.F., Reneke, P., and Jones, W.W., (January 2000b), "CFAST, the Consolidated Model of Fire Growth and Smoke Transport, Version 4.0.1", NIST Technical Note 1431, National Institute of Standards and Technology, Gaithersburg, MD.

Peacock, R.D., Reneke, P.A., Forney, C.L, and Kostreva, M.M. (1998), "Issues in Evaluation of Complex Fire Models," Fire Safety Journal 30, 103-136.

Peacock, R.D., Jones, W.W., and Bukowski, R.W., (1993), "Verification of a Model of Fire and Smoke Transport," Fire Safety J. 21, 89-129.

Rockett, J.A., (June 1997), "Zone Model Plume Algorithm Performance," Thirteenth Meeting of the UJNR Panel on Fire Research and Safety, March 13-20, 1996, Beall, K.A., ED., NISTIR 6030, Gaithersburg, MD: National Institute of Standards and Technology.

Setchkin, N.P., (1949), National Bureau of Standards Journal of Research, National Bureau of Standards, Gaithersburg, MD.

Scheffey, J.L., Williams, F.W., Hill, S.A., Toomey, T.A., Darwin, R.L., Leonard, J.T., and Smith, D.E., (May 31, 1999), "Post-Flashover Fires in Shipboard Components Aboard ex-USS Shadwell: Phase V-Fire Dynamics," NRL/MR/6180-99-9902.

Scheffey, J.L., DiNenno, P.J., Tatem, P.A., and Williams, F.W., (April 22, 1992), "Review of Fire Spread Parameters for TSS/FT Fire Spread Model," NRL Ltr Rpt Ser 6180-107.

Trelles, J., Hunt, S.P., and Williams, F.W., "Verifying HEATING 7.3 Against the Swedish National Testing and Research Institute's Suite of Fire Resistance Examples," NRL Report in preparation.

White, D.A., Rhodes, B.T., Mack, E.C., Scheffey, J.L., Farley, J.P., Williams, F.W., and Tatem, P.A., (June 15, 2001), "Heat and Smoke Management Guidelines and Fire Fighting Doctrine for the LPD-17 Well Deck and Vehicle Stowage Areas," NRL/MR/6180-01-8558.

White, D.A., Scheffey, J.L., Farley, J.P., and Williams, F.W., (June 26, 2000), "LPD17 Amphibious Dock Ship: Fire Hazard Assessment of the Forward and Aft AEM/S System Masts," NRL/MR/6180-00-8467.

White, D.A., Scheffey, J.L., Szepesi, D.B., and Williams, F.W., (November 3, 1997), "Dry Deck Shelter Fire Hazard Analysis," NRL Ltr Rpt Ser 6180/0545.

White, D.A., Rhodes, B.T., DiNenno, P.J., Tatem, P.A., and Kay, D., (September 30, 1997), "Smoke and Fire Spread Evaluations: LPD-17 Amphibious Transport Dock Ship Total Ship Survivability and Battle Damage Repair Assessments (U)," NRL/MR/6180-97-7985, 30 (Confidential).

White, D.A., Scheffey, J.L., Sincaglia, P.E., Williams, F.W., and Farley, J.P., (June 25, 1996), "Advanced Enclosed Mast/Sensor System Fire Hazard Analysis," NRL Ltr Rpt Ser 6180/0316.

Wickstrom, U., (1999), "An Evaluation Scheme of Computer Codes for Calculating Temperature in Fire Exposed Structures," in S. Grayson (ED.), Interflam '99 (pp. 1033-1044), London:Interscience Communications Ltd.

Williams, F.W., Toomey, T.A. and Carhart, H.W., (September 1992), "The ex-SHADWELL Full Scale Fire Research and Test Ship," NRL Memorandum Report, NRL/MR/6180-01-8576, August 24, 2001.

APPENDIX A

VERIFICATION AND VALIDATION OF CONSOLIDATED FIRE AND SMOKE TRANSPORT (CFAST)

CONTENTS
APPENDIX A

FIGURES

1.0 CHARACTERIZATION OF SECONDARY DAMAGE IN THE PDA(F)

1.1 Development and Assumptions of the Fire Model

In the current methodology (Back, March, 2003), the multi-compartment zone fire model used for characterizing the environment in primary damage area that includes vent-connected spaces for each hit scenario is Consolidated Fire and Smoke Transport (CFAST) Version 3.1.7 (Peacock et al, January 2000; January 2000). APDA(F) and BAPDA(F) spaces are not included in the fire model. CFAST is a member of a class of models referred to as zone or finite element models. This means that each room is divided into a small number of volumes (called layers), each of which is assumed to be internally uniform. That is, the temperature, smoke and gas concentrations within each layer are assumed to be exactly the same at every point. In CFAST, each room is divided into two layers. Since these layers represent the upper and lower parts of the room, conditions within a room can only vary from floor to ceiling, and not horizontally. This assumption is based on experimental observations that in a fire, room conditions do stratify into two distinct layers. While we can measure variations in conditions within a layer, these are generally small compared to differences between the layers.

CFAST is based on solving a set of equations that predict state variables (pressure, temperature and so on) based on the enthalpy and mass flux over small increments of time. These equations are derived from the conservation equations for energy, mass, and momentum, and the ideal gas law. The conservation equations are always correct, everywhere. Thus any errors made by the model cannot come from these equations, but rather come from simplifying assumptions or from processes having been omitted. Examples of each source of error will be highlighted in the following discussion.

1.1.1 Fires

CFAST uses a specified fire. This requirement is probably the most important restriction on the use of CFAST. The input heat release rate of the fuel, specified by the user, is critical to achieving accurate model predictions of temperature (one of the primary parameters used in the validation process). This fuel is converted into enthalpy (the conversion factor is the heat of combustion) and mass (the conversion factor is the yield of a particular species) as it burns. Burning can take place in the portion of the plume in the lower layer (if any), in the upper layer or in a door jet. For an unconstrained fire (i.e., not oxygen-limited), CFAST always uses the specified heat release rate. Burning will all take place within the fire plume. For a constrained fire, the heat release rate can be reduced below the user-specified level if there is insufficient oxygen to support that combustion rate. Burning will take place where there is sufficient oxygen. In the simulation analyses, constrained fires are typically used with conservative worst case fire growth rates. This leads to oxygen-limited fires that are as large as can be supported. In general this results in a conservative prediction.

Specification of the heat release rate by the user means that this version of CFAST (3.7.1), like all current zone fire models, does not include a pyrolysis model to predict fire growth.

Rather pyrolysis rates for each fire modeled define the fire history. The similarity of that input to the real fire problem of interest will determine the accuracy of the resulting calculation. The user must account for any interactions between the fire and the pyrolysis rate. Generally, more severe fires are postulated.

Another issue that must be considered carefully when executing CFAST is the fuel load since the user is specifying a time-dependent description of the growth of the fire. Since CFAST does not model the fire itself but the effects of the fire on the environment, the amount of fuel consumed in the fire is based on the user-specified fire growth descriptions. Back, March 2003, and Hoover and Tatem, June 2000, provide excellent guidelines for factors to be considered by the user in making this selection. Typically, aggregate fuel loading is assumed to be present since it is difficult to preclude the presence of combustible material.

1.1.2 Vent Flows

Flow through vents is the dominant phenomenon in a fire model because it fluctuates most rapidly and transfers the greatest amount of enthalpy on an instantaneous basis of all the source terms. Also, it is most sensitive to changes in the environment. There are two primary means for flow through vents. The first is referred to as horizontal gas flow through vertical vents. It is the flow that is normally thought of when discussing fires. It encompasses flow through doors, windows and other vertical openings. The other is vertical gas flow through horizontal vents and can occur if there is a hole in the ceiling or floor of a compartment (e.g. ship hatches and scuttles). This latter phenomenon is particularly important for shipboard vent flow and for roof venting in structural fires.

Flow through vents is governed by the pressure difference across a vent. There are two situations which give rise to flow through vents. The first, and usually thought of in fire scenarios, is that of air or smoke which is transported from a compartment primarily by buoyancy. The second type of flow is due to expansion that is particularly important when conditions in the fire environment are changing rapidly. Rather than depending entirely on density differences between the two gases, the flow is forced by volumetric expansion. The earlier versions of CFAST did not solve this part of the problem entirely correctly. In most cases the differences are small except for rapidly changing situations. However, these small differences become very important if we wish to follow flows due to small pressure differences, such as will occur in a mechanical ventilation system. Atmospheric pressure is about 100,000 Pa; fires produce pressure changes from 1 to 1,000 Pa and mechanical ventilation systems typically involve pressure differentials of about 1 to 100 Pa. In order to solve these interactions correctly, we must be able to follow pressure differences of 0.1 Pa out of 100,000 Pa for the overall problem, or 10^{-4} for adjacent compartments.

Natural ventilation may be provided by holes in the skin of the ship (resulting from the weapon hit) and openings between PDA(F) compartments. At a minimum, oxygen for combustion is provided naturally through any openings to weather that result from the weapon hit. Forced ventilation may be provided in vital spaces where ventilation is not secured under

materiel condition ZEBRA. In order to handle the flows for natural and forced ventilation, small pressure differences are followed in later versions of CFAST.

1.1.3 Non-Navy-Funded Verification and Validation of CFAST

Jones et al., 2000, reviewed a number of studies that have compared the predictions from CFAST to real-scale fires. Nelson, 1989, used simple computer fire models along with existing experimental data to develop an analysis of a large high-rise building fire. This analysis showed the value of available analytical calculations in reconstructing the events involved in a multiple-story fire.

Bukowski, 1990; 1992; 1995, has applied the FAST and CFAST models in several fatal fire reconstructions. Details of the fires including temperatures, vent flows, and gas concentrations were consistent with observed conditions and witness accounts.

Several studies comparing model predictions with experimental measurements are available. Deal, 1990, reviewed four computer fire models (CCFM, FIRST, FPETOOL and FAST) to ascertain the relative performance of the models in simulating fire experiments in a small room. All the models simulated the experimental conditions including temperature, species generation, and vent flows "quite satisfactorily".

Duong, 1990, studied the predictions of several computer fire models (CCFM, FAST, FIRST, and BRI), comparing the models with one another and with large fires in an aircraft hanger. For a 4 MW fire size, he concluded that all the models are "reasonably accurate." At 36 MW, however, "none of the models did well." Beard, 1990; 1992, evaluated four fire models (ASET, FAST, FIRST, and JASMINE) by modeling three well-documented experimental fires, ranging in scope from single compartments to a large-department-store space with closed doors and windows. He provides both a qualitative and quantitative assessment of the models ability to predict temperature, smoke obscuration, CO concentration, and layer interface position (for the zone-based models).

Peacock et al., 1993, 1998, compared the CFAST model to a range of experimental fires. The model provided predictions of the magnitude and trends (time to critical conditions and general curve shape) for the experiments studied which range in quality from within a few % to a factor of two or three of the measured values.

Other peer-reviewed publications have also compared the results of CFAST with experimental data. For completeness, these comparisons are reported here with brief synopses of conclusions drawn. More detailed discussions can be obtained from the citations.

Dembsey, et al., 1995, compared predictions from CFAST 2.1 with experiments and found the predictions of upper layer gas temperatures to be higher. The authors conjectured that the difference was due to insufficient heat transfer out of the simulated compartment. (Version 3.1.7 of CFAST has an improved vertical heat transfer sub-model.)

Collier, 1995, compared experiments in an actual multi-room house. Comparisons between the predicted interface height (CFAST 2.x) and the compartments' temperatures with actual data provided varying degrees of agreement depending upon the time and compartment being compared.

Chow, 1996 made multi-room comparisons of the upper layer temperature and interface height with predictions from CFAST 2.0. Again, there are varying degrees of agreement depending upon the time and the compartment being compared.

Davis, et al., 1996, compared ceiling jet temperature predictions using CFAST 2.0 to experimental data from a 15 m tall hangar. Results from the predictions were consistently higher than those of the experiments.

Rockett, 1997, evaluated the accuracy of plume algorithms in CFAST 2.0. He compared CFAST predictions and experimental values for the vent flow, dependent upon heat release rate.

Luo, 1997, compared CFAST 2.0.1 and experimental data for interface height and upper layer temperatures and showed the predictions to be higher than the actual.

He, et al., 1998, looked at two methods for determining interface height in CFAST (version unknown) and compared both methods to data from large scale experiments. CFAST predictions compared poorly with actual measurements by significantly over-predicting upper layer temperatures.

1.1.4 Navy-Funded Verification and Validation of CFAST

1.1.4.1 Natural and Forced Vent Flow Validation

1.1.4.1.1 General

Smoke ejection system (SES) fire tests conducted by the Naval Surface Warfare Center/Carderock (CD/NSWC), Code 633, onboard ex-USS SHADWELL were used to validate the concept of vertical gas flow through horizontal vents and smoke control through fan pressures and closures (Bailey, 1994). Because of the presence of scuttles and hatches, as well as the presence of heating, ventilation and air conditioning (HVAC) systems and their use to control smoke movement, both of these concepts are important phenomena that must be accounted for in naval platforms. The experimental data from the SES tests were compared to predictions from CFAST version 1.6.4.

The forward area of ex-USS SHADWELL, frames 0 to 36, was modified to resemble the DDG 51 design criteria (Figure A-1). The test area consisted of a machinery space connected to a mock DC passageway, hereafter referred to as DC passageway, by a vestibule. The vestibule was located directly above the machinery overhead and was divided into two compartments –

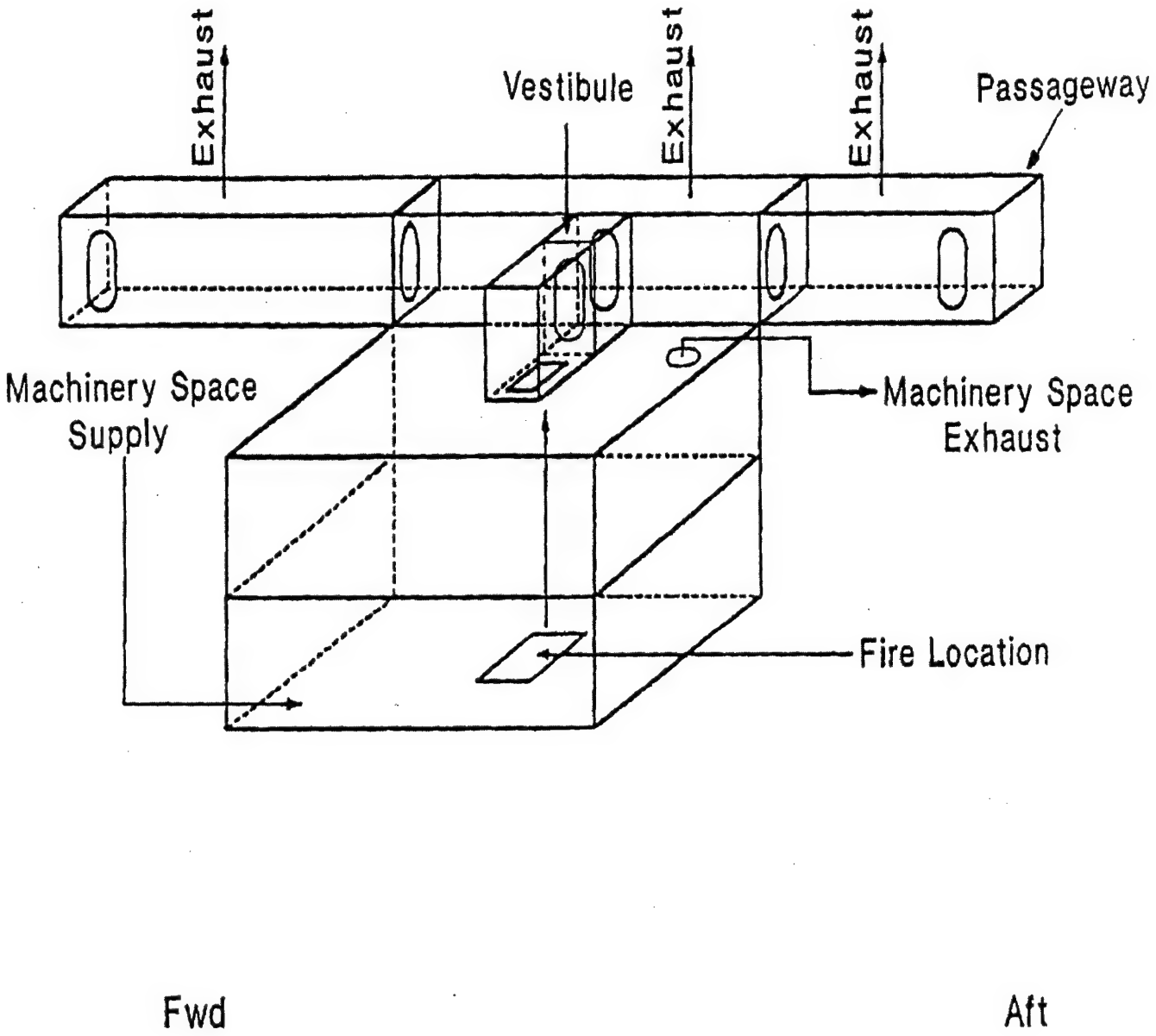

SES Test Area

Fig. A-1 - SES Test Area

inboard and outboard - by a standard Navy archway. The fuel for the machinery space fire was a diesel spray, which was ignited by a heptane pan fire. The machinery space was equipped with both a supply and exhaust fan. The DC passageway subdivisions also had mechanical ventilation. There were vertical thermocouple trees in the machinery space, both the inboard and outboard vestibules, and the DC passageway. These temperature measurements from these thermocouple trees were compared with the temperatures predicted in the compartment by CFAST.

1.1.4.1.2 Limitations:

1. The model predicts the average temperatures in an upper and lower layer, whereas the experiments, in some cases, measure a single point. In other cases where several points are measured, an average layer temperature must be determined based on limited individual measurements at discrete locations.

2. The accuracy of the model predictions depends on accurate inputs. The unavailability of any experimental setup information may have led in this V&V exercise to best "guess-timates" for input parameters.

In the machinery space, all of the thermocouple data were averaged to give an average compartment temperature. These temperatures were compared to a volume-average of the model-predicted temperatures. With the horizontal vent open in the space, the model and experiment both showed that the compartment temperature increases when the fire size is increased and decreases when fire size is decreased. Though the temperature trends are consistent, the absolute temperature is under-predicted by the model when the horizontal vent is open. These observations imply that the model is over-predicting the flow through the horizontal vent. This over-prediction is seen consistently when comparing temperatures in the DC passageway.

The inboard vestibule was connected to the machinery space via a horizontal vent and to the outboard vestibule by an archway. In the inboard vestibule the model and experimental data show a substantially higher temperature relative to the machinery space. Model-predicted and experimentally calculated temperatures also show the same increasing and decreasing trends. The absolute temperatures are close during the first 40 minutes of the experiment but then begin to deviate substantially.

In the outboard vestibule, the model-predicted and experimentally determined temperature profiles were very similar to their counterparts in the inboard vestibule. Both the model and the experiment, however, show that the temperatures in the outboard vestibule are lower than those in the inboard vestibule throughout the experiment.

In the DC passageway, the model over-predicted the temperatures relative to the experimentally determined values. Some factors that may contribute to this only fair comparison have been addressed in later modifications to CFAST, e.g., horizontal and vertical heat transfer and "corridor" effects for long passageways. The improved corridor sub-model, which is

discussed later, is transient – it only affects the upper layer during the initial ceiling jet flow. After that, everything reverts to the old algorithm for handling smoke movement. Other factors that still need to be addressed are horizontal placement of mechanical ventilation openings and flame extension through horizontal vents.

1.1.5 Vertical Heat Transfer Algorithm (Heat Conduction Through Decks)

1.1.5.1 General

The vertical heat transfer algorithm was added to CFAST to correctly account for conductive heat transfer in the vertical direction through metal decks in naval platforms. The addition of this phenomenon in shipboard environments is necessary since rising temperatures in adjacent steel compartments as a result of fire can cause materials to reach ignition levels even though no breach has occurred in the initial fire compartment.

Comparisons were made using CFAST version 2.1 (with the vertical heat transfer turned on [2.1 +] and off [2.1]) and experimental data from real scale fire tests conducted onboard ex-USS SHADWELL in the Internal Ship Conflagration Control (ISCC) test area in the port wing wall (Figure A-2) (Bailey and Tatem,1995).

The compartments that comprised the ISCC test area (Figure A-2) were Berthing 2, Ricer 2, CIC and Pilot House. The experimental conditions were produced by a post-flashover fire in Berthing 2, created by diesel spray fires ignited by burning heptane pool fires. The measurements of interest in the validation process were the compartment temperatures as measured by thermocouples. Since CFAST is a zone model, it divides the compartments into two layers – an upper and a lower. Each layer is assumed to be of uniform temperature and composition. The same limitations described in this report under the Section "Natural and Forced Vent Flow Validation" for model and experimental temperatures apply to those parameters in this validation.

Model assumptions and experimental limitations must be specified for accurate interpretation of the comparisons. A limitation that existed in the experiment was accurate assessment of the vent openings. Inherent in the aftermath of burning are the formation of cracks in the structure that must be approximated as "vent openings". Also the mass loss rate of the fuel was approximated based on the use of both diesel spray and heptane pool sources.

The model assumes that each compartment is a rectangular parallelpiped. Since none of the compartments were rectangular parallelpipeds, their dimensions were adjusted to conserve actual compartment volume. Also the compartment walls varied in thickness within a given compartment. A weighted average based on actual surface area was used as input to the model for these compartments. The model uses the wall thickness to calculate conductive heat transfer through the walls.

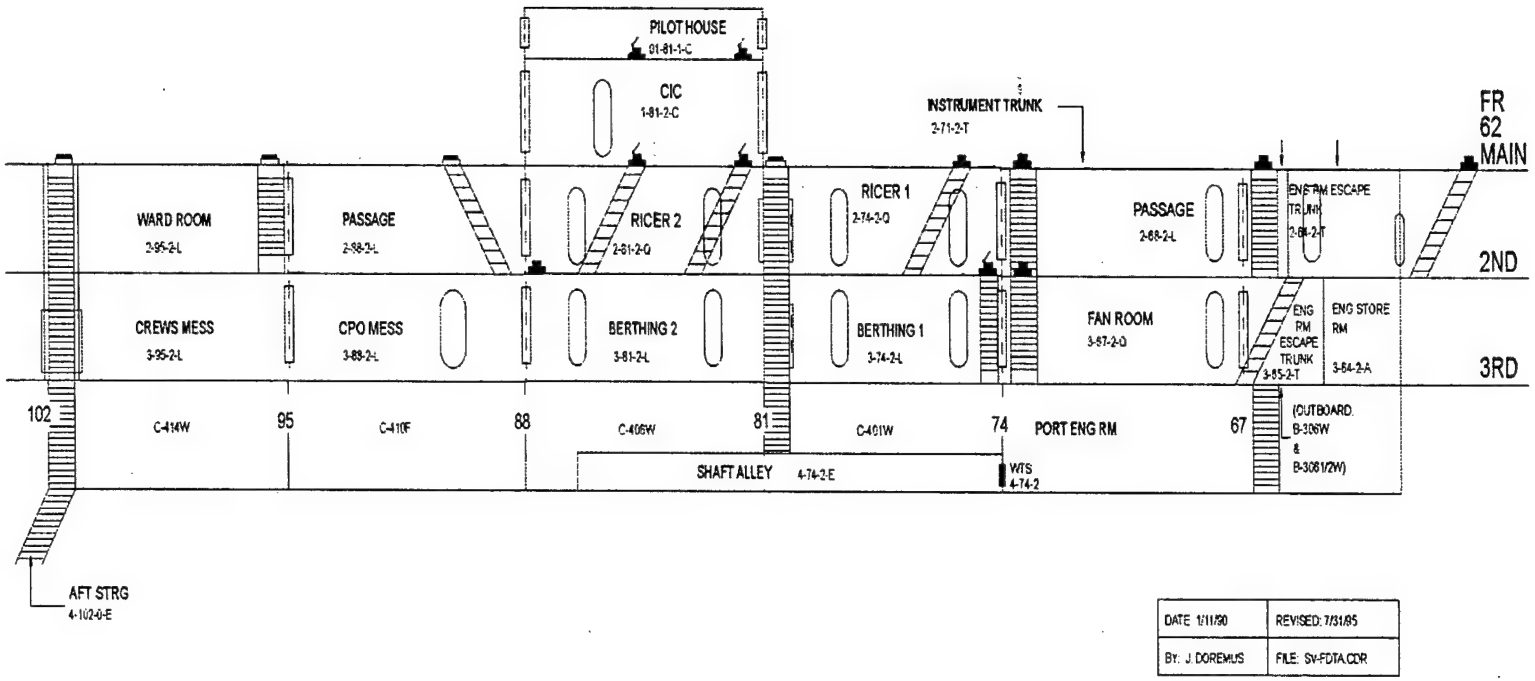

Fig. A-2 - ex-SHADWELL, section view, port wing wall ISCC test area

1.1.5.2 Results

Prior to incorporation of the algorithm into CFAST which properly accounts for vertical heat transfer by conduction, the model predicted that the temperatures in the compartments and decks above a fire compartment would not increase above ambient. After incorporating the algorithm, the model predicted much more realistic results. These predictions compared reasonably well with experimental results for the fire compartment (Berthing 2) as well as for the deck and compartment directly above it (Ricer 2). The model over-predicted the temperatures of the compartments and decks not directly adjacent to the fire compartment (CIC and Pilot House). For Berthing 2, both the model and experimental data results show that almost the entire compartment was in the upper layer during the experiments. The temperature predictions from version 2.1+ were higher than those from version 2.1. This is because in version 2.1 the model assumes the energy is conducted through the fire compartment overhead into the ambient environment which remains at a constant temperature. In version 2.1+, the heat is conducted into Ricer 2 which heats up as energy is accumulated in the compartment.

In Ricer 2, version 2.1 of CFAST predicts that the deck will remain at ambient (room) temperature throughout the experiment. Clearly, the predictions from the enhanced model (2.1+) are much more realistic. Version 2.1+ predictions for Ricer 2 air temperatures compared reasonably well at the beginning and the end with experimental data, but are different by about 50 degrees Celsius in the middle portion. However, since version 2.1 does not contain the vertical heat transfer algorithm the comparison between model and experiment was very poor throughout the entire time period.

The largest over-prediction by CFAST 2.1+ as compared to experimental data was in CIC deck. There was also an over-prediction in the air temperature of CIC but not of the same magnitude. This could be a result of the over-prediction in the Ricer 2 air temperature and also the representative experimental temperature data for the CIC deck (one, rather than several, thermocouple readings).

The deck and air temperatures in the Pilot House are over-predicted also, but is viewed as relatively insignificant since at these locations the increase above ambient is quite small for both the predictions and the experiments.

Additional validations were performed with the ISCC SHADWELL data and CFAST 3.1. In these comparisons, CFAST 3.1 consistently under predicted the temperatures (Bailey, et al., 1998). In the second validation, in order to model Ricer 2, the CIC and the Pilot House as one zone each, the SHAFT option was used (see Section 1.1.6).

1.1.6 Improved Radiation Transport Sub-Model

One of the assumptions originally made by CFAST was the use of constant (rather than time- variant) extinction coefficients in the upper and lower layers to calculate the

absorbance or radiation effect of the combustion gases. In order to address this deficiency, CFAST was modified to permit the absorbance of each layer to be calculated as a function of the time-variant concentration of carbon dioxide, water vapor and soot (Hoover et al., 1997; Hoover, 1995; Hoover and Bailey, 2000.).

With the new algorithm, the total absorbance is calculated analytically from the gas absorbance and various soot parameters and the gas absorbance is estimated by interpolation of values stored in lookup tables. This absorbance functionality was incorporated into CFAST version 2.2.1. Predictions from the modified CFAST, known in this document as CFAST 2.2.1+, were compared to those from CFAST 2.2.1 and, where possible, with data from experiments on ex-USS SHADWELL fire tests in the Integrated Ship Conflagration Control (ISCC) test area. This experimental description and configuration is given in this report under Section "Vertical Heat Transfer Algorithm (Heat Conduction Through Decks) (Hoover et al., 1996).

The compartments that comprised the ISCC test area were Berthing 2, Ricer 2, CIC and the Pilot House. Berthing 2 was handled as a "two-zone" space, comparing the experimental upper layer temperatures to CFAST 2.2.1 and CFAST 2.2.1+. There were no experimental temperature data for the lower layer, so only the predictions from the two CFAST model versions could be compared. There was very good agreement between the predicted upper layer air temperatures for the two CFAST model versions and the corresponding experimental values. The lower layer of Berthing 2 is the zone in which the largest differences among the various models are seen. The changes in the temperature predictions between the two models are consistent with expectations but, since there are no experimental data for this zone, there is no way to determine which of the models is better.

In general, errors in the predictions accumulate as one moves farther from the compartment of origin and it becomes much harder to make meaningful comparisons with experimental data. However, some useful conclusions can be drawn from the results obtained in this particular validation.

For the air temperature in Ricer 2, CFAST 2.2.1+ is more accurate than CFAST 2.2.1, while, in CIC, there is little difference between the two, as long as a reasonable value of the calculated total absorbance is used. In the case of the Pilot House, conditions are so close to ambient that there is little effect, regardless of which model or what value of the calculated total absorbance is used. Inconsistencies observed in the Berthing 2 upper layer air temperatures and the Ricer 2 deck temperature (common boundary) were possibly related to the mechanism for calculating horizontal heat transfer through the bulkheads. This phenomenon is accounted for in a higher version of CFAST.

The SHAFT option was used in this validation of the gas absorbance algorithm. When this option is invoked on a particular compartment, the model uses a single set of parameters (i.e., temperature and gas concentration) to represent the entire compartment volume, rather than two sets (one for each layer). This is appropriate whenever the compartment gases are well mixed and may therefore be represented by a single zone. With the SHAFT option in effect, the temperature at the top of a compartment is affected

by heat conducted from the compartment below; therefore, energy transfer from Ricer 2 to CIC and CIC to the Pilot House is handled correctly. With this in mind, users must be aware that the original, hard-coded extinction value used for the upper layer in CFAST 2.2.1 is inappropriate for compartments which accumulate little, if any, combustion products; for example, those compartments far from the fire. If the SHAFT option is used for one of these compartments, the upper layer extinction will be applied to the entire compartment and the results for the whole compartment will be in error. This problem will, of course, be moot if CFAST 2.2.1+ or higher is used because, in that case, the extinction will be calculated on the fly.

One final consideration: when CFAST 2.2.1+ or higher is used, it is vital that some reasonable value of the total gas absorbance be specified in the input file (i.e., non-zero). If no value is explicitly defined, a value of zero will be assumed and this results in the soot in the model being "turned off", which is rarely a reasonable thing to do.

1.1.7 Corridor Flow or Hybrid Smoke Movement (CFD Correlation) Sub-Model

The Corridor Flow or Hybrid Smoke Movement Sub-model, developed by NIST, was validated by NRL using an experiment from the SHADWELL/688 test series and CFAST versions 4.0.1 and 3.1.3 (Bailey, et al., 2002, Bailey and Tatem, 1998). Prior to addition of the new sub-model, CFAST did not properly account for the time it took a ceiling jet, entering at one end of a corridor, to travel down to the other end. Previously, CFAST assumed an isothermal upper layer would immediately cover the entire ceiling area along the entire length of the corridor. The new sub-model enables CFAST to predict the flow of the ceiling jet down the corridor with time. CFAST also calculates, at any given time, the temperature distribution of the gases inside the ceiling jet. Results presented here are predictions from the enhanced version of CFAST (4.0.1) that contains the new sub-model and to experimental data from the SHADWELL/688 test series.

A section of the port wing wall on ex-USS SHADWELL was configured to represent the forward compartment of an SSN 688 Class submarine (Figure A-3). The test area was comprised of 14 compartments, located on four levels. The compartments were connected with various hatches, watertight doors and a mechanical ventilation system. The experiments consisted essentially of igniting a pan fire in one of the compartments and then manipulating variables to observe the effect on the smoke flow within the test area.

There was only one compartment within the test area, the Laundry Room, which contained a corridor. Both exhaust and supply terminals were located near the ceiling in the corridor of this compartment. The Corridor Flow Sub-model does not take into account any effects of forced ventilation on the flow of the ceiling jet. Therefore, an experiment chosen for validation purposes did not employ the mechanical ventilation system.

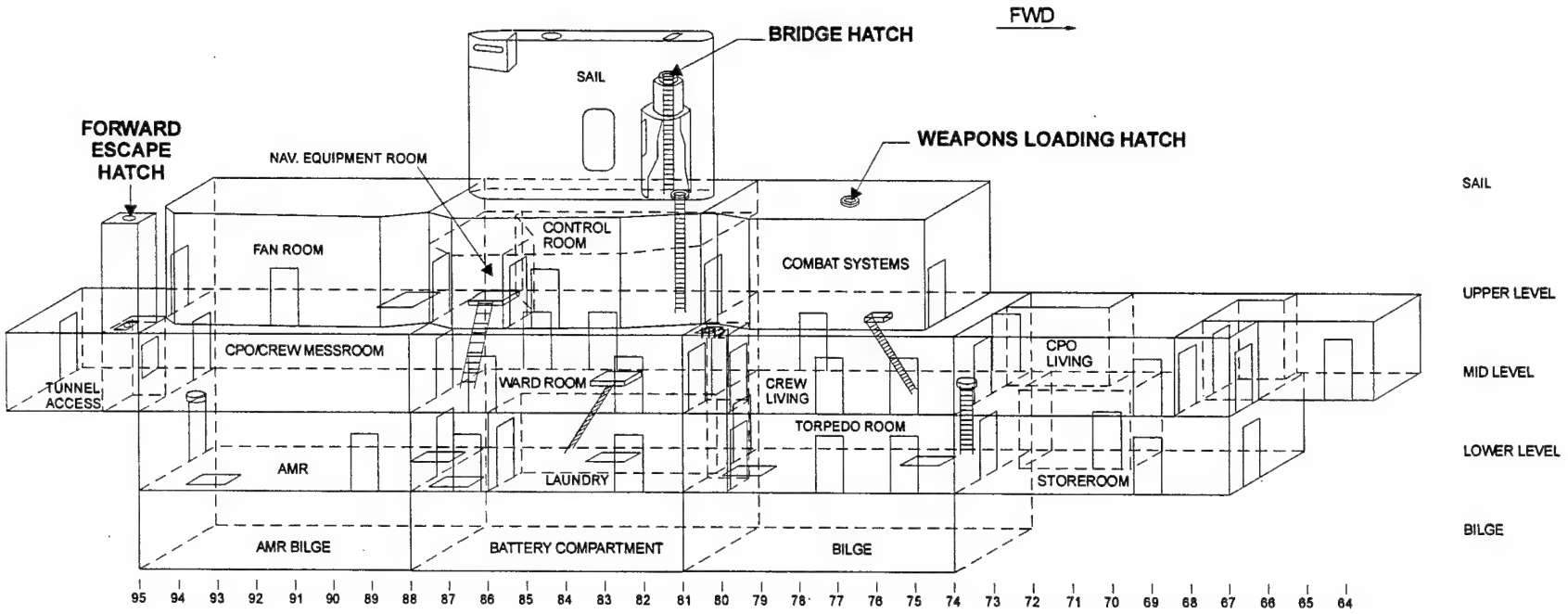

Fig. A-3 - Forward Compartment of an SSN 688 Class Submarine

The Laundry Room was actually subdivided into two sub-compartments. The sub-compartment which contained the fire is the Fire Compartment and the remaining sub-compartment is the Passageway. The Fire Compartment contained a fire pan filled with diesel fuel, facilitated in its ignition with a small amount of heptane. The temperature comparisons used for CFAST predictions were obtained from thermocouples located in the Fire Compartment and at two locations referred to as A and B, in the Passageway.

The assumptions that had to been made for these comparisons were similar to the previous validations reported: mass loss rate estimated based on temperature data from inside the Fire Compartment; translation of experimental temperatures, measured at distinct locations, to an overall zone temperature as predicted by CFAST; and conservation of compartment volume due to non-rectangular geometry in the test area.

The experiment to be modeled began with ignition of a diesel pan fire at time zero. Times were noted for (1) time of pan fire ignition, (2) time at which combustion products flowed into the Passageway through the Fire Compartment door, (3) time at which ceiling jet reached Location A, (4) time at which ceiling jet reached Location B, and (5) time at which ceiling jet reached the end of the Passageway. Experimental times for Events 1, 3, and 4 can be obtained from thermocouple readings and were 0, 27, and 32 s, respectively. CFAST 4.0.1, without the Corridor Flow Sub-model invoked, assumes that a thin hot gas layer forms along the length of the entire corridor ceiling the instant that the hot gases pass under the Fire Compartment door soffit, so there is no transient nature in the smoke movement along the long Passageway. The enhanced model (CFAST 4.0.1 with the Corridor Flow Sub-model invoked) predicted transient smoke movement so that Events 3 and 4 occurred at 29 and 40 s, respectively. Therefore, the enhanced model provides a more realistic prediction of the delay that occurs as the ceiling jet travels down the Passageway.

Experimental temperatures, as well as time, were correlated with the original and enhanced model predictions. There is remarkably good agreement between the temperatures of the experiment and the enhanced model at Location A, whereas the predicted temperature from the original model deviates significantly. At Location B, the enhanced model agrees better with the experiment than the original model, but the agreement is not as good as at Location A.

1.1.8 Horizontal Heat Transfer Algorithm (Heat Conduction Through Bulkheads)

The horizontal heat transfer algorithm was added to CFAST to correctly account for conductive heat transfer in the horizontal direction through metal bulkheads in naval platforms (Jones et al., 2002). The addition of this phenomenon in shipboard environments is necessary since rising temperatures in adjacent steel compartments as a result of fire can cause materials to reach ignition levels even though no breach has occurred in the initial fire compartment.

Heat transfer between horizontally connected compartments is modeled by merging the connected surfaces for the connected horizontal compartments. A heat conduction problem is solved for the merged walls using a temperature boundary condition for both the near and far wall. Temperatures are determined by the solver so that the heat flux striking the wall surface (both interior and exterior) is consistent with the temperature gradient at that surface.

For horizontal heat transfer between compartments, the connections can be between partial wall surfaces, expressed as a fraction of the wall surface. CFAST first estimates conduction fractions analogous to radiative configuration factors. For example, a conduction fraction between a rear wall in room 1 and a front wall in room 2 is the heat flux fraction from the room 2 wall that strikes and hence contributes to room 1's heat transfer.

CFAST version 4.0.1 (and, by default, Version 5.0 also) contains the horizontal heat conduction (wall/wall) phenomenon as well as the Hybrid Smoke Movement Sub-Model, as stated above. Although Version 4.0.1 was validated for the corridor flow algorithm, there was not sufficient experimental data in any of the ex-SHADWELL fire test series to provide surface temperature readings to be used for complete validation of the horizontal heat conduction algorithm in CFAST Version 4.0.1. A preliminary validation of the horizontal heat transfer algorithm was conducted using CFAST 4.0.1 and ISCC experiments (See Section "Vertical Heat Transfer Algorithm"). This Version of CFAST still requires more extensive experimental validation for this phenomenon.

APPENDIX B

A METHODOLOGY FOR PREDICTING FIRE AND SMOKE SPREAD FOLLOWING A WEAPON HIT

3905
Ser 6180/0014

From: Commanding Officer, Naval Research Laboratory
To: Commander, Naval Surface Warfare Center/Carderock Division (Code 66 Wolk)

Subj: A Methodology for Predicting Fire and Smoke Spread Following a Weapon Hit

Encl: (1) Two copies of subject report

1. Enclosure (1) is forwarded for your information and comment.

2. The purpose of this report is to generically document the fire and smoke spread methodology used for the CVNX Vulnerability Assessment Report (VAR) and to make recommendations for future methodology. Particular emphasis is placed on the definitions used for the PDA (Primary Damage Area) and the APDA (Adjacent to Primary Damage Area).

3. The definitions for the PDA and APDA have varied depending on the application. We recommend that the PDA for fire and smoke spread be designated as PDA(F) (Primary Damage Area (Fire)). Since fire and smoke spread and the availability of oxygen for combustion is controlled by vents, we recommend that the PDA(F) spaces include any adjoining spaces that have free communication including open doors and scuttles. These spaces are in addition to those that experience weapon induced structural alternatives such as bulkhead failure or holing in deck, overhead and bulkheads.

The APDA(F) would then by definition be all spaces (including above and below) that share a common deck, bulkhead or overhead with PDA(F) spaces. The definition for BAPDA(F) would be the compartments once removed from the APDA(F).

4. The Naval Research Laboratory's point of contact is Dr. Frederick W. Williams, Code 6180: (202) 767-2002/e-mail: fwilliam@ccs.nrl.navy.mil.

Copy to:
COMNAVSEASYSCOM (Code 05P6 Hunstad, Satterfield)

6180/0014A:FWW
March 17, 2003

A Methodology For Predicting Fire And Smoke Spread Following A Weapon Hit

GERARD G. BACK
ERIN C. MACK
MICHELLE J. PEATROSS
JOSEPH L. SCHEFFEY
DEREK A. WHITE

Hughes Associates, Inc.
Baltimore, MD

FREDERICK W. WILLIAMS
JOHN P. FARLEY

Navy Technology Center for Safety and Survivability
Chemistry Division

DAVID SATTERFIELD

Naval Sea Systems Command

Code 05P4

Encl (1) to NRL Ltr
3905
Ser 6180/0014

CONTENTS
APPENDIX B

TABLES

FIGURES

ACRONYMS AND NOMENCLATURE

APDA	Adjacent to Primary Damage Area
APDA(F)	Adjacent to Primary Damage Area for Fire & Smoke Spread
ASAP	Advanced Survivability Assessment Program
ASTM	American Society for Testing and Materials
BAPDA	Beyond Adjacent to Primary Damage Area
BAPDA(F)	Beyond Adjacent to Primary Damage Area for Fire & Smoke Spread
BDRA	Battle Damage Repair Assessment
CFAST	Consolidated Model of Fire Growth and Smoke Transport
CVNX	The next generation aircraft carrier
DC	Damage Control
DC-ARM	Damage Control Automation for Reduced Manning
FFE	Firefighting Ensemble
HEATING	Finite difference heat conduction model
HVAC	Heating, Ventilation and Air Conditioning
ISCC	Internal Ship Conflagration Control
LFT&E	Live Fire Testing and Evaluation
LPD 17	Amphibious transport dock
NIST	National Institute of Standard and Technology
NRL	Naval Research Laboratory
NSWC/CD	Naval Surface Warfare Center, Carderock Division
PDA	Primary Damage Area
PDA(F)	Primary Damage Area for Fire & Smoke Spread
SCBA	Self Contained Breathing Apparatus
SVM	Ship Vulnerability Model
TSS	Total Ship Survivability
VAR	Vulnerability Assessment Report
VC	Vital Component
V&V	Verification and Validation
VV&A	Verification, Validation and Accreditation
WR/WC/SH	Washrooms, Water Closets and Showers
WET	Weapons Effects Test

A METHODOLOGY FOR PREDICTING FIRE AND SMOKE SPREAD FOLLOWING A WEAPON HIT

1.0 INTRODUCTION

A methodology has been developed and refined to predict smoke and fire spread after a weapon hit. This methodology was developed to comply with the congressionally mandated Live Fire Testing and Evaluation (LFT&E) program. Under the LFT&E program for each ship platform, a vulnerability assessment is undertaken and a Vulnerability Assessment Report (VAR) is prepared. The VAR provides an evaluation of the survivability of the ship platform and ship mission against simulated weapon threats. The vulnerability assessment process includes the simulation of weapon damage, characterization of secondary damage (e.g., flooding, fire and smoke), and description of the battle damage repair activities and effectiveness. These activities are generally referred to as a Total Ship Survivability (TSS) and Battle Damage Repair Assessment (BDRA). The overall objective of the TSS/BDRA is to identify specific weaknesses and/or shortcomings as well as high payoff research and development efforts that might increase the survivability of the particular ship platform.

The current TSS/BDRA process involves consideration of various weapon hits. For each specific weapon threat scenario (shot line), the initial damage is identified by utilizing a blast damage model. Secondary damage, such as fire and smoke spread that results from the blast damage, must also be characterized. The methodology described in this document outlines the framework through which a conservative estimate of the secondary fire and smoke damage can be established. This document also uses a refined set of definitions for fire and smoke spread in damaged areas of the ship.

2.0 APPROACH

The current approach for the characterization of secondary damage associated with a weapon hit has evolved over several TSS/BDRA evaluations. The genesis of the current methodology was rudimentary fire spread times, developed by the Naval Research Laboratory (NRL) and Hughes Associates, Inc. based on USS *Stark* incident data and testing [1]. This information was implemented in a TSS model developed by the Naval Surface Warfare Center, Carderock Division (NSWC/CD). The fire spread methodology was improved and the framework was expanded to allow for smoke spread during the evaluation performed for the LPD 17 VAR 2 [2]. Most recently, the methodology was further refined during the CVNX assessment [3]. This report reflects the most current methodology used for the CVNX assessment. The framework incorporates a combination of computer fire modeling using the Consolidated Model of Fire Growth and Smoke Transport (CFAST) program and prescriptive rules for fire spread. CFAST is specifically used to characterize the environment in the primary damage area which includes vent connected spaces.

Estimates of the worst plausible fire spread scenario for each hit are used to determine the extent of damage control (DC) operations that are required to control and secure the fire. As part

of this conservative assessment framework, the effects of fixed fire suppression systems or manual firefighter activities normally associated with DC operations are **not considered** in the initial secondary damage assessment. In some instances, intact suppression systems may be evaluated on a case by case basis. Estimates of the rate of smoke production, extent of smoke migration and the temperature of the smoke layer are used to identify the potential exposures to shipboard equipment, personnel and DC parties.

Describing the methodology for predicting fire and smoke spread requires an understanding of the shipboard damage zones developed for these evaluations. The zones are categorized in three ways:

Primary Damage Area (PDA) compartments: PDA compartments are those that incur significant damage from the weapon hit (e.g., failed deck/bulkhead and shock holing). **It should be noted that compartments that are only vent connected to PDA compartments as a result of door/hatch failure have not been considered part of the PDA in certain contexts.** This definition differs from that used in Damage Control Automation for Reduced Manning (DC-ARM) testing [4-6] and Weapons Effect Test (WET) for the ex-*Caron* fire and smoke spread [7], where all compartments that are vent connected as a result of the blast damage are considered PDA compartments. From the standpoint of fire and smoke spread, including the vent connected spaces makes more sense. This is due to the fact that the vents provide a means for spreading fire and smoke directly as well as supplying additional oxygen for the fires. **Therefore, in the future we recommend designating the fire and smoke spread PDA (noted as PDA(F)) where vent connected spaces are included.**

Adjacent to Primary Damage Area (APDA) compartments: These compartments share a common boundary (bulkhead, overhead or deck) with a PDA compartment. Historically these compartments included spaces with a communicable opening (e.g., vent connection) between PDA compartments and the APDA compartment, such as a failed door or hatch. Our recommended definition for fire and smoke spread for adjacent compartments, APDA(F), excludes any compartments that have vent openings to the PDA. This is a result of those vented compartments becoming part of the PDA(F).

Beyond Adjacent to Primary Damage Area (BAPDA) compartments: These compartments border APDA spaces. They can be otherwise described as "twice removed" from the PDA. These spaces may be a concern due to potential fire spread later into the event. It is typically assumed that there are no communicable openings (i.e., vents, ducts, open doors or open hatches) between BAPDA and APDA spaces. This definition for BAPDA(F) remains the same for fire and smoke concerns as weapon effect concerns.

For illustrative purposes, Figure B-1 shows an example of the compartment categorization of spaces for a hypothetical weapon hit using the PDA, APDA and BAPDA definitions (as compared to PDA(F), APDA(F) and BAPDA(F)). As indicated in the legend, PDA compartments are marked in red, APDA compartments are marked in yellow and BAPDA compartments are marked in blue. The PDA consists of those compartments that are structurally affected by the blast overpressure. The APDA compartments on the Third Deck and First Platform are horizontally adjacent to the PDA on those decks. In addition, there are APDA

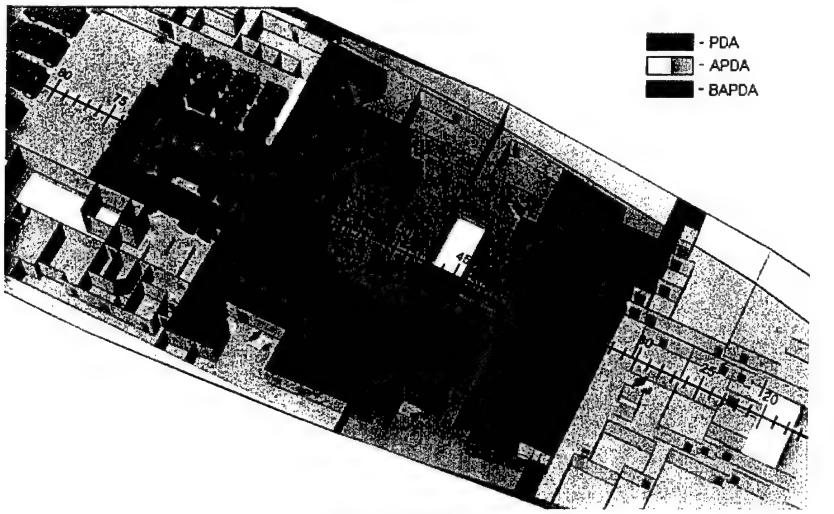

Second Deck

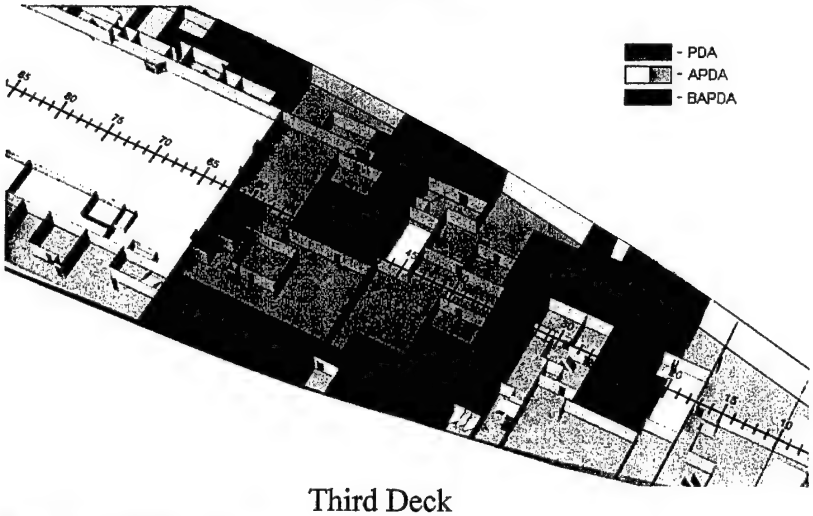

Third Deck

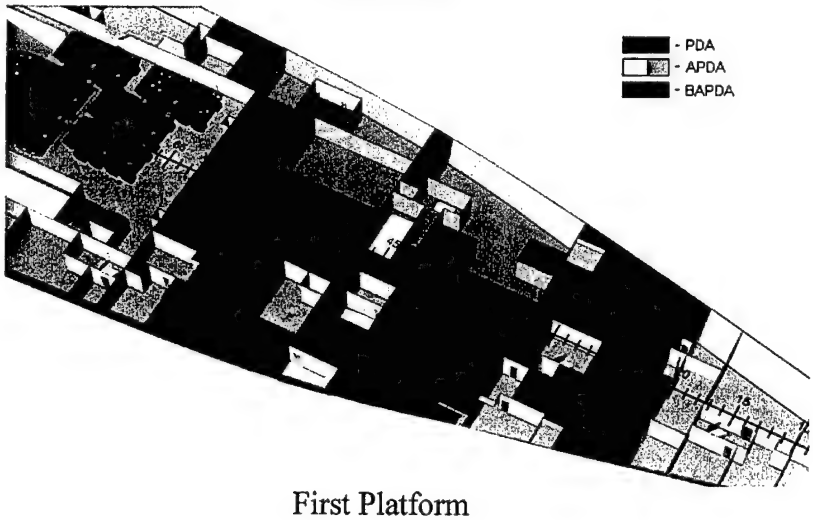

First Platform

Fig. B-1 - Example of compartment damage characterization after hypothetical weapon hit using PDA, APDA and BAPDA compartment designations

compartments on the Second Deck directly over the PDA compartments on the Third Deck. The BAPDA compartments are either horizontally adjacent to or above or below APDA compartments.

Figure B-2 shows how changing the definition of the PDA, APDA and BAPDA to PDA(F), APDA(F) and BAPDA(F) would affect the definition of spaces. Irrespective of the terminology, vent connected spaces have always been included (and will continue to be included) in the fire model used to assess the spread of smoke and fire associated with the fires that start immediately following the weapon detonation. As a result, the definitions used for PDA and APDA spaces will not impact the results that are obtained from the analysis. **From this point forward, the recommended definitions for PDA(F), APDA(F) and BAPDA(F) are used in this methodology report.**

3.0 METHODOLOGY

The methodology for predicting fire and smoke spread follows the steps listed below. Each process is described in further detail in the following sections.

1. Establish the primary damage;
2. Review the primary damage information;
3. Characterize the secondary damage (fire and smoke spread) in the PDA(F);
4. Characterize the secondary damage to PDA(F) spaces;
5. Characterize the secondary damage to APDA(F) and BAPDA(F) compartments; and
6. Document the time dependent secondary damage estimates in snapshot format.

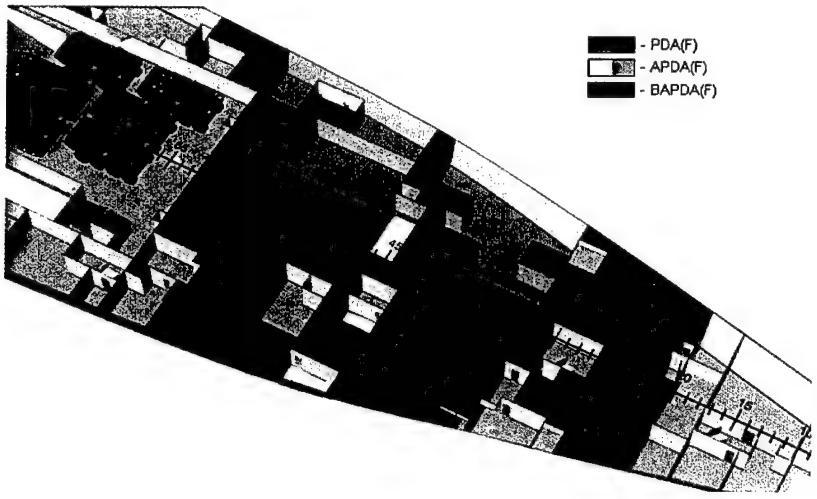

Second Deck

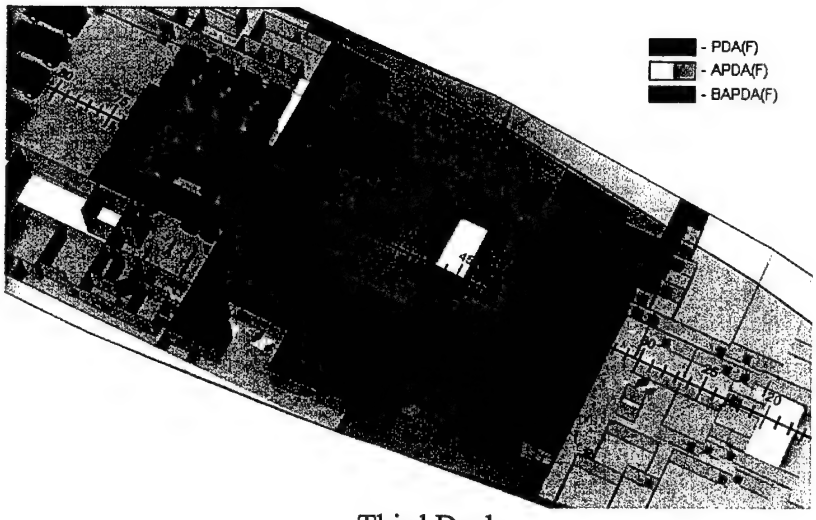

Third Deck

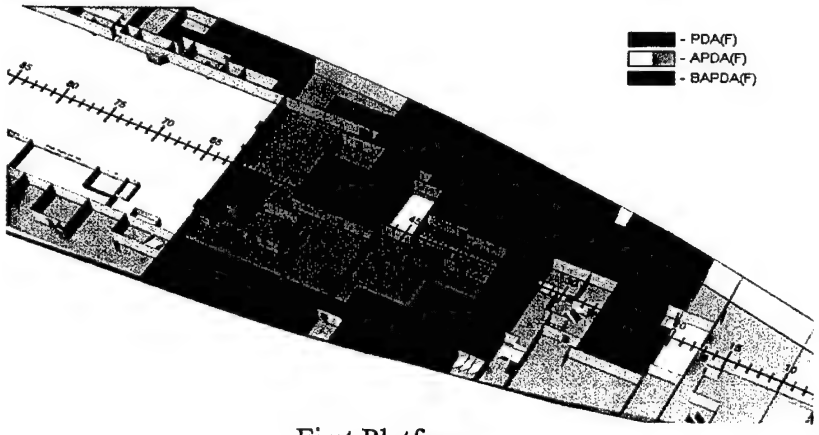

First Platform

Fig. B-2 - Example of compartment damage characterization after hypothetical weapon hit using PDA(F), APDA(F) and BAPDA(F) compartment designations

3.1 Establishment of the PDA(F)

The primary damage from the weapon hit is established based on output from either the Ship Survivability Model (SVM) or the Advanced Survivability Assessment Program (ASAP) model [8, 9]. Both models are designed to simulate initial ship damage from a weapons attack. The output from either model provides information such as the locations of failed bulkheads and decks, shock holing, failed doors and hatches, overpressures, bulkhead and deck deflection, fragment damage to vital components (VCs) and damage to distributive systems. Equipment specific damage as a result of thermal or smoke exposures during the detonation and burning of the residual fuel from the weapon is not specifically included in this methodology.

The output from the ASAP or SVM model is used to establish the location of PDA(F), APDA(F) and BAPDA(F) compartments. Since the blast damage models do not provide the output in terms of PDA, APDA and BAPDA or PDA(F), PADA(F) and BAPDA(F), the characterization of space type is done as part of the fire and smoke damage assessment. Based on the model output provided, PDA(F) compartments consist of those compartments where bulkheads or decks have failed, or where shock holing has occurred. In addition, PDA(F) spaces include those compartments that are vent-connected. Vent connections may consist of failed doors or hatches, or openings created by shock holing. The structural damage incurred from a weapon detonation is translated into ventilation opening sizes based on advice from NSWC/CD Code 665. For shock holing, it is assumed that the area can be treated as a single opening with an area equivalent to 100% of the shock holing value.

In addition, it is assumed that the fire insulation attached to boundaries that experience less than a specific amount of deflection (as reported in Reference 2) remains intact and performs to specifications. For deflections greater than this value, the boundary is modeled as a bare steel bulkhead or deck.

3.2 Review of Primary Damage Information

The assumptions for each assessment consist of general assumptions that apply for each analysis and those that are specific to the hit (shot line). General assumptions include the following:

1. The ship is at general quarters prior to each hit (e.g., material condition ZEBRA is set throughout the ship). This assumption implies that all ZEBRA doors, hatches and fittings are closed.
2. Unless otherwise stated, heating, ventilation and air conditioning systems (HVAC) are not considered. Engineering judgment can be used in specific instances to account for the effects associated with failure of ventilation ducts. In some cases, such as with smoke ejection systems, these HVAC systems may help mitigate smoke spread or accumulation;
3. For compartments that contain combustible materials, the fuel load is considered as sufficient to support post flashover fires during the evaluation;

4. Thermally thin combustible materials (i.e., readily ignitable) are located such that fire spread may occur across an intact boundary. These materials may normally be in this arrangement or may be redistributed against bulkheads and decks as a result of the shock impact or over pressure;
5. Transient opening and closing of doors and hatches between compartments is not considered (from people exiting the area or investigators performing an assessment);
6. The weapon hit precipitates ignition in all PDA(F) spaces that are intimate with compartment containing the point of detonation and that have a combustible fuel load (due to unspent propellant or hot fragments); a fire growth rate curve is followed for the specific fuel load. The oxygen concentration in the space could have considerable affect on the fire growth curve;
7. Toxicity issues related to unspent missile propellant are not considered;
8. Generally, firefighting activities and fire mitigation effects are not considered;
9. For compartments that are not included in the fire model (APDA(F) and BAPDA(F) spaces), smoke production or accumulation is not characterized. Rather, it is assumed that these spaces become untenable for unprotected personnel once fire spreads to them; and
10. The fuel load and air supply in APDA(F) and BAPDA(F) compartments are not considered. Rather, it is assumed that there is a sufficient quantity of fuel and air to support flashover conditions. In reality, these compartments would not necessarily become fully involved, particularly if they are closed (e.g., limited ventilation).

An example of a shot specific assumption is one where a ventilation system remains operational after the weapon hit. For example, this situation could occur if a well deck and/or vital spaces are part of the PDA(F). Including the effects of forced ventilation systems could result in an increase in fire intensity, particularly for cases where the fire would be oxygen starved otherwise.

3.3 Characterization of Secondary Damage in the PDA(F)

3.3.1 Development of the Fire Model

A fire model is used to characterize the environment in PDA(F) spaces for each hit scenario. APDA(F) and BAPDA(F) spaces are not included in the fire model. Currently, the multi-compartment zone fire model used for this analysis is CFAST version 3.1.7 [10,11].

In developing the input for CFAST, the ventilation conditions must be defined. These conditions include those provided by natural and forced ventilation. Natural ventilation may be provided by holes in the skin of the ship (resulting from the weapon hit) and openings between PDA(F) compartments. At a minimum, oxygen for combustion is provided naturally through any openings to weather that result from the weapon hit. Forced ventilation may be provided in vital spaces where ventilation is not secured under material condition ZEBRA.

Another consideration for the model input is the fuel load in each space. The types of fuel consist of unspent missile propellant, Class A material and Class B fuel. Examples of Class A material include paper products found in storerooms and offices, electrical cable insulation, pipe insulation and bedding in berthing spaces. Class B fuels may be introduced by JP-5 (or equivalent) fuel storage tanks that are breached or damage to fuel lines. The following assumptions are used for characterizing the fires in these spaces:

- The fuel load is evenly distributed through the compartment;
- Trunks, voids and enclosed ladders do not participate in fire spread;
- In general, passageways do not have concentrated fuel loads except possibly cabling and pipe insulation. For passageways that serve as companionways or ladderways, there is no appreciable fuel load and fire cannot spread to or from the space. For long passageways (either athwartship or fore-to-aft), cabling and pipe insulation is installed in the overhead. Fire cannot spread from below to these spaces but can spread from adjacent compartments. In addition, once a fire is established in the overhead of these passageways, fire can spread to adjacent compartments or the compartment(s) above; and
- It is assumed that the doors to washrooms, water closets and showers (WR/WC/SH) that serve living areas are open when a fire begins. These areas will become involved in the fire simultaneously with the contiguous space; however, any resulting fire is likely to be very limited given the low fuel loads in washroom spaces. Since WR/WC/SH areas typically do not have a substantial fuel load associated with them, it is assumed that they do not propagate fire spread.

For the initial CFAST run, only the fuel load in PDA(F) compartments is considered. It is assumed that fires ignite in all PDA(F) compartments that are intimate with the compartment containing the burst point and have available fuel at the time of the weapon detonation . This is a very aggressive assumption. Since specific details about the fuel loading are not usually available, fire growth rates associated with the type of materials expected in the spaces are used for these typical materials. More specifically, it is assumed that the fires follow "t squared" fire growth curves. This type of fire growth curve is represented by Equation 1:

$$\dot{Q} = \alpha t^2 \qquad (1)$$

where $\dot{Q}$ is the heat release rate of the fire (kW), α is the fire growth constant typically associated with the type of materials in the space (kW/s^2) and t is the length of time the fire has burned (s).

A medium fire growth rate ($\alpha = 0.0117\ kW/s^2$) is used to represent Class A materials. This value was adopted after analysis of potential fire threats [12] and was validated during a weapons effects test (WET) conducted on the ex-USS *Dale* (CG-19) [13]. An ultra-fast fire growth rate ($\alpha = 0.1876\ kW/s^2$) is used to represent Class B pool fires involving JP-5 or equivalent diesel fuel [14].

3.3.2 Interpretation of Fire Modeling Results

The results from the fire modeling are used to predict the temperatures, interface heights (demarcation between smoke and relatively smoke free zones) and smoke levels in PDA(F) compartments. The temperature data are used to determine when or if fire will spread to these spaces. The interface height and smoke density data, in addition to the temperature data, are used to determine how tenable these compartments would be for protected and unprotected personnel. The criteria used for tenability are described in Section 3.4. This information is the most basic output provided by the fire model. It has been validated and verified extensively [15-19].

3.4 Fire and Smoke Spread within the PDA(F)

Fire may spread to compartments within the PDA(F) via either hot gases passing through an open vent or heating of an intact boundary (bulkhead or deck). In this situation, fires resulting from the weapon detonation in the immediate vicinity of the burst point would spread to other compartments within the PDA(F). Both modes of fire spread are examined when evaluating fire spread to these PDA(F) compartments to determine which mode results in a faster (more conservative) fire spread time.

3.4.1 Fire Spread Through Vents

Fire spread through vents that connect compartments within the PDA(F) may result from several different scenarios. The highest probability of spreading fire occurs when a PDA(F) compartment reaches flashover. In this situation, hot gases that are in excess of 500 C (932°F) will flow into the adjacent space resulting in a radiant heat flux exposure of at least 20 kW/m^2. These fluxes exceed the critical radiant heat flux for piloted ignition of wood and select plastic materials [20]. The configuration or orientation of the fuel in vent connected spaces will not affect how readily it is ignited.

Another ignition scenario occurs when the fire is located in close proximity to the door, hatch or vent opening. The radiation from the flame can pass through the opening and ignite combustible materials in the adjacent space. In order to achieve ignition, the exposure must exceed the critical ignition heat flux associated with the combustible material. Critical ignition heat fluxes can be as low as 10-15 kW/m^2 [21]. This ignition mechanism is difficult to apply in a typical TSS/BDRA since it is dependent on the relative location and geometry of both the fire and the target fuel source.

The final scenario results from convective heating produced by hot gases (below 500°C (932 F)) flowing into the adjacent compartment. These hot gases can potentially heat combustibles in the vent connected PDF(F) compartments to their auto-ignition temperature. The presence of glowing embers or firebrands may cause ignition more quickly. The auto-ignition temperature of materials can be measured through the use of the Setchkin Furnace [22].

The standardized procedure for measuring these temperatures, ASTM D 1929 [23], has been used for a wide range of materials. Review of published test data show that paper will ignite at approximately 230°C (446°F) and various polymers will ignite between 330-450°C (626-842°F) [24, 25].

Based on the review of these potential ignition scenarios, it is conservatively assumed that ignition via hot gases will occur in a PDA(F) compartment when the accumulated fire gas temperatures reach 230°C (446 °F) in that adjacent space.

3.4.2 Fire Spread through Intact Boundaries

Fire spread within the PDA(F) may also occur via heat transfer through the thermally thin steel bulkheads [24, 26-28]. This scenario occurs globally during post flashover fires. It could also occur locally with smaller fires if the burning material is in close proximity to the boundary. This would be considered fire spread across an unbreached boundary.

When flames impinge directly on a steel boundary, the temperature of the boundary will increase until it begins to glow red at approximately 350°C (572°F). Depending on the heat source, the temperatures could reach values as high as 650°C (1202°F). The boundary serves as a fairly efficient radiant heat source that will increase the temperature of nearby objects significantly [20]. The amount of energy that is transferred through a bare steel boundary resulting from direct flame impingement can approach 50 kW/m^2 [20]. This energy consists of both convective (~50%) and radiative (~50%) components. As shown in Figure B-3, the worst case heat flux exposures decrease from 25 kW/m^2 at the boundary surface to approximately 1.0 kW/m^2 at a distance of ten meters away from the boundary. As points of reference, spontaneous ignition of combustible materials typically occurs around 20 kW/m^2, piloted ignition of combustibles occurs around 10 kW/m^2 and bare skin begins to blister for short exposures (less than one minute) around 5 kW/m^2 [21, 29, 30]. Under worst case conditions, spontaneous ignition can occur as far away as 0.8 m (2.5 ft) away from the boundary.

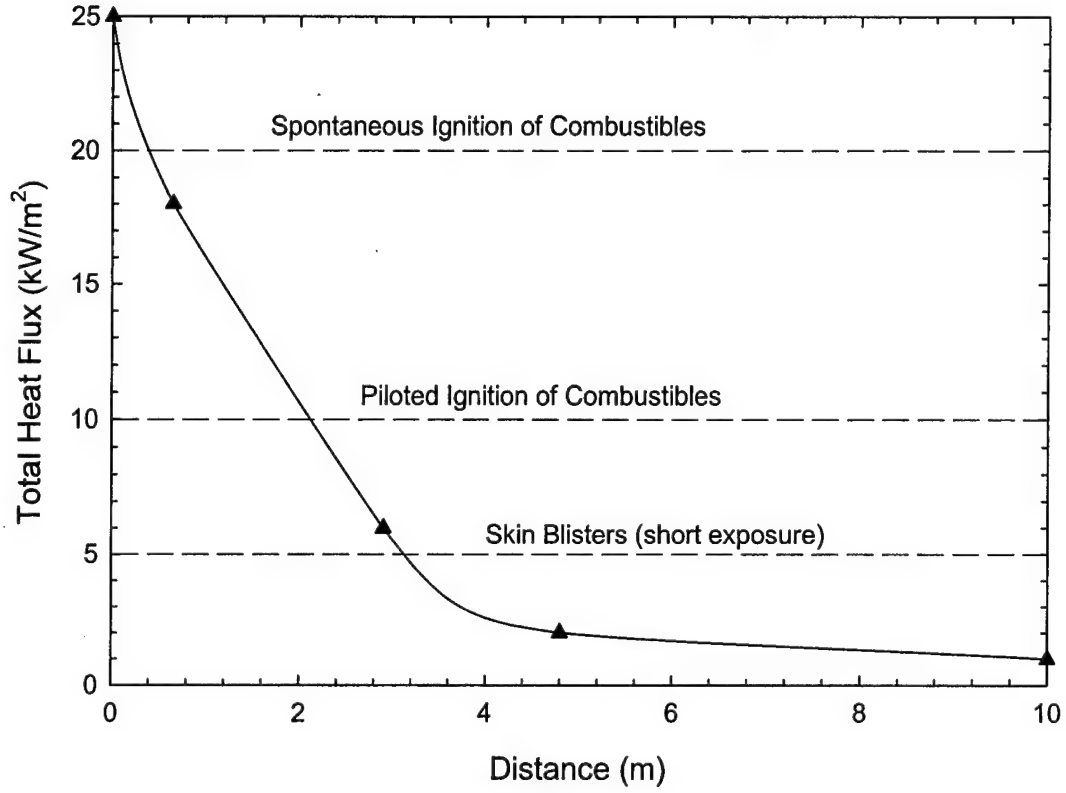

Fig. B-3 - Worst case heat flux exposures as a function of distance from a bulkhead or deck

For aluminum the heat transfer would be difficult and failure of the bulkhead could be expected under extreme conditions. The melting point of pure aluminum is 660°C while aluminum alloys can melt around 500°C [31]. Also aluminum loses one half of its structural strength at 330°C. There is a significant difference for composites. As composites are insulators, the heat transfer would be significantly delayed. It should be kept in mind that most composites in general use today could become fuels with time/temperature insult. This would eventually result in a breached boundary.

Ignition can also occur when combustible materials are in contact with the hot boundary and the temperature exceeds the auto-ignition temperature of the material (230°C (446 °F)). Although both mechanisms (contact or radiant heating) are realistic scenarios, fire spread will occur the most quickly with contact heating. However, this type of scenario is difficult to model without knowledge of the fuel load distribution. Even in cases where the normal distribution is known, it is likely that items will be relocated as a result of the impact from the weapon hit. As a result, it was assumed that smaller, pre-flashover fires could cause ignition of ordinary combustibles due to thermal penetration of steel boundaries on the same time scale as post flashover fires.

In order to determine the amount of time, t_{spread}, that is required to spread fire across a boundary (e.g., heat it to 230°C (446°F)), Equation 2 is used:

$$t_{spread} = t_{growth} + t_{penetration} \qquad (2)$$

where t_{growth} is the time for the fire to reach flashover in the initiating compartment and $t_{penetration}$ is the time required to transfer heat through the boundary. All times are measured in minutes.

This equation applies to both vertical and horizontal spread independent of the fire source (post flashover or localized heating).

The fire growth time (t_{growth}) is a function of the fuel loading and configuration in the compartment, the oxygen available for combustion (ventilation) and the size of the compartment. Since the fuel loading and configuration is unknown at the time of the hit, it is assumed that there is adequate fuel to sustain a fully developed fire for the duration of this simulation.

The fire growth times were determined by modeling a range of compartment sizes using CFAST. The compartment footprints (A_f) ranged from 9.3 to 464.5 m^2 (100 to 5000 ft^2). The compartment height was taken as 3.0 m (10 ft), a typical deck-to-deck height. It was assumed that the fire is unconstrained (i.e., ample oxygen to support combustion) in a closed compartment. In addition, a Class A fire growth curve was used ($\alpha = 0.0117$ kW/sec^2). The Class A growth curve was selected since most shipboard spaces will contain Class A fuels as opposed to Class B fuels. The growth time was defined as the number of minutes required for the upper layer temperature to reach 500°C (932°F).

The fire growth times that were conservatively developed based on the fire modeling results are summarized in Table B-1. It should be noted that the growth time for vertical spread from any compartment and horizontal spread from any PDA(F) compartment is 5 minutes, regardless of the compartment size. Since fires can quickly expose the overhead to high heat fluxes, vertical fire spread to taller spaces (multi-deck) may be handled on a case-by-case basis (i.e., hit specific assumption).

Table B-1 - Fire Growth Times (T_{growth}) For A Range Of Compartment Footprints

Spread Direction	Compartment Footprint (A_f) [m^2 (ft^2)]	T_{growth} (minutes)
Vertical	any compartment	5
Horizontal	any PDA(F) compartment	5
Horizontal	0 (0) < A_f < 93 (1000)	5
Horizontal	93 (1000) ≤ A_f < 139 (1500)	7
Horizontal	139 (1500) ≤ A_f < 186 (2000)	9
Horizontal	186 (2000) ≤ A_f < 232 (2500)	11
Horizontal	232 (2500) ≤ A_f < 279 (3000)	13
Horizontal	279 (3000) ≤ A_f < 325 (3500)	15
Horizontal	325 (3500) ≤ A_f < 372 (4000)	17
Horizontal	372 (4000) ≤ A_f < 418 (4500)	19
Horizontal	418 (4500) ≤ A_f < 465 (5000)	21
Horizontal	A_f ≥ 465 (5000)	23

The thermal penetration time ($t_{penetration}$) was determined using the finite difference heat conduction model – HEATING (Version 7.3 [32]). Steel plate thicknesses between 12.7 mm (0.5 in.) and 101.6 mm (4.0 in.) were modeled. The results in Table 2 are based on the following conservative boundary conditions applied to the exposed steel surface: the surface temperature was set at 1000°C (1832°F), an emissivity of 0.7 was used and a convective heat transfer coefficient of 10 W/m^2K was imposed. Based on numerous tests on *Shadwell* , a steel temperature of 600°C is rare as is a flame temperature above 800°C in ship compartments. The penetration time was defined as the number of minutes required to heat the unexposed surface to 230°C (446°F) by direct flame impingement on the opposite side. The Verification and Validation (V&V) of HEATING has been accomplished previously and is being summarized as part of the V&V process of another ship platform VAR. Results from this analysis are summarized in Table B-2.

Table B-2 - Penetration times ($t_{penetration}$) for various plate thicknesses

Plate Thickness (P_t) [mm (in.)]	$t_{penetration}$ (minutes)
P_t < 12.6 (0.49)	1
12.7 (0.5) ≤ P_t < 19.0 (0.74)	2
19.1 (0.75) ≤ P_t < 25.3 (0.99)	3
25.4 (1.0) ≤ P_t < 31.7 (1.24)	4
31.8 (1.25) ≤ P_t < 50.7 (1.99)	5
50.8 (2.0) ≤ P_t < 76.1 (2.99)	7
76.2 (3.0) ≤ P_t < 101.5 (3.99)	11
P_t = 101.6 (4.0)	15

It should be recognized that the times shown in Table 2 are conservative/generic guidelines. They do not account for the effects of insulation or bulkhead/deck treatments which could significantly impede thermal penetration or prevent it altogether.

In summary, the amount of time required to spread fire through an intact boundary is determined by identifying the fire growth time and the thermal penetration time. The fire growth time is a function of the type of compartment (PDA(F) as compared to APDA(F) or BAPDA(F)) and/or compartment size (Table 1). The thermal penetration time is a function of the bulkhead or deck thickness (Table 2).

3.4.3 Assessment of Tenability

The tenability guidelines are divided into two categories: those for unprotected personnel and those for protected personnel (DC parties). It is assumed that protected personnel are outfitted with self-contained breathing apparatus (SCBAs) and firefighting ensembles (FFEs).

For unprotected personnel, conditions are considered untenable when the smoke is too hot to breathe or the visibility is too poor for evacuation activities. Untenable conditions are assumed to occur when a smoke layer is below 1.5 m (4.9 ft), combined with one or both of the following conditions [33]:

- Upper layer temperature > 100°C (212 °F) and/or
- Visibility < 4 m (13 ft) for transported troops and < 1.7 m (5.6 ft) for unprotected ship personnel.

The smoke layer height of 1.5 m (5.0 ft) is significant because it is below the normal head height. This condition would result in the potential exposure of standing personnel to hot gases or reduced visibility. The temperature criteria was chosen based on the fact that personnel exposed to gases above 100°C (212°F) will experience pain and potential damage to their respiratory tract [34-36]. Burning of the respiratory tract can result in severe injury or incapacitation for any person forced to breathe these gases. The failure criteria of 100°C is conservative as compared to the human tolerance temperatures in the NSTM 555, which indicate incapacitation after an exposure for 5 minutes to gases of 149°C (300°F) and incapacitation after an exposure for 35 minutes to gases of 93°C (199°F) [21].

Visibility throughout the primary and secondary damage compartments is important from a life safety/egress standpoint. Successful egress is contingent upon personnel being able to locate the ladders, hatches and the appropriate egress paths. Visibility degradation relates to the ability of occupants to egress through areas that may be smoke logged. It is possible for personnel to become disoriented in the event the visibility becomes significantly reduced. The minimum visibility for egress activities is dependent upon the occupant. Since some ships may transport troops that are not familiar with the ship's layout, more visibility would be required for egress activities than for ship personnel. This difference is accounted for by assuming a visibility criterion for ship personnel that corresponds to the more generous limit identified in the literature of 1.7 m (5.6 ft) [33]. This value corresponds to data that indicate it is the point where egressing

occupants will decrease their walking speed significantly [37]. A more stringent criterion of 4.0 m (13 ft) visibility is used for troops that are being transported [33, 38, 39].

Failure criteria for protected personnel were established based on the conditions that would not permit necessary firefighting operations to proceed. A smoke temperature of 200°C (326°F) was conservatively chosen. Certainly, firefighters in FFEs could tolerate higher exposure temperatures for short durations. Tests have shown that a firefighter in an FFE may be forced to abandon a space after 5 minutes when the temperatures are approximately 260°C (500 F) at head level. This translates to a temperature gradient in the compartment of 163°C (325°F) at waist level and 63°C (145°F) at knee level. Well-trained Navy fire fighters that have been through the ex-USS *Shadwell* experience can withstand hot gas layers above these and at higher temperatures [40]. For the purpose of evaluating the fire modeling results, it was assumed that a layer interface height of 0.6 m (2.0 ft) and an upper layer temperature of 200°C (392°F) constitute untenable conditions for protected personnel.

3.5 Characterization of Secondary Damage to APDA(F) and BAPDA(F) Spaces

Fire spread from APDA(F) spaces and BAPDA(F) spaces occurs via heat transfer through intact bulkheads and decks. This mode of fire spread is the most predominant since these spaces normally do not have vent connections to the spaces with fires. As a result, the methodology described in 3.4.2 is used to characterize secondary damage to these spaces. The tenability of these spaces is not assessed. Rather, it is assumed that they are untenable for unprotected personnel as soon as fire spreads to them. The analysis continues until the fire spread times are larger than the length of time that is specified for the analysis. For example, if secondary damage is only a concern for 30 minutes after the weapon hit, fire spread times longer than 30 minutes are not considered.

In many situations, the use of these prescriptive rules is conservative since it is assumed that there is an unlimited amount of fuel and air available in each compartment. In the event that there is a small amount of fuel in the compartment or the compartment is closed, fire spread may be delayed or may not occur at all.

3.6 Documentation of Secondary Damage Estimates

The secondary damage for a particular weapon hit is reported in a snapshot format. These snapshots show which spaces contain fires at particular points in time. In addition, the tenability for PDA(F) spaces is shown. Fire suppression effects are shown in situations where suppression systems are considered. Figures B-4 thru B-6b show examples of these snapshots 5, 10 and 15 minutes, respectively, after the hypothetical weapon hit represented in Figures B-1 and B-2. Compartments containing fire are marked in red. Compartments that are not tenable for unprotected personnel are designated with blue. Those compartments that are untenable for all personnel (unprotected and protected) are shown in yellow. It should be noted that the rules-based fire spread framework was used for the development of these examples. These results would be contingent on the incorporation of CFAST results.

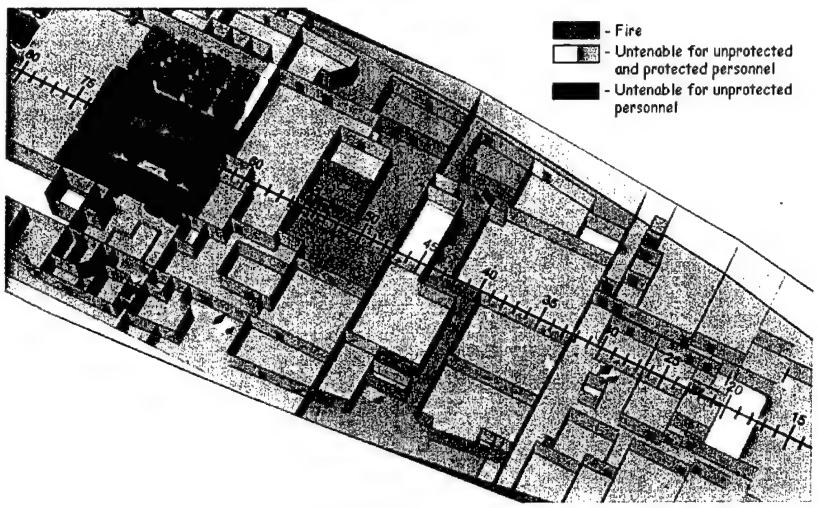

Second Deck

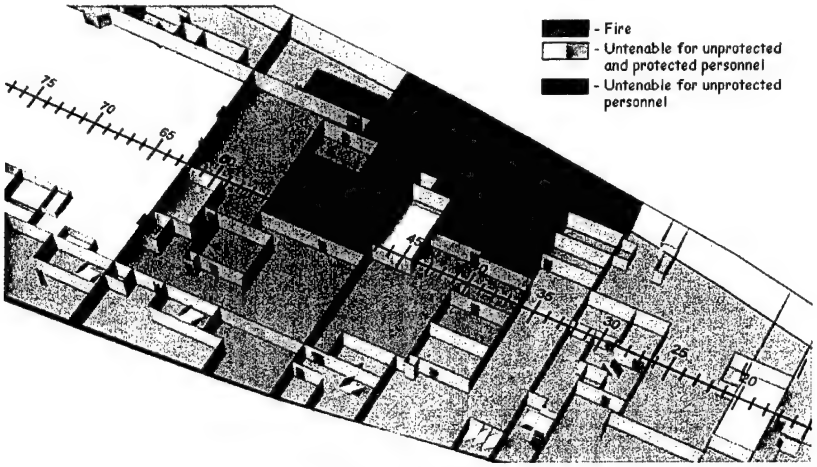

Third Deck

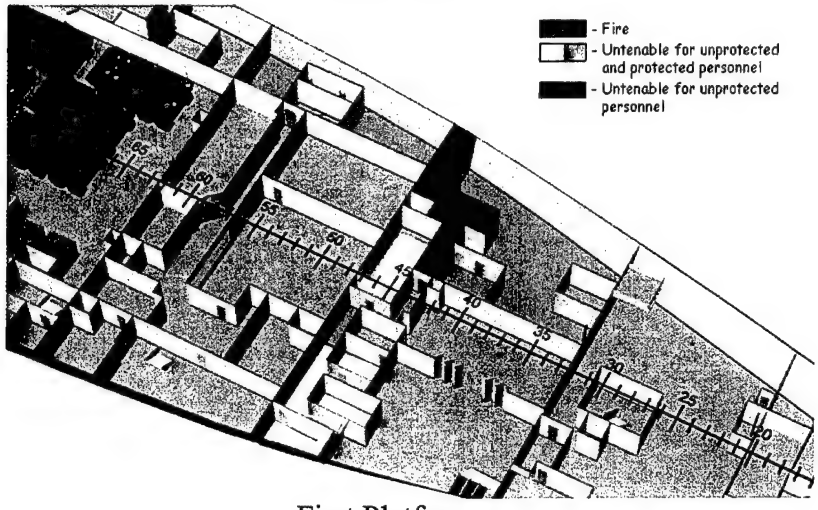

First Platform

Fig. B-4 - Example of secondary damage 5 minutes after hypothetical weapon hit

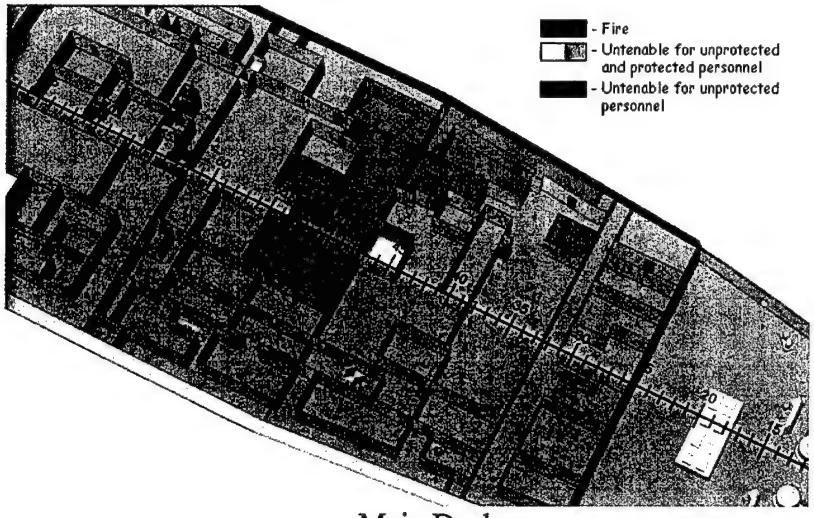

Main Deck

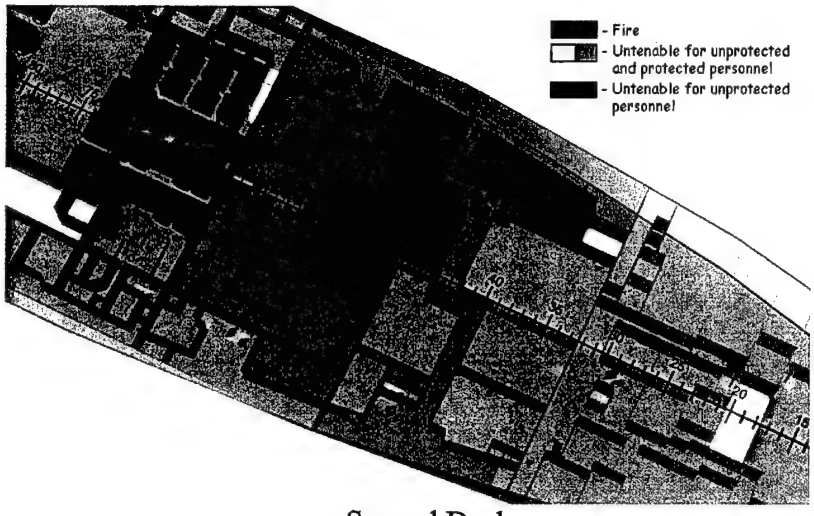

Second Deck

Fig. B-5a - Example of secondary damage 10 minutes after hypothetical weapon hit

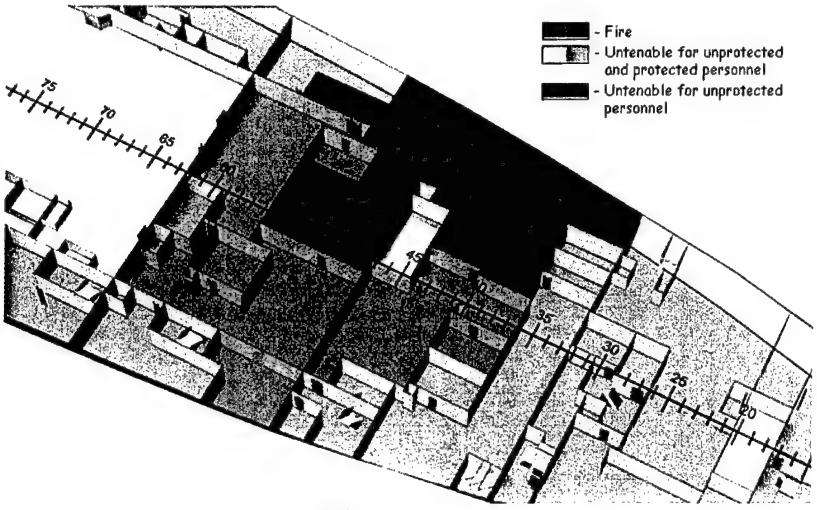

Third Deck

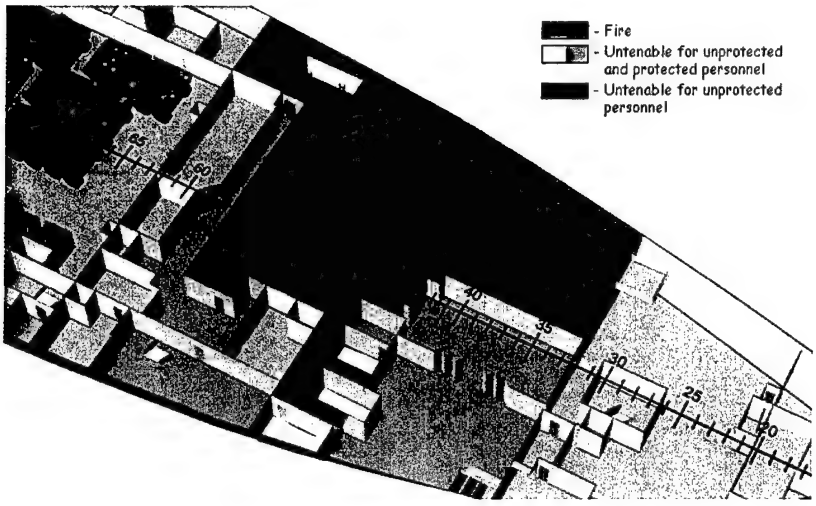

First Platform

Fig. B-5b - Example of secondary damage 10 minutes after hypothetical weapon hit (continued)

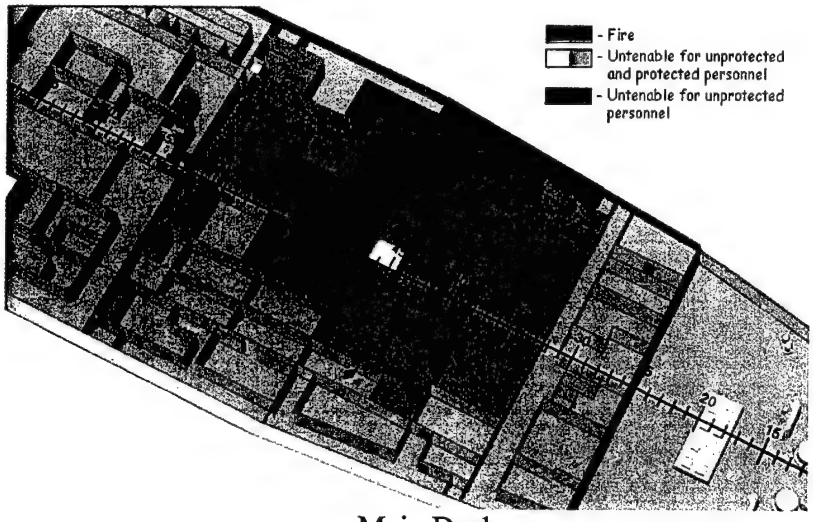

Main Deck

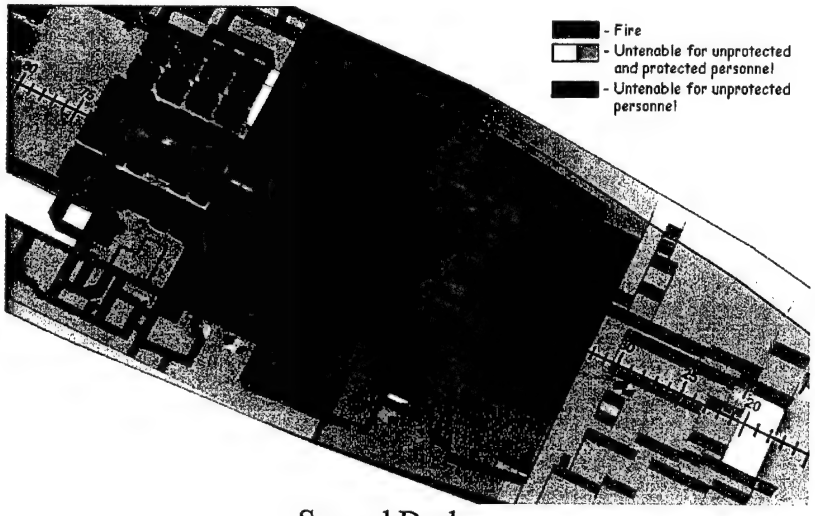

Second Deck

Fig. B-6a - Example of secondary damage 15 minutes after hypothetical weapon hit

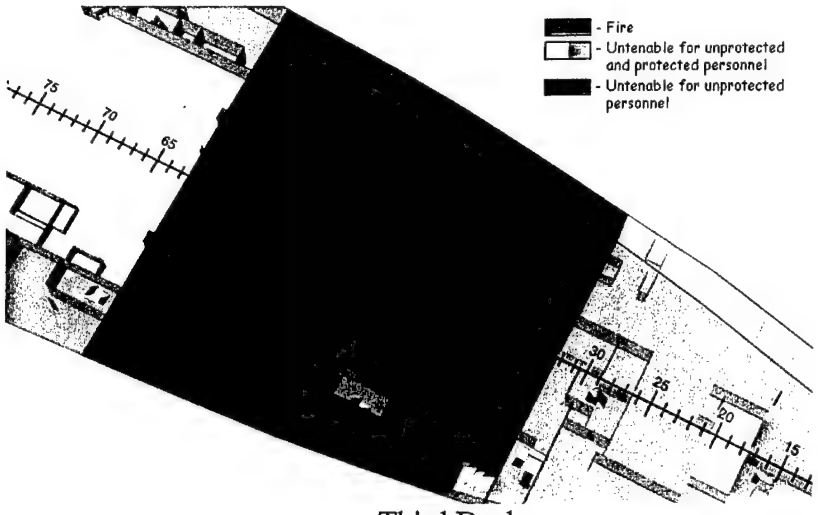

Third Deck

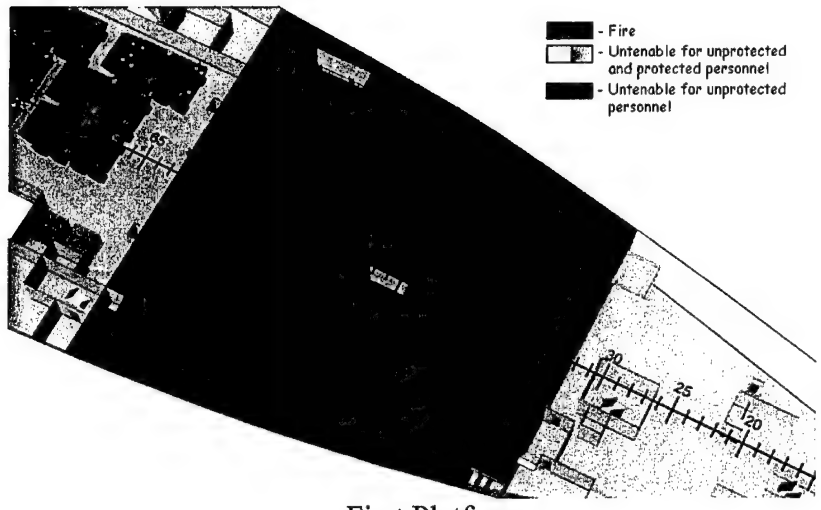

First Platform

Fig. B-6b - Example of secondary damage 15 minutes after hypothetical weapon hit (continued)

The methodology is summarized in the flowchart shown in Figure B-7. Figure B-8 is a flowchart for tenability. The process involves modeling PDA(F) compartments with the multi-compartment zone fire model CFAST. The use of CFAST allows for a more complete characterization of these compartments. The output from CFAST is used to predict fire spread times and assess tenability conditions. Fire spread beyond these compartments to APDA(F) and BAPDA(F) compartments is predicted using a conservative set of prescriptive rules.

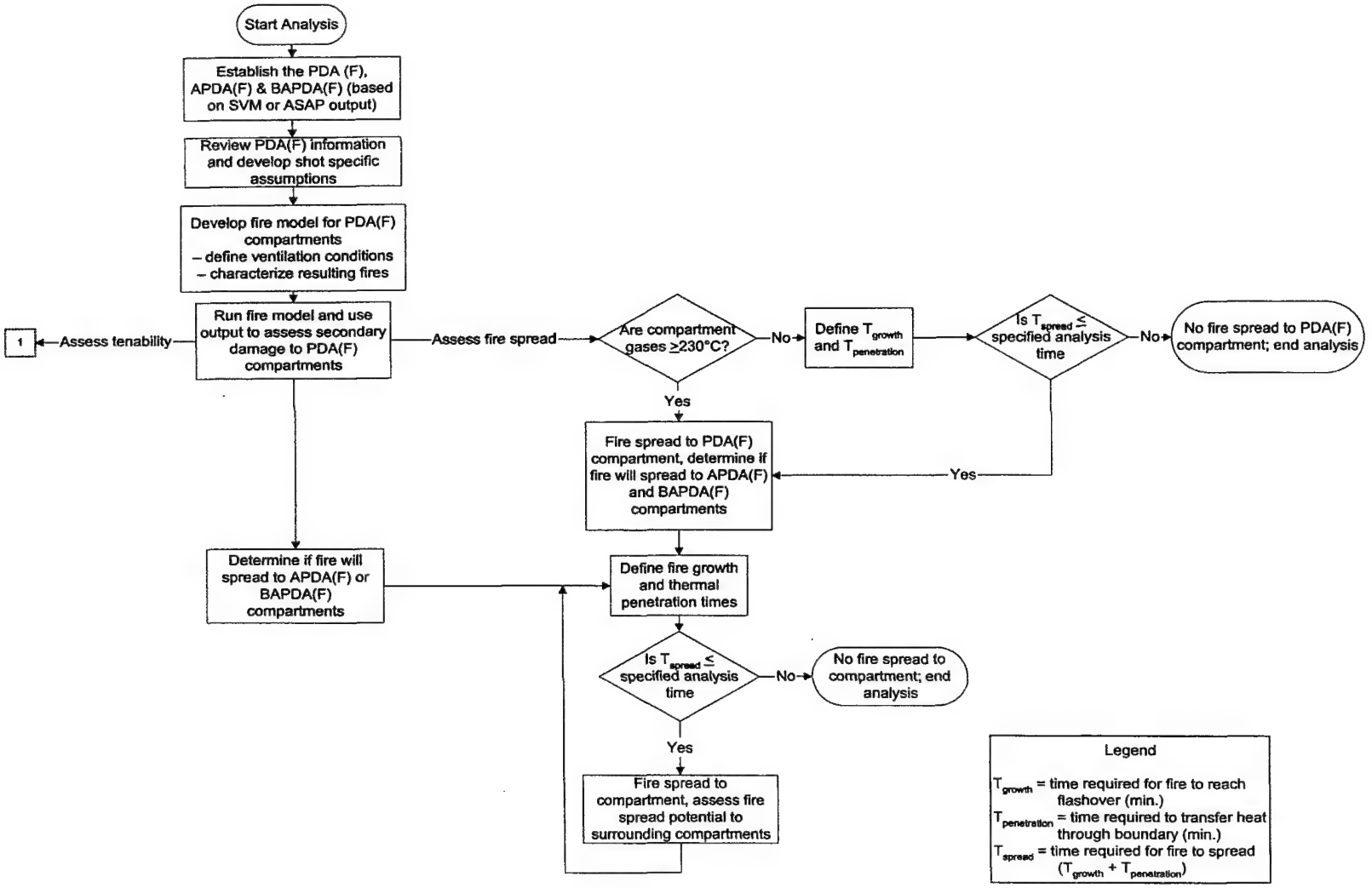

Fig. B-7 - Flowchart for fire and smoke spread methodology

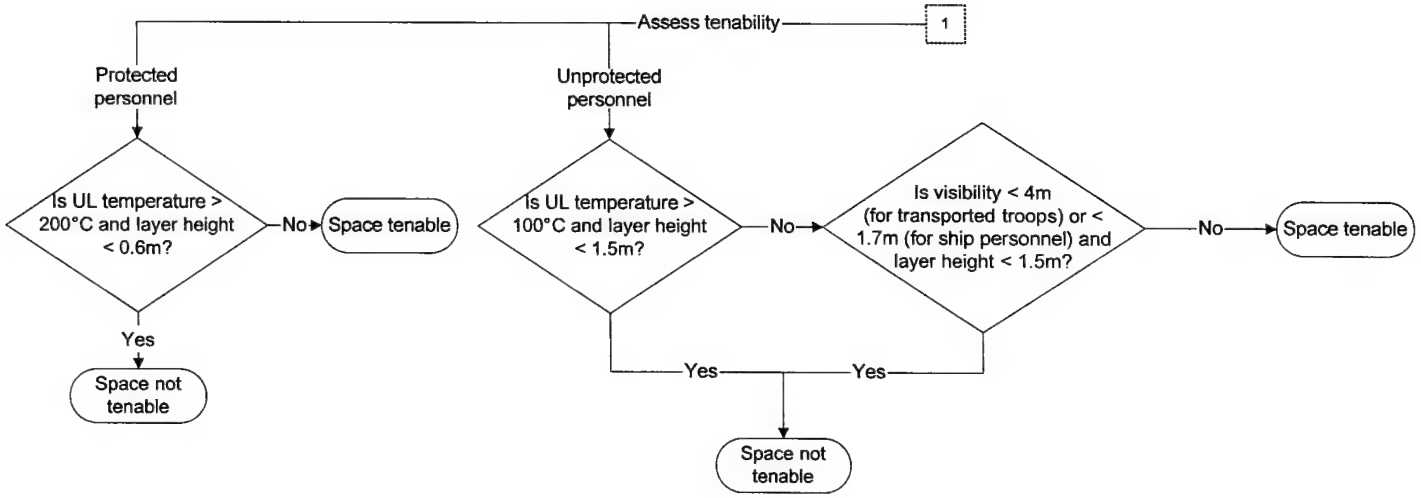

Fig. B-8 - Flowchart for fire and smoke spread methodology for tenability

4.0 SUMMARY

A methodology has been developed as part of a congressionally mandated LFT&E programs to predict smoke and fire spread after a weapon hit. The objective of the current methodology is to identify specific weaknesses and/or shortcomings that might increase survivability.

5.0 FUTURE DEVELOPMENTS

The methodology described in this report is currently being applied in the VAR 3 process for the LPD 17 platform detailed design. Any further developments or improvements in the methodology will be documented and reflected in a future revision of this report. Separate efforts are underway to develop a network fire model [41]. The network fire model would provide a physics based model that could quickly assess fire and smoke spread for ship platforms. Plans also include accounting for fire detection and suppression effects. This type of model would provide better far field secondary damage characterization capabilities. It is unclear if the network fire model will replace the current methodology or if it will be used in conjunction with the method or portions of the method described in this report. Significant changes in direction for predicting secondary damage associated with LFT&E efforts will be documented in future reports.

6.0 REFERENCES

1. Williams, F.W., Scheffey, J.L, Tatem, P.A., and DiNenno, P.J., "Review of Fire Spread Parameters for Total Ship Survivability/Fleet Training (TSS/FT) Fire Spread Model, NRL Ltr Rpt Ser 6180-107, 22 April 1992.

2. White, D.A., Rhodes, B.T., DiNenno, P.J., Tatem, P.A., and Kay, D., "Smoke and Fire Spread Evaluations: LPD-17 Amphibious Transport Dock Ship Total Ship Survivability and Battle Damage Repair Assessments (U)," NRL/MR/6180-97-7985, 30 September 1997 (Confidential).

3. Back, G.G., Darwin, R.L., Hopkins, D., Mack, E.C., Scheffey, J.L., White, D.A., Tatem, P.A., Williams, F.W., and Hunstad, M., "CVNX1 Vulnerability Report (2) and Battle Damage Repair Assessment: Fire and Smoke Spread Evaluation (U)," NRL report in preparation, 18 March 2002 (Secret).

4. Luers, A.C., Gottuk, D.T., Pham, H.V., Scheffey, J.L., Wong, J.T., Downs, R., Runnerstrom, E., Farley, J.P., Williams, F.W., Tatem, P.A., Durkin, A., Nguyen, X., and Buchanan, J., "FY 2001 DC-ARM Final Demonstration Report," NRL/MR/6180-02-8623, 31 May 2002.

5. Peatross, M.J., Luers, A.C., Pham, H.V., Scheffey, J.L., Wong, J.T., Farley, J.P., Williams, F.W., Tatem, P.A., Nguyen, X., and Rose-Pehrsson, S.L., "Results of the FY 2000 DC-ARM Demonstration," NRL Ltr Rpt Ser 6180/0029, 07 February 2001.

6. Parker, A.P., Strehlen, B.D., Scheffey, J.L., Wong, J.T., Darwin, R.L., Pham, H., Runnerstrom, E., Lestina, T., Downs, R., Bradley, M., Toomey, T.A., Farley, J.P., Williams, F.W. and Tatem, P.A., "Results of 1998 DC-ARM/ISFG Demonstration Tests," NRL Ltr Rpt Ser 6180/0032, March 12, 1999.

7. Back, G.G., Scheffey, J.L. and Williams, F.W., "Spruance Class Weapon Effects Test – Fire Spread Evaluation: Preliminary Report," NRL Ltr Rpt 6180/0584, December 26, 2002

8. "Ship Vulnerability Model Program Maintenance/Analyst Manual (U) Volume I. Simulation Model Part 1," Tom Carroll Associates, November 1985.

9. Adamchak, J., *et al*, "Advanced Survivability Assessment Program Verification and Validation Plan (U)," April 2002.

10. Peacock, R.D., Reneke, P.A., Jones, W.W., Bukowski, R.W., and Forney, G.P., "A User's Guide for FAST: Engineering Tools for Estimating Fire Spread and Smoke Transport," Special Publication 921 2000 Edition, National Institute of Standards and Technology, Gaithersburg, MD, January 2000.

11. Peacock, R.D., Forney, G.F., Reneke, P., and Jones, W.W., "CFAST, the Consolidated Model of Fire Growth and Smoke Transport, Version 4.0.1 " NIST Technical Note 1431, National Institute of Standards and Technology, Gaithersburg, MD, January 2000.

12. Back, G.G., Iqbal, N., William, F.W., and Scheffey, J.L., "Potential Compartment Fire Growth Curve Resulting from a Missile Hit," NRL Ltr Rpt 6180/0526, 27 October 1998.

13. Back G.G., Darwin, R.L. and Williams, F.W., "Weapons Effects Test (EX-USS DALE [CG-19]) Compartment Fire Evaluation (U)," NRL Ltr Rpt 6180/0022, 04 February 2002 (Confidential).

14. Evans, D.D., "Ceiling Jet Flows," *The Society of Fire Protection Engineers (SFPE) Handbook of Fire Protection Engineering*, 2nd Edition, National Association of Fire Protection Engineers, Quincy, MA, 1995.

15. Bailey, J.L. and Tatem, P.A., "Validation of Fire/Smoke Spread Model (CFAST) Using ex-USS *Shadwell* Internal Ship Conflagration Control (ISCC) Fire Tests," NRL Memorandum Report 6180-05-7781, 30 September 1995.

16. Bailey, J.L. and Tatem, P.A., "Validation of Fire/Smoke Spread Model (CFAST) Using ex-USS *Shadwell* Smoke Ejection System Fire Tests," NRL Ltr Rpt, 6180/0007.2, 24 January 1994.

17. Hoover, J.B., Bailey, J.L. and Tatem, P.A, "Validation of Gas Phase Absorbance Algorithm in the Consolidated Fire Growth and Smoke Transport CFAST Model," NRL Ltr Rpt, 6180/0020, 8 March 1996.

18. Nelson, H.E., and Deal, S. (1991), "Comparing Compartment Fires with Compartment Fire Models," *Fire Safety Sciences-Proceedings of the Third International Symposium*, Elsevier, NY, pp. 719-728.

19. Peacock, R.D., Jones, W.W., and Bukowski, R.W., "Verification of a Model for Fire and Smoke Transport," *Fire Safety Journal,* **21**, 1993, pp. 89-129.

20. Back, G.G., Darwin, R.L., and Beyler C.L., "An Evaluation of the Cooling Capabilities of Water Spray Systems in Cargo Holds," Hughes Associates Report, 10 February 2000.

21. Department of the Navy "Naval Ships' Technical Manual Chapter 555-Volume **1**, Surface Ship Firefighting," S9086-S3-STM-010/CH-555V1R9, 1 December 2001.

22. Setchkin, N.P., *National Bureau of Standards Journal of Research,* National Bureau of Standards, Gaithersburg, MD, 1949.

23. American Society of Testing and Materials, "ASTM D1929, Standard Test Method for Ignition Properties of Plastics," Philadelphia, PA, 1983.

24. Darwin, R.L., Leonard, J.T., and Scheffey, J.L., "Fire Spread by Heat Transmission Through Steel Bulkheads and Decks," Proceedings of IMAS Conference on Fire Safety on Ship, Institute of Marine Engineers, London, England, May 1994.

25. Drysdale, D., "An Introduction to Fire Dynamics," Second Edition, John Wiley & Sons, Chichester, 1999.

26. Back, G., Beyler, C., DiNenno, P., and Tatem, P., "Wall Incident Heat Flux Distributions Resulting from an Adjacent Fire," *Fire Safety Science-Proceedings of the Fourth International Symposium,* 1994, pp. 241-252.

27. Back, G.G., Leonard, J.T., Fulper. C.R., Darwin, R.L., Scheffey, J.L., Willard, R.L., DiNenno, P.J., Steel, J.S., Ouellette, R.J., and Beyler, C.L., "Post-flashover Fires in Simulated Shipboard Compartments: Phase I – Small Scale Studies," NRL/MR/6180--9886, 3 September 1991.

28. Scheffey, J.L., Hill, S.A., Toomey, T.A., Leonard, J.T., Williams, F.W., Smith, D.E., and Darwin, R.L., "Post-flashover Fires in Shipboard Compartments Aboard ex-USS *Shadwell*: Phase V Fire Dynamics," NRL/FR/6180-99-9902, 31 May 1999.

29. Vegthe, J.J., "Human Exposure to High Radiant Environments," Aerospace Medicine, Vol. **44**, pp. 1147-1157, 1973.

30. Stoll, A.M. and Chianta, M.A., "Evaluation of Thermal Protection," Aerospace Medicine, Vol. **11**, pp. 1232-1238, 1989.

31. White, F.M., "Heat Transfer," Addison-Wesley Publishing Company, Inc., Reading Massachusetts, 1984.

32. Oak Ridge National Laboratory, "HEATING," Multidimensional Finite-Difference Heat Conduction Analysis Code System Version 7.3, ORNL, Oak Ridge, Tennessee, 1999.

33. Peacock, R.D., Jones, W.W., Bukowski, R.W., and Forney, C.L, "Technical Reference Guide for HAZARD I Fire Hazard Assessment Method, Version 1.1," NIST Handbook 146, Volume II, National Institute of Standards and Technology, Gaithersburg, MD, June 1991.

34. Purser, D.A., "Toxicity Assessment of Combustion Products," *The Society of Fire Protection Engineers (SFPE) Handbook of Fire Protection Engineering*, 2nd Edition, National Association of Fire Protection Engineers, Quincy, MA, 1995.

35. Bryan, J.L., "Damageability of Buildings, Contents and Personnel from Exposure to Fire," *Fire Safety Journal*, **11**, 1986, pp. 15-31.

36. Vegthe, J.H., "Design Criteria for Fire Fighters' Protective Clothing," Jansville Apparel, 1st Edition, September 1981.

37. Jin, T., "Visibility Through Fire Smoke," Report of Fire Research Institute of Japan, **2 (33)**, 1971, pp. 12-18.

38. Budnick, E.K., "Mobile Home Living Room Fire Studies: The Role of Interior Finish," NBSIR 78-1530, National Bureau of Standards, Gaithersburg, MD, September 1978.

39. Malhotra, H.L., "Movement of Smoke on Escape Routes, Part 1 – Instrumentation and Effect of Smoke on Visibility," Joint Fire Research Organization, Borehamwood Fire Research Note 651, England, January 1967, p. 21.

40. Scheffey, J.L., Jonas, L.A., Toomey, T.A., Byrd, R., and Williams, F.W., "Analysis of Quick Response Fire Fighting Equipment on Submarines – Phase II, Full Scale Doctrine and Tactics Tests," NRL Memorandum Report 6632, 10 July 1990.

41. Floyd, J., Scheffey, J., Haupt, T., Al Habbash, H., Hodge, B., Norton, O., Williams, F., and Tatem, P., "Requirements for a Shipboard, Network Fire Model," NRL Ltr Rpt 6180/0469, January 23, 2003.

APPENDIX C

HEATING REF A

Verifying HEATING 7.3 Against the Swedish National Testing and Research Institute's Suite of Fire Resistance Examples

JAVIER TRELLES
SEAN P. HUNT

Hughes Associates, Inc.
Baltimore, MD

FREDERICK W. WILLIAMS

Naval Research Laboratory
Naval Technology Center for Safety and Survivability
Washington, DC

April 10, 2003

CONTENTS

TABLES

FIGURES

1.0 INTRODUCTION

A series of eight benchmark reference cases were proposed by Wickström and Pålsson [1999] for use in verifying two-dimensional heat conduction computer programs [Wickström *et al.*, 1999; Pålsson *et al.*, 2000]. These entail thermal calculations of increasing complexity. The reference cases were developed to address the following aspects of a numerical heat transfer calculation:

- Convergence;
- Variable convective and radiative boundary conditions;
- Variable thermal material properties;
- Multiple materials;
- Phase change of material constituents; and
- Radiation and convection in voids.

Convergence is verified by starting with a coarse grid in each domain and then by increasing the number of nodes until a desired error tolerance is met. The remaining aspects are verified when the difference between the converged numerical results and the touchstone calculations is below an acceptable error threshold.

In this study, the eight reference cases will be solved with the finite volume conduction program HEATING 7.3. HEATING stands for heat engineering and transfer in nine geometries. HEATING was developed at the Oak Ridge National Laboratory's (ORNL) Radiation Safety Information Computational Center (RSICC) [Childs, 1998]. HEATING was created to analyze the thermal impact of the U.S. Energy Department's various high energy projects, including all aspects of radiation shielding. It has one of the longest development histories of any computational heat transfer software package: [Fowler & Volk, 1959; Liguori & Stephenson, 1961; Turner & Crowell, 1969; Turner & Siman-Tov, 1971; Turner et al., 1977; Becker, 1977; Elrod et al., 1984; Bryan et al., 1986; Childs, 1990; Childs et al., 1990; Childs, 1991]. Verification studies and tools for HEATING can be found in [Bryan et al., 1986; Chu, 1989].

HEATING is a field model. It solves, using finite volume techniques [Patankar, 1980; Childs, 1998], the heat equation [Arpaci, 1966; Carslaw & Jaeger, 1959],

$$\rho c \frac{\partial T}{\partial t} = \nabla \cdot \left(k \nabla T \right) + \dot{q}''', \qquad (1)$$

subject to the general boundary condition

$$\dot{q}_s'' = -k\frac{\partial T_s}{\partial n} = \left\{h_f + h_n\left|T_s - T_\infty\right|^{h_e} + h_r\left(T_s^2 + T_\infty^2\right)\left(T_s + T_\infty\right)\right\}\left(T_s - T_\infty\right)$$

or (2)

$$T_s = f_s(\mathbf{x}, t)$$

The variables are as follows: T is the material internal temperature, ρ is the density, c is the specific heat, t is the time, $\dot{q}'''$ is the volumetric heat generation rate, $\dot{q}_s''$ is the heat flux for surface s, n is the coordinate normal to the surface, k is the thermal conductivity, T_s is the material surface temperature, f_s is a temperature function associated with surface s, T_∞ is the ambient temperature, h_f is the heat transfer coefficient for forced convection, h_n is the heat transfer coefficient for natural convection, h_e is the exponent for natural convection, h_r is the radiative transfer coefficient, and ∇ and ∂ are partial derivative operators.

HEATING 7.2i and 7.3 are the most recent developments in a series of heat-transfer codes distributed by RSICC as SCA-1/HEATING5 and PSR199/HEATING 6. HEATING7 can solve steady-state and/or transient heat conduction problems in one-, two-, and three-dimensional Cartesian, cylindrical, or spherical coordinates. A model may include multiple materials, and the thermal conductivity, density, and specific heat of each material may be both time- and temperature-dependent. The thermal conductivity may also be anisotropic. Materials may undergo change of phase. Thermal properties of materials may be input or may be extracted from a material properties library. Heat-generation rates may be dependent on time, temperature, and position. Boundary temperatures may be time- and position-dependent. The boundary conditions, which may be surface-to-environment or surface-to-surface, may be specified temperatures or any combination of prescribed heat flux, forced convection, natural convection, and radiation. The boundary condition parameters may be time- and/or temperature-dependent. General gray-body radiation problems may be modeled with user-defined factors for radiant exchange. Surfaces that are not in contact can exchange heat via custom connectors. The mesh spacing may be variable along each axis.

2.0 VERIFICATION

[Wickström & Pålsson, 1999] published a suite of eight configurations suitable for the verification of heat transfer programs that can predict the temperature in structures exposed to fires. They used TASEF [Sterner and Wickström, 1990] as the benchmark for verifying other computer codes. TASEF stands for "Temperature Analysis of Structures Exposed to Fire." It employs the finite element method in order to analyze heat transfer in two-dimensional Cartesian and axisymmetric cylindrical coordinates. These region may be composed of multiple materials and voids. TASEF is general enough to account for nonlinearities in the boundary conditions and in the material properties. As the constituents of its acronym imply, TASEF was specifically developed to determine the response of structural assemblies and components to fire. The first

reference case in the suite is a linear problem that has an exact analytic solution. The following five reference cases are non-linear problems that do not have exact solutions available. The last two examples in this suite deal with heat transfer in enclosures. The results produced by HEATING 7.3 are to be evaluated for these eight cases.

The computer model INST2D [Rudolphi and Müller, 1980] has been verified using the first seven benchmark reference cases [Hamann *et al.*, 1999]. Hamann *et al.* demonstrate reasonable agreement between TASEF and INST2D. SAFIR, another finite element heat transfer program, has been used to successfully solve Reference Case 7 [Pintea and Franssen, 1997]. These two favorable outcomes add credibility to the verification suite based on results from TASEF. This document summarizes the benchmark verification process per [Wickström and Pålsson, 1999] for the finite volume heat transfer computer code HEATING, version 7.3 [Childs, 1998].

It is worthwhile to take the opportunity now to clarify some points that will make the following comparison between TASEF and HEATING more sensible. HEATING is a finite volume program that offers first and second order accuracy in space and time, depending on the algorithm that is used. Spatial accuracy can only be improved by increasing the number of cells. TASEF is a finite element program. Spatial accuracy is likewise governed by the number of elements but it is also affected by the order of the multidimensional polynomial serving as the basis function for each finite element. The geometrical shape of the subvolumes for each of the two methods also matters. Hence a finite element model composed of 20 fourth order multidimensional polynomial quadrilaterals is expected to be more accurate than a second order finite volume simulation with 20 cells. When percent differences are presented, the "actual" is taken to be the solution from an analytic expression, if available. Otherwise, the answer provided by TASEF is employed. All the specifications for the examples, unless otherwise noted, are taken from the publications [Wickström and Pålsson, 1999; Wickström, 1999; Pålsson & Wickström, 2000]. The HEATING calculations were done on a Linux workstation with two Pentium III Xeon processors, 1 GByte of memory, and 19 Gbytes of storage and a Silicon Graphics, Inc. Octane2 graphics workstation with V6® graphics, two R12,000A processors, 2 Gbytes of RAM memory, and in excess of 136 Gbytes of storage. The October 1999 release of HEATING 7.3 was used for this investigation.

2.1 Reference Case 1: Comparison Against Analytical Results, Constant Material Properties

Reference Case 1 consists of a square section of a generic material whose thermal properties are to be determined from the stipulation that its thermal diffusivity ($\alpha = k / \rho c$) and Biot number ($\mathrm{Bi} = h L / k$) are both unity. L is the half-length of the side of the square section. The material, initially at 0°C, is subjected to a surface gas temperature of 1,000°C. Convection is the means of heat transfer between the square section and the surrounding gas. The specific material

properties are arbitrary in this case. Refer to Figure C-1 for a depiction of the calculation domain. The implicit Crank-Nicolson method [Childs, 1998; Smith, 1987; Jaluria & Torrance, 1986] is used to solve for the temperature within the square. The tolerance for convergence is 10^{-6}.

The temperature at the center of the square region is presented as a function of dimensionless time (i.e., the Fourier number). The Fourier number, Fo, is $\alpha t / L^2$. Figure C-2 shows the results of HEATING and TASEF for grids using 4 through 256 elements. This plot shows that both TASEF and HEATING converge to a solution with fewer than 64 elements. Table C-1 compares HEATING with the exact solution for a 64 cell grid. Table C-1 demonstrates excellent agreement with the results of the analytical solution reported in [Wickström and Pålsson, 1999] which is based on the formulae in [Carslaw & Jaeger, 1959].

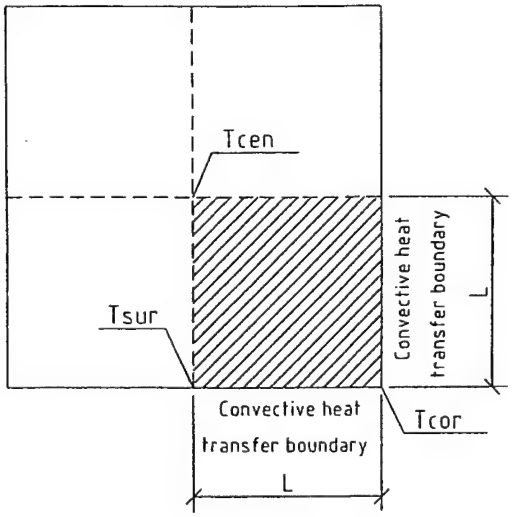

Fig. C-1 - Diagram of benchmark Reference Case 1.

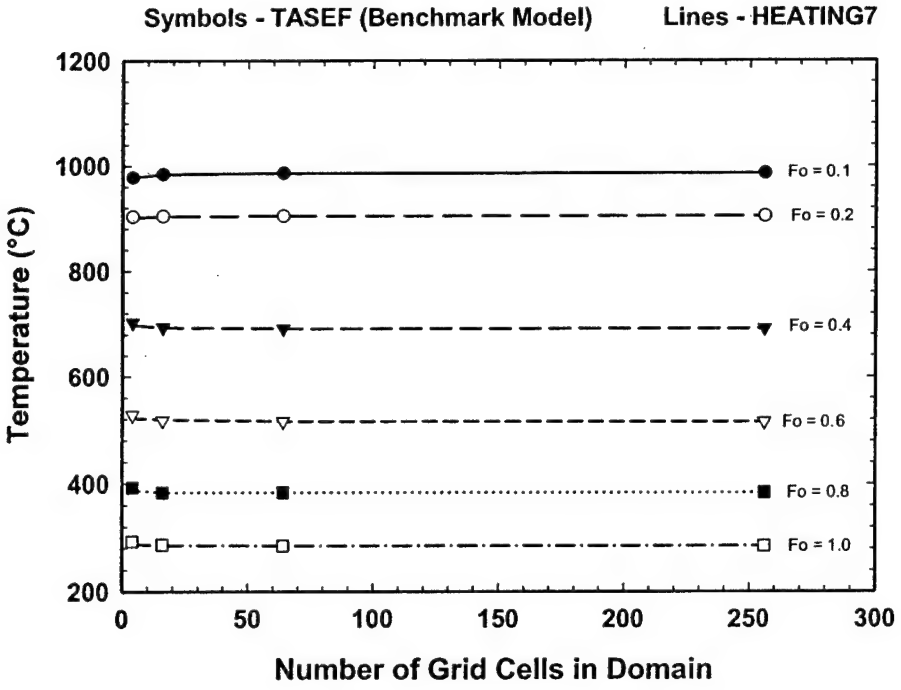

Fig. C-2 - Center temperature for Reference Case 1 as a function of the number of grid cells.

Table C-1 - Comparison of HEATING to Analytical Solution for the Reference Case 1.

Fourier Number	Center Temperature [°C]		
	HEATING (64 Cells)	Analytical Solution	% Difference
0.1	986	986	0.000
0.2	904	904	0.000
0.4	691	690	0.145
0.6	515	515	0.000
0.8	384	383	0.261
1.0	285	285	0.000

2.2 Reference Case 2: Non-Linear Boundary Conditions and Constant Material Properties

Reference Case 2 consists of a square section of a concrete-like material with constant properties. Figure C-3 shows the region. The dimensions and material properties are as follows:

- Length: 0.1 m
- Thermal conductivity: 1.0 W/(m·K)
- Heat capacity: 1,000 J/kg
- Density: 2,400 kg/m^3.

- Density: 2,400 kg/m^3.

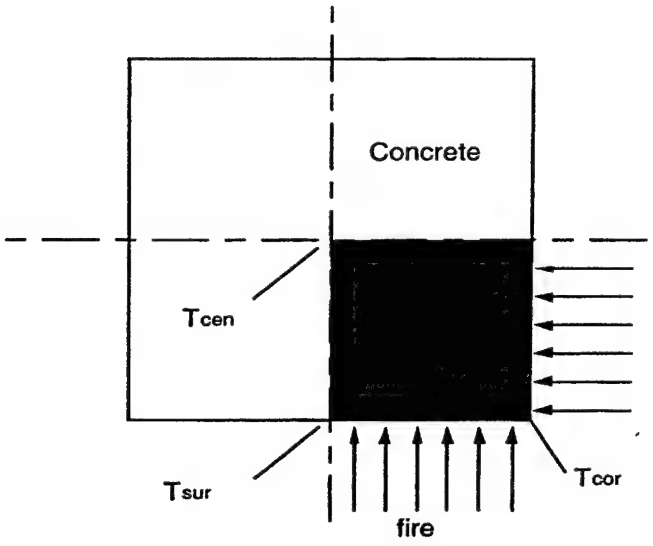

Fig. C-3 — Diagram of benchmark Reference Case 2

The boundary condition is applied in the following form:

$$\dot{q}'' = \sigma\varepsilon\left(T_s^4 - T_\infty^4\right) + h\left(T_s - T_\infty\right) \qquad (3)$$

where $\dot{q}''$ is the boundary heat flux (W/m^2), ε is the surface emissivity, σ is the Stefan-Boltzman constant (5.669×10^{-8} W/m^2·K^4), T_∞ is the exposure temperature (K), T_s is the surface temperature (K), and h is the convective heat transfer coefficient (W/m^2·K). The boundary condition parameters are as follows:

- Emissivity: 0.8
- Convection coefficient: 10 W/(m2·K)
- Initial temperature (T_0): 0 °C
- Exposure temperature (1): 1,000 °C
- Exposure temperature (2): $T_0 + 345\log_{10}(8t+1)$, where t is in minutes.

The implicit Crank-Nicolson scheme [Childs, 1998; Smith, 1987; Jaluria & Torrance, 1986] is used. The convergence tolerance is 10^{-6}. Figures C-4 and C-5 compare the temperature predictions of TASEF and HEATING for the three locations shown in Figure C-3: the center, the surface, and the corner. The time window within which the temperatures are compared is 30 minutes to 180 minutes. The figures show that HEATING and TASEF are in agreement when 64 or more cells are used for the reference case.

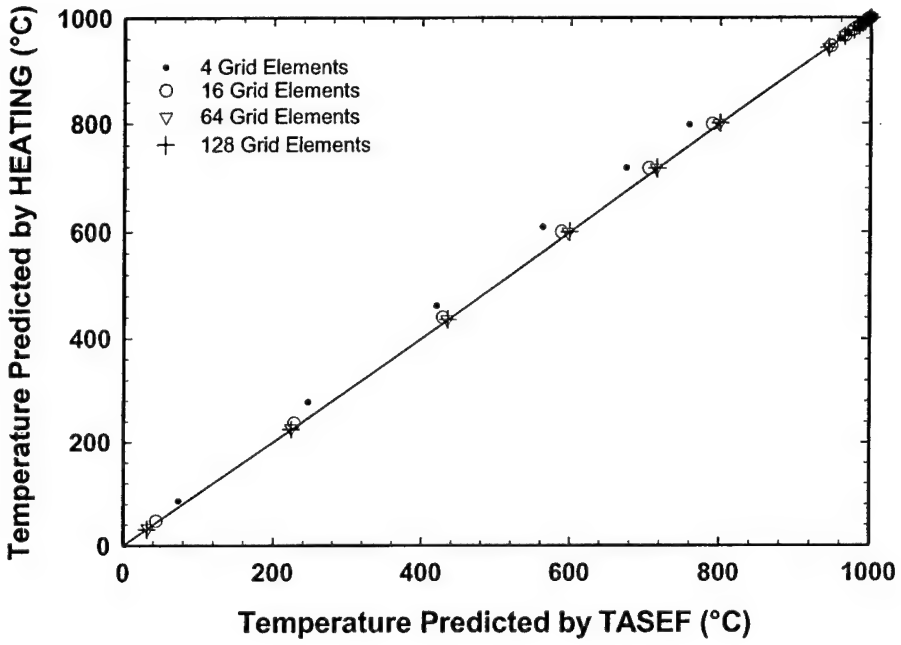

Fig. C-4 — HEATING and TASEF temperature predictions for Reference Case 2 – constant 1,000 °C exposure temperature.

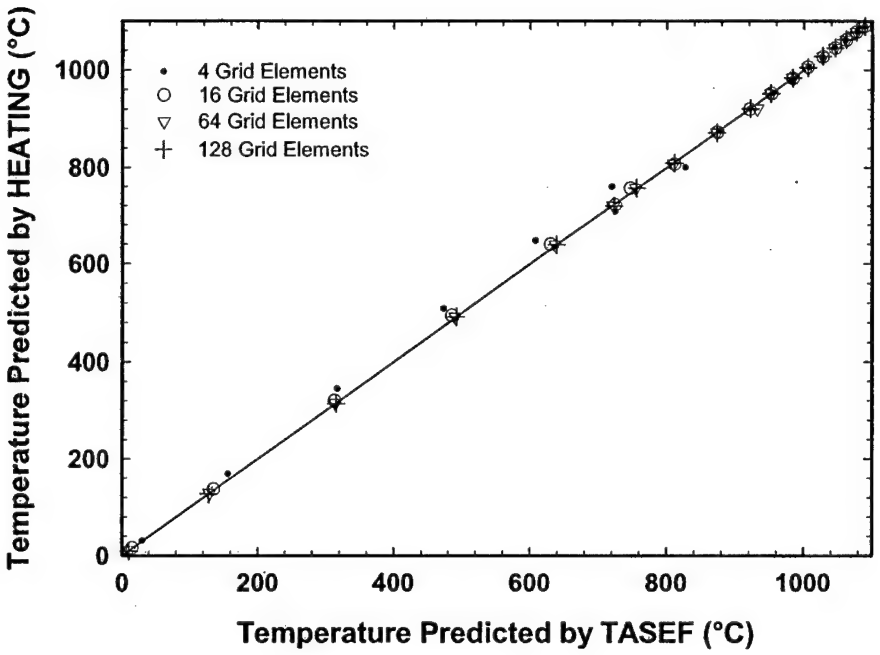

Fig. C-5 — HEATING and TASEF temperature predictions for Reference Case 2 – transient exposure temperature.

2.3 Reference Case 3: Non-Linear Boundary Conditions and Temperature Dependent Material Properties

Reference Case 3 is the same as Reference Case 2 except that the thermal conductivity of the square region is temperature-dependent as follows in Table C-2.

Table C-2 - Time-dependant thermal conductivity of the square region.

Temperature [°C]	Thermal Conductivity [W/(m·K)]
0	1.5
200	0.7
1000	0.5

(HEATING linearly interpolates the data in Table C-2.) Figures C-6 and C-7 compare the temperature predictions of TASEF and HEATING for the three locations indicated in Figure 3. The time interval when the temperatures are compared is 30 minutes to 180 minutes. The figures show that HEATING and TASEF are in agreement when 64 or more cells are used.

2.4 Reference Case 4: Latent Heat Due to Water Content – A Concrete Block with Moisture

Reference Case 4 is the same as Reference Case 3 except that a five percent by weight moisture content is assumed in the material. The change of phase of the liquid water within the concrete-like material alters the thermal response because the latent heat of vaporization of the water acts as a heat sink for the whole composite. This effect is modeled by (discontinuously) stepping the specific heat c up from 5650 J/(kg·K) to 6858 J/(kg·K) in the temperature range of 100°C to 120°C. The implicit Crank-Nicolson scheme [Childs, 1998; Smith, 1987; Jaluria & Torrance, 1986] is used. The convergence tolerance is 10^{-5}.

Figures C-8 and C-9 compare the temperature predictions of TASEF with HEATING for the three locations shown in Figure C-3. The times at which the temperatures are compared vary from 30 minutes to 180 minutes. The figures show that HEATING and TASEF are in agreement when 64 or more cells are used for the reference case.

2.5 Reference Case 5: Composite, Steel and Concrete

Reference Case 5 is the same as Reference Case 4 except that a 10 mm steel-like tube surrounds the concrete-like core material. The properties of the steel-like material are as follows:

- Thermal conductivity @ 20°C: 54 W/(m·K)
- Thermal conductivity @ 800°C: 27 W/(m·K)
- Thermal conductivity @ 1,000°C: 27 W/(m·K)
- Heat capacity: 600 J/(kg·K)
- Density: 7,850 kg/m3

Reference Case 5 is shown in Figure C-10. The implicit Crank-Nicolson scheme [Childs, 1998; Smith, 1987; Jaluria & Torrance, 1986] is used. The convergence tolerance is 5×10^{-4}.

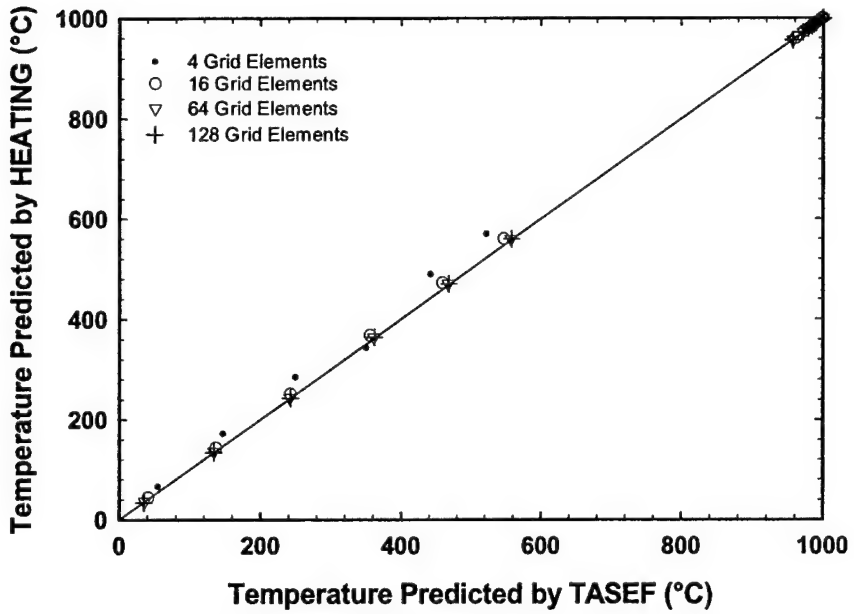

Fig. C-6 — HEATING and TASEF temperature predictions for Reference Case 3 – constant 1,000 °C exposure temperature.

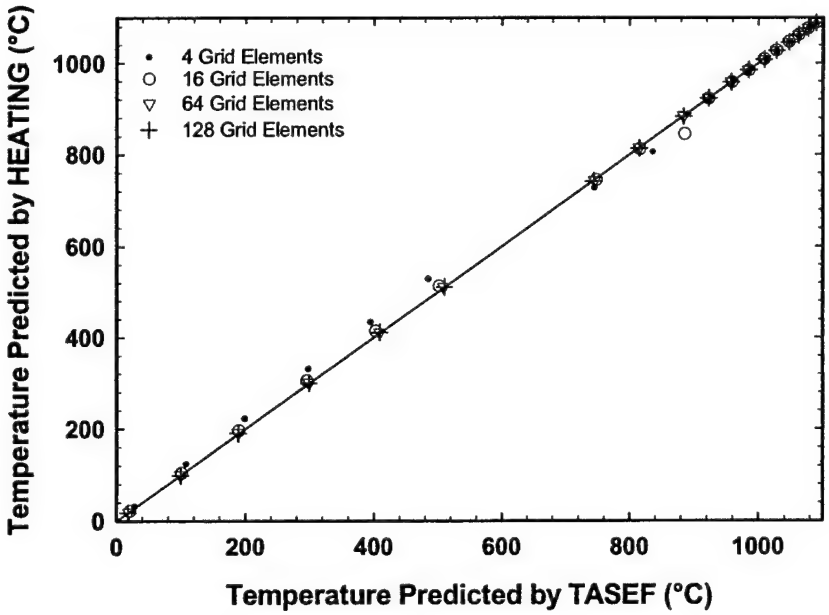

Fig. C-7 — HEATING and TASEF temperature predictions for Reference Case 3 – transient exposure temperature.

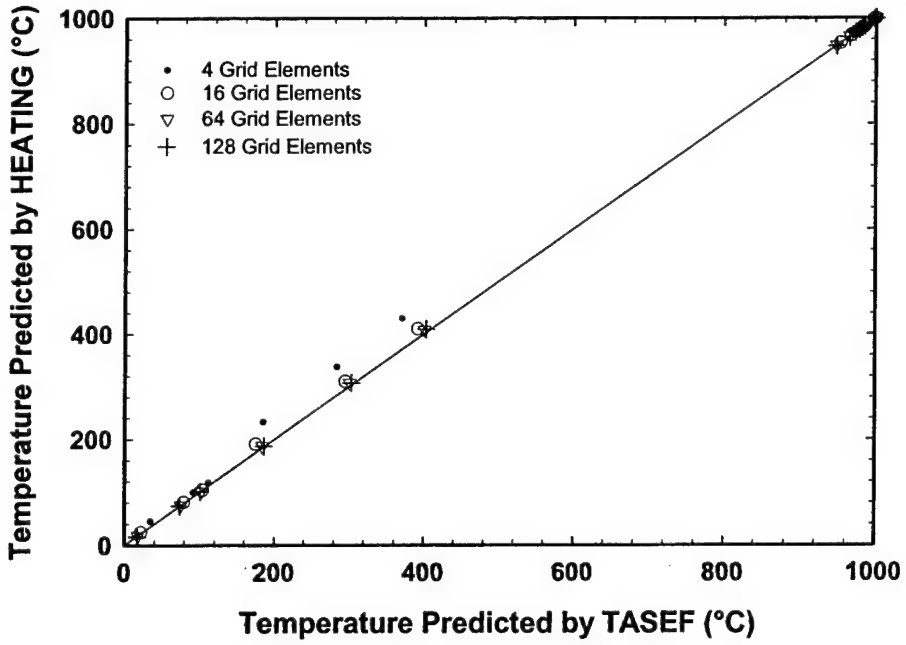

Fig. C-8 — HEATING and TASEF temperature predictions for Reference Case 4 – constant 1,000 °C exposure temperature.

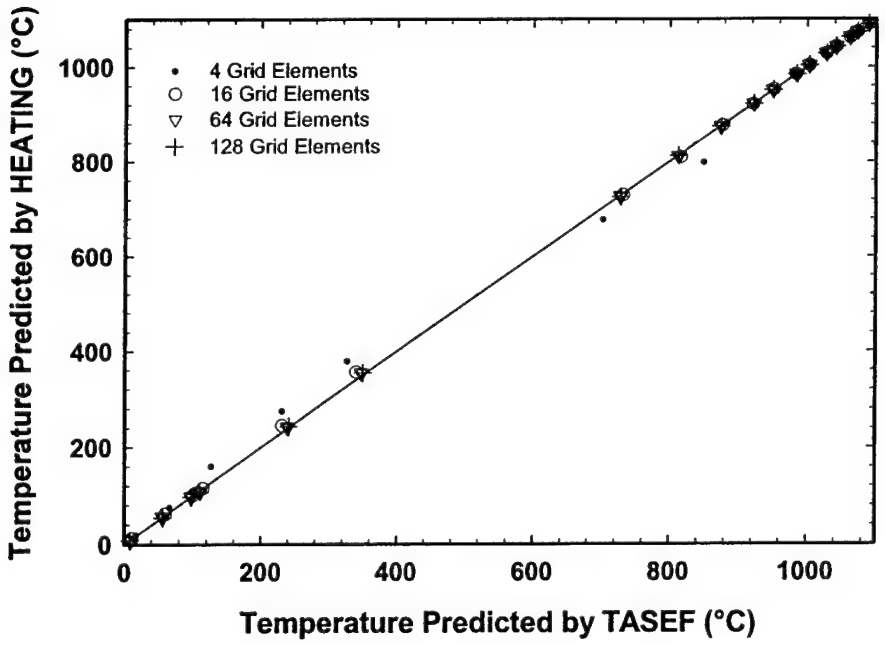

Fig. C-9 — HEATING and TASEF temperature predictions for Reference Case 4 – transient exposure temperature.

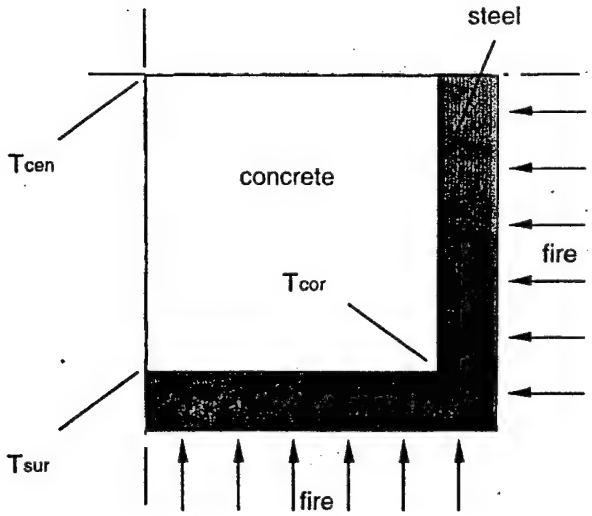

Fig. C-10 - Diagram of benchmark Reference Case 5.

Figures C-11 and C-12 compare the temperature predictions of TASEF and HEATING for the three locations shown in Figure C-10 in the time window from 30 minutes to 180 minutes. The figures show that HEATING and TASEF are in agreement when 64 or more cells are used.

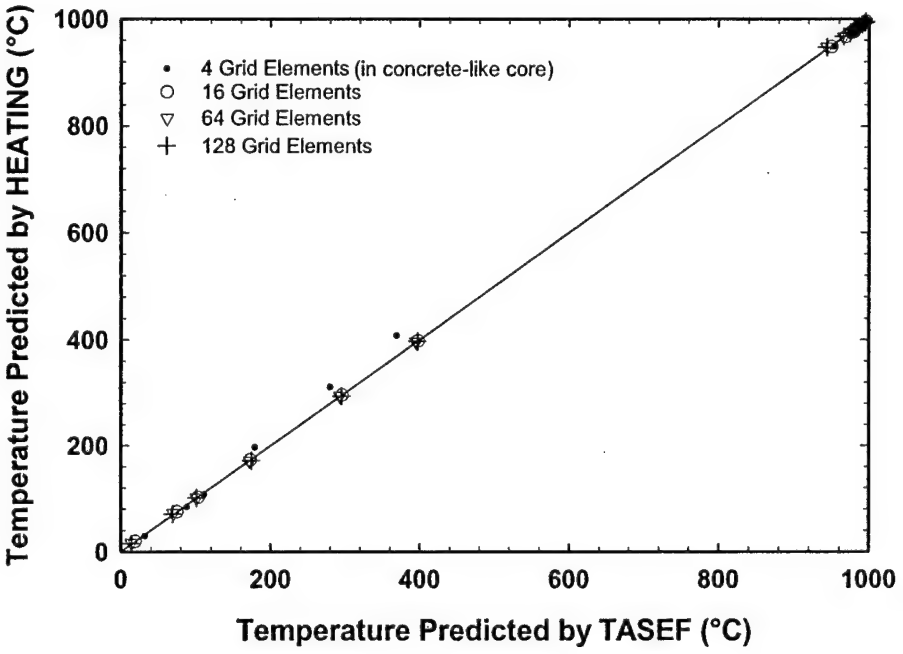

Fig. C-11 — HEATING and TASEF temperature predictions for Reference Case 5 – constant 1,000 °C exposure temperature.

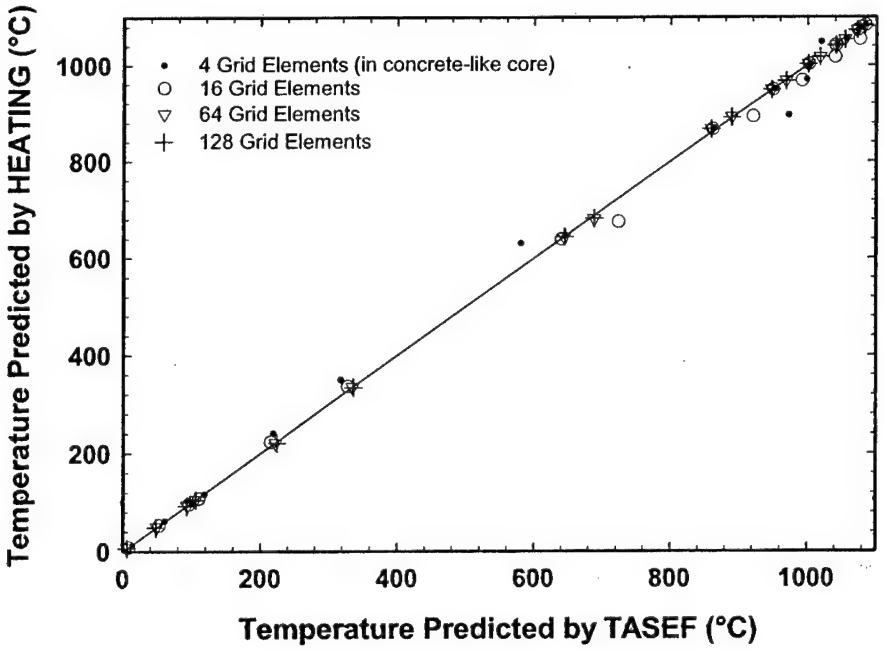

Fig. C-12 — HEATING and TASEF temperature predictions for Reference Case 5 – transient exposure temperature.

2.6 Reference Case 6: Composite, Steel and Mineral Wool

Reference Case 6 is the same as Reference Case 5 except that the concrete-like core is replaced with a mineral wool-like material. The properties of the mineral wool-like material are as follows:

- Thermal conductivity: 0.05 W/(m·K)
- Heat capacity: 1,000 J/(kg·K)
- Density: 50 kg/m3

Reference Case 6 is shown in Figure C-13. The implicit Crank-Nicolson method [Childs, 1998; Smith, 1987; Jaluria & Torrance, 1986] is used. The convergence tolerance is 5×10^{-4}.

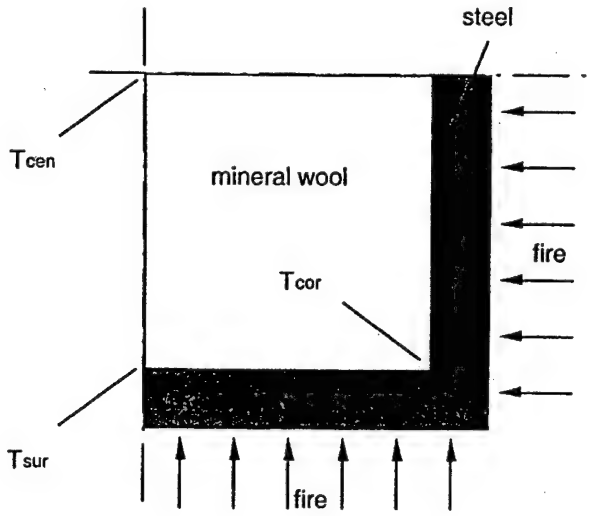

Fig. C-13 — Diagram of benchmark Reference Case 6.

Figures C-14 and C-15 compare the temperature predictions of TASEF with HEATING for the three locations shown in Figure C-13 in the time interval from 15 minutes to 180 minutes. The figures show that HEATING and TASEF are in agreement when 64 or more cells are used for the reference case.

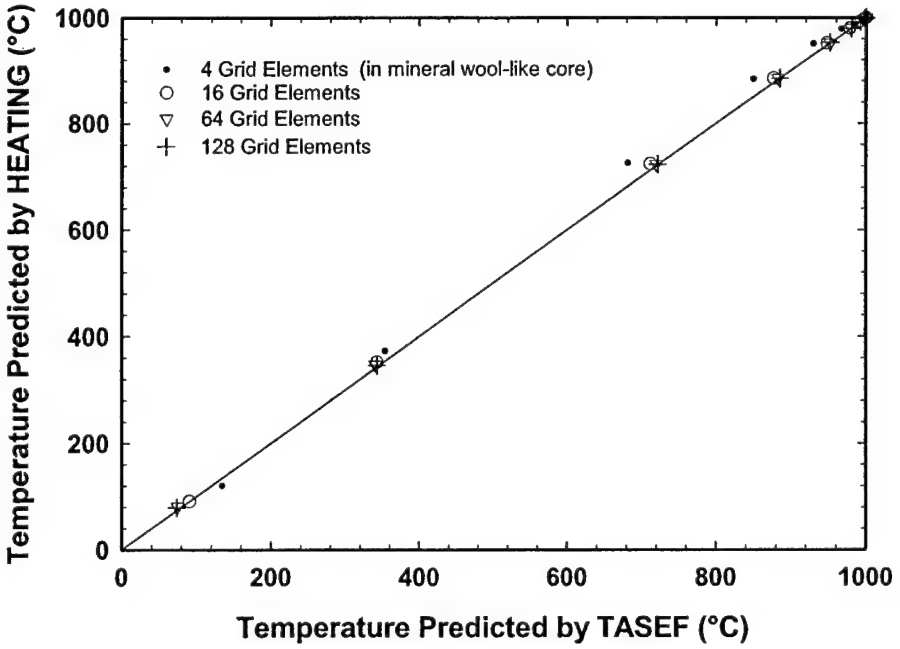

Fig. C-14 — HEATING and TASEF temperature predictions for Reference Case 6 – constant 1,000 °C exposure temperature.

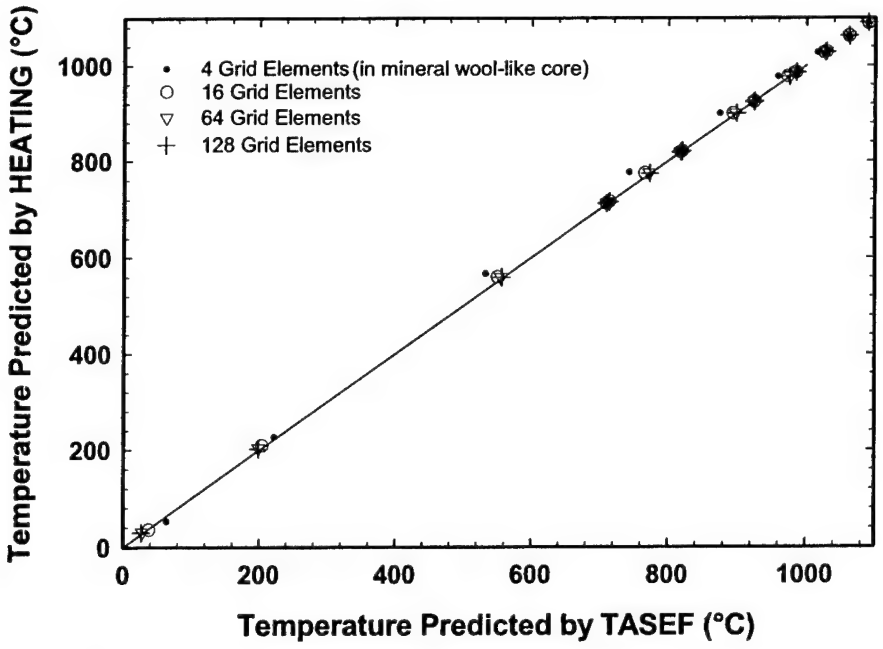

Fig. C-15 — HEATING and TASEF temperature predictions for Reference Case 6 – transient exposure temperature.

2.7 Reference Case 7: Radiative Transfer Across an Oblong Rectangular Cavity

These examples demonstrate the effect of radiation in an enclosure. HEATING needs the results of external calculations in order to determine the transfer factor. Appendix A describes the procedure used to obtain the transfer factor. The domain consists of a rectangular cavity that is ten times longer in one dimension than the other. The rectangular enclosure has a wall thickness of 5 mm. The dimensions of the cavity are 100 mm in the x–direction and 10 mm in the y. (See Figure C-16). If a temperature difference is applied across the 10 mm gap, the transfer is essentially one-dimensional. When the temperature difference is applied across the 100 mm gap, the transfer is two-dimensional. The thermal properties of the case are $k = 1$ W/(m·K), $c = 1000$ J/(kg·K), $\rho = 1000$ kg/m^3, and $\varepsilon = 0.8$. A steady-state solution is sought. The temperature used to initiate the iterations is 500°C.

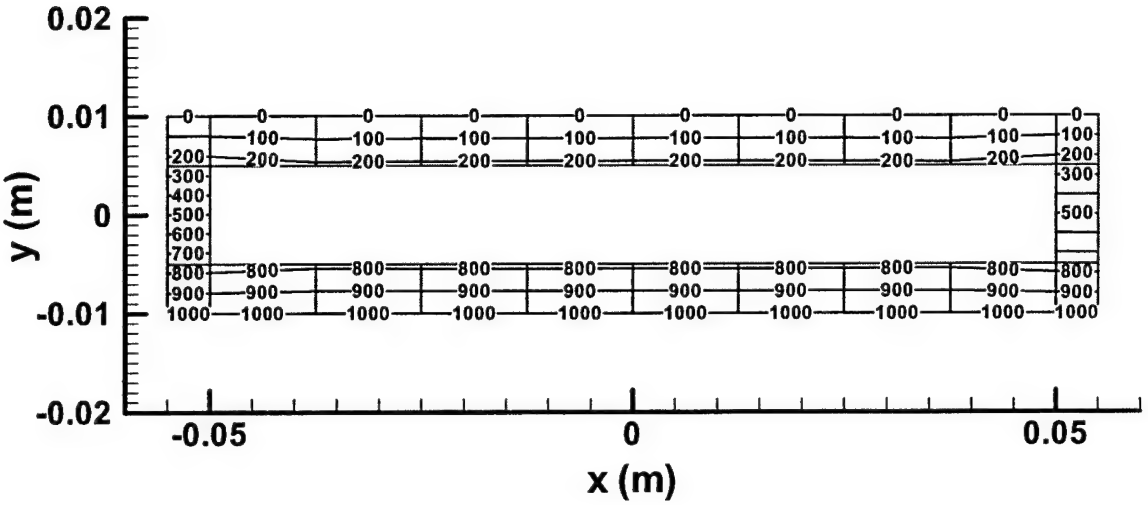

Fig. C-16 — Contours of the steady-state temperature (in °C) for Reference Case 7a.

The tolerance for convergence is 10^{-6}. The solution methods that have been used are the iterative successive over-relaxation (SOR) and conjugate gradient procedures as well as direction solution of the linear algebraic system of equations using a numerical procedure. All three were found to yield results that were identical to three significant figures or more. The results of the conjugate gradient solution are presented.

2.7.1 Temperature Difference Applied Across the *y*-Coordinate

For this case (7a), the bottom temperature is 1000°C, the top temperature is 0°C, and the left and right sides are adiabatic. These sides refer to the outer surface of the solid enclosure. The results that are presented in Table C-3 clearly show (rapid) convergence and excellent agreement with the results of the analytical solution reported in [Wickström and Pålsson, 1999]. The contour plot presented in Figure 16 confirms that the heat transfer is essentially one-dimensional.

Table C-3 - Temperature [°C] at two different locations for heat transfer along the narrow gap (Reference Case 7a).

Void Location	Number of Bottom Cells	TASEF	Analytical	HEATING	% Difference
Lower, Center	2	789	779.4	779.6	0.0257
	4	774		779.6	0.0257
	8	779		779.6	0.0257
Upper, Center	2	198	220.6	219.4	0.544
	4	229		220.0	0.272
	8	221		220.0	0.272

2.7.2 Temperature Difference Applied Across the *x*-Coordinate

For this case (7b), the left temperature is 1000°C, the right temperature is 0°C, and the top and bottom sides are adiabatic. The results are plotted in Figure C-17. Table C-4 compares the HEATING results with those of TASEF as well as SAFIR [Pintea and Franssen, 1997]. The comparison is plotted in Figure C-18.

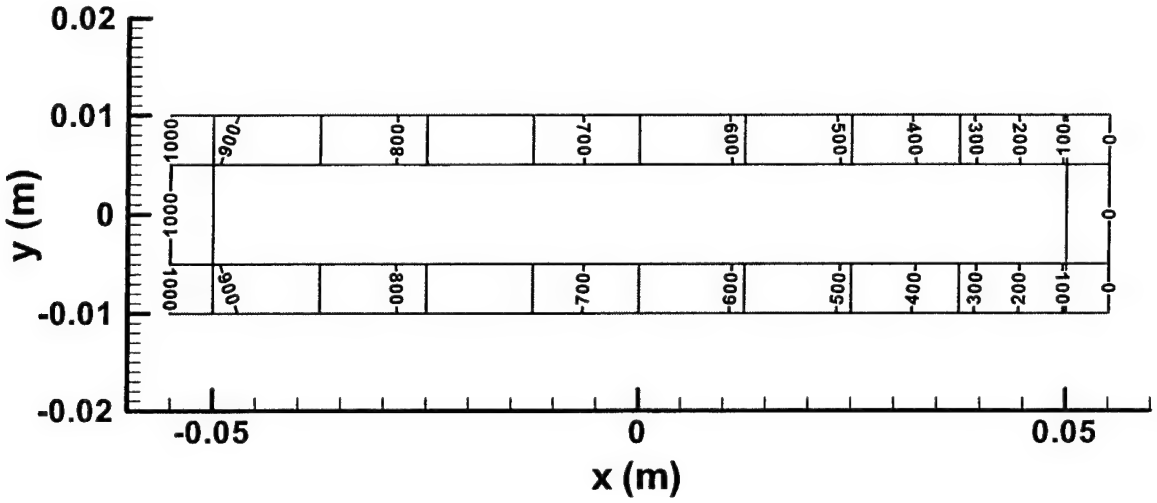

Fig. C-17 — Contours of the steady-state temperature (in °C) for Reference Case 7b.

Table C-4 - Temperature [°C] at several *x*-locations (in mm) for heat transfer across the wide gap (Reference Case 7b). *n* refers to the number of bottom cells.

MODEL	*n*	*x* [mm]								
		0	12.5	25	37.5	50	62.5	75	87.5	100
TASEF	2	881				629				117
HEATING		860				663				140
% Difference		2.38				5.41				19.7
TASEF	4	898		748		675		499		98
HEATING		891		785		672		503		107
% Difference		0.780		4.95		0.444		0.802		9.18
SAFIR	8	917	820	777	724	662	586	484	344	90
TASEF		906	820	779	723	662	587	485	335	89
HEATING		904	837	785	730	667	591	490	340	91.8
% Difference		0.221	2.07	0.777	0.968	0.755	0.681	1.03	1.49	3.15

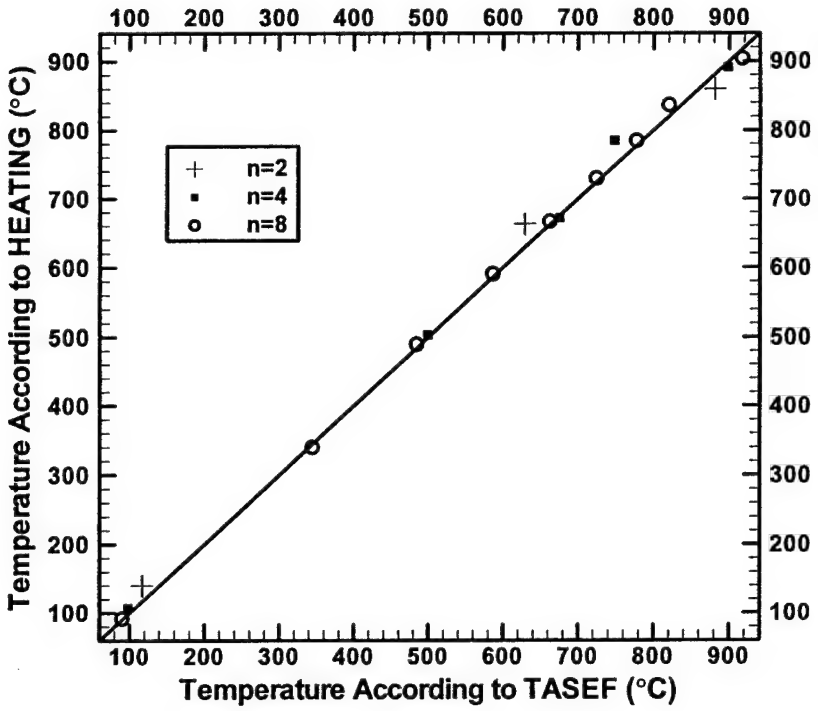

Fig. C-18 — Comparison of the results for Reference Case 7b at the positions indicated in Table 4. ***n*** represents the number of bottom cells.

2.8 Reference Case 8: Exposure of an HE200B Beam Section

This example demonstrates the effects of radiative and convective heat transfer in cavities. Appendix A describes the steps taken to accomplish this with HEATING. For this case, an HE200B beam section is protected by a 10 mm thick rectangle of Promatek insulation boards. The outer dimensions of the section are 200 mm × 200 mm. The thickness of the web is 9 mm and that of the flange is 15 mm. Four cavities are formed when the beam is thus enclosed. The one above the top flange has a 10 mm gap in the y–direction. The other dimension is 100 mm long. The gap below the bottom flange has identical dimensions. The two remaining gaps measure 45.5 mm by 70 mm. (See Figure C-19.) The exterior of the Promatek is exposed to an ISO 834 fire curve:

$$T_{ISO834} = T_0 + 345\log_{10}(8t+1), \qquad (4)$$

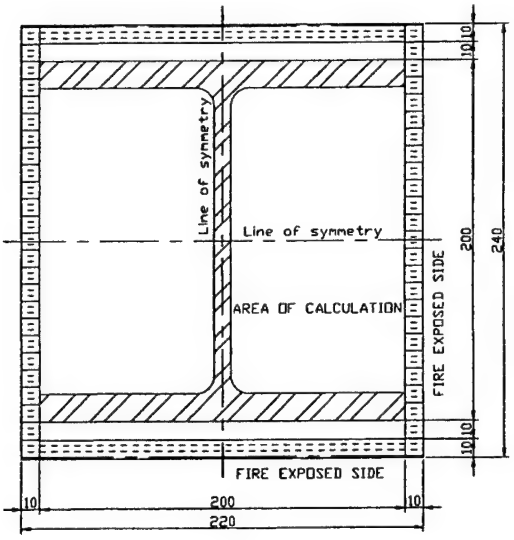

Fig. C-19 — Diagram of benchmark Reference Case 8.

where t is in minutes and the temperature is in °C (or K). The initial temperature, T_0, is 20°C. For the outside of the the assembly, $\varepsilon = 0.8$ and $h = 10$ W/(m^2·K). The thermal properties for the steel are $c = 600$ J/(kg·K), $\rho = 7850$ kg/m^3, $\varepsilon = 0.8$, and the thermal conductivity is given in Table C-5.

Table C-5 - Thermal conductivity of the steel for Reference Case 8.

Temperature T [°C]	**Thermal Conductivity k [W/(m·K)]**
20	54.0
800	27.3
1200	27.3

The thermal properties of the Promatek are $c = 1130$ J/(kg·K), $\rho = 870$ kg/m^3, $\varepsilon = 0.8$, and the thermal conductivity is given in Table C-6. As was stated previously, radiative and convective heat transfer can occur within the four gaps. The heat transfer coefficient for the top and bottom gaps is 1.5 W/(m^2·K) and it is 2.0 W/(m^2·K) for the left and right cavities. Four different meshes are used for the HEATING calculations. (See Figure C-20.) Although HEATING can match the grids used by TASEF, for the sake of simplicity these meshes are more uniform than those employed by [Wickström & Pålsson, 1999]. A transient solution is sought. The Crank-Nicolson implicit algorithm [Childs, 1998; Smith, 1987; Jaluria & Torrance, 1986] is used. The tolerance for convergence is 10^{-4}.

Table C-6 - Thermal conductivity the Promatek insulation boards for Reference Case 8.

Temperature T [°C]	Thermal Conductivity k [W/(m·K)]
0	0.174
250	0.188
1100	0.188

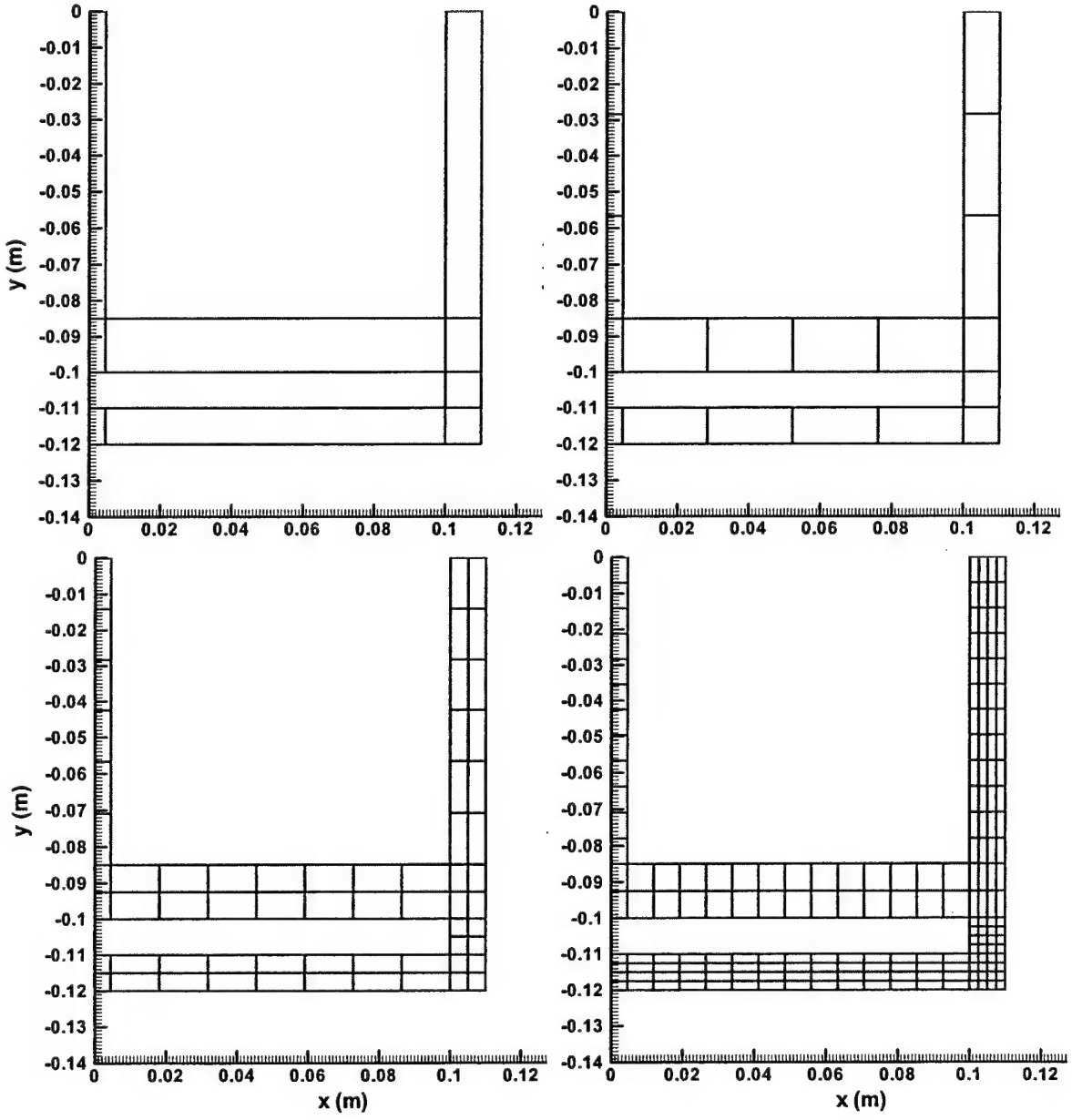

Fig. C-20 — These are quarter domains showing the four grids used for Reference Case 8. The upper left is Mesh 0, the upper right is Mesh 1, the lower left is Mesh 2, and the lower right is Mesh 3.

Figure C-21 shows the temperature contours with both radiative and convective heat transfer within the cavities after two hours of exposure to the ISO834 fire. Table C-7 shows the results for the middle flange temperature. HEATING and TASEF are in good agreement when only radiation is occurring in the cavities. The addition of convection to the cavities has a more pronounced impact on TASEF than HEATING. For both cases, the agreement between the two models improves as t increases from 30 min. Figure C-22 shows the time histories of the middle flange (x = 0 m, y = –0.0925 m) temperature. HEATING is clearly converging to its

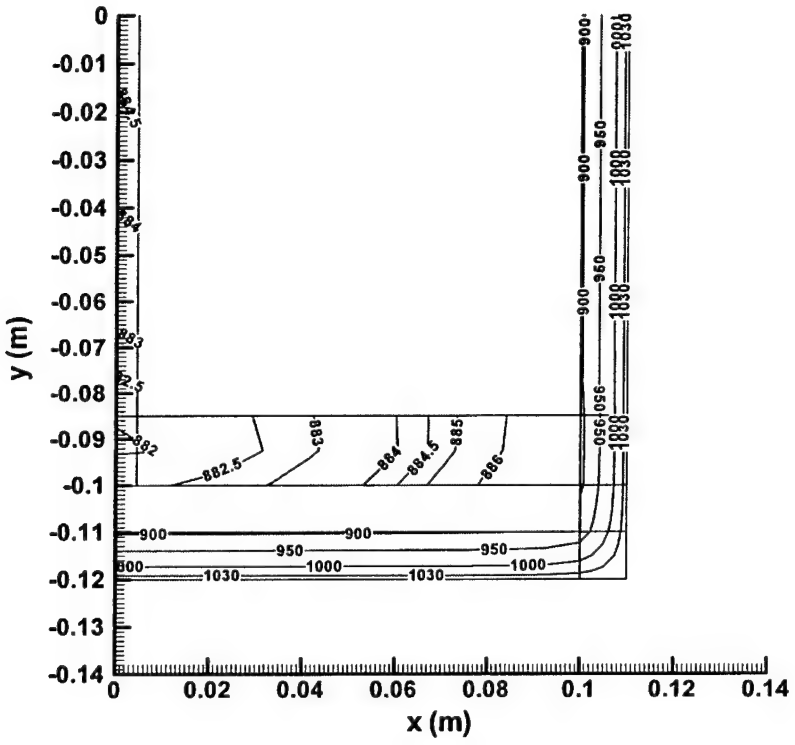

Fig. C-21 — Contours of the temperature (in °C) @ t = 120 min in a quarter of the domain for Reference Case 8 for Mesh 3.

Table C-7 - Middle flange temperature [°C] for the two models under different conditions for Mesh 3 (Reference Case 8).

Time (min)	Radiation Only			Radiation + Convection		
	TASEF	HEATING	% Diff.	TASEF	HEATING	% Diff.
30	226	230	1.77	246	232	5.69
60	518	521	0.579	536	523	2.43
90	736	738	0.272	746	739	0.938
120	879	880	0.114	885	881	0.452

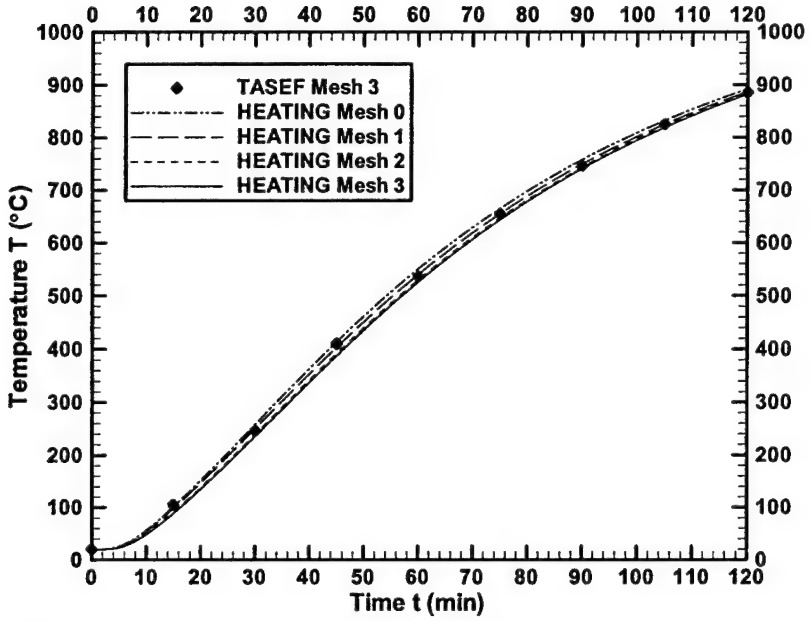

Fig. C-22 — Temperature at the center of the bottom flange for Reference Case 8. Heat transfer is by radiation and convection within the cavities.

own solution. This tends to be lower than TASEF's in the mid-time range. However, the two solutions approach each other as the temperature begins to level out. The temperature after one hour of exposure to the ISO834 fire along the L-shaped path traced from the center of the section (0 m, 0 m) to the center of the bottom flange (0 m, –0.0925 m) to the bottom right-edge of the flange (0.1 m, –0.0925 m) is shown in Figure C-23. Once again it is evident that HEATING is converging to a solution that is slightly lower than TASEF's during the temperature-rise time range.

3.0 CONCLUSIONS

HEATING has compared successfully with Reference Cases 1 through 8 of the benchmark proposed by [Wickström *et al.*, 1999]. It was found that for Cases 1 through 6, 64 cells are sufficient for satisfactory convergence with either the analytical solution or with the results calculated by TASEF. For Reference Case 7, two bottom cells suffice to yield excellent results for the one-dimensional transfer Case (7a). For the two dimensional case (7b), 8 bottom cells result in differences smaller than 3.2%. For the more complex geometry of Reference Case 8, the results for the most refined mesh are in excellent agreement with TASEF when only radiative transfer is occurring in the cavities. When convective heat transfer was added to the cavities, HEATING yielded moderately lower temperatures than TASEF.

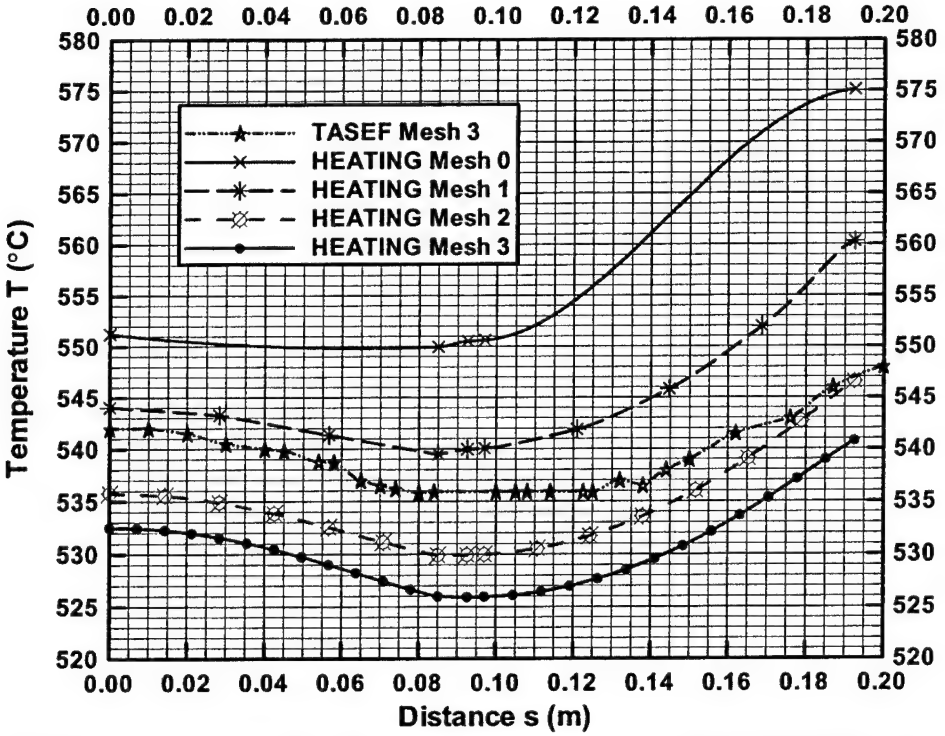

Fig. C-23 — Temperature @ t = 60 min along the L-shaped path traced from the center to the bottom right-edge of the flange for Reference Case 8. Heat transfer is by radiation and convection within the cavities.

4.0 ACKNOWLEDGMENTS

The authors would like to thank Kenneth Childs and Ulf Wickström for their comments and Heimo Tuovinen for his review of the TASEF work.

5.0 REFERENCES

1. Anderson, E., Bai, Z., Bischof, C., Blackford, S., Demmel, J., Dongarra, J., Du Croz, J., Greenbaum, A., Hammarling, S., McKenney, A., Sorensen, D. (1999), *LAPACK Users' Guide*, 3rd ed., Philadelphia, PA: SIAM.

2. Arpaci, V. S. (1966), *Conduction Heat Transfer*, Reading, MA: Addison-Wesley.

3. Becker, B. R. (1977), "A Direct Solution Technique for Solving Steady-State Problems Using the HEATING6 Heat Transfer Code," Technical Report K/CSD/TM-15, Union Carbide Corp., Nuclear Div., Gaseous Diffusion Plant, Oak Ridge, Tennessee.

4. Bryan, C. B., Childs, K. W., & Giles, G. E. (1986), "HEATING6 Verification," Technical Report K/CSD/TM-61, Oak Ridge National Laboratory, Oak Ridge, Tennessee.

5. Burden, R. L. & Faires, J. D. (1989), *Numerical Analysis*, 4th ed., Boston: PWS-Kent.

6. Carslaw, H. S., & Jaeger, J. C. (1959), *Conduction of Heat in Solids*, 2nd ed., Oxford, England: Clarendon.

7. Childs, K. W. (1990), HEATING 7.0 User's Manual, Technical Report K/CSD/INF/90-32, Martin Marietta Energy Systems, Inc., Gaseous Diffusion Plant, Oak Ridge, Tennessee.

8. Childs, K. W. (1991), "HEATING 7.1 User's Manual," Technical Report K/CSD/TM-96, Martin Marietta Energy Systems, Inc., Gaseous Diffusion Plant, Oak Ridge, Tennessee.

9. Childs, K. W. (1998), "HEATING 7: Multidimensional, Finite-Difference Heat Conduction Analysis Code System, Versions 7.2i and 7.3," RSICC Report PSR-199, Oak Ridge, Tennessee: Oak Ridge National Laboratory.

10. Childs, K. W., Giles, G. E., Bryan, C. B., & Cobb, C. K. (1990), "HEATING: A Computer Program for Multidimensional Heat Transfer Analysis (Version 6.1), Sect. F10 of SCALE: A Modular Code System for Performing Standardized Computer Analysis for Licensing Evaluation," Technical Report ORNL/NUREG/CSD-2/V2/R3, Martin Marietta Energy Systems, Inc., Oak Ridge National Laboratory, Oak Ridge, Tennessee.

11. Chu, W. (1989), "HEATCHEK: A Computer Program to Automate Verification of New Versions of HEATING," Technical Report K/CSD/INF-89/4, Union Carbide Corp., Nuclear Div., Gaseous Diffusion Plant, Oak Ridge, Tennessee.

12. Edwards, A. L. (1969), "A Compilation of Thermal Property Data for Computer Heat-Conduction Calculations," Technical Report UCRL-50589, University of California Lawrence Radiation Laboratory, Berkeley, California.

13. Edwards, A. L. & Williams, P. T. (1990), "Thermal Material Properties Library, Sect. M5 of SCALE: A Modular Code System for Performing Standardized Computer Analysis for Licensing Evaluation," Technical Report ORNL/NUREG/CSD-2/V2/R6, Oak Ridge National Laboratory, Oak Ridge, Tennessee.

14. Elrod, D. C., Giles, G. E., & Turner, W. D. (1984), "HEATING6: A Multidimensional Heat Conduction Analysis with the Finite-Difference Formulation, Sect. F10 of SCALE: A Modular Code System for Performing Standardized Computer Analysis for Licensing Evaluation," Technical Report NUREG/CR-0200, Rev. 2, U.S. Nuclear Regulatory Commission, Washington, D.C.

15. Fowler, T. B. & Volk, E. R. (1959), "Generalized Heat Conduction Code for the IBM-704 Computer," Technical Report ORNL-2734, Union Carbide Corp., Nuclear Div., Oak Ridge National Laboratory, Oak Ridge, Tennessee.

16. Gebhart, B. (1971), *Heat Transfer*, 2nd ed., New York: McGraw Hill.

17. Hamann, J., Müller R., Rudolphi, R., Schriever, R., & Wickström, U. (1999), "Anwendung von Temperatur-Berechnungsprogrammen auf kritische Referenzbeispiele des Brandschutzes," Forschungsbericht 229, Bundesanstalt für Materialforschung und-prüfung, Berlin, 1999.

18. Jaluria, Y. & Torrance, K. E. (1986), *Computational Heat Transfer*, Washington, DC: Hemisphere.

19. Liguori, T. B. & Stephenson, J. W. (1961), "The HEATING Program," Technical Report ASTRA 417-5.0, ASTRA Inc., Raleigh, NC.

20. Pålsson, J., & Wickström, U. (2000), "A Scheme for the Verification of Computer Codes for Calculating Temperature in Fire Exposed Structures," First International Workshop on Structures in Fires.

21. Patankar, S. V. (1980), *Numerical Heat Transfer and Fluid Flow*, Washington, DC: Hemisphere.

22. Pintea, D., and Franssen, J.-M. (1997), "Evaluation of the Thermal Part of the Code SAFIR by Comparison with the Code TASEF," in M. Ivan (Ed.), *Proceedings of the Eigth International Conference on Steel Structures*, vol. 2, (pp. 636-643), MIRTON, Timisoara.

23. Press, W. H., Teukolsky, S. A., Vetterling, W. T., & Flannery, B. P. (1996), *Numerical Recipes in FORTRAN 90: the Art of Parallel Programming*, 2nd ed., Cambridge, England: Cambridge University Press.

24. Press, W. H., Teukolsky, S. A., Vetterling, W. T., & Flannery, B. P. (1992), *Numerical Recipes in FORTRAN: the Art of Scientific Programming*, 2nd ed., Cambridge, England: Cambridge University Press.

25. Rudolphi, R., & Müller, R. (1980), "ALGOL – Computerprogramm zur Berechnung zweidimensionaler instationärer Temperaturverteilungen mit Anwendungen aus dem Brand- und Wärmeschutz", Forschungsbericht 74, Bundesanstalt für Materialprüfung, Berlin, 1980.

26. Siegel, R., & Howell, J.R. (1992), *Thermal Radiation Heat Transfer*, 3rd ed., Washington, DC: Hemesphere.

27. Smith, G. D. (1987), *Numerical Solution of Partial Differential Equations: Finite Difference Methods*, 3rd (corrected) ed., Oxford, England: Clarendon.

28. Sterner, E., & Wickström, U. (1990), "TASEF - Temperature Analysis of Structures Exposed to Fire," SP Report 1990:05, SP Swedish National Testing and Research Institute, Borås, Sweden, 1990.

29. Turner, W. D. & Crowell, J. S. (1969), "Notes on HEATING - An IBM 360 Heat Conduction Program," Technical Report CTC/INF-980, Union Carbide Corp., Nuclear Div., Oak Ridge National Laboratory, Oak Ridge, Tennessee.

30. Turner, W. D., Elrod, D. C., & Siman-Tov, I. I. (1977), "HEATING5 - An IBM 360 Heat Conduction Program," Technical Report ORNL/CSD/TM-15, Union Carbide Corp., Nuclear Div., Oak Ridge National Laboratory, Oak Ridge, Tennessee.

31. Turner, W. D. & Siman-Tov, I. I. (1971), HEATING3 – "An IBM 360 Heat Conduction Program," Technical Report ORNL/TM-3208, Union Carbide Corp., Nuclear Div., Oak Ridge National Laboratory, Oak Ridge, Tennessee.

32. Wickström, U. (1979), "A Numerical Procedure for Calculating Temperature in Hollow Structures Exposed to Fire," Report 79-3, Lund, Sweden: Lund Institute of Technology.

33. Wickström, U. (1999), "An Evaluation Scheme of Computer Codes for Calculating Temperature in Fire Exposed Structures," in S. Grayson (Ed.), *Interflam '99* (pp. 1033-1044), London: Interscience Communications Ltd.

34. Wickström, U., & Pålsson, J. (1999), "A Scheme for the Verification of Computer Codes for Calculating Temperature in Fire Exposed Structures," SP Report 1999:36, Borås, Sweden: SP Swedish National Testing and Research Institute.

6.0 NOMENCLATURE

Roman

A	Area [m^2]
c	Specific heat [J/(kg·K)]
c_p	Specific heat at constant pressure [J/(kg·K)]
$\mathbf{E}$	Emissivity-shape factor matrix []
$\mathbf{F}$	Shape factor matrix []
f	A generic function [varies]
$\mathbf{G}$	Absorption factor matrix []
$\mathbf{H}$	Effective conductance matrix [m^2]
h	Heat transfer coefficient or exponent [W/(m^2·K)]
k	Thermal conductivity [W/(m·K)]
L	Distance [m]
M	A number of nodes []

N	The number of nodes in a cavity []
n	Normal coordinate [m]
q	Heat (energy) [J]
$\mathbf{R}$	Reflectivity-shape factor matrix []
S	Distance [m]
s	Distance [m]
T	Temperature [°C]
t	Time [s]
V	Volume [m^3]
w	Width [m]
$\mathbf{x}$	The Cartesian position vector, equal to (x, y, z) [(m,m,m)]
x	The first Cartesian coordinate [m]
y	The second Cartesian coordinate [m]
z	The third Cartesian coordinate [m]

Greek

α	Thermal diffusivity [m^2/s]
γ	Ratio of the specific heats []
Δ	Difference operator []
Φ	Transfer factor matrix []
ρ	Density [kg/m^3]
ρ	Reflectivity []
σ	Stefan-Boltzmann constant [5.669×10^{-8} $W/(m^2\cdot K^4)$]

Superscripts

$\bullet$	Quantity per unit time [s^{-1}]
$'$	First derivative
$'$	Quantity per unit length [m^{-1}]
$''$	Quantity per unit area [m^{-2}]
$'''$	Quantity per unit volume [m^{-3}]

Subscripts

0	Denotes an initial quantity

e	Denotes a natural convection exponent
i	An index
j	An index
k	An index
l	An index
n	An index ; denotes a natural convection quantity
f	Denotes a forced convection quantity
G	Denotes a gas quantity
r	Denotes a radiation quantity
S	Denotes a solid quantity
s	Denotes a surface quantity
x	Denotes an x-coordinate quantity
y	Denotes a y-coordinate quantity
z	Denotes a z-coordinate quantity
∞	Denotes an ambient quantity

APPENDIX A: DEVELOPMENT OF CAVITY HEAT TRANSFER ALGORITHMS

INTRODUCTION

This appendix details the methods employed to facilitate the calculation of heat transfer in voids using HEATING 7.3. The term "connectors" is used to describe data blocks for the radiative and convective conductance between any two nodes. The results have been verified using the two relevant examples recommended in [Wickström & Pålsson, 1999; Wickström, 1999; Pålsson & Wickström, 2000].

DIFFUSE, GRAY SURFACE RADIATIVE HEAT TRANSFER

It is assumed that the surfaces participating in radiative exchange have emissivities that essentially do not vary with the wavelength of the radiation (i.e., they are gray) and that reflections off of a surface are diffuse. The ratio of the mean surface roughness to the median (or bounding) radiation wavelength serves as a measure for the type of reflection [Siegel & Howell, 1992]. If it is less than one, the reflections are specular. If it is greater than one, it is diffuse. A FORTRAN 95 program, h7_3radconn, has been written to create the CONNECTORS file for two dimensional, diffuse-gray radiative transfer. As its name implies, h7_3radconn is intended to work in conjunction with version 7.3 of HEATING. It performs two basic tasks: it calculates the node-to-node shape and transfer factors.

SHAPE FACTORS

The method of crossed strings [Siegel & Howell, 1992] is used to determine the shape factors between cells. The area for the i^{th} cell is denoted A_i. The shape factor from cell i to cell j is F_{ij}. The method of crossed strings makes use of the two shortest distances from cell edges, S_{ij1}, S_{ij2} (these are the "straight strings"), and the two longest distances that can be measured from one cell's edge to another, L_{ij1}, L_{ij2} (these are the "crossed strings"). The formula for the shape factor is

$$A_i F_{ij} = \frac{1}{2}\left(L_{ij1} + L_{ij2} - S_{ij1} - S_{ij2}\right) \qquad (5)$$

HEATING 7.3 actually needs values at nodes so the area for each node is the sum of half the area of the two cells surrounding the node. (The emissivity for the node adjoining two disparate surfaces is determined in a similar fashion. The half-cell-area average of the emissivities of the two abutting materials is used.) However, for internal corners, the projected area (i.e., the hypotenuse) is used.

ABSORPTION FACTORS

HEATING's method for calculating the radiative heat transfer for node i, $\dot{q}_i$, is

$$\dot{q}_i = \sigma A_i \sum_{j=1}^{N} \Phi_{ij} \left(T_i^4 - T_j^4 \right). \qquad (6)$$

Φ_{ij} is the (Hottel) transfer factor. It is the fraction of the black body thermal energy between cells i and j that can be exchanged due to the geometry and reflectivity of ALL the participating surfaces (nodes in this case). Φ_{ij} can be related to the absorption factor, G_{ij}, via the formula

$$\Phi_{ij} = \varepsilon_i G_{ij}. \qquad (7)$$

ε_i is the emissivity for surface i. The reflectivity for surface k, ρ_i, is

$$\rho_i = (1 - \varepsilon_i). \quad (8)$$

G_{ij} is the fraction of the emission from surface i that reaches surface j and is absorbed. Like the shape factor, it sums to unity for each surface. I.e.,

$$\sum_{j=1}^{N} G_{ij} = 1 \qquad \forall i. \qquad (9)$$

The reciprocity relation is

$$A_i \varepsilon_i G_{ij} = A_j \varepsilon_j G_{ji}. \qquad (10)$$

Note that this implies that

$$A_i \Phi_{ij} = A_j \Phi_{ji}, \qquad (11)$$

which is completely analogous with the shape factor reciprocity relation. Although for a flat surface $F_{ii} = 0$, this is generally not so for G_{ii} since energy emitted by surface i can be reflected back to surface i and be subsequently (fractionally) absorbed. An analysis of the energy that is absorbed by each surface [Gebhart, 1971; Siegel & Howell, 1992] results in the matrix equation

$$\mathbf{RG} = \mathbf{E}. \qquad (12)$$

The components of the reflectivity-shape factor matrix, $\mathbf{R}$, are

$$R_{ij} = \begin{cases} -\rho_j F_{ij} & i > j \\ 1 & i = j \\ -\rho_i F_{ji} & j > i \end{cases} \qquad (13)$$

and for the emissivity-shape factor matrix, $\mathbf{E}$, they are

$$E_{ij} = \varepsilon_j F_{ij}. \qquad (14)$$

Experience has shown that if all the $\varepsilon_i < 1$, then the matrix $\mathbf{R}$ is generally dense, strictly row-and-column diagonally dominant, and non-symmetric. If all the $\varepsilon_i = 1$, then the matrix $\mathbf{R}$ is generally sparse, strictly row-and-column diagonally dominant, and symmetric.

The program that determines the shape factor also solves Equation (**Error! Reference source not found.**). The user can choose different numeric methods to achieve the solution. The available methods are LU decomposition [Anderson et al., 1999], Gauss-Jordan elimination [Press et al., 1996; Press et al., 1993], diagonal pivoting [Anderson et al., 1999], QR decomposition [Anderson et al., 1999], and singular value decomposition [Anderson et al., 1999]. It is recommended that for each new geometry, the HEATING 7.3 connections file be determined by at least two of these methods.

CONVECTIVE HEAT TRANSFER IN A CAVITY

HEATING 7.3 can readily model convective heat transfer at external solid boundaries because the ambient temperature is assumed to be known. If the boundary is part of a closed cavity, the background temperature will be changing. A method is presented in this appendix that addresses this issue of determining $T_\infty(t)$, the background temperature as a function of time. As before, HEATING 7.3 needs values at nodes so the area for each node is the sum of half the area of the two cells surrounding the node. For any corner, the half area of each branch is used since convection depends on the "wetted" area.

[Wickström & Pålsson, 1999] suggest letting $T_\infty(t)$ be equal to the average temperature for all the cells in the cavity. In order to impliment this in HEATING using connections, first consider how HEATING models convective heat transfer for node i:

$$\dot{q}_i = A_i h_i \left(T_i - T_\infty(t)\right). \qquad (15)$$

For now it is assumed that the heat transfer coefficient, h_i, is constant. HEATING also allows node i to participate with any number (say, M) of nodes,

$$\dot{q}_i = h_i \sum_{j=1}^{M} H_{ij} \left(T_i - T_j\right), \qquad (16)$$

where H_{ij} is the effective conductance matrix associated with nodes i and j. The effective conductance is

$$h_i H_{ij}. \qquad (17)$$

Applying Wickström and Pålsson's suggestion to Equation (**Error! Reference source not found.**) results in

$$\dot{q}_i = A_i h_i \left(T_i - \frac{\oint_A T(s,t)\mathrm{d}s}{A} \right), \qquad (18)$$

where A is the total length (per unit depth) of the cavity perimeter and s is the coordinate about the closed loop of the cavity. Replacing the integral with the middle Riemann sum (i.e., by the mid-point method [Burden & Faires, 1989]) yields

$$\dot{q}_i = A_i h_i \left(T_i - \frac{\sum_{j=1}^{N} A_j T_j}{A} \right). \qquad (19)$$

For the present two-dimensional Cartesian coordinate system, A_j is the cell length associated with node j. Equation (**Error! Reference source not found.**) can be written as

$$\dot{q}_i = A_i h_i \left(\frac{\sum_{j=1}^{N} A_j T_i}{A} - \frac{\sum_{j=1}^{N} A_j T_j}{A} \right) \qquad (20)$$

because $\sum_{j=1}^{N} A_j = A$. Further rearrangement results in

$$\dot{q}_i = h_i \sum_{j=1}^{N} \frac{A_i A_j}{A} \left(T_i - T_j \right). \qquad (21)$$

Here, $A_i A_j / A$ is, by comparison with Equation (**Error! Reference source not found.**), the conductance matrix. This conductance matrix,

$$H_{ij} = \frac{A_i A_j}{A}, \qquad (22)$$

is calculated as the input for HEATING 7.3 CONNECTOR lines. Note that the procedure presented in this section could also have been carried out by using the arithmetic mean. The result would replace the term A_j / A in Equation (**Error! Reference source not found.**) with $1/N$. In fact, if the step-size around the cavity is constant, $A_j / A = 1/N$. However, for nonuniform gridding, the area-averaged approach is clearly the correct one.

APPENDIX D

HEATING VALIDATION

HEATING 7.3 Validation For Fire Resistive Applications IN SUPPORT OF T-AKE Test And Evaluation

SEAN P. HUNT
JAVIER TRELLES

Hughes Associates, Inc.
Baltimore, MD

FREDERICK W. WILLIAMS

Naval Research Laboratory
Naval Technology Center for Safety and Survivability
Washington, DC

August 21, 2003

CONTENTS

TABLES

FIGURES

HEATING 7.3 VALIDATION FOR FIRE RESISTIVE APPLICATIONS

1.0 INTRODUCTION

A series of eight validation cases were selected to validate the thermal computer model HEATING. These entail thermal calculations of increasing complexity. The algorithms used by HEATING have been previously verified in Trelles *et al.* [2003] and Bryan *et al.* [1986]. The focus of these validation cases is to compare the calculated results of HEATING with test data for various configurations.

The validation cases were selected to address the following aspects of a numerical heat transfer calculation:

- Variable convective and thermal radiation boundary conditions;
- Variable thermal material properties;
- Multiple materials; and
- Radiation and convection in voids.

In addition, the sensitivity of the results to the boundary condition parameters, material properties, convergence criteria, and the numerical solution method were investigated. This was accomplished by varying the boundary condition parameters and material properties for which there are degrees of uncertainty, increasing the resolution of the solution grid, using different numerical methods, and changing the solution error tolerances.

The validation cases were selected from available test data involving fire tests of building materials, insulation materials, and composite materials. The availability of material properties, the type of exposure conditions, and the reliability of the exposure and sample temperature data were also factors in selecting the validation cases.

2.0 BACKGROUND

HEATING was developed at the Oak Ridge National Laboratory's (ORNL) Radiation Safety Information Computational Center (RSICC) [Childs, 1998]. The model was created to analyze the thermal impact of the U.S. Energy Department's various high energy projects, including all aspects of radiation shielding. It has one of the longest development histories of any computational heat transfer software package [Fowler *et al.*, 1959; Liguori *et al.*, 1961; Turner *et*

al., 1969; Turner *et al.*, 1971; Turner *et al.*, 1977; Becker, 1977; Elrod *et al.*, 1984; Bryan *et al.*, 1986; Childs, 1990; Childs *et al.*, 1990; and Childs, 1991]. Verification studies and tools for HEATING can be found in Bryan *et al.* [1986], Chu, 1989], and more recently in Trelles *et al.* [2003].HEATING is a field model. It solves, using finite volume techniques [Patankar, 1980; Childs, 1998], the following heat equation [Arpaci, 1966; Carslaw *et al.*, 1959]:

$$\rho c \frac{\partial T}{\partial t} = \nabla \cdot (k \nabla T) + \dot{q}''', \qquad 23)$$

subject to the general boundary condition:

$$\dot{q}_s'' = -k \frac{\partial T_s}{\partial n} = \left\{ h_f + h_n \left| T_s - T_\infty \right|^{h_e} + h_r \left(T_s^2 + T_\infty^2 \right) \left(T_s + T_\infty \right) \right\} \left(T_s - T_\infty \right)$$

or (24)

$$T_s = f_s(\mathbf{x}, t)$$

where T is the material internal temperature (K), ρ is the density (kg/m^3), c is the specific heat (kJ/kg), t is the time (s), $\dot{q}'''$ is the volumetric heat generation rate (kJ/kg-s), $\dot{q}_s''$ is the heat flux for surface s (kW/m^2), n is the coordinate normal to the surface, k is the thermal conductivity (kW/m-K), T_s is the material surface temperature (K), f_s is a temperature function associated with surface s, T_∞ is the ambient temperature (K), h_f is the heat transfer coefficient for forced convection (kW/m^2-K), h_n is the heat transfer coefficient for natural convection (kW/m^2-K^{h_e}), h_e is the exponent for natural convection, h_r is the thermal radiation heat transfer coefficient (kW/m^2-K^4).

HEATING 7.2i and 7.3 are the most recent developments in a series of heat-transfer codes distributed by RSICC as SCA-1/HEATING5 and PSR199/HEATING 6. HEATING7 can solve steady-state and/or transient heat conduction problems in one-, two-, and three-dimensional Cartesian, cylindrical, or spherical coordinates. The following are some notable features of HEATING 7.

- Multiple materials may be used.
- Material properties may be both time- and/or temperature-dependent. Thermal conductivity may be anisotropic and materials may undergo a phase change.
- Material properties may be inputed directly or extracted from a material properties library provided with the model.
- Heat generation rates may be a function of time, temperature, and/or position.
- Boundary temperatures may be time- and/or position-dependent.
- Boundary conditions may be surface-to-environment or surface-to-surface. They may consist of a specified temperature or a combination of prescribed heat flux, forced convection, natural convection, and thermal radiation.
- Boundary condition parameters may be time- and/or temperature dependent.

- General gray-body radiation problems may be modeled with user-defined factors for radiant exchange. Surfaces that are not in contact can exchange heat via custom connectors. The mesh spacing may be variable along each axis.

The HEATING calculations were performed on the following computer systems:

- Linux workstation with two Pentium III Xeon processors, 1 GB of RAM memory, and 19 GB of storage;
- Silicon Graphics, Inc. Octane2 graphics workstation with V6® graphics, two R12,000A processors, 2 GB of RAM memory, and more than 136 GB of storage; and;
- Dell workstation with a single Pentium 4 processor, 1 GB of RAM memory, and 80 GB of storage.

3.0 VALIDATION

The validation set for HEATING consists of eight cases of increasing complexity. The basis for comparison between a validation case and HEATING includes temperatures at a specific time and location, transient temperatures at a specific position, and average temperature at a specific time. The particular metrics vary among the validation cases due to the nature of the data available for comparison. The validation cases and the comparison basis are summarized in Table D-1 below.

Table D-1 — Summary of HEATING Validation Cases

Validation Case	Description	Key Elements	Validation Basis
1	Bare steel plate heated by known transient temperature profile.	1-D thermal analysis, material properties of steel well documented, boundary conditions deduced from measurements.	Transient surface temperatures.
2	Concrete section heated by ASTM E119 Standard Time-Temperature profile.	1-D thermal analysis, properties for concrete documented, includes water vaporization in concrete, thermocouple pads.	Fire resistance rating, unexposed surface temperature at a fixed time.
3	Aluminum protected with Unifrax high temperature mineral fiber blanket; assembly exposed to test conditions specified by IMO A.754(18).	1-D thermal analysis with multiple materials. Thermal material properties of insulation material are proprietary, thermocouple pads.	Fire resistance rating, transient surface temperatures.
4	Steel protected with mineral fiber insulation – exposed to an empirical furnace curve	1-D thermal analysis, material properties of steel and Structo-gard are well documented.	Transient surface temperatures.

Table D-1 — Summary of HEATING Validation Cases (Continued)

Validation Case	Description	Key Elements	Validation Basis
5	Unprotected steel column filled with concrete in web area exposed to ASTM E119 Standard Time-Temperature profile.	2-D thermal analysis analogous to Validation Case 2.	Transient average temperatures, fire resistance rating.
6	Steel beam protected with Blazeshield D-C/F insulation exposed to ASTM E119 Standard Time-Temperature profile (UL Design J907).	2-D thermal analysis involving steel W8X28 beam protected with Blazeshield D-C/F spray applied mineral fiber insulation supporting unprotected concrete floor, material properties documented.	Fire resistance rating, average steel temperature at a fixed time.
7	Steel beam protected with Blazeshield D-C/F insulation exposed to ASTM E119 Standard Time-Temperature profile (UL Design P809).	2-D thermal analysis involving steel W8X28 beam and concrete floor protected with Blazeshield D-C/F spray applied mineral fiber insulation, material properties documented.	Fire resistance rating, average steel temperature at a fixed time.
8	Gypsum-steel wall assembly exposed to CAN/ULC-S101-M89 Standard Time-Temperature profile.	2-D thermal analysis involving a radiation and convection heat transfer in a cavity space, material properties of gypsum and steel well documented.	Transient surface temperatures.

Convergence was verified for each validation case by increasing the number of nodes, decreasing the time step, decreasing the error tolerance, and/or altering the solution method.

3.1 Validation Case 1: Bare Steel Deck Exposed to Known Transient Temperature

Validation Case 1 consists of bare steel deck exposed to a post-flashover fire environment. The post-flashover fire was approximated in a cubical enclosure measuring 2.4 m by 2.4 m by 2.4 m using a JP-5 spray fire [Leonard *et al.*, 1991]. The enclosure was constructed of 0.95 cm thick steel plates. The temperature in the compartment as well as the exposed and unexposed surface temperatures of the steel were measured as a function of time.

The validation basis is the average deck exposed and unexposed temperature as a function of time. The input parameters include the thermal material properties of the steel and the exposed and unexposed surface boundary conditions. A one-dimensional thermal analysis is used to calculate the exposed and unexposed surface temperature of the steel plate as a function of time. Figure D-1 depicts the configuration modeled by HEATING. The thermal material properties for steel were obtained from Abrams [1979]. Figure D-2 shows the thermal conductivity and heat capacity as a function of temperature for A36 steel. The spike in the heat capacity

corresponds to the perlite-austenite transformation, which typically occurs between 700°C and 850°C [Abrams, 1979]. A density of 7,800 kg/m^3 is assumed for the steel [Holman, 1990].

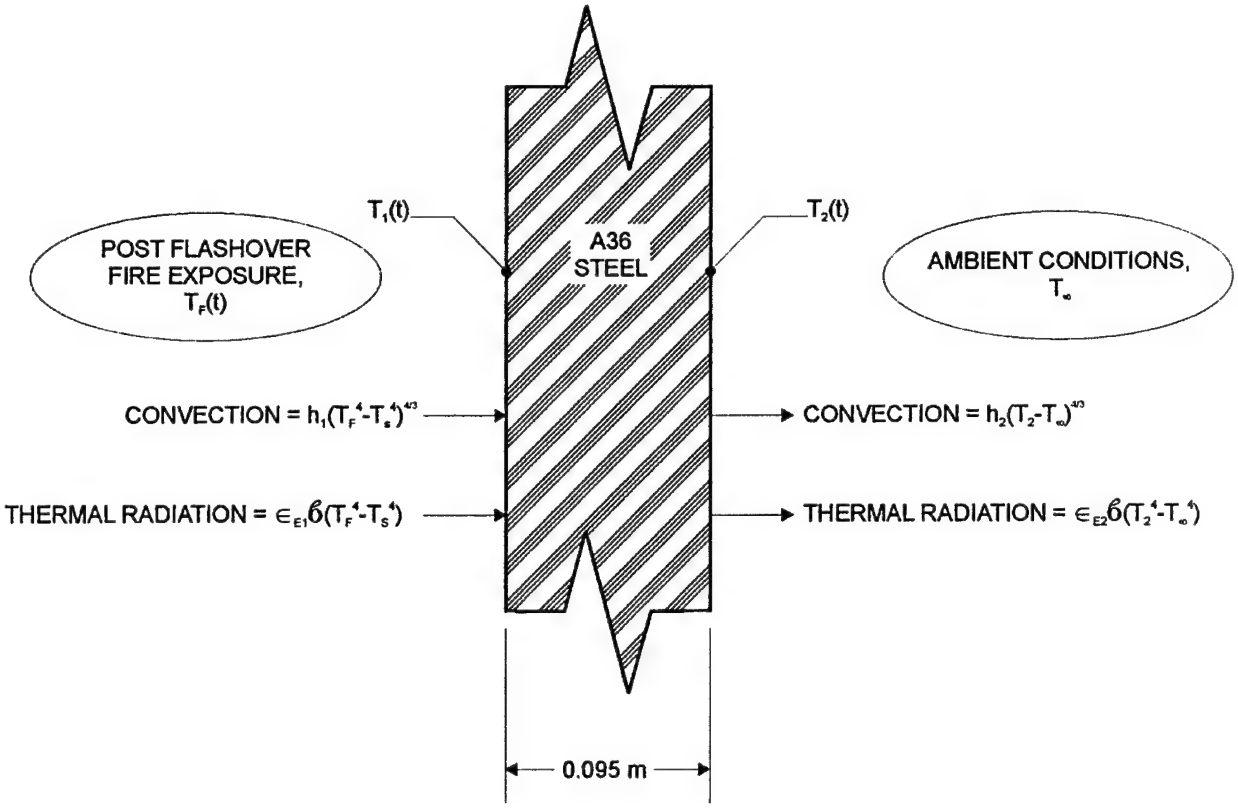

Fig. D-1 — Validation Case 1 (Not to Scale)

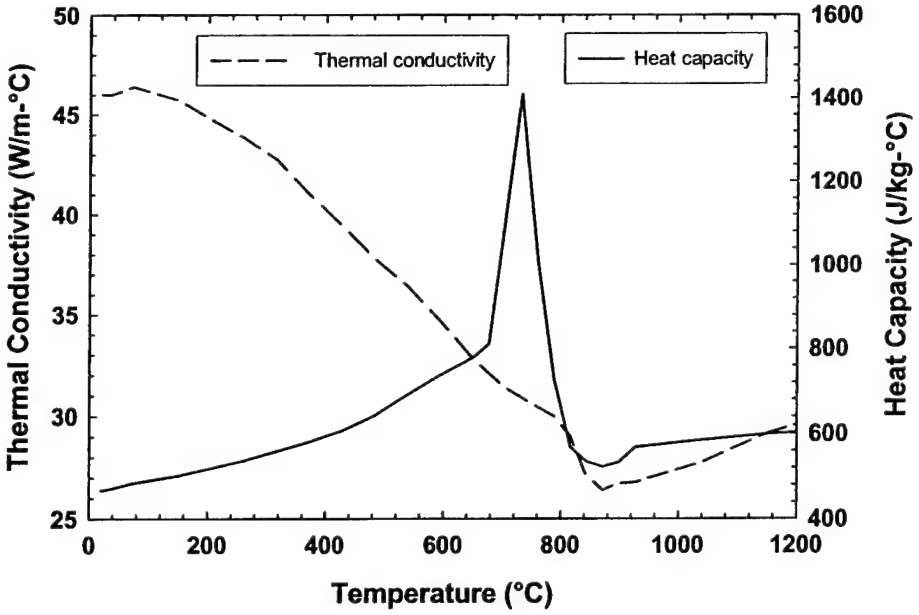

Fig. D-2 — Thermal Material Properties for A36 Steel [Abrams,1979]

Boundary Conditions

A natural convection boundary condition was applied to the exposed and unexposed surface of the steel in the following form [Holman, 1990]:

$$\dot{q}_c'' = h_n \cdot \left(\left|T_s - T_A\right|\right)^{4/3} \qquad (3)$$

where $\dot{q}_c''$ is the convective heat flux boundary condition (W/m^2), h_n is the effective natural convection coefficient (W/m^2-°C$^{4/3}$), T_s is the steel surface temperature (K), and T_A is the ambient/exposure temperature (K). Equation 3 is applicable to heated plates facing up (on the unexposed boundary) or cooled plates facing down (on the exposed boundary condition) when the convection coefficient is 1.52 W/m^2-°C$^{4/3}$ [Holman, 1990].

A thermal radiation boundary condition was applied to the exposed and unexposed surface of the steel in the following form assuming a gray gas and/or surfaces that have the same radiosity [Holman, 1990; Bird *et al.* 1960]:

$$\dot{q}_r'' = \varepsilon_E \sigma F\left(T_s^4 - T_A^4\right) \qquad (4)$$

where $\dot{q}_r''$ is the thermal radiation heat flux boundary condition (W/m^2), ε_E is the resultant (effective) emissivity between the steel surface and the ambient environment, and F is the view factor between the exposure and the surface. Note that the heat flux would be negative (*i.e.* the steel gains energy) if the ambient temperature is greater than the steel temperature and *vice*

versa. The resultant effective emissivity was determined using the following equation [Barnett, 1989; Bird *et al.* 1960; Pettersson *et al.*, 1976]:

$$\varepsilon_E = \frac{1}{1/\varepsilon_A + 1/\varepsilon_S - 1} \qquad (5)$$

where ε_A is the emissivity of the ambient environment and ε_S is the emissivity of the steel. The emissivity of steel is 0.8 and the emissivity of the ambient environment on the unexposed side of the steel is assumed to be 0.95 [Holman, 1990; Sparrow *et al.*, 1978; Incropera *et al.*, 1985]. The emissivity of the fire exposure/compartment surfaces was determined from the test data to be approximately 0.7, which takes into account surfaces which may be at different temperatures due to the formation of a smoke layer in the test compartment. The view factor was unity between ambient environment and the steel on the exposed and unexposed surfaces. As such, the effective emissivity on the exposed steel surface was 0.6 and 0.77 on the unexposed steel surface.

Results

The implicit Crank-Nicolson method [Childs, 1998; Smith, 1987; Jaluria *et al.*, 1986] was used to solve for the steel plate surface temperature. The tolerance for convergence was 1×10^{-6} and the solution time step was 0.5 seconds. Decreasing the tolerance, decreasing the time step, or using the Classical Explicit Procedure or Classical Implicit Procedure produced the same results.

The validation results are shown in Figure D-3 for a model using twenty cells. Also shown in Figure D-3 is the measured exposure temperature profile. The results did not change when the number of cells was increased to one hundred.

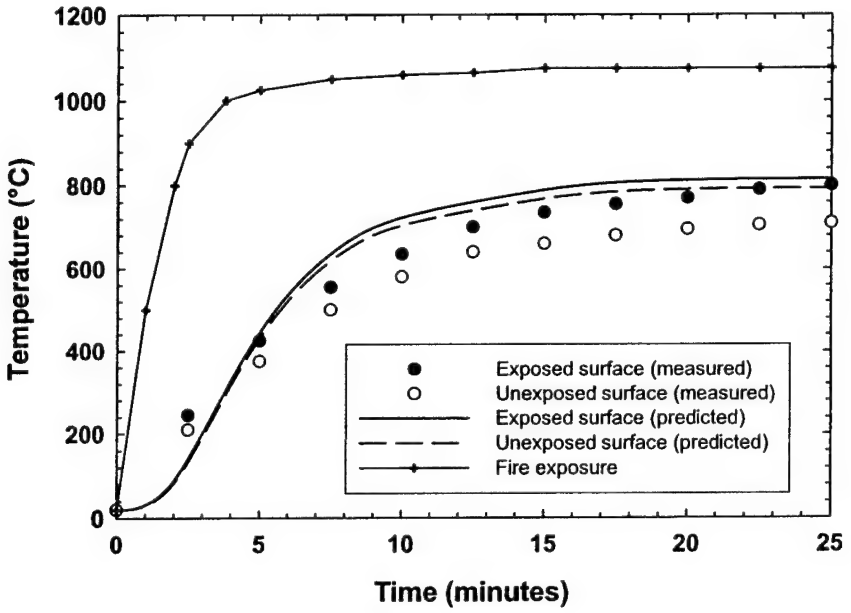

Fig. D-3 — Validation Case 1 Temperature Results – Twenty Cell Model

Figure D-3 shows good agreement between the measured and calculated exposed steel surface temperature. However, the measured unexposed surface temperature is considerably lower than the calculated unexposed surface temperature. The test data indicate that there is an approximately 90 °C temperature difference between the exposed and unexposed steel surfaces whereas the calculated temperature difference is approximately 20 °C. The measured temperature difference likely includes heat loss effects around the thermocouples that are not included in the thermal model. This may be seen when considering the quantity of energy that

the steel transmits via conduction from one surface to the other. The following equation from Holman [1990] can be used to calculate this effect:

$$\dot{q}_s'' = \frac{k}{\delta}(T_1 - T_2) \qquad (6)$$

where $\dot{q}_s''$ is the energy conducted through the steel (kW/m^2), k is the thermal conductivity of the steel (kW/m-°C), δ is the thickness of the steel (m), and T_1 and T_2 are the exposed and unexposed surface temperatures (°C), respectively. The thermal conductivity of steel is about 0.03 kW/m-°C when the steel temperature is 800 °C, as seen in Figure D-2. If the temperature difference between the exposed and unexposed surfaces were 90 °C as measured 25 minutes after initial exposure, then the energy conducted through the steel would be about 284 kW/m^2, as calculated using Equation 6 for 9.5 mm thick steel. Because the steel temperature is increasing slowly at 25 minutes, most of this energy would have to be radiated and convected into the ambient area. This would require a blackbody surface temperature around 1,200°C, which greatly exceeds the measured surface temperatures, exposed or unexposed. If the temperature difference between the exposed and unexposed surfaces is closer to 20°C, as calculated by HEATING, then the energy conducted through the steel would be about 60 kW/m^2, which is closer to the expected boundary heat loss for a blackbody surface temperature in the 800°C range and an ambient temperature of 20°C.

Sensitivity of Results to Input Parameter Assumptions

The sensitivity of the calculated temperatures to the assumed boundary conditions was investigated by increasing and decreasing the effective emissivity of the exposed and unexposed surfaces. The convection coefficient was also increased and decreased by twenty-five percent. The results are shown in Figure D-4 for the exposed steel surface temperature. The figure indicates that the calculated steel surface temperature may vary by plus or minus 50°C depending on the selection of the effective emissivity. The calculated temperature is less sensitive to the convection coefficient. The figure also indicates that increasing the effective emissivity has opposite impacts on the calculated temperature when applied to the exposed versus unexposed surface. The same is true for decreasing the effective emissivity. This suggests that there is some compensating effects such that the combined impact of an incorrect effective emissivity would be less than that shown in Figure D-4, as it is unlikely that the effective emissivity would be increased on one surface and decreased on another.

3.2 Validation Case 2: Concrete Wall Section Exposed to the ASTM E119 Standard Time-Temperature Fire Exposure

Validation Case 2 involves a concrete wall section exposed to the ASTM E119 Standard Time-Temperature Curve. The ASTM E119 Standard Time-Temperature fire exposure is intended to bound a compartment fire temperature exposure during post-flashover fire conditions [ASTM E119-98, 1999; Lie, 1995]. The wall is assumed to consist of one of three types of concrete: carbonate aggregate normal weight concrete, siliceous aggregate normal weight concrete, and lightweight aggregate concrete. Carbonate aggregate normal weight concrete is concrete made with aggregate consisting mainly of calcium carbonate or magnesium carbonate,

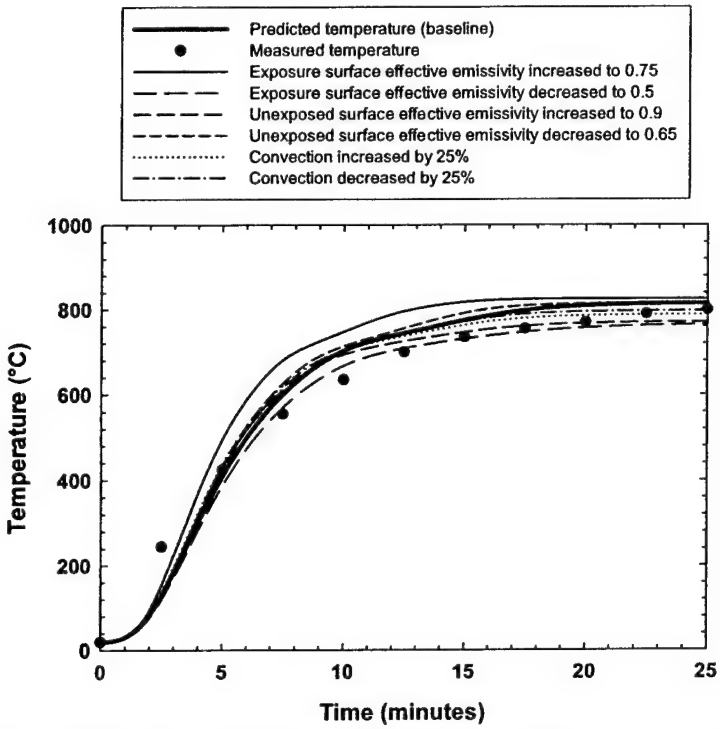

Fig. D-4 — Sensitivity of the Calculated Exposed Steel Surface Temperature Predictions to Uncertainty in the Boundary Condition Parameters

typically limestone or dolomite, and has a dry unit weight between 2,200 kg/m3 and 2,400 kg/m3 [ASCE 29-99, 1998; Harmathy, 1983; Lie, 1972]. Siliceous aggregate normal weight concrete also has a dry unit weight between 2,200 kg/m^3 and 2,400 kg/m^3 and is made with aggregate consisting mainly of silica or compounds other than calcium carbonate or magnesium carbonate [ASCE 29-99, 1998; Harmathy, 1983; Lie, 1972]. Lightweight aggregate concrete is made with aggregates of expanded clay, shale, slag, slate or sintered fly ash and has a dry unit weight of 1,360 – 1,840 kg/m^3 [ASCE 29-99, 1998; Lie, 1972]. Because the thermal material properties vary with the nature of the aggregate, the fire resistance rating of a concrete wall varies with the type of aggregate. As such, this section considers wall sections made with each of the three aggregates separately.

The basis for the validation case is the fire resistance rating of the concrete wall, which is defined as a temperature rise of 139°C on the unexposed side of the wall per ASTM E119 [1999]. A one-dimensional thermal analysis is used to calculate the fire resistance rating of the concrete wall sections. Figure D-5 depicts the configuration modeled by HEATING. Fire resistance ratings between 1 hr and 4 hrs for each of the three types of concrete noted above are used for the validation basis [ASCE 29-99, 1998; Fleischmann, 1995]. The fire resistance ratings for the wall sections are based on tests reported by Abrams *et al.* [1968]. Per ASTM

E119, thermocouples used to measure the unexposed wall surface temperature are covered with pads in an attempt to simulate contact with a combustible material. Because the thermocouple pads affect the temperature profile in the wall, they are included in the thermal model used in this validation case.

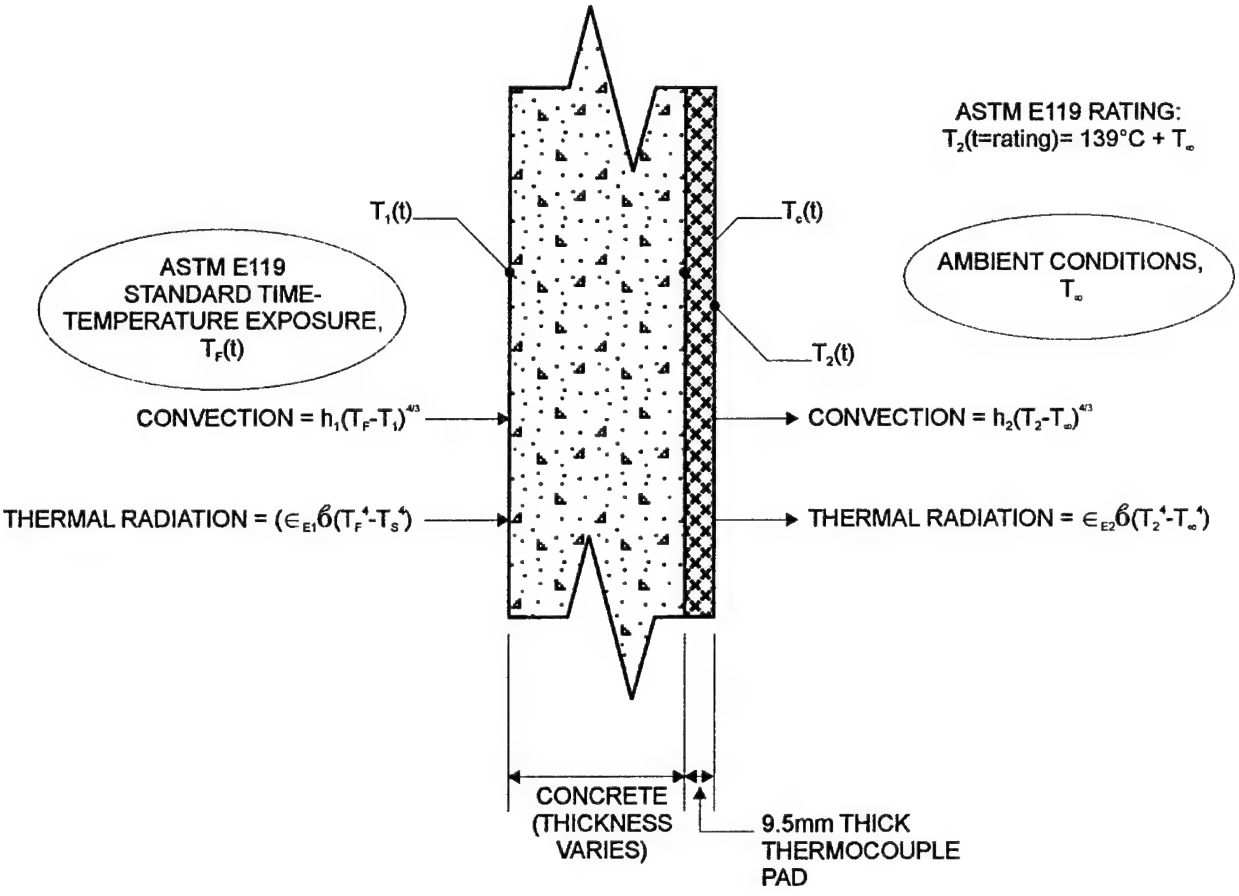

Fig. D-5 — Validation Case 2 (Not to Scale)

Material Properties

The material properties that are necessary for calculating the fire resistance rating of the concrete wall section are the thermal conductivity, the heat capacity, the density, and the percent moisture content of the concrete and the thermal conductivity, heat capacity, and the density of the thermocouple pad. Figures D-6 and D-7 show the thermal conductivity and heat capacity as a function of temperature for carbonate and siliceous aggregate normal weight concretes and lightweight concrete assumed in this evaluation [Harmathy, 1983; Lie, 1972]. Material properties vary considerably amongst concretes [Flynn, 1999] and were the primary focus of the sensitivity evaluation. The actual material properties of the concrete that was the basis for the fire resistance ratings was unknown. A general assumption applied to this validation case was that the upper bound thermal conductivity values for the particular aggregate apply. The density of each concrete is as follows:

- Carbonate aggregate, normal weight: 2,136 kg/m^3;
- Siliceous aggregate, normal weight: 2,300 kg/m^3; and
- Lightweight: 1,150 kg/m^3.

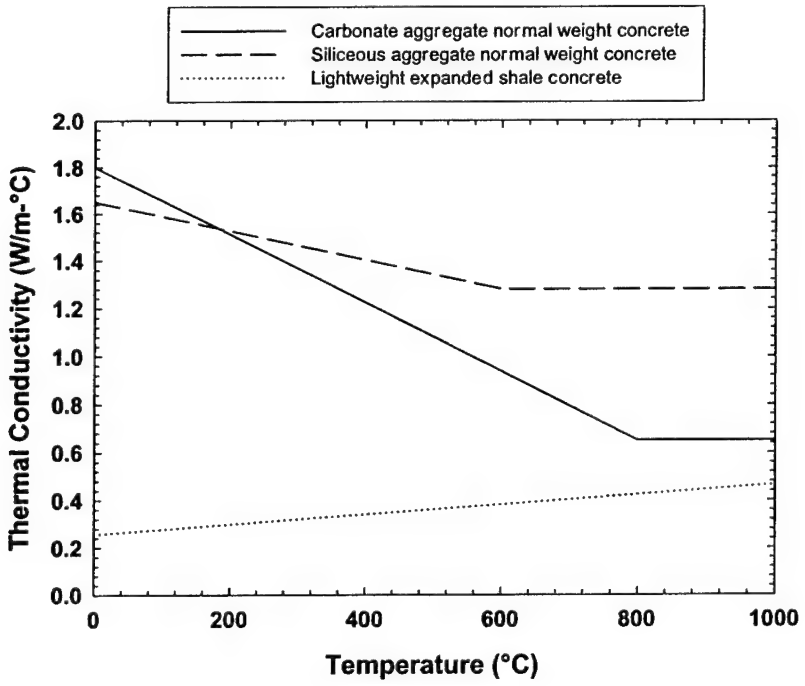

Fig. D-6 — Thermal Conductivity of Various Concrete Aggregates

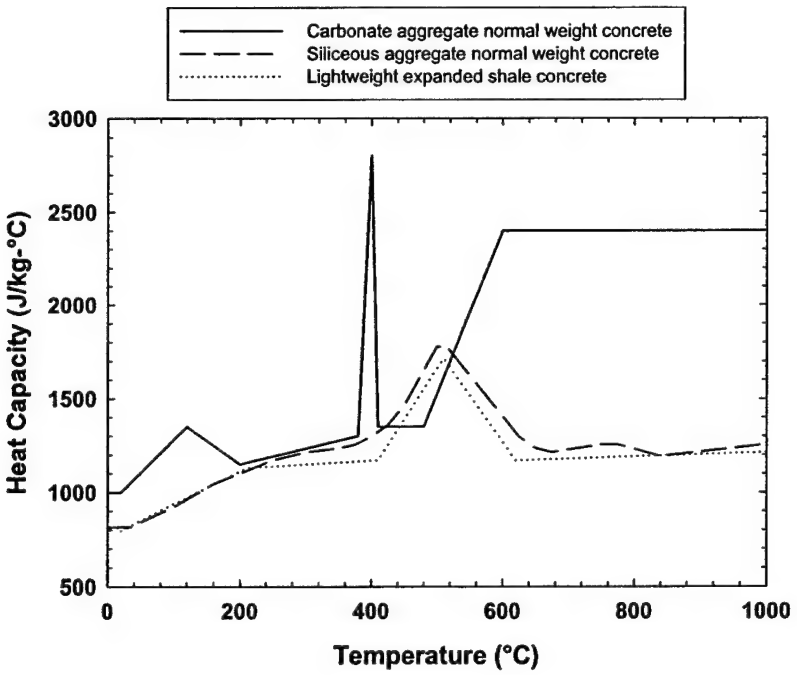

Fig. D-7 — Heat Capacity of Various Concrete Aggregates

The moisture content of the concrete may vary depending on the local environmental conditions, the cure time, and other factors. The moisture content may range from zero percent to twelve percent or greater [Flynn, 1999]. A 1½ percent by mass moisture content is the minimum moisture content of the samples tested by Harmathy [1983] and is assumed for this validation case. The vaporization of the moisture is included in the model by applying the total vaporization energy to the heat capacity term in HEATING over a 10°C range starting at 100°C. The heat of vaporization of water at 100°C and 1 atm pressure is 2,258 kJ/kg [Jones *et al.*, 1986]. The resulting vaporization energy and values added to the heat capacity terms in HEATING are summarized in Table D-2.

Table D-2 — Moisture Vaporization Energy for Concrete

Concrete	Density (kg/m3)	Moisture Mass Density (kg/m^3)	Vaporization Energy (kJ/kg)	Heat Capacity Increase (kJ/kg-°C)
Carbonate	2,136	32	72,260	7,230
Siliceous	2,300	34.5	77,900	7,790
Lightweight	1,150	17.3	39,100	3,910

The thermal conductivity and (indirectly) the density of the thermocouple pads are prescribed by ASTM E119-98 [1999]. The thermal conductivity of refractory fiber pads should be 0.053 plus or minus 0.004 W/m-K and the density should be 305 kg/m^3 but may fall between 159 kg/m^3 and 519 kg/m^3. The large density range is the result of tolerances in the pad area, thickness, and dry weight. Due to the uncertainty in the density of the pad material, an average heat capacity for mineral fiber over a 600 °C temperature range [Harmathy, 1983] was assumed (960 kJ/kg-K).

Boundary Conditions

A natural convection boundary condition was applied to the exposed concrete surface and unexposed thermocouple pad surface as described by Equation 3. The convection coefficient for vertical planes was assumed to be 1.31 W/m^2-°C$^{1.33}$ [Holman, 1990]. A thermal radiation boundary condition was applied to the exposed and unexposed surface of the concrete as described by Equation 4. An emissivity of 0.91 was assumed for the concrete surfaces and the thermocouple pad and a value of 0.95 was assumed for all ambient surroundings (exposed and unexposed) [Holman, 1990; Sparrow *et al.*, 1978; Incropera *et al.*, 1985]. The resultant or effective emissivity for the exposed and unexposed surfaces, as calculated using Equation 5, was 0.87. The view factor was unity between ambient environment and the concrete and the thermocouple pad surfaces.

The exposure temperature was the ASTM E119-98 Standard Time-Temperature profile [1999], which may be estimated using the following curve fit equations:

$$T_f(t) = \frac{908t}{3.14+t} + \frac{745t}{490+t} - (17.8) \qquad t \le 120$$

$$T_f(t) = 1010 + \left(\frac{t-120}{120}\right)\cdot(83) \qquad 120 < t \le 240 \tag{7}$$

where T_f is the exposure temperature (°C) and t is the time after the start of the exposure (minutes). The ambient exposure temperature is 23.9°C such that the critical unexposed surface temperature is 162.8°C.

Results

The implicit Crank-Nicolson method [Childs, 1998; Smith, 1987; Jaluria *et al.*, 1986] was used to solve for the unexposed concrete surface temperature. The tolerance for convergence was 1 X 10^{-6} and the solution time step was 0.5 seconds. Decreasing the tolerance, decreasing the time step, or using the Classical Explicit Procedure or Classical Implicit Procedure produced the same results. A total of one hundred cells was used in the concrete and twenty in the thermocouple pad. The results did not change when the number of cells was increased in either material.

The thickness of the concrete varies with the fire resistance rating and the type of concrete aggregate [ASCE 29-99, 1998; Fleischmann, 1995]. Table D-3 summarizes the wall thickness

and ASTM E119 fire resistance rating for the cases considered. The thickness of the thermocouple pads is 9.5 mm as specified by ASTM E119-98 [1999]. The calculated fire resistance rating, which is the time at which the unexposed concrete surface reaches 163°C assuming an initial temperature of 24°C, is compared to the listed fire resistance rating in Table D-3.

Table D-3 — Concrete Wall Fire Resistance – 120 Cell Model

Type of Concrete	Thickness (mm)	Listed Fire Resistance (min)	Calculated Fire Resistance (min)
Normal Weight Carbonate Aggregate	81	60	64 (+ 6.7%)
	102	90	95 (+ 5.6%)
	117	120	121 (+ 1.0%)
	145	180	179 (- 1.0%)
	168	240	235 (- 2.0%)
Normal Weight Siliceous Aggregate	89	60	67 (+ 11.1%)
	109	90	93 (+ 3.3%)
	127	120	121 (+ 1.0%)
	157	180	176 (- 2.2%)
	178	240	220 (- 8.3%)
Light Weight Expanded Shale	64	60	64 (+ 6.7%)
	79	90	93 (+ 3.3%)
	91	120	120 (–)
	112	180	175 (- 2.8%)
	130	240	231 (- 3.8%)

Table D-3 indicates that the calculated fire resistance is within eleven percent and typically within five percent or less of the actual fire resistance rating.

Sensitivity of Results to Input Parameter Assumptions

A sensitivity analysis of the material properties and boundary conditions was performed to determine critical parameters. Figure D-8 shows the impact of uncertainty in the thermal material properties of the concrete for the carbonate aggregate. Figure D-8 indicates that there is a considerable range in the predicted fire resistance with a material property uncertainty of twenty-five percent. This uncertainty is within the range of data for various concrete aggregates [Harmathy, 1983; Lie, 1972; Flynn, 1999], thus identification of the correct aggregate and thermal properties is essential when modeling concrete materials with HEATING. Similar results are observed for siliceous and expanded shale aggregates.

Figure D-9 shows the impact of boundary condition uncertainty and Figure D-10 shows the impact of variations in the thermocouple pad material properties and physical dimensions. Also shown in Figure D-10 is the temperature of the concrete without thermocouple pads, indicating a significant improvement in performance. This is consistent with observations of temperature measurements made with and without thermocouple pads that demonstrated an increase of up to 30 minutes in the fire resistance rating and an overall temperature difference of 44°C between the bare and covered thermocouples [Carlson *et al.*, 1962]. Collectively, Figures D-9 and D-10 suggest that the boundary conditions and the material properties of the thermocouple pad

(provided it is included in the model) are not significant parameters when modeling the performance of concrete with HEATING.

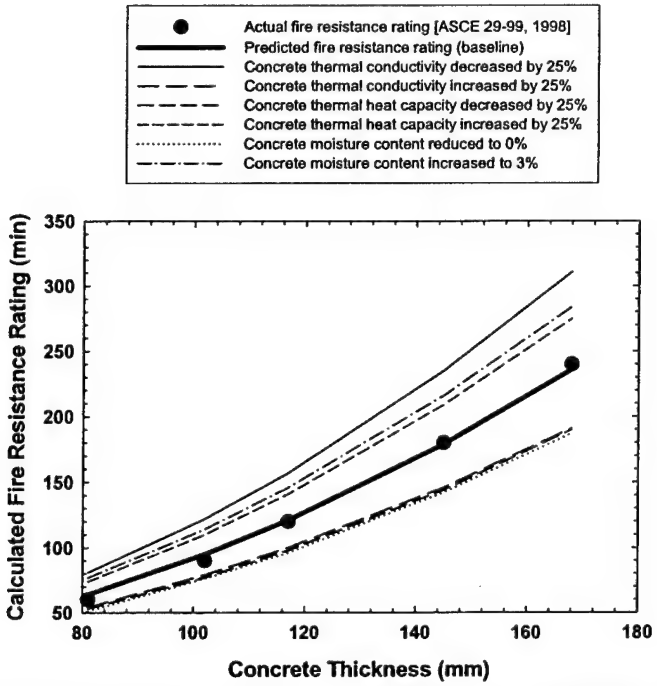

Fig. D-8 — Sensitivity of Carbonate Aggregate Normal Weight Concrete Predicted Temperature to Uncertainty in the Thermal Material Property Data

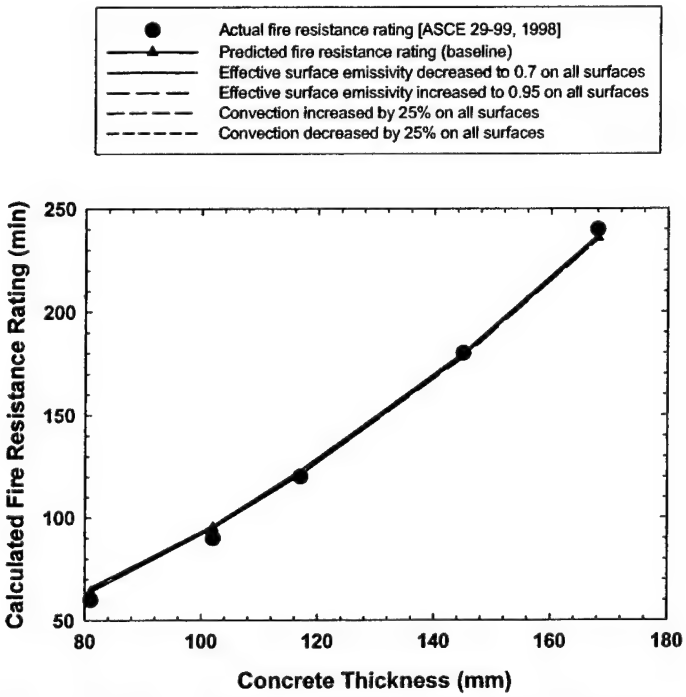

Fig. D-9 — Sensitivity of Carbonate Aggregate Normal Weight Concrete Predicted Temperature to Uncertainty in the Boundary Condition Parameters

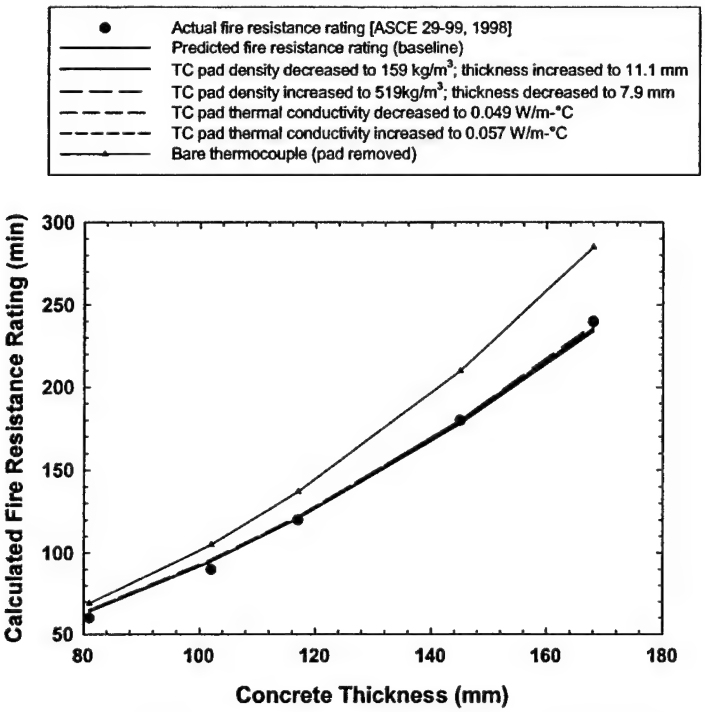

Fig. D-10 — Sensitivity of Carbonate Aggregate Normal Weight Concrete to Variations in Thermocouple Pad Dimensions and Thermal Material Properties

3.3 Validation Case 3: Aluminum Plate Protected with Mineral Fiber Blanket Insulation Exposed to ISO 6944 Test Conditions

Validation Case 3 is a bulkhead/deck assembly that involves a 6 mm thick aluminum plate and Unifrax Insulfrax mineral fiber blanket fire insulation. The test data available for this assembly includes two designs tested in accordance with A.754(18) [1993], which uses the ISO 834 Standard Time-Temperature Profile [IMO A.754(18), 1993; ISO 834, 1999]]. The two assembly ratings are A30 (30 minutes) and A60 (60 minutes). The material properties of the Insulfrax insulation are proprietary to Unifrax; however the test results (exposure temperature and aluminum temperature versus time) and the rating of the assembly may be used and form the comparison basis for this validation case [DIFST, 2002a; DIFST, 2002b; DIFST, 2002c, and DIFST, 2002d].

The specific basis for the validation case is the fire resistance rating of the aluminum-insulation assembly and the transient aluminum temperature. A one-dimensional thermal analysis is used to calculate the aluminum temperature as a function of time. Figure D-11 depicts the configuration modeled by HEATING. Per IMO A.754(18) [1993], thermocouples used to measure the unexposed aluminum surface temperature are covered with pads in an attempt to simulate contact with a combustible material. As noted in Section 3.2, the presence of thermocouple pads impacts the fire resistance rating and the unexposed surface temperature of the assembly. As such, they are included in the thermal model used in this validation case.

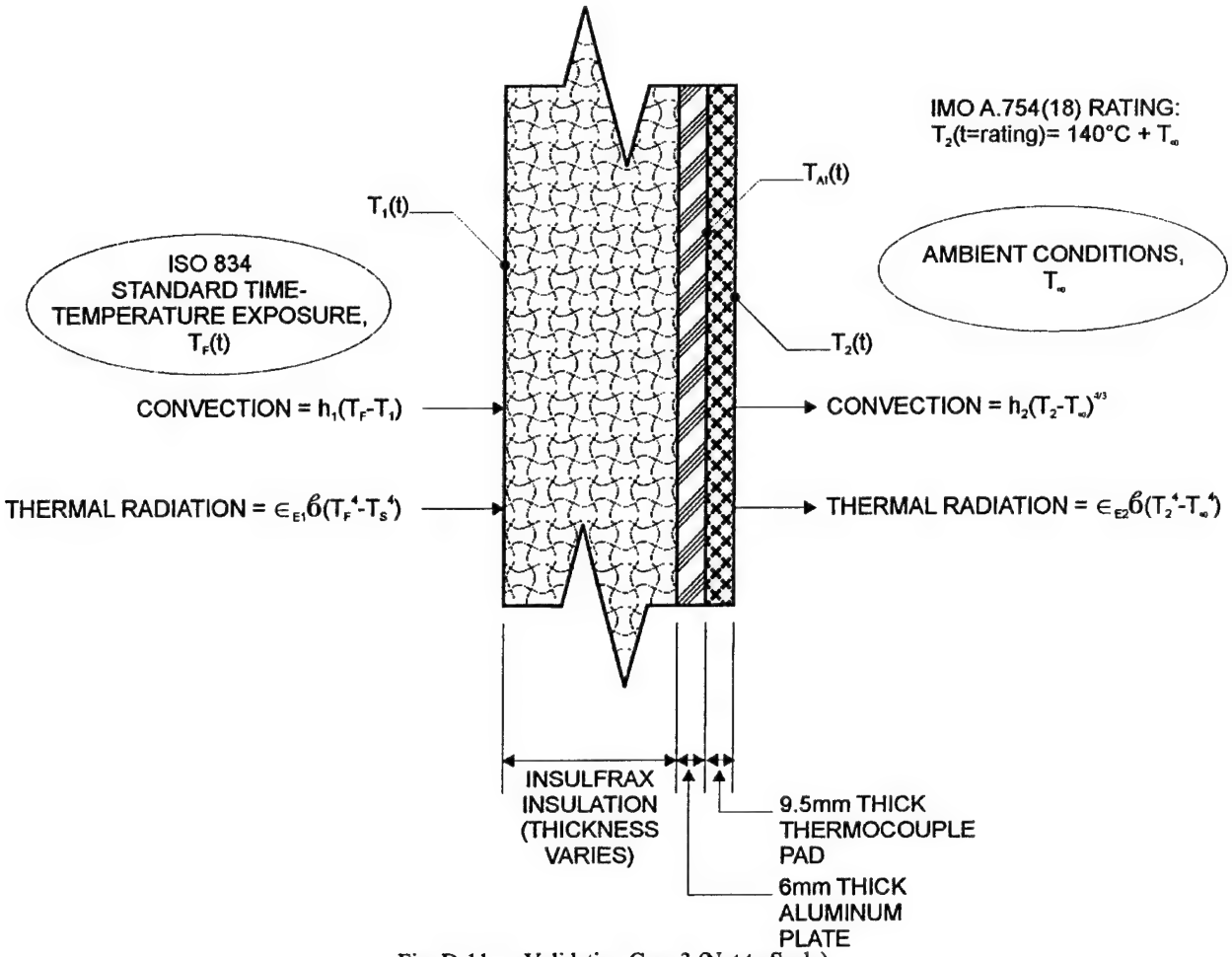

Fig. D-11 — Validation Case 3 (Not to Scale)

Material Properties

The material properties that are necessary for calculating the fire resistance rating of the Insulfrax-aluminum bulkhead/deck assembly are the thermal conductivity, heat capacity, and density of all materials involved, including the thermocouple pads. The thermal conductivity and the heat capacity of the mineral fiber blanket were provided by Insulfrax but are proprietary and therefore are not plotted in this document. The density for each material is as follows.

- Aluminum: 2,787 kg/m^3 [Holman, 1990];
- Insulfrax: 96 kg/m^3 [DIFST, 2002a; DIFST, 2002c]; and
- Thermocouple pad: 300 kg/m^3 [ASTM E119-98, 1999].
- The heat capacity for the aluminum and thermocouple pad is as follows:
- Aluminum: 883 J/kg-°C [Holman, 1990]; and
- Thermocouple pad: 960 J/kg-°C, assumed (typical mineral fiber) [Harmathy, 1983].

The thermal conductivity for aluminum is a function of temperature as shown in Table D-4 [Holman, 1990]. The thermal conductivity for the thermocouple pad is 0.55 W/m-°C. Note that this is greater than the value prescribed by ASTM E119. Due to the considerable uncertainty in the thermocouple pad thickness, density, and thermal conductivity, this parameter, along with the emissivity of the thermocouple pad, was used to correlate the data and the value is thus not likely the true thermal conductivity.

Table D-4 — Thermal Conductivity of Aluminum [Holman, 1990]

Temperature (°C)	Thermal Conductivity (W/m-°C)
0	159
100	182
200	194
500	194

Boundary Conditions

A forced convection boundary condition was applied to the exposed surface of the bulkhead/deck assembly and a natural convection boundary condition was applied to the unexposed surface. The following form was used in both cases [Holman, 1990]:

$$\dot{q}_c'' = h\left(\left|T_S - T_A\right|\right)^n \qquad (8)$$

where n is an exponent that ranges from unity (forced convection) to about 1.33 (natural convection) and all other terms have been defined in Section 3.1. A convection coefficient of 15 W/m^2-°C and an exponent of unity were applied to the exposed surface of the assembly and a convection coefficient of 1 W/m^2-°C$^{1.25}$ and an exponent of 1.25 were applied to the unexposed thermocouple pad surface. These values are consistent with furnace exposures [Barnett, 1989; Issen, 1974].

A thermal radiation boundary condition was applied to the exposed and unexposed surfaces as described by Equation 4. The emissivity of the Insulfrax surface is also proprietary and is thus not provided. The emissivity of the exposure source was 0.686 and the effective emissivity of the ambient thermocouple pad surface was 0.53. The view factor was unity between the ambient environment and the Insulfrax and the thermocouple pad surfaces.

The exposure fire was the ISO 834 Standard Time-Temperature profile. The temperature as a function of time is as follows [ISO 834, 1999]:

$$T_f(t) = T_\infty + 345\log 8t \qquad (9)$$

where T_∞ is the initial ambient temperature (°C) and t is the time in minutes.

Results

The implicit Crank-Nicolson method [Childs, 1998; Smith, 1987; Jaluria *et al.*, 1986] was used to solve for the aluminum temperature. The tolerance for convergence was 1×10^{-4} and the solution time step as 1.0 second. Decreasing the tolerance, decreasing the time step, or using the Classical Explicit Procedure or Classical Implicit Procedure resulted in a less than 3°C fluctuation in the maximum temperature predictions. Twenty-five cells were used in the Unifrax Insulfrax, four cells were used in the aluminum, and five cells were used in the thermocouple pad. The maximum temperature predictions changed by less than 1°C when the number of cells was quadrupled in each of the three materials.

The thickness of the insulation for the A60 assembly is 50 mm [DIFST, 2002a; DIFST, 2002b] and for the A30 bulkhead/deck assembly it is 38 mm [DIFST, 2002c; DIFST, 2002d]. The calculated average aluminum temperature is compared to the measured test data in Figures D-12 and D-13 for the A60 and A30 assemblies. The figures indicate that the calculated results are in agreement with the test data, particularly 10-20 minutes after test initiation.

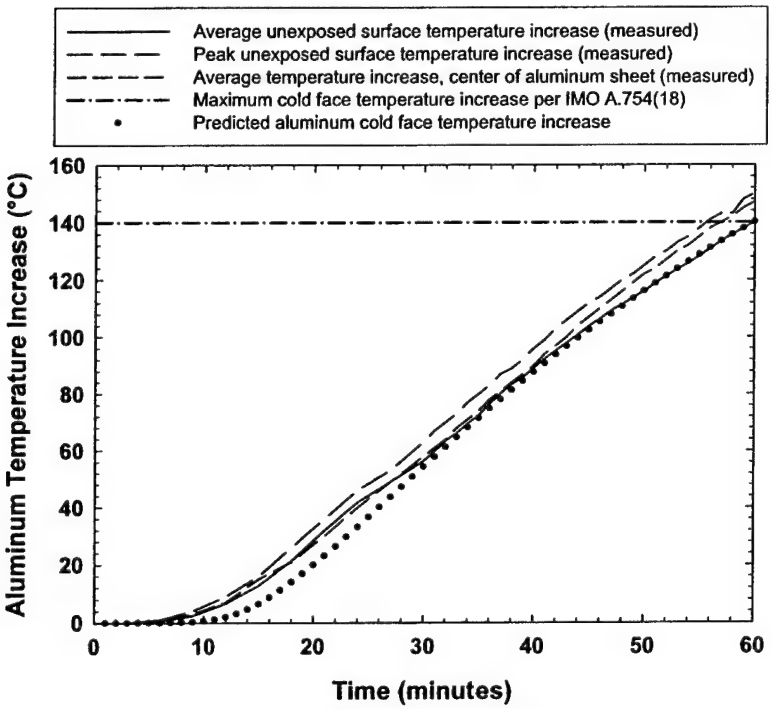

Fig. D-12 — Predicted versus Measured Aluminum Temperature for A60 Bulkhead/Deck Assembly – 34 Cell Model

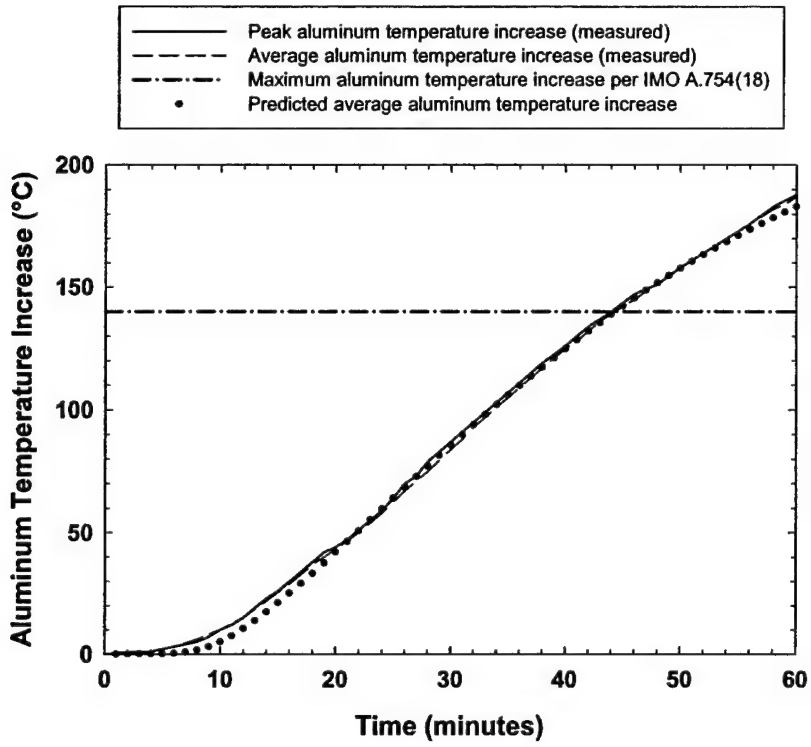

Fig. D-13 — Predicted versus Measured Aluminum Temperature for A30 Bulkhead/Deck Assembly – 34 Cell Model

The calculated time to reach a 140°C temperature rise on the unexposed surface is compared in Table D-5. The rating of the bulkhead/deck assemblies is not strictly based on the time to reach a 140°C temperature increase. The aluminum temperature must not exceed 200°C at 60 minutes for load bearing sections. This is confirmed in Table D-5 for both the A60 and A30 bulkhead/deck assemblies. As such, HEATING accurately predicts the rating of the assemblies relative to the IMO A.754(18) test criteria.

Table D-5 — Time Aluminum Reaches Critical Temperature for Bulkhead/Deck Test Assemblies – 34 Cell Model

Test	Measured Time to 140°C Aluminum Temperature Rise (minutes)	Calculated Time to 140°C Aluminum Temperature Rise (minutes)
A60	60	60
A30	44	44

Sensitivity of Results to Input Parameter Assumptions

The sensitivity of the calculation results to the material properties and boundary conditions was determined. Figure D-14 shows the impact of uncertainty in the thermal material properties of the insulation and the thermocouple pad for the A30 bulkhead/deck assembly. Figure D-15

shows the sensitivity of the temperature predictions to the boundary condition parameters for the A30 bulkhead/deck assembly. Similar results are observed for the A60 bulkhead/deck assembly.

Figures D-14 and D-15 suggest that there are two critical parameters: the thermal conductivity of the insulation material and the effective emissivity of the exposed surface. The other parameters impact the results by less than five percent.

3.4 Validation Case 4: Steel Protected with Mineral Fiber Insulation Exposed to UL 1709 Rapid Temperature Rise Fire Exposure

Validation Case 4 is a steel plate protected with Stucto-gard mineral fiber insulation that is exposed to the Underwriters Laboratories (UL) 1709 [1998] Rapid Temperature Rise fire exposure. The test data available for this assembly are the fire exposure temperature as a function of time and the temperature at the Structo-gard–steel interface as a function of time. The total test duration was seventy five minutes.

The specific basis for the validation case is transient temperature at the Structo-gard–steel interface of the assembly. A one-dimensional thermal analysis is used to calculate the temperature profile. Figure D-16 depicts the configuration modeled by HEATING. Although the UL 1709 test requires thermocouple pads on the unexposed surface, the location where the interface temperature was measured was not near areas in which there were thermocouple pads on the unexposed steel [Leonard *et al.*, 1993; Soriathia *et al.*, 1998].

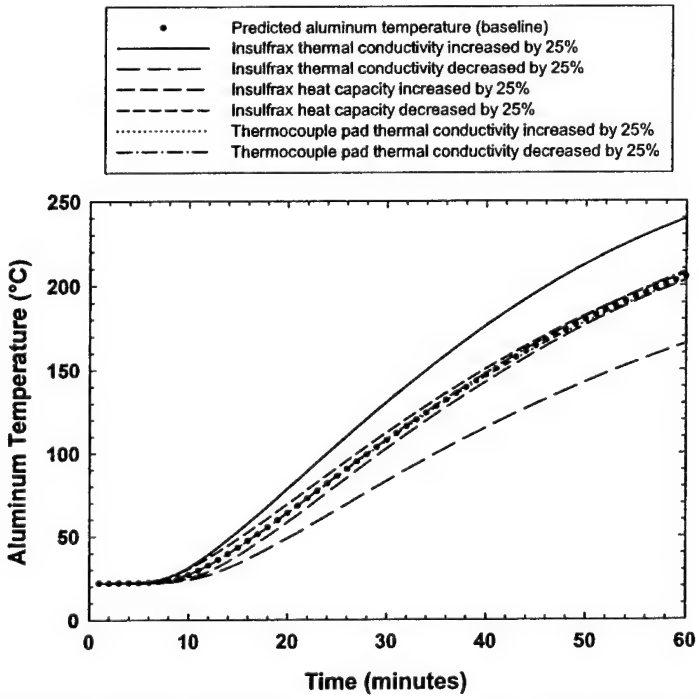

Fig. D-14 — Sensitivity of the A30 Bulkhead/Deck Predicted Temperature to Uncertainty in the Material Property Data

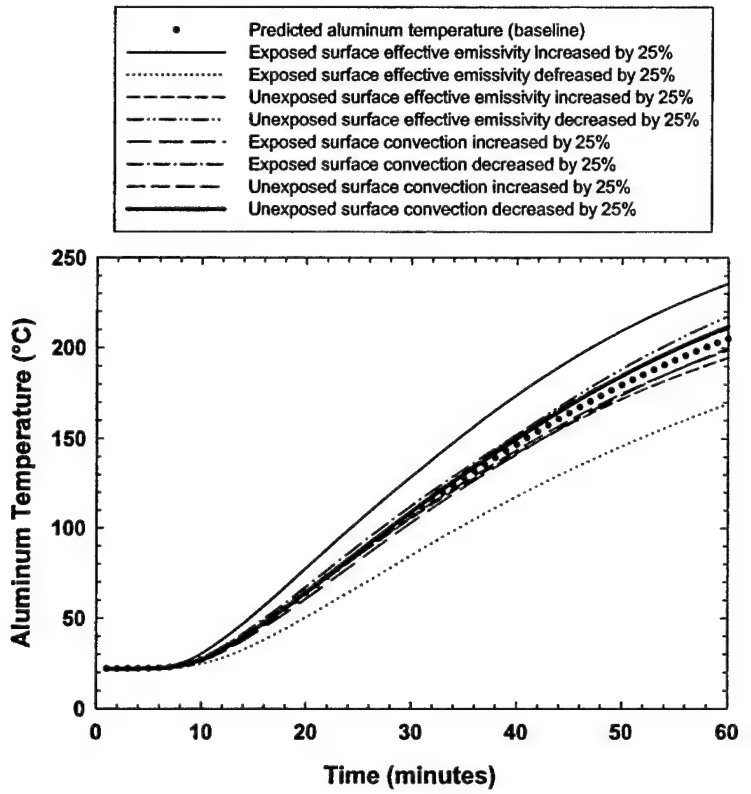

Fig. D-15 — Sensitivity of the A30 Bulkhead/Deck Predicted Temperature to the Uncertainty in the Boundary Condition Parameters

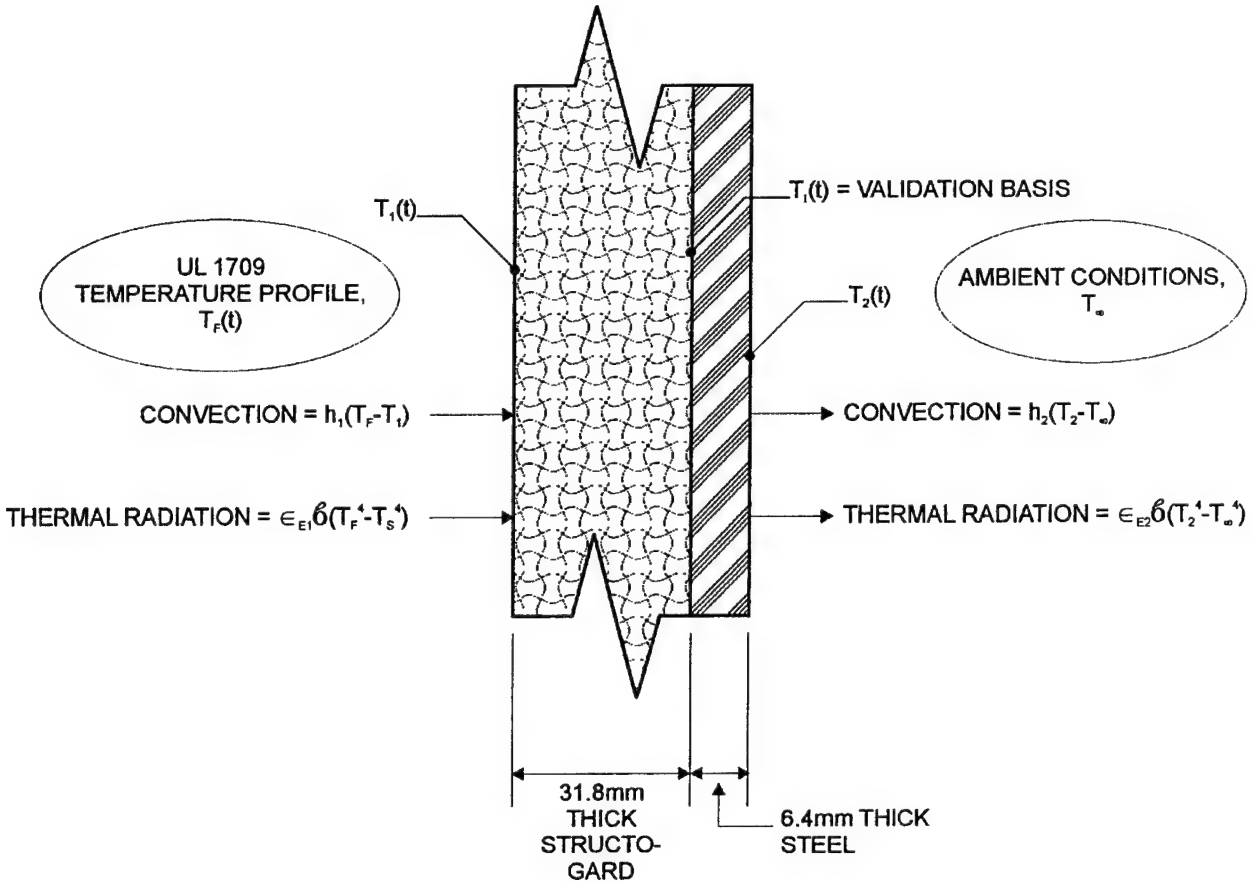

Fig. D-16 — Validation Case 4 (Not to Scale)

Material Properties

The material properties necessary for this validation case are the thermal conductivity, the heat capacity, and the density of the Structo-gard and steel. The properties for structo-gard were obtained from the manufacturer [Thermal Ceramics, 2000] and the properties for the steel were obtained from the HEATING material library database for carbon steel [Childs, 1998]. Figure D-17 shows the thermal conductivity and heat capacity for the insulation and steel as a function of temperature. The density of the two materials is as follows:

- Steel – 7,860 kg/m^3 [Childs, 1998]; and
- Structo-Gard – 102.5 kg/m^3 [Thermal Ceramics, 2000].

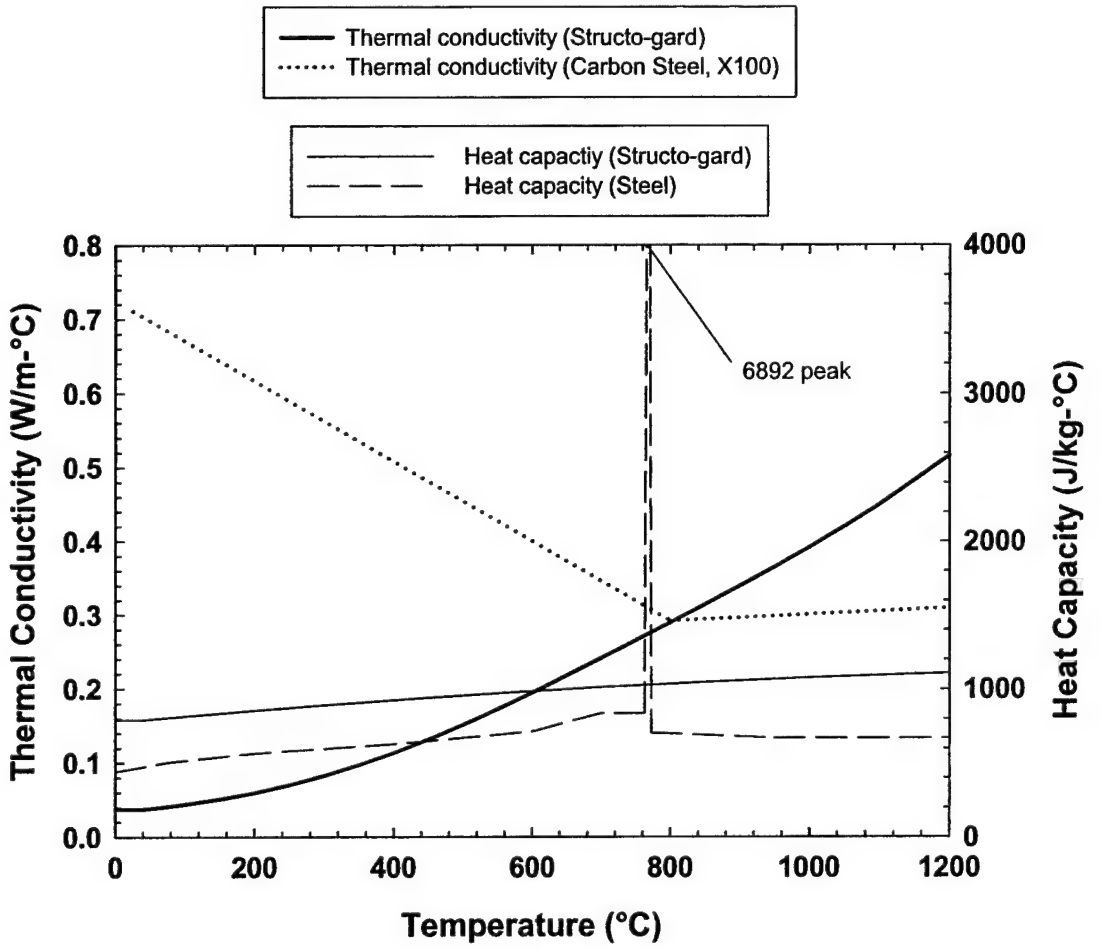

Fig. D-17 — Thermal Material Properties of Structo-gard and Steel

Boundary Conditions

A forced convection boundary condition was applied to the exposed and unexposed surfaces of the Structo-gard – steel assembly as described by Equation 8. A convection coefficient of 15 W/m^2-°C was used for both surfaces.

A thermal radiation boundary condition was applied to the exposed and unexposed surfaces as described by Equation 4. The ambient emissivity was assumed to be 0.95. The emissivity of the Structo-gard was assumed to be 0.95 and the emissivity of the steel was assumed to be 0.8. As such, the effective emissivity calculated using Equation 5 of the exposed (Structo-gard) surface was 0.9 and the effective emissivity of the unexposed (steel) surface was 0.77. The view factor was unity between the ambient environment (exposed and unexposed) and the all surfaces.

The exposure fire for the tests was the UL 1709 as shown in Figure D-18. The actual average temperature data, also shown in Figure D-18, was used as the input for the validation model.

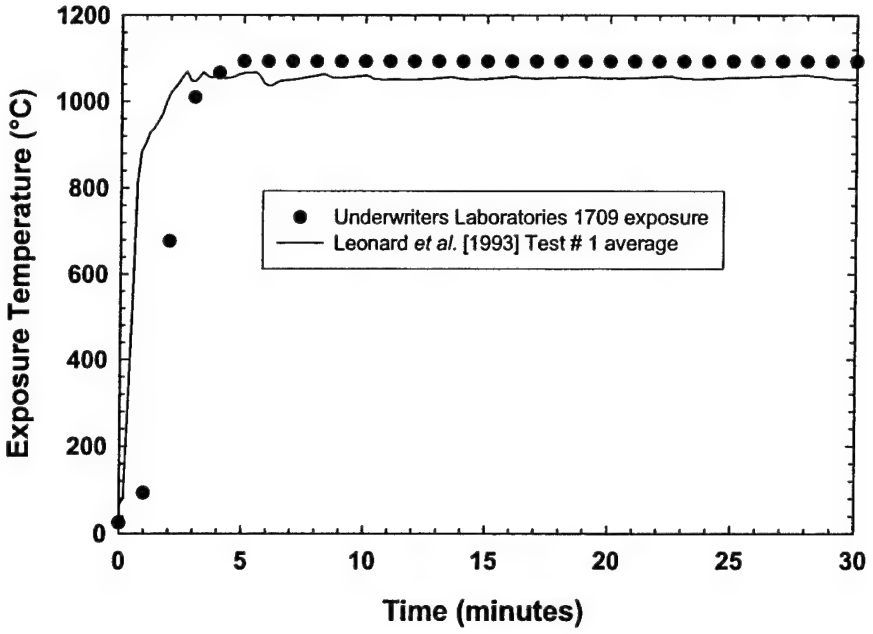

Fig. D-18 — Fire Exposure for Leonard *et al.* [1993] Test # 1

Results

The Classical Implicit Scheme [Childs, 1998; Smith, 1987; Jaluria *et al.*, 1986] was used to solve for the unexposed concrete surface temperature. The tolerance for convergence was 1 X 10^{-7} and the solution time step was 2.0 seconds. Decreasing the tolerance, decreasing the time step, or using the Classical Explicit Procedure or Crank-Nicolson Method resulted in a less than 1°C fluctuation in the maximum temperature predictions at the Structo-gard – steel interface. Eighty- cells were used in the Structo-gard and sixteen cells were used in the steel. Increasing the number of cells in either material did not alter the temperature results.

The measured temperature at the Stucto-gard – steel interface is compared with the calculated temperature in Figure D-19 for the first thirty minutes of Test #1 in Leonard *et al.* [1993]. The results are conservative (*i.e.*, overestimate the interface temperature) and are within ten percent of the measured data.

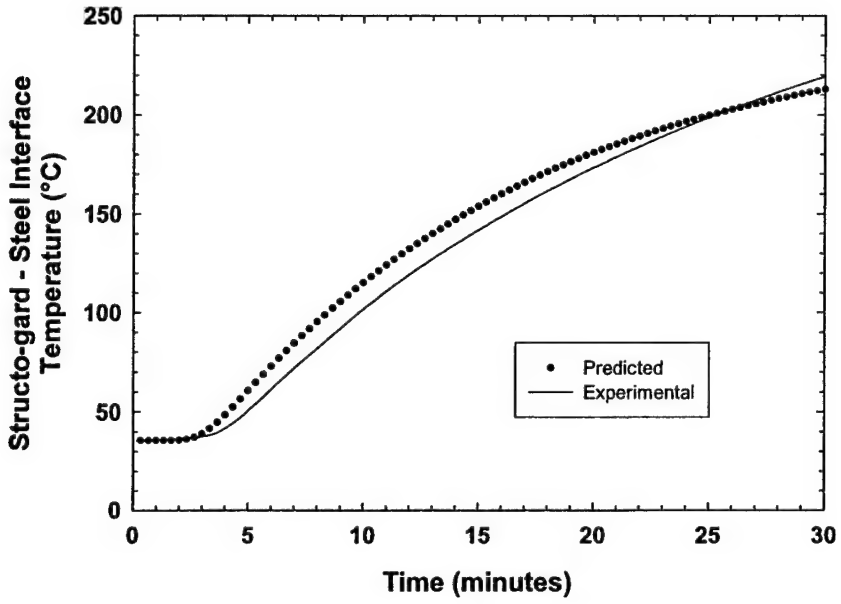

Fig. D-19 — Predicted versus Measured Structo-gard – Steel Interface Temperature (96 Cell Model)

Sensitivity of Results to Input Parameter Assumptions

The sensitivity of the calculation results to the material properties and boundary conditions was determined. Figure D-20 shows the impact of uncertainty in the thermal material properties of the Structo-gard insulation. The material properties of steel are well established and were not varied. Figure D-21 shows the sensitivity of the temperature predictions to the boundary condition parameters on the exposed and unexposed surfaces.

Figures D-20 and D-21 indicate that the thermal conductivity of the Structo-gard is the most critical parameter. The other parameters impact the results by less than five - ten percent.

3.5 Validation Case 5: Unprotected Steel Column Filled with Concrete in Web Area Exposed to ASTME119 Test Conditions

Validation Case 5 involves fire tests on two unprotected steel W-shape columns with the area between flanges filled with concrete [Underwriters Laboratories, 1919]. The columns are exposed to the ASTM E119 Standard Time-Temperature profile and the steel temperatures are measured at several locations and the failure time of the columns noted. The flange area for the column in Test#14 was filled with carbonate aggregate normal weight concrete; siliceous aggregate normal weight concrete was used in the same manner for Test #15.

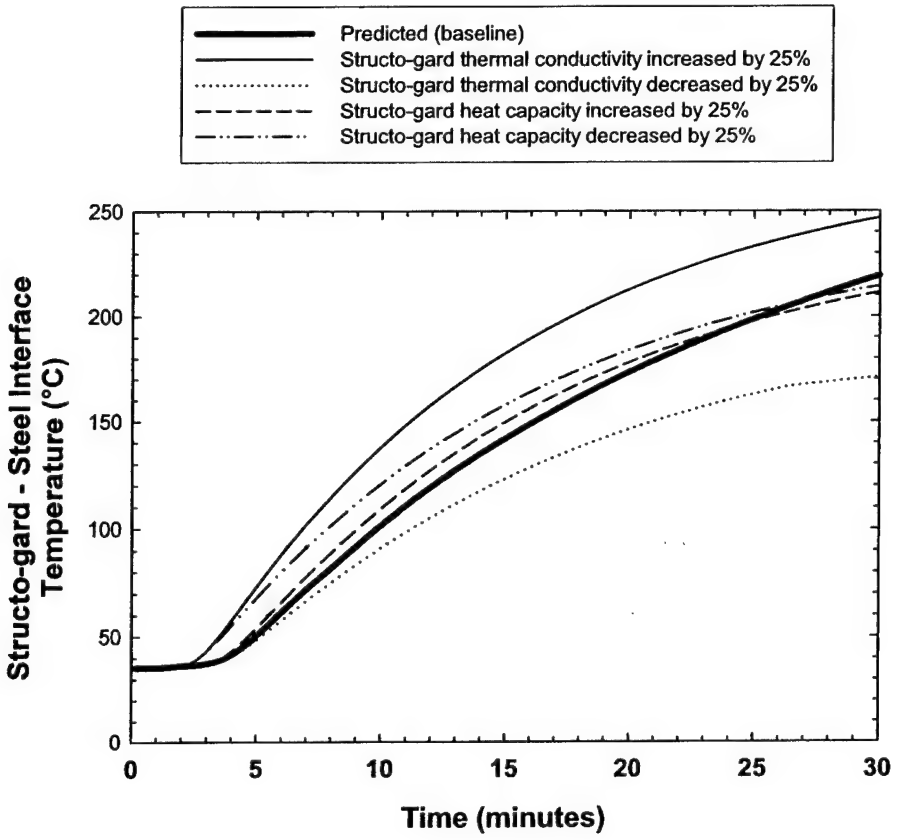

Fig. D-20 — Sensitivity of Structo-gard – Steel Interface Predicted Temperature to Uncertainty in the Material Property Data

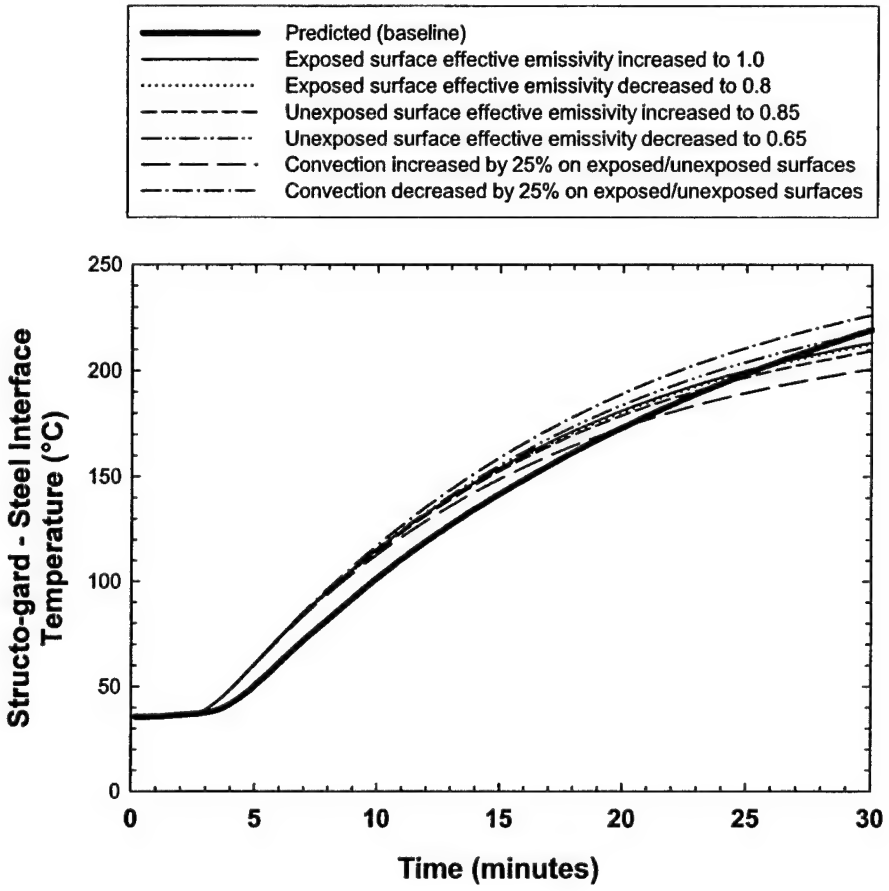

Fig. D-21 — Sensitivity of Structo-gard – Steel Interface Predicted Temperature to Uncertainty in the Boundary Condition Parameters

The specific basis for the validation case is transient temperature at various locations on the steel and the time that the steel columns exceed the ASTM E119 critical steel temperatures. A two-dimensional thermal analysis is used to calculate the temperature profiles. Figure D-22 depicts the configuration modeled by HEATING. The ASTM E119 criteria for rating steel beams is an average temperature of 538°C or a peak temperature of 649°C, whichever occurs first [ASTM E119-98, 1999]. The peak and average temperature are derived from measurements taken at three locations, which are shown in Figure D-22 [ASTM E119-98, 1999].

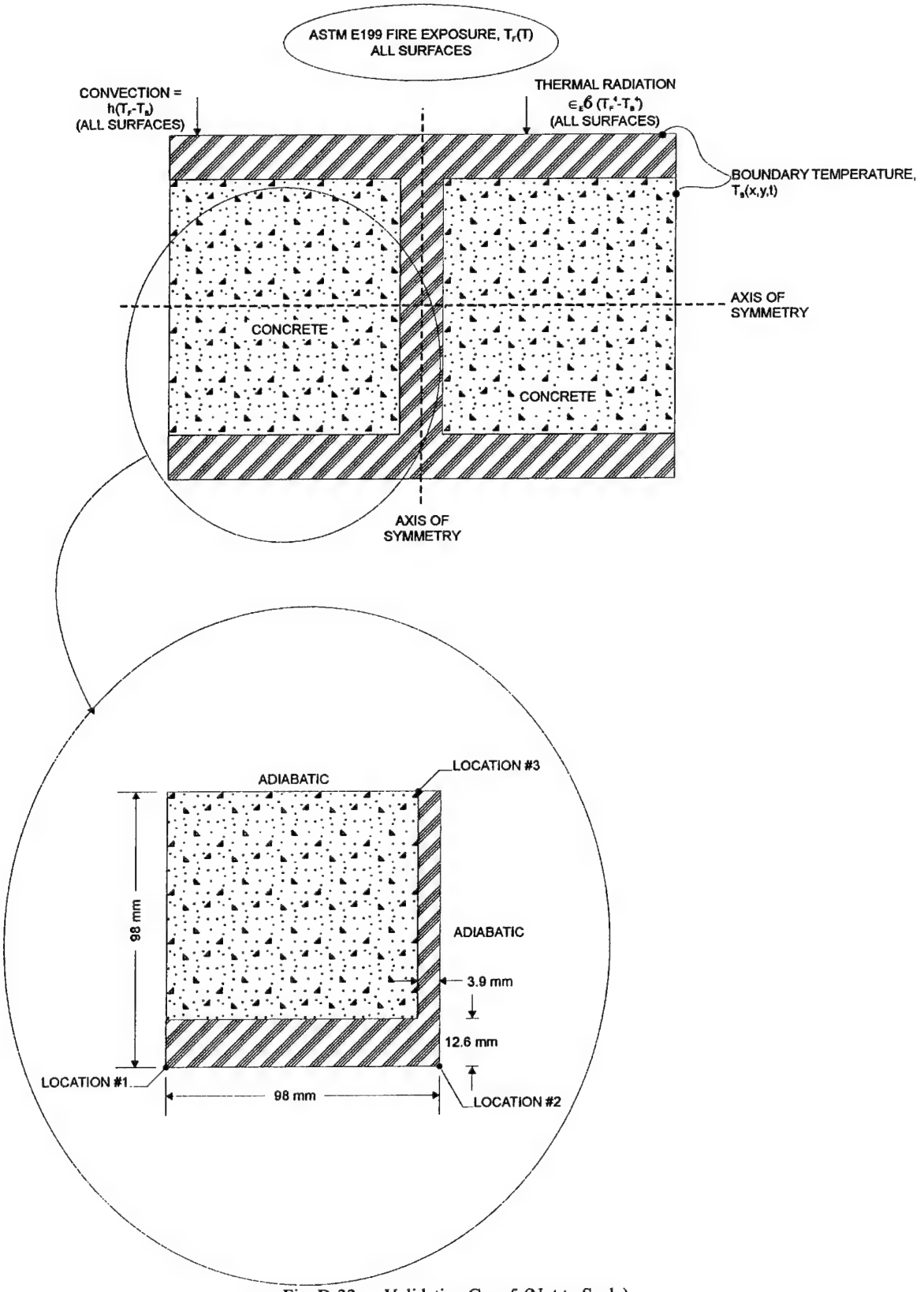

Fig. D-22 — Validation Case 5 (Not to Scale)

Material Properties

The material properties for steel are as described for Validation Case 1. The material properties for the concrete are as described for Validation Case 2 for the carbonate and siliceous aggregate normal weight concretes.

Boundary Conditions

The column was modeled as a quarter section due to symmetry, as shown in Figure D-22. An adiabatic boundary condition was thus applied to all symmetry axes.

A forced convection boundary condition was applied to the exposed surfaces of the steel and concrete as described by Equation 8. A convection coefficient of 15 W/m^2-°C was used for both surfaces.

A thermal radiation boundary condition was applied to the exposed steel and concrete as described by Equation 4. The emissivity of the steel was assumed to be 0.8 and the concrete 0.91 [Holman, 1990; Sparrow et al., 1978; Incropera *et al.*, 1985]. The emissivity of the exposure source and surroundings was determined from the test data to be approximately 0.8; thus the effective emissivity for the steel surface was 0.63 and for the concrete surface 0.7. The view factor was unity between the ambient exposure environment and the all surfaces.

The exposure fire for the tests was the ASTM E119 Standard Time-Temperature Profile [1998] as shown in Figure D-23. The actual average temperature data for Test #14 and Test #15, also shown in Figure D-23, was used as input for the validation model.

Results

Levy's Explicit Procedure [Childs, 1998; Levy, 1968] was used to solve for the temperature distribution in the column assemblies. The solution time step is determined from the stability criteria and a multiplier, which was set to 2.0. Decreasing the time step multiplier, or using the implicit Crank-Nicolson method or the Classical Implicit Procedure resulted in maximum temperature predictions that varied by less then 4°C. Thirty cells were used in each dimension in the concrete and five cells were used in the narrow dimension of the steel for a total of 1,225 cells. The temperature predictions did not significantly change when the number of total cells was increased to 5,041 with increases in each dimension and each material.

The model was validated by comparing the transient temperature profile at three locations on the steel in each test (shown in Figure D-22). Location #1 corresponds to the edge of the flange; location #2 corresponds to the middle of the flange; and location #3 corresponds to the middle of the web. The results are shown in Figures D-24 and D-25 for Test #14 and Test #15, respectively. Figure D-26 shows the temperature contours in the Test #14 column at 45 minutes, the approximate time at which the beam exceeds the ASTM E119 critical peak temperature of 649°C.

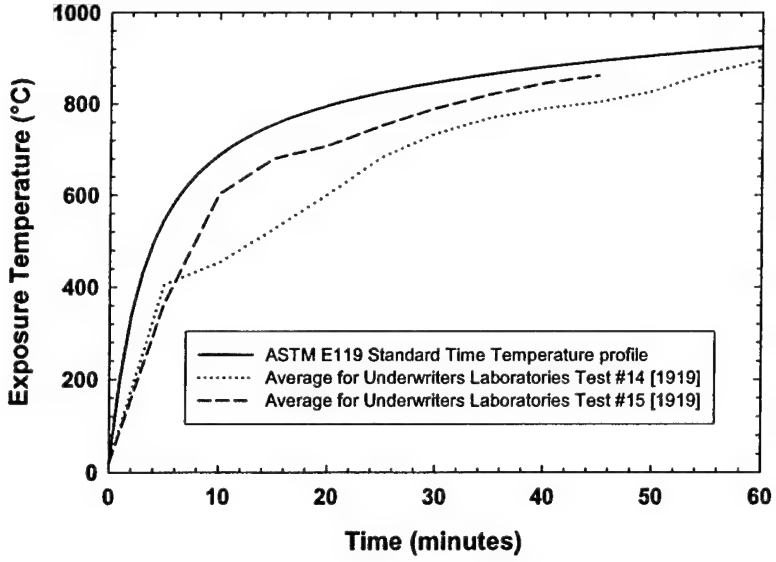

Fig. D-23 — Measured Exposure Temperature for Test #14 and Test #15

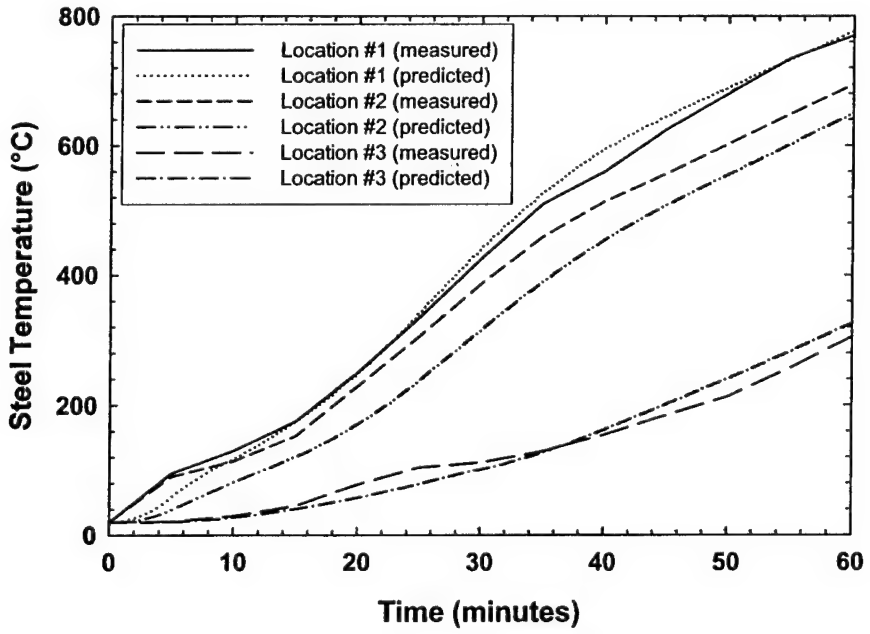

Fig. D-24 — Predicted versus Measured Temperatures for Test #14 Column - 1,225 Cell Model

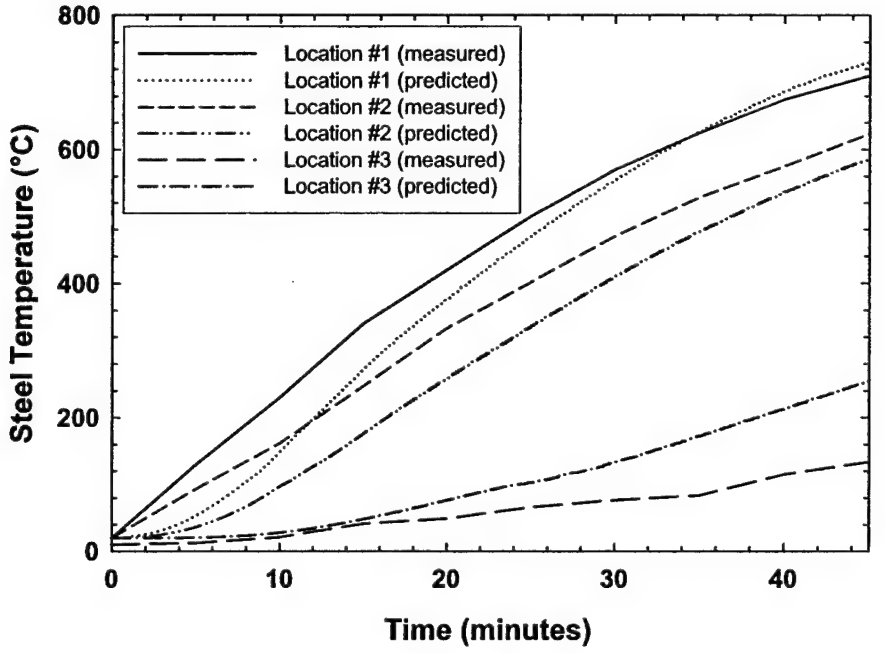

Fig. D-25 — Predicted versus Measured Temperatures for Test #15 Column – 1,225 Cell Model

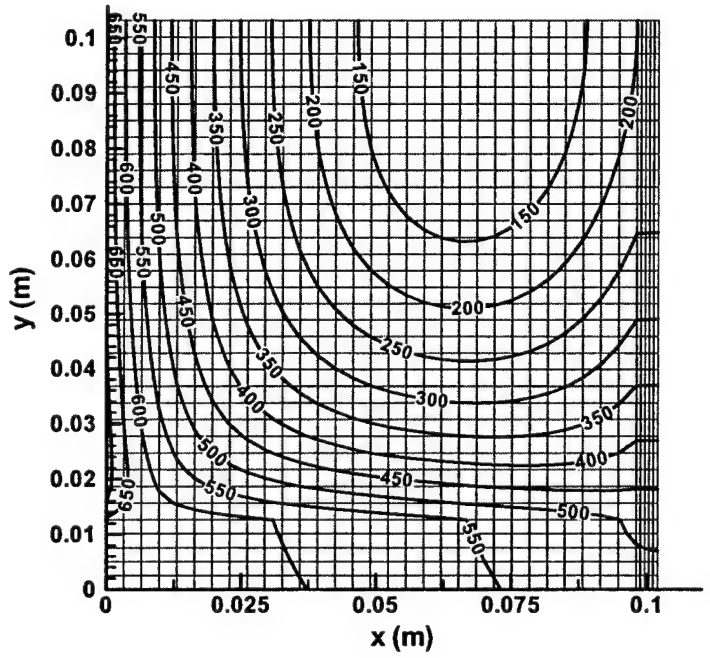

Fig. D-26 — Predicted Isotherms (°C) in Test #14 Column 45 minutes after Test Start – 1,225 Cell Model

The time to exceed the ASTM E119 critical steel temperatures for columns (*viz.*, an average temperature of 538 °C or a peak temperature of 649°C, whichever occurs first [ASTM E119, 1998]) was also used as a validation criterion. The average temperature is based on four locations per ASTM E119 [1998]: three on the upper and lower flanges and one in the web. The predicted time to exceed the ASTM E119 temperature criteria is compared with the measured time in Table D-6.

Table D-6 — Calculated and Predicted Time to Exceed ASTM E119 Critical Steel Temperatures for Columns – 1,225 Cell Model

Test	Time to Exceed Average Temperature of 538°C (min)		Time to Exceed Peak Temperature of 649°C (min)	
	Measured	Predicted	Measured	Predicted
14	49	49 (–)	47	45 (+ 4.4%)
15	38	41 (+ 7.9%)	44	37 (- 16%)

Table D-6 indicates that HEATING predicted the average and peak temperature for Test #14. The predicted fire resistance rating for this test was 45 minutes, as compared to 47 minutes measured. The average temperature prediction for Test #15 was also predicted well, however the peak temperature was over-predicted in the model. The predicted fire resistance rating for the assembly is 37 minutes, as compared to 38 minutes measured. Note that the limiting criteria is different in the predicted and measured cases for Test #15, however the predicted versus measured fire resistance rating is nearly identical.

Sensitivity of Results to Input Parameter Assumptions

The sensitivity of the calculation results to the material properties and boundary conditions was investigated for Test #14, Location #1. Similar results are observed for other locations and for Test #15.

The sensitivity of the transient temperature of Test #14, Location #1 to uncertainty in material property data is shown in Figure D-27. Likewise, Figure D-28 shows the sensitivity of the transient temperature at the same location to boundary condition uncertainty. Table D-7 shows the variation in the predicted time for the Test #14 column to reach an average temperature of 538°C and a peak temperature of 649°C as a result of material property and boundary condition uncertainty.

Figures D-27, D-28 and Table D-7 indicate that the column-concrete system is not especially sensitive to uncertainty in the material property or boundary condition parameters. The effective emissivity may impact the maximum predicted temperatures by plus or minus 50°C; the remaining parameters have significantly less of an impact.

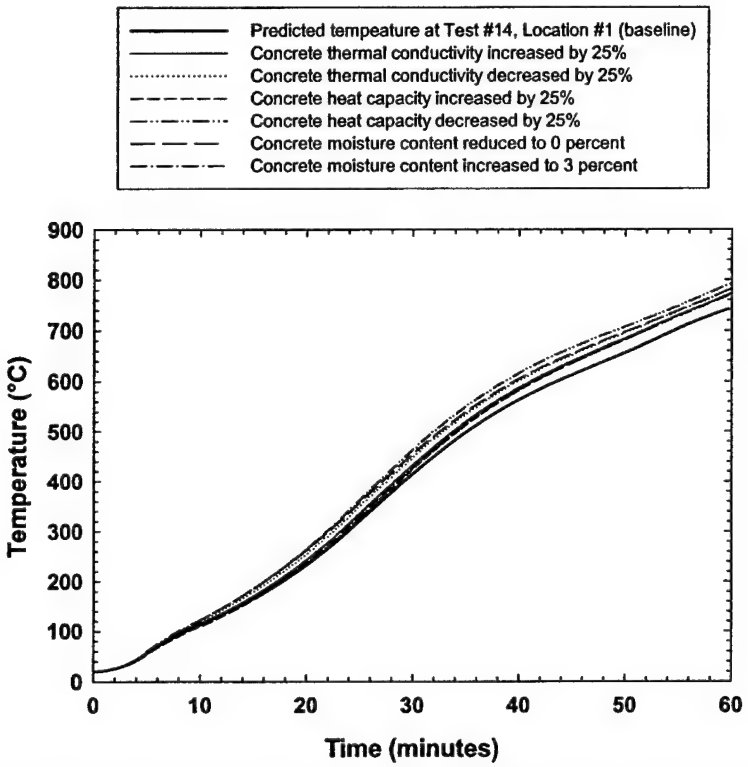

Fig. D-27 — Sensitivity of Test #14, Location #1 Temperature Predictions to Material Property Parameter Uncertainty

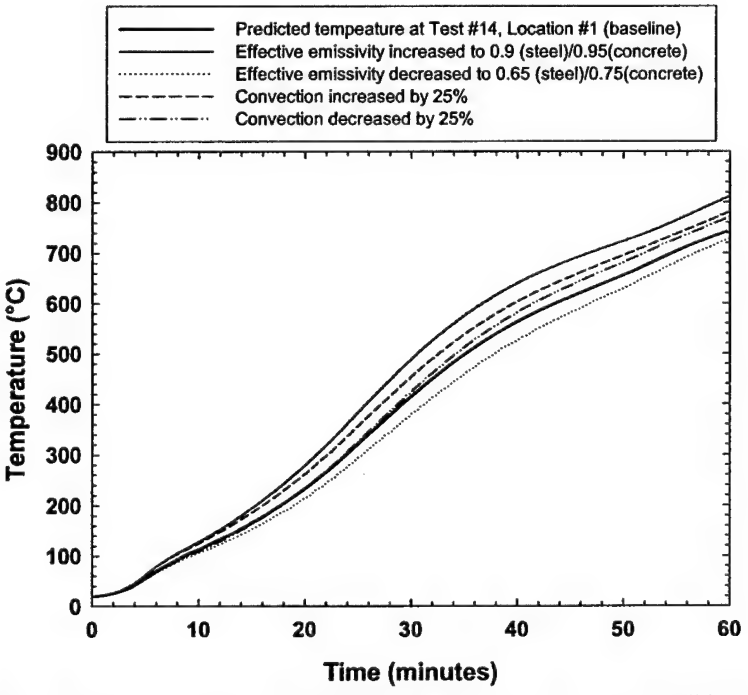

Fig. D-28 — Sensitivity of Test #14, Location #1 Temperature Predictions to Boundary Condition Parameter Uncertainty

Table D-7 — Sensitivity of the Predicted Time to Exceed ASTM E119 Critical Steel Temperatures to Material Property and Boundary Condition Parameter Uncertainty

Sensitivity Parameter Modification	Predicted time to Reach 538°C Average (min)	Predicted time to Reach 649°C Peak (min)
No modifications (baseline)	49.4	45.5
Concrete conductivity increased by 25%	49.7 (+ 0.6%)	46.1 (+ 1.3%)
Concrete conductivity decreased by 25%	48.5 (- 1.8%)	44.7 (- 1.8%)
Concrete heat capacity increased by 25%	52.1 (+ 5.5%)	47.4 (+ 4.2%)
Concrete heat capacity increased by 25%	45.8 (- 7.3%)	41.1 (- 9.7%)
Concrete moisture reduced to 0%	47.1 (- 4.7%)	44.4 (- 2.4%)
Concrete moisture increased to 3%	51.1 (+ 3.4%)	46.4 (+ 2.0%)
Effective emissivity increased by ~25%	45.2 (- 8.5%)	40.8 (- 10.0%)
Effective emissivity decreased by ~25%	54.8 (+ 10.9%)	51.9 (+ 14.1%)
Convection increased by 25%	48.5 (- 1.8%)	44.5 (- 2.2%)
Convection decreased by 25%	50.3 (+ 1.8%)	46.4 (+ 2.0%)

3.6 Validation Case 6: Steel Beam Protected with Blazeshield Exposed to ASTME119 Test Conditions (UL Design J907)

Validation Case 6 is Underwriters Laboratories (UL) Design Number P907 [UL, 2003]. The UL "P" designs feature roof or ceiling assemblies that are unprotected, however the steel framing that supports the assemblies is typically protected with insulation or a membrane. UL Design No. P907 involves a W8X28 beam that supports fluted galvanized steel-form insulating concrete (*i.e.*, lightweight concrete) floor units. The UL Design No. P907 roof-ceiling assembly is rated for 2 hours fire resistance when exposed to the ASTM E119 Standard Time-Temperature profile provided the steel is protected with a 31.7 mm thick coating of Blazeshield D-C/F sprayed fire resistive material [UL, 2003].

The specific basis for the validation case is the unrestrained beam fire resistance rating for the ceiling-roof assembly using the ASTM E119 critical steel temperature criteria [ASTM E119-98, 1999]. A two-dimensional thermal analysis is used to calculate the temperature profiles within the assembly. Figure D-29 depicts the configuration that was modeled with HEATING. The ASTM E119 criteria for rating steel beams is an average temperature of 593°C or a peak temperature of 704°C, whichever occurs first [ASTM E119-98, 1999]. The peak and average temperature are derived from measurements taken at four locations, which are shown in Figure D-29 [ASTM E119-98, 1999].

Material Properties

The material properties for lightweight concrete are as described for the lightweight expanded shale aggregate concrete used in Validation Case 2 in Section 3.2. The material properties for steel are as described for Validation Case 1 in Section 3.1.

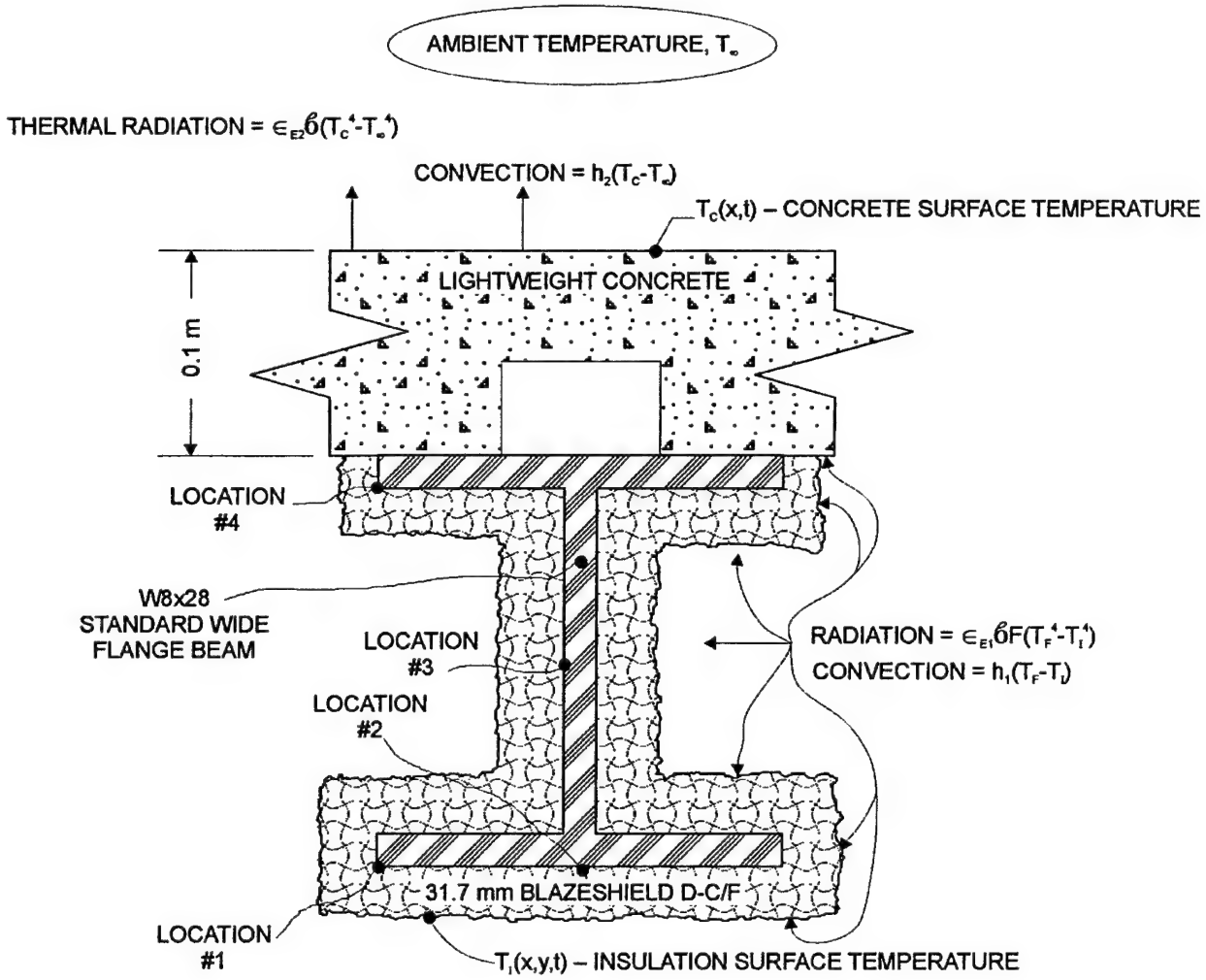

Fig. D-29 — Validation Case 6 (Not to Scale)

The thermal conductivity and heat capacity of Blazeshield D-C/F vary with temperature and are shown in Figure D-30 [Harmathy, 1983]. The insulation density is 309 kg/m^3 [Harmathy, 1983].

Boundary Conditions

A forced convection boundary condition was applied to all exposed and unexposed surfaces of the concrete and Blazeshield D-C/F insulation as described by Equation 8. A convection coefficient of 15 kW/m^2 was assumed on all surfaces where convection was applied.

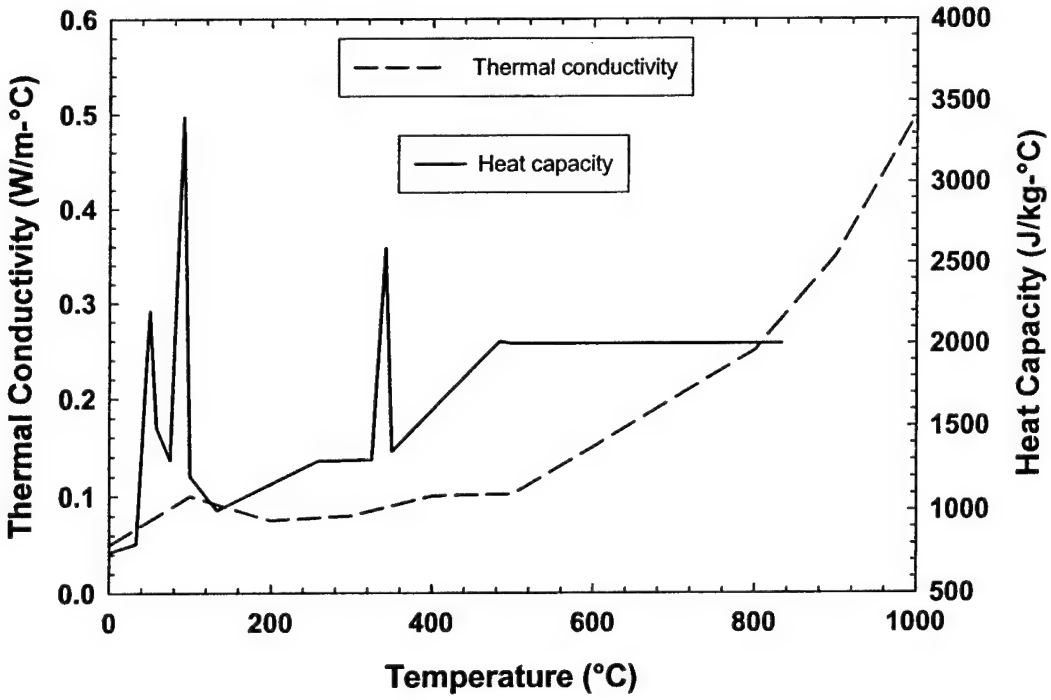

Fig. D-30 — Thermal Conductivity and Heat Capacity of Blazeshield D-C/F [Harmathy, 1983]

A thermal radiation boundary condition was applied to the exposed and unexposed surfaces as described by Equation 4. The emissivity of the insulation was assumed to be 0.9 and the concrete emissivity was assumed to be 0.91, as described for Validation Case 1 [Holman, 1990; Sparrow *et al.*, 1978; Incropera *et al.*, 1985]. The emissivity of the exposed and unexposed ambient environment was assumed to be 0.95. Thus the effective emissivity for the exposed surfaces was 0.86 and for unexposed surfaces 0.87 as calculated using Equation 5. The thermal radiation configuration factor was assumed unity on all surfaces except for those associated with the inner flange and the web areas. The following equation was used to calculate the configuration factor between the web and the exposure source [Howell, 1982]:

$$F = \sqrt{1 + \frac{h}{w}} - \frac{h}{w} \qquad (10)$$

where F is the configuration factor between the web surface and the exposure source (*i.e.*, fraction of radiant energy incident on the web surface originating from the exposure source), h is the exposed height of the web surface, equal to the web height minus the insulation thickness on the upper and lower flanges (m), and w is the exposed length of the inner flange, roughly equal to

one-half the flange width (m). Likewise, the configuration factor between the inner flange surfaces and the exposure source is given by the following [Howell, 1983]:

$$F = 0.5 \cdot \left(1 + \frac{s}{d} - \sqrt{1 + \frac{s}{d}} \right) \qquad (11)$$

where F is the configuration factor between the inner flange surfaces and the exposure source, s is the exposed height of the web surface, equal to the web height minus the insulation thickness on the upper and lower flanges (m), and d is the exposed length of the inner flange, roughly equal to one-half the flange width (m). The resulting configuration factors for a W8X28 beam protected with 31.7 mm of insulation were 0.323 between the web surfaces and the exposure source and 0.339 between the inner flange surfaces and the exposure source.

The use of equations 10 and 11 to calculate a configuration factor between the surface and the exposure source implies that the insulation surfaces on the unexposed web in flange areas are approximately at the same temperature. As such there would be no net radiation heat exchange between these surfaces.

The exposure source temperature is the ASTM E119-98 [1999] given by Equation 6 in Section 3.2.

Results

The implicit Crank-Nicolson method [Childs, 1998; Smith, 1987; Jaluria *et al.*, 1986] was used to solve for the temperature distribution in the beam assembly. The tolerance for convergence was 1×10^{-6} and the solution time step was 2.0 seconds. Decreasing the tolerance, decreasing the time step, or using the Classical Explicit Procedure or Classical Implicit Procedure did not result in significant changes in the temperature predictions. Typically, four or five cells were used in the insulation through the dimension with the greatest temperature gradient. The total number of cells was 1,064. The flutes in the galvanized steel used to form the concrete were simulated as a 110 mm by 56 mm adiabatic void positioned above the center of the beam. The temperature predictions and predicted fire resistance rating did not significantly change when the number of total cells was increased to 4,024, with resolution increases in each dimension and in each material.

The model was validated by comparing the calculated fire resistance rating using the ASTM E119-98 temperature criteria for steel beams to the listed fire resistance rating for UL Design No. P907 with 31.7 mm Blazeshield D-C/F insulation. The listed fire resistance rating for this assembly is 2 hours. The predicted fire resistance is as follows:

Predicted time average temperature exceeds 593°C:	123.5 minutes
Predicted time peak temperature exceeds 704°C:	132.8 minutes

Thus, the predicted fire resistance of the assembly is 123.5 minutes, 3.5 minutes, or about three percent, greater than the actual listing for the assembly modeled.

The predicted temperature at the four locations used to estimate the fire resistance rating is shown in Figure D-31. Figure D-32 shows the predicted temperature distribution within the entire two-dimensional model domain at 120 minutes after start of ASTM E119 temperature exposure.

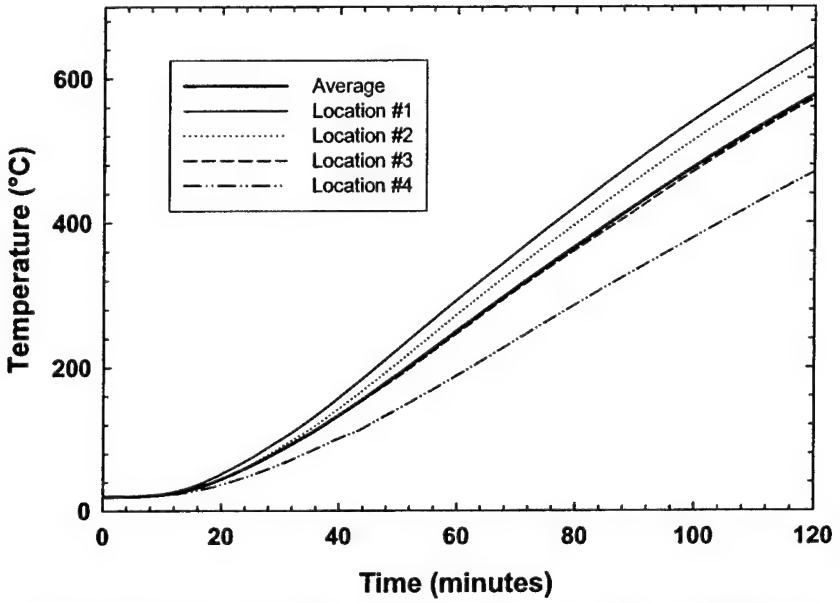

Fig. D-31 — Predicted Temperature at Locations Used to Obtain Fire Resistance Rating for UL Design No. P907 – 1,064 Cell Model

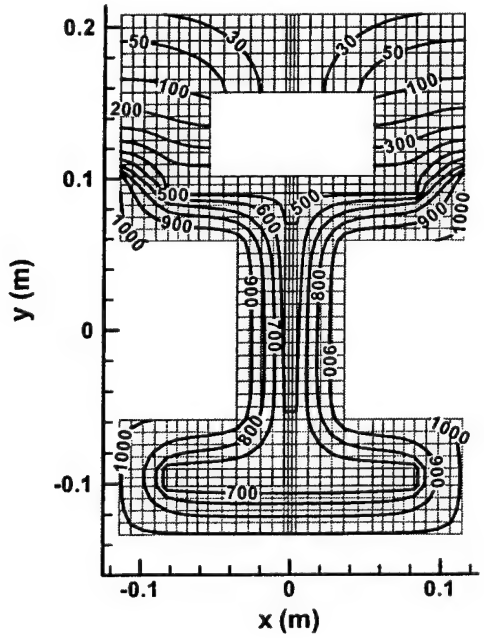

Fig. D-32 — Calculated Temperature Distribution (°C) in UL Design No. P907 at 120 minutes after Start of Exposure – 1,064 Cell Model

Sensitivity of Results to Input Parameter Assumptions

The sensitivity of the calculation results to uncertainty in the material properties and boundary conditions is assessed relative to the predicted fire resistance rating of the floor or ceiling-roof assembly. The material properties of the Blazeshield D-C/F and concrete were varied by plus or minus 25 percent. Similarly, the radiation and convection boundary conditions were increased and decreased in order to determine the change in the predicted fire resistance rating. The results are summarized in Table D-8.

Table D-8 — Sensitivity of the Calculated Fire Resistance of UL Design No. P907 to Uncertainty in the Material Property Data and Boundary Condition Parameters

Modified Parameter	Average temperature of 593°C		Peak Temperature of 704°C	
	Time (min)	Difference (min)	Time (min)	Difference (min)
Predicted (unmodified baseline)	123.5	–	132.8	–
Blazeshield D-C/F conductivity increased by 25%	106.9	- 16.6 (- 13.4%)	114.0	-18.8 (- 14.2%)
Blazeshield D-C/F conductivity decreased by 25%	149.8	+ 26.3 (+ 21.3%)	162.9	+ 30.1 (+ 22.3%)
Blazeshield D-C/F heat capacity increased by 25%	129.3	+ 5.8 (+ 4.7%)	138.9	+ 6.1 (+ 4.6%)
Blazeshield D-C/F heat capacity increased by 25%	117.8	- 5.7 (- 4.6%)	126.7	- 6.1 (- 4.6%)
Concrete conductivity increased by 25%	123.7	+ 0.2 (+ 0.2%)	132.8	– (–)
Concrete conductivity decreased by 25%	123.4	- 0.1 (- 0.1%)	132.8	– (–)
Effective emissivity of insulation and concrete increased by ~25%	122.8	- 0.7 (- 0.6%)	132.1	- 0.7 (- 0.5%)
Effective emissivity of insulation and concrete decreased by ~25%	124.7	+ 1.2 (+ 1.0%)	133.8	+ 1.0 (+ 0.8%)
Convection increased by 25%	123.3	- 0.2 (- 0.2%)	132.7	- 0.1 (- 0.1%)
Convection increased by 25%	123.8	+ 0.3 (+ 0.2%)	133.0	+ 0.2 (+ 0.2%)

Table D-8 indicates that the calculated fire resistance rating for UL Design No. P907 is relatively insensitive to uncertainty in the material properties and boundary condition parameters with the notable exception of the thermal conductivity of the Blazeshield D-C/F insulation material. In this case, a twenty five percent increase or decrease in the thermal conductivity value could result in a 15 – 25 percent increase or decrease in the predicted fire resistance rating using the ASTM E119-98 [1999] critical steel temperature criteria.

3.7 Validation Case 7: Steel Beam Protected with Blazeshield Exposed to ASTME119 Test Conditions (UL Design P809)

Validation Case 7 is Underwriters Laboratories (UL) Design Number J809 [UL, 2003]. The UL "J" designs feature concrete floor, roof, or ceiling assemblies where the concrete and steel, if present, is protected with a sprayed fire resistive material. UL Design No. J809 involves a W8X28 beam that supports normal weight siliceous or carbonate aggregate concrete floor or roof-ceiling assembly. The UL Design No. J809 floor or roof-ceiling assembly is rated for 2 hours fire resistance when exposed to the ASTM E119 Standard Time-Temperature profile provided the steel is protected with a 25.4 mm thick coating of Blazeshield D-C/F sprayed fire resistive material and the exposed portions of the concrete is protected with a 14.2 mm thick coating of Blazeshield D-C/F [Underwriters Laboratories, 2003]. The concrete thickness for this particular rating and insulation thickness is 88.9 mm [Underwriters Laboratories, 2003].

The specific basis for the validation case is the unrestrained beam fire resistance rating for the ceiling-roof assembly using the ASTM E119 critical steel temperature criteria [ASTM E119-98, 1999]. A two-dimensional thermal analysis is used to calculate the temperature profiles within the assembly. Figure D-33 depicts the configuration that was modeled with HEATING. The ASTM E119 criteria for rating steel beams is an average temperature of 593°C or a peak temperature of 704°C, whichever occurs first [ASTM E119-98, 1999]. The peak and average temperature are derived from measurements taken at four locations, which are shown in Figure D-33 [ASTM E119-98, 1999].

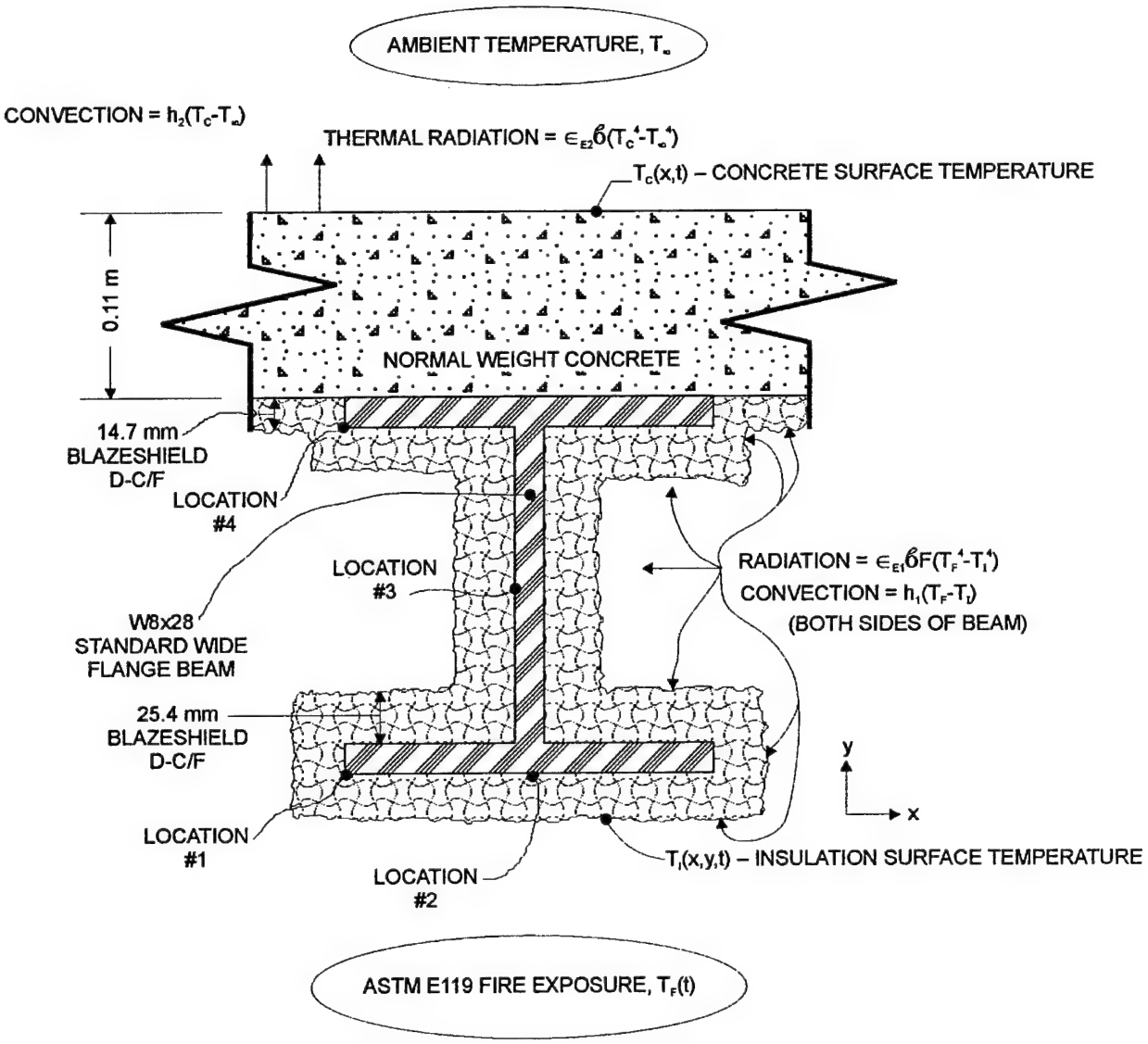

Fig. D-33 — Validation Case 7 (Not to Scale)

Material Properties

The material properties for the steel and Blazeshield D-C/F sprayed fire resistive material are as described in Section 3.6 for Validation Case 6. The material properties for siliceous aggregate normal weight are as described in Section 3.2 for Validation Case 2.

Boundary Conditions

The boundary conditions are as described for Validation Case 6 with the exception of the radiation configuration factor. Because there is 6.3 mm less Blazeshield D-C/F insulation on the steel than Validation Case 6, the radiation configuration factors, calculated using Equations 10 and 11, are different from those calculated in Section 3.6. The resulting configuration factors for

a W8X28 beam protected with 25.4 mm of insulation are 0.281 between the web surfaces and the exposure source and 0.36 between the inner flange surfaces and the exposure source.

Results

The implicit Crank-Nicolson method [Childs, 1998; Smith, 1987; Jaluria *et al.*, 1986] was used to solve for the temperature distribution in the beam assembly. The tolerance for convergence was 1×10^{-6} and the solution time step was 2.0 seconds. Decreasing the tolerance, decreasing the time step, or using the Classical Explicit Procedure or Classical Implicit Procedure did not result in significant changes in the temperature predictions.Typically, four or five cells were used in the insulation through the dimension with the greatest temperature gradient. The total number of cells was 1,436. The temperature predictions and predicted fire resistance rating did not significantly change when the number of total cells was increased to 5,529, with resolution increases in each dimension and in each material.

The model was validated by comparing estimating the fire resistance rating using the ASTM E119-98 [1999] temperature criteria for steel beams to the listed fire resistance rating for UL Design No. J809 with 25.4 mm Blazeshield D-C/F insulation on the steel beam and 14.7 mm on the exposed portions of the concrete floor or ceiling-roof slab. The listed fire resistance rating for this assembly is 2 hours. The predicted fire resistance is as follows:

Predicted time average temperature exceeds 593°C: 130.5 minutes

Predicted time peak temperature exceeds 704°C: 116.3 minutes

Thus, the predicted fire resistance of the assembly is 116.7 minutes, 3.7 minutes, or about three percent, less than the actual listing for the assembly modeled.

The predicted temperature at the four locations used to estimate the fire resistance rating is shown in Figure D-34. Figure D-35 shows the predicted temperature distribution within the entire two-dimensional model domain at 120 minutes after start of ASTM E119 temperature exposure.

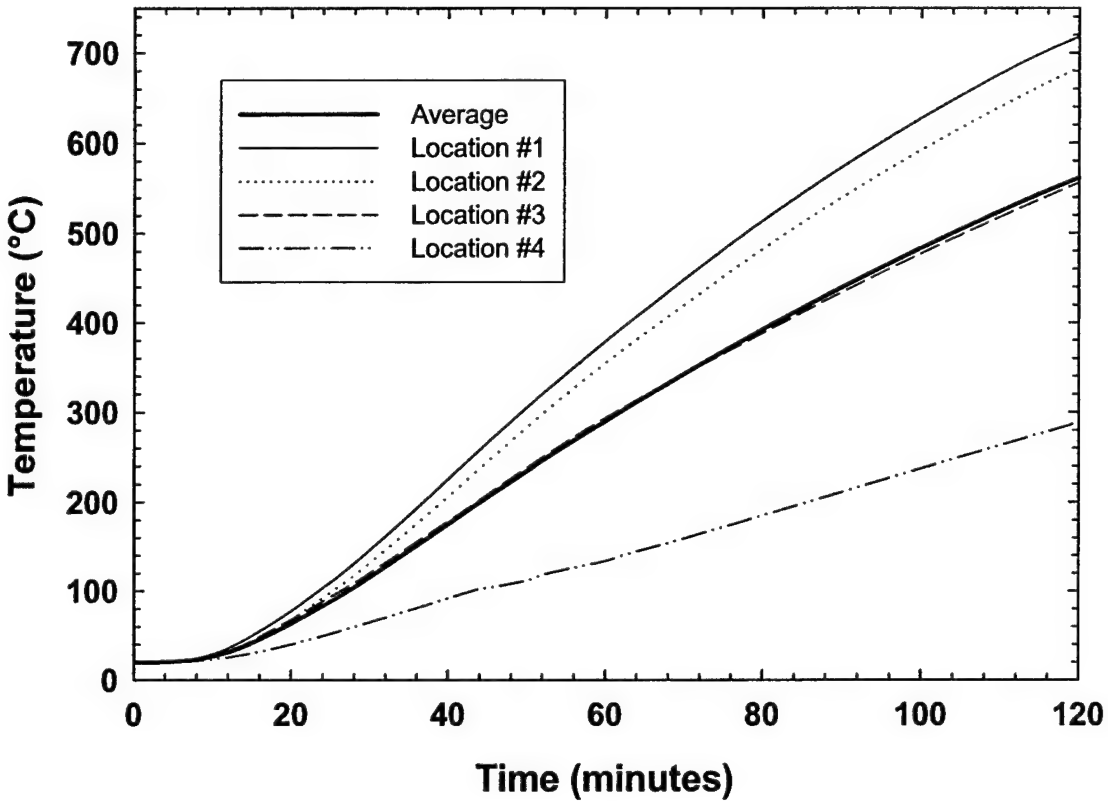

Fig. D-34 — Predicted Temperature at Locations Used to Obtain Fire Resistance Rating for UL Design No. J809 – 1,436 Cell Model

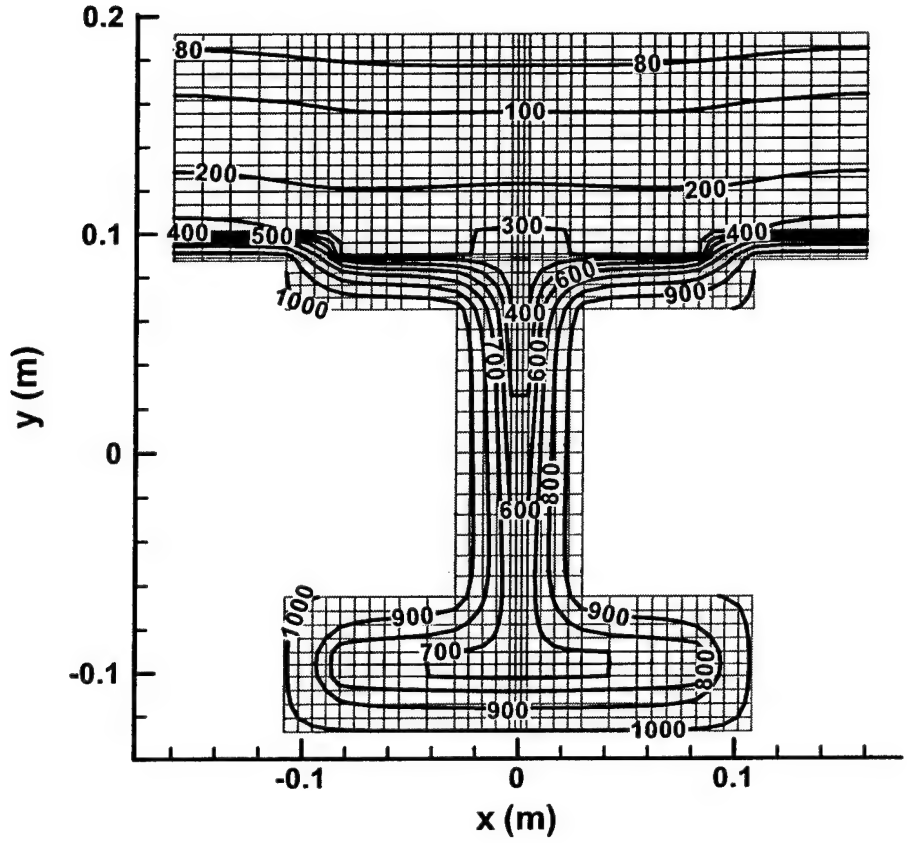

Fig. D-35 — Calculated Temperature Distribution (°C) in UL Design No. J809 at 120 minutes after Start of Exposure – 1,436 Cell Model

Sensitivity of Results to Input Parameter Assumptions

The sensitivity of the calculation results to uncertainty in the material properties and boundary conditions is assessed relative to the predicted fire resistance rating of the floor or ceiling-roof assembly. The material properties of the Blazeshield D-C/F and concrete were varied by plus or minus 25 percent. Similarly, the radiation and convection boundary conditions were increased and decreased in order to determine the change in the predicted fire resistance rating. The results are summarized in Table D-9.

Table D-9 — Sensitivity of the Calculated Fire Resistance of UL Design No. J809 to Uncertainty in the Material Property Data and Boundary Condition Parameters

Modified Parameter	Average temperature of 593°C		Peak Temperature of 704°C	
	Time (min)	Difference (min)	Time (min)	Difference (min)
Predicted (unmodified baseline)	130.5	–	116.3	–
Blazeshield D-C/F conductivity increased by 25%	111.3	- 19.2 (- 14.7%)	99.3	- 17.0 (- 14.6%)
Blazeshield D-C/F conductivity decreased by 25%	163.2	+ 32.7 (+ 25.0%)	145.0	+ 28.7 (+ 24.7%)
Blazeshield D-C/F heat capacity increased by 25%	134.5	+ 4.0 (+ 0.3%)	120.5	+ 4.2 (+ 3.6%)
Blazeshield D-C/F heat capacity increased by 25%	126.5	- 4.0 (- 0.3%)	112.2	- 4.1 (- 3.5%)
Concrete conductivity increased by 25%	133.5	+ 3.0 (+ 2.2%)	116.8	+ 0.5 (+ 4.2%)
Concrete conductivity decreased by 25%	127.0	- 3.5 (- 2.7%)	115.8	- 0.5 (- 4.2%)
Effective emissivity of insulation and concrete increased by ~25%	128.8	- 1.7 (- 1.3%)	115.2	- 1.1 (- 9.4%)
Effective emissivity of insulation and concrete decreased by ~25%	133.5	+ 3.0 (+ 2.2%)	118.7	+ 2.4 (+ 2.1%)
Convection increased by 25%	130.3	- 0.2 (- 0.2%)	116.2	- 0.1 (- 0.1%)
Convection increased by 25%	130.8	+ 0.3 (+ 2.2%)	116.7	+ 0.4 (+ 0.3%)

Table D-9 indicates that the calculated fire resistance rating for UL Design No. J809 is relatively insensitive to uncertainty in the material properties and boundary condition parameters with the notable exception of the thermal conductivity of the Blazeshield D-C/F insulation material. In this case, a twenty five percent increase or decrease in the thermal conductivity value could result in a 15 – 25 percent increase or decrease in the predicted fire resistance rating using the ASTM E119-98 [1999] critical steel temperature criteria.

3.8 Validation Case 8: Gypsum-Steel Stud Wall Assembly Exposed to CAN/ULL-S101-M89 Test Conditions

Validation Case 8 consists of an uninsulated steel-stud wall assembly constructed and tested in accordance with CAN/ULC-S101-M89 [1989; Sultan, 1996; Alfawakhiri *et al*, 2000]. The wall assembly of interest consists of 90 mm by 30 mm by 0.46 mm thick steel studs spaced 600 mm on center. Type X gypsum 15.9 mm was attached to the exposed and unexposed sides of the steel studs. The wall assembly was exposed to the CAN/ULC-S101-M89 time-temperature profile until the average temperature of the unexposed wall surface (measured using thermocouple pads) increased to 140°C above ambient [CAN/ULC-S101-M89, 1989; Sultan,

1996], the fire resistance rating of the assembly. This occurred at 54 minutes for the test used to validate HEATING.

The specific basis for the validation case is the transient temperature within the cavity space on the exposed and unexposed gypsum surfaces and the average temperature on the unexposed side of the wall. The latter measurements were made with and without thermocouple pads, thus both measurements techniques are used in this validation case. The fire resistance rating of the assembly was also used as a validation basis, defined by CAN/ULC-S101-M89 [1989] as an average temperature increase on the unexposed surface of 140°C or a peak single point temperature increase of 180°C. Both measurements include thermocouple pads.

A two-dimensional thermal analysis is used to calculate the temperatures at the various locations as well as determining the fire resistance rating of the wall assembly. A single wall cavity section was modeled due to symmetry. Heat transfer within the void space was included in the model. Figure D-36 depicts the configuration modeled where there is no thermocouple pad. The same configuration was also modeled with a thermocouple pad present as noted above.

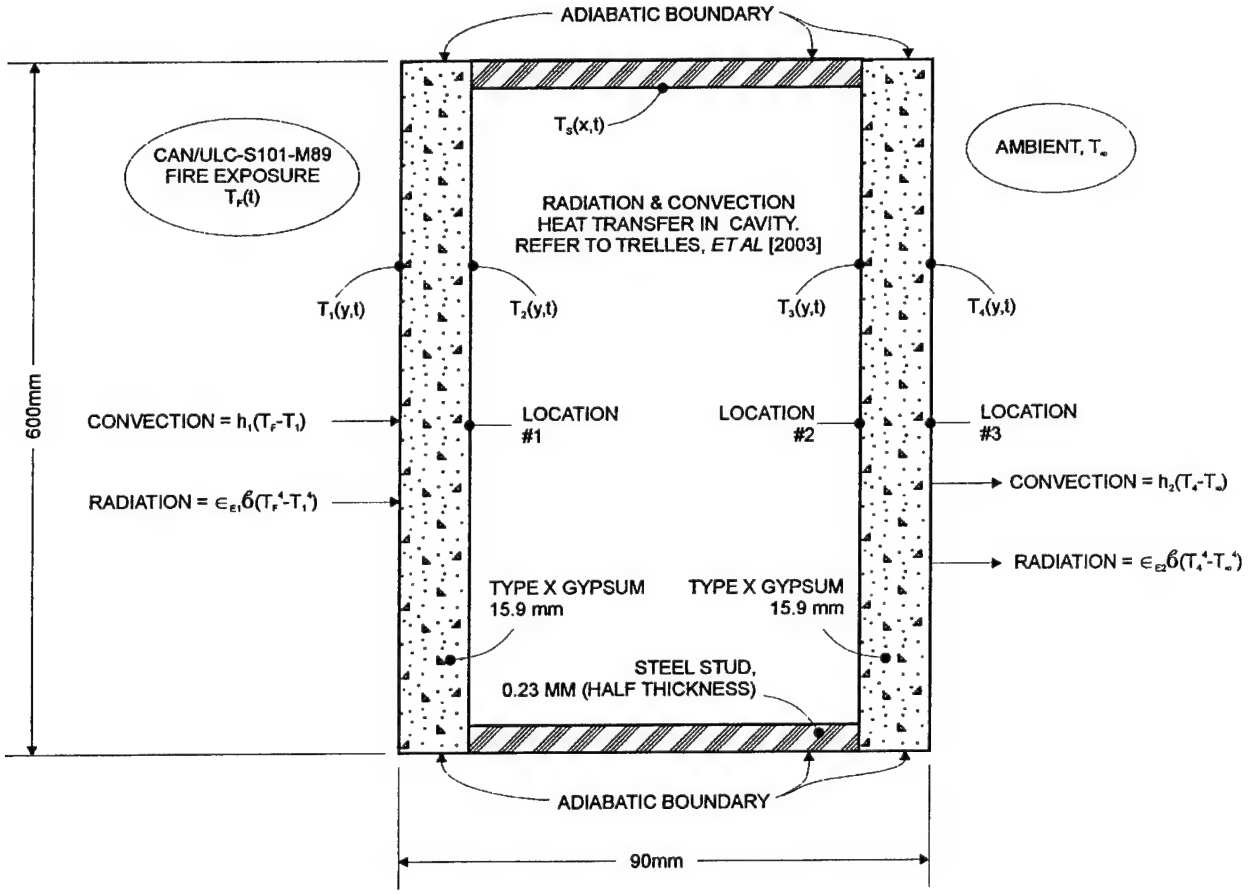

Fig. D-36 — Validation Case 8 – Thermocouple Pad not Shown (Not to Scale)

Material Properties

The material properties for steel and the thermocouple pad are as described for Validation Case 1.

The thermal conductivity, heat capacity, and density of gypsum vary with temperature [Harmathy, 1993; Sultan, 1996; Alfawakhiri, 2000]. Figure D-37 shows the thermal conductivity and heat capacity of Type X gypsum as a function of temperature [Sultan, 1996; Alfawakhiri, 2000]. The density is as follows [Sultan, 1996]:

- 698 kg/m^3 – 20°C to 80°C; and
- 576 kg/m^3 – over 80°C.

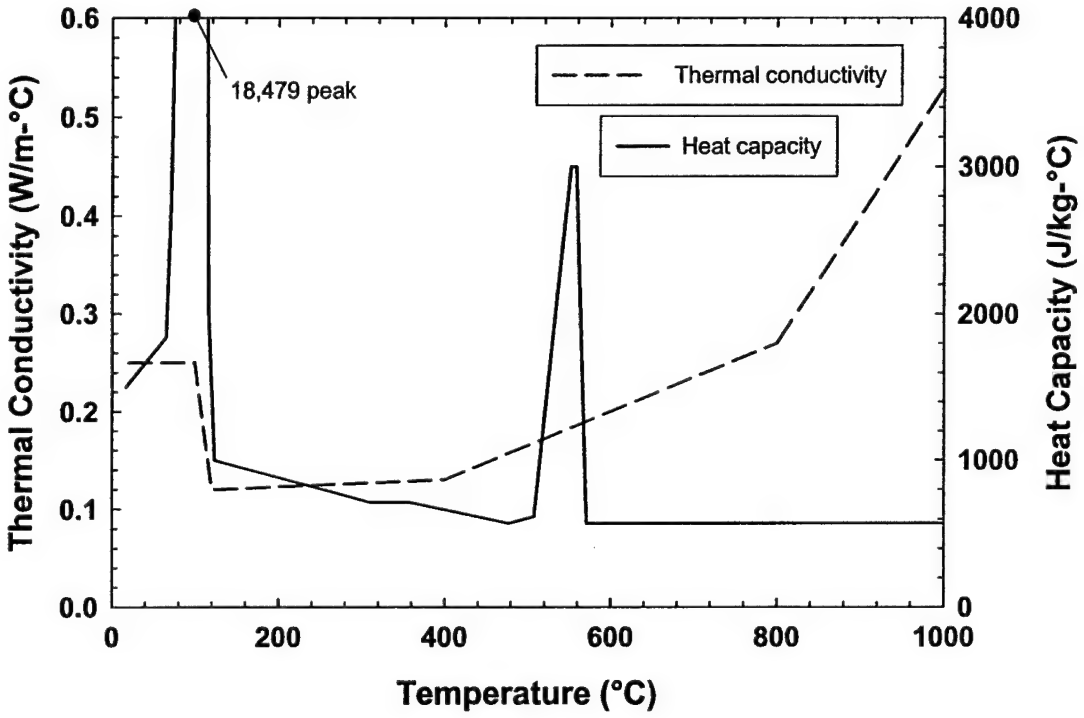

Fig. D-37 — Thermal Conductivity and Heat Capacity of Type X Gypsum [Sultan, 1996; Alfawakhiri, 2000].

Boundary Conditions

A natural convection boundary condition was applied to all exposed and unexposed wall surfaces, as described by Equation 3, except for inside the cavity and the axes of symmetry, which are by definition adiabatic. A forced convection boundary condition was applied inside the cavity. The natural convection coefficient and exponent for the non-cavity surfaces was 1.31 W/m^2-°C$^{1.33}$ and 1.33, respectively [Holman, 1990], as described in Section 3.2 for wall surface boundary conditions. The forced convection coefficient applied to the cavity boundaries was derived from natural convection information provided by Sultan [1996]. Based on this

information, the equivalent forced convection coefficient, assuming a 100°C temperature difference within the cavity space, a cavity height of 3.05 m, and a cavity width of 90 mm, is 7.3 W/m^2-°C. Trelles *et al.* [2003] describes the manner in which convection boundary conditions are applied to cavity space boundaries using HEATING.

A thermal radiation boundary condition was applied to all exposed and unexposed surfaces, including inside the cavity, of the gypsum and steel wall assembly as described by Equations 4 and 5, except for the axes of symmetry, which are by definition adiabatic. The emissivity of the steel was assumed to be 0.8, the emissivity of the thermocouple pad was assumed to be 0.91, and the emissivity of the gypsum was assumed to be 0.84 [Sparrow *et al.*, 1978; Holman, 1990; and Incropera *et al.*, 1985; Sultan, 1996]. The ambient emissivity was assumed to be 0.95. The resultant or effective emissivity for the exposed surface, as calculated using Equation 5, is thus 0.8 and for the unexposed surface it is 0.87 (thermocouple pad present) or 0.8 (no thermocouple pad). The view factor was unity between ambient environment and the concrete and the thermocouple pad surfaces. The effective emissivity and view factor vary from node to node inside the wall cavity. Refer to Trelles *et al.* [2003] for a description of the calculation procedure for thermal radiation heat transfer in cavity spaces.

The exposure temperature was the Standard CAN/ULC-S101-M89 [1989] Time-Temperature profile, a similar exposure to the ASTM E119-98 [1999] Standard Time-Temperature profile. The CAN/ULC-S101-M89 temperature profile may be determined using the following equation [Sultan, 1996]:

$$T_f(t) = T_\infty + 750\left[1 - \exp\left(-3.79553\sqrt{t}\right)\right] + 170.41\sqrt{t} \quad (12)$$

where $T_f(t)$ is the exposure temperature (°C) at time t (hr).

Results

The implicit Crank-Nicolson method [Childs, 1998; Smith, 1987; Jaluria *et al.*, 1986] was used to solve for the temperature distribution in the wall assembly. The tolerance for convergence was 1×10^{-6} and the solution time step was 1.0 seconds. Decreasing the tolerance, decreasing the time step, or using the Classical Explicit Procedure or Classical Implicit Procedure produced the same results. Two distinct domain models were prepared: one in which thermocouple pads were absent and one in which thermocouple pads were present. The width of the thermocouple pads was assumed to be 0.15 m, as prescribed by CAN/ULC-S101-M89 [1989]. A total of 714 cells were used to model the configuration lacking the thermocouple pads and 1,029 cells were used to model the configuration that included the thermocouple pads. Increasing the number of cells to 2,668 and 3,868 for the two configurations did not significantly change the temperature predictions.

The model was validated by comparing the predicted and measured average temperature of the gypsum at various locations within the wall assembly, shown in Figure D-36. The tranient temperatures at these locations are shown in Figure D-38. Figure D-39 and Figure D-40 show the temperature profile within the wall assemblies after 45 minutes exposure to the CAN/ULC-S101-M89 [1989] temperature profile.

The fire resistance rating, based on an average temperature increase of 140°C or a peak temperature increase of 180°C on the unexposed surface when measured using thermocouple pads, was also used as a comparison basis. In both cases, the temperature measurement includes a thermocouple pad. The results are as follows [Sultan, 1996]:

- Predicted time average temperature rise exceeds 140°C above ambient: 48.5
- Measured time average temperature rise exceeds 140°C above ambient: 54.0

- Predicted time peak temperature rise exceeds 180°C above ambient: 49.3
- Measured time peak temperature rise exceeds 180°C above ambient: 52.0

The predicted fire resistance rating of the assembly is thus 48.5 minutes and the measured fire resistance rating was 52 minutes.

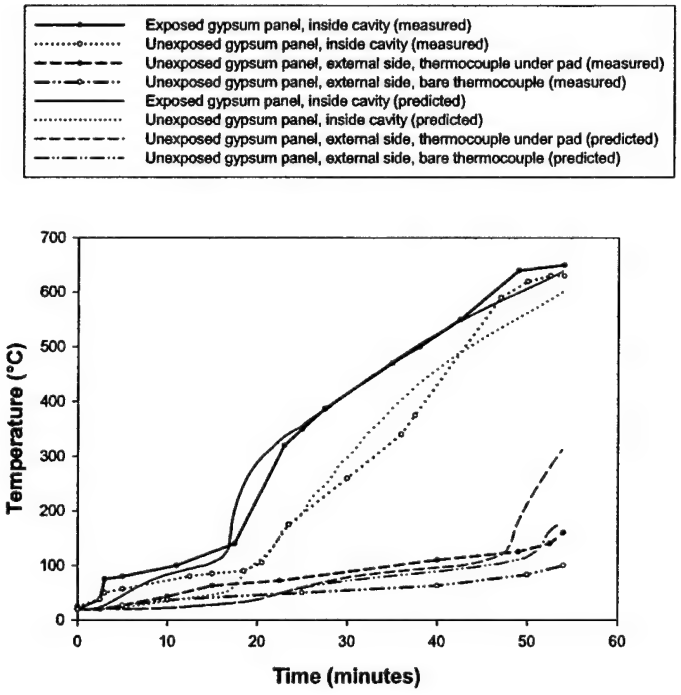

Fig. D-38 — Predicted versus Measured Gypsum Surface Temperatures for Wall Assembly – 714 and 1,029 Cell Models [Sultan, 1996; Alfawakhiri, 2000].

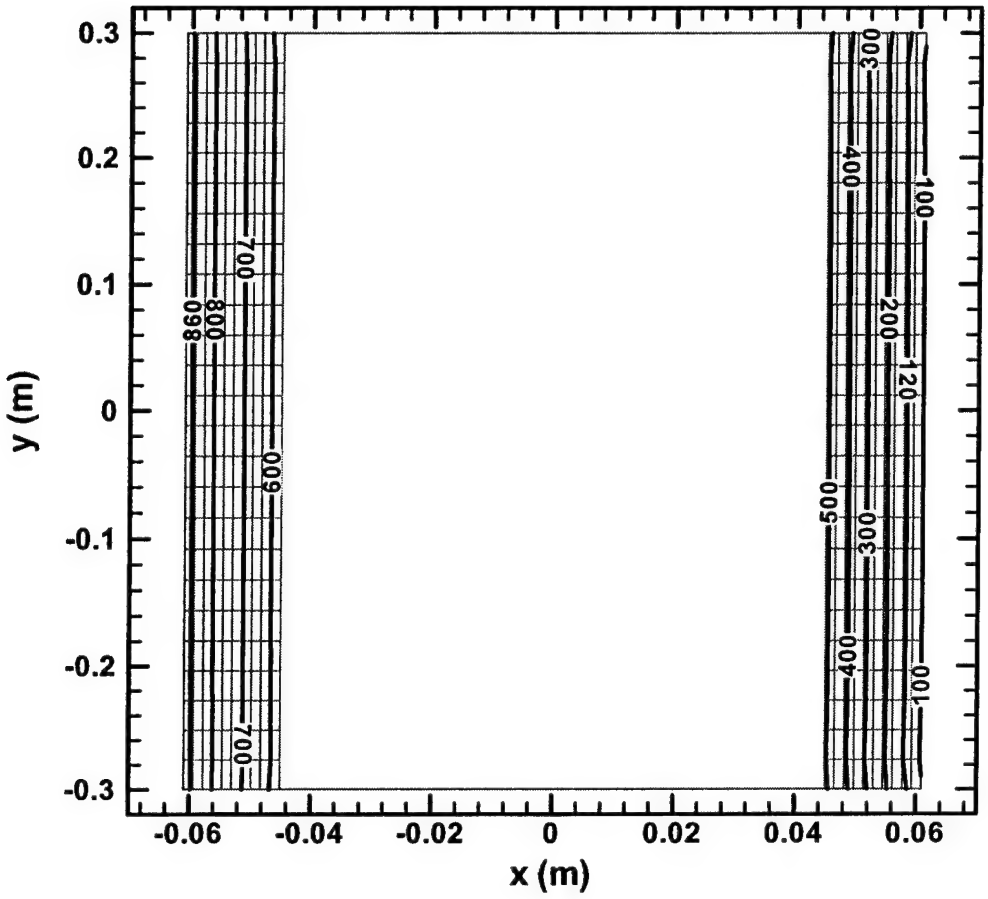

Fig. D-39 — Temperature Profile in Wall Assembly 45 Minutes after Start of CAN/ULC-S101-M89 [1989] Exposure – 714 Cell Model, No Thermocouple Pads (Note: x an y Axes Use Different Scales)

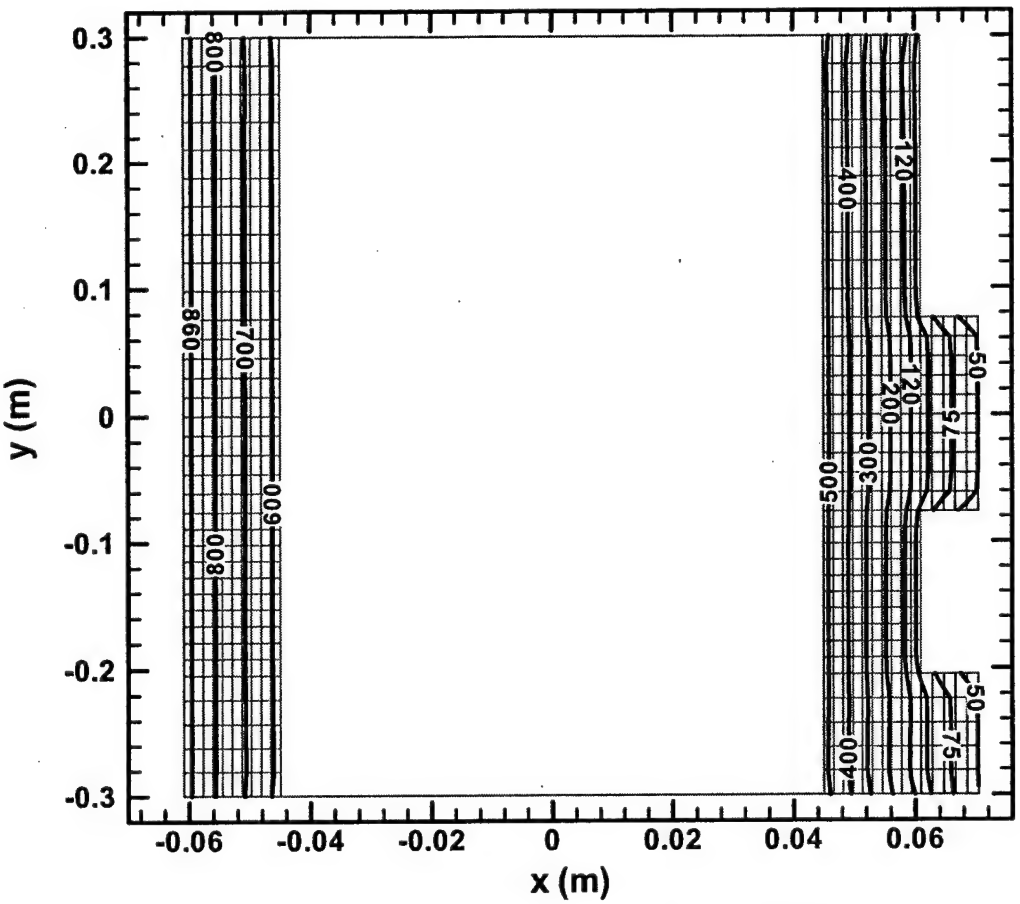

Fig. D-40 — Temperature Profile in Wall Assembly 45 Minutes after Start of CAN/ULC-S101-M89 [1989] Exposure – 1,029 Cell Model, Thermocouple Pads Included (Note: *x* an *y* Axes Use Different Scales)

Sensitivity of Results to Input Parameter Assumptions

The sensitivity of the calculation results to uncertainties in the material properties and the boundary conditions is assessed relative to predicted transient average temperature at specific locations and to the predicted fire resistance rating of the wall assembly. The material properties of the gypsum were varied by plus or minus 25 percent. Similarly, the radiation and convection boundary conditions on all surfaces, including the cavity boundaries, were increased and decreased in order to determine the change in the predicted fire resistance rating. Figures D-41 and 42 show the sensitivity of the transient average temperature at Location #2 to uncertainty in the material properties and boundary conditions, respectively. Likewise, Figures D-43 and 44 show the sensitivity of the temperature predictions at Location #3 (bare thermocouple). Similar results are observed for Location #1 and Location #3 (with thermocouple pads). Table D-10 summarizes the sensitivity of the predicted fire resistance rating to parameter uncertainty.

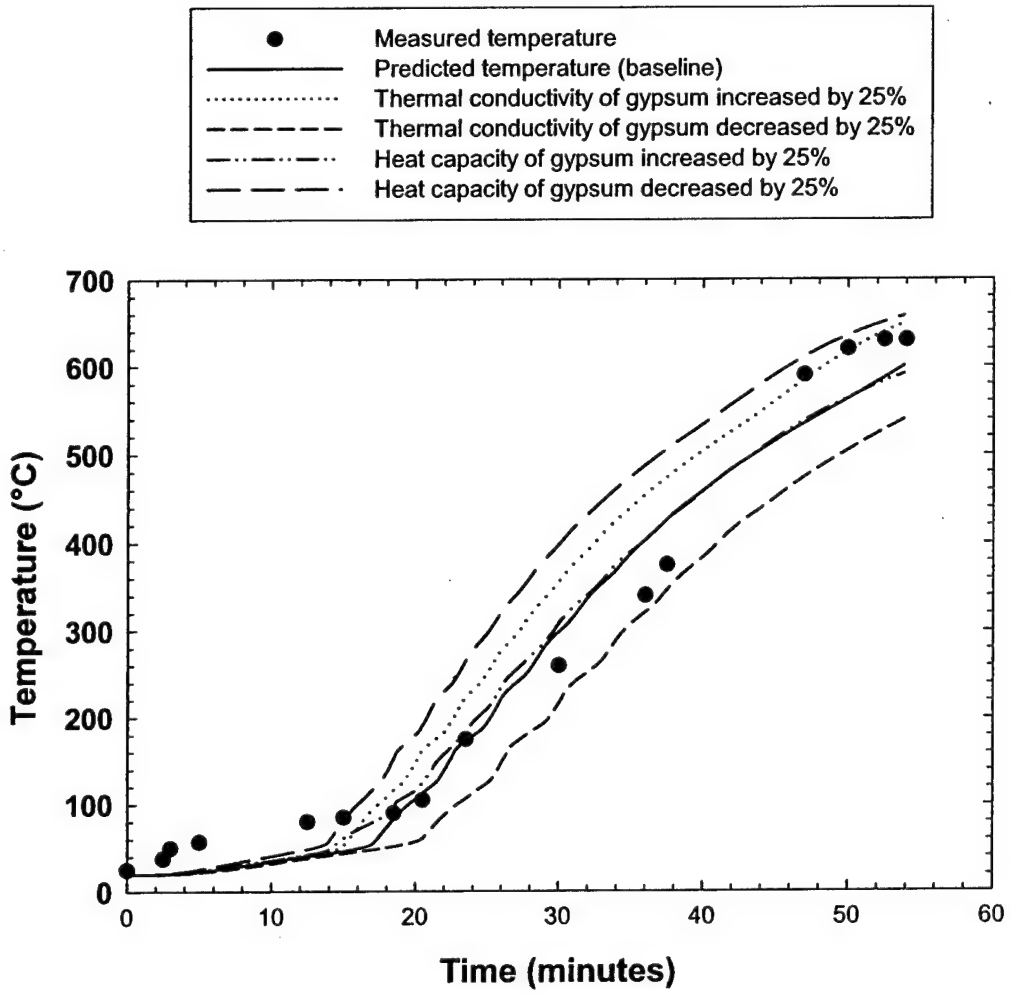

Fig. D-41 — Sensitivity of Location #2 Temperature Predictions to Material Property Uncertainty

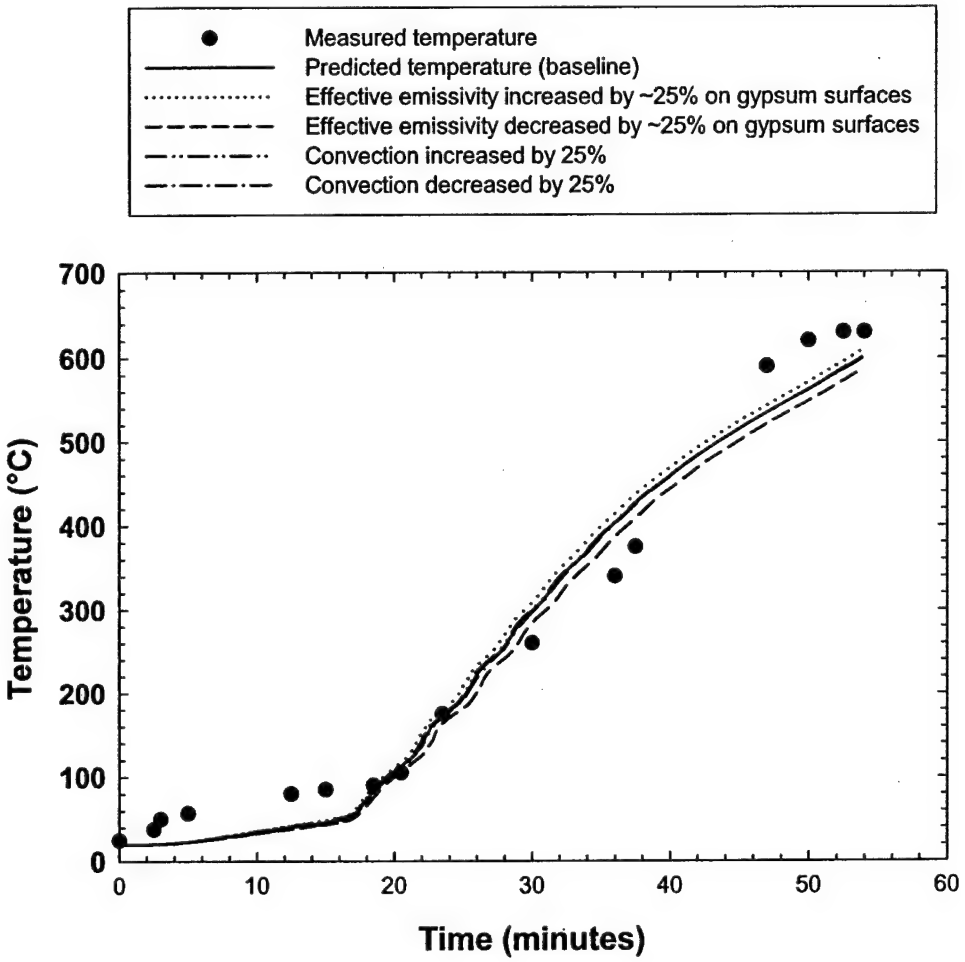

Fig. D-42 — Sensitivity of Location #2 Temperature Predictions to Boundary Condition Parameter Uncertainty

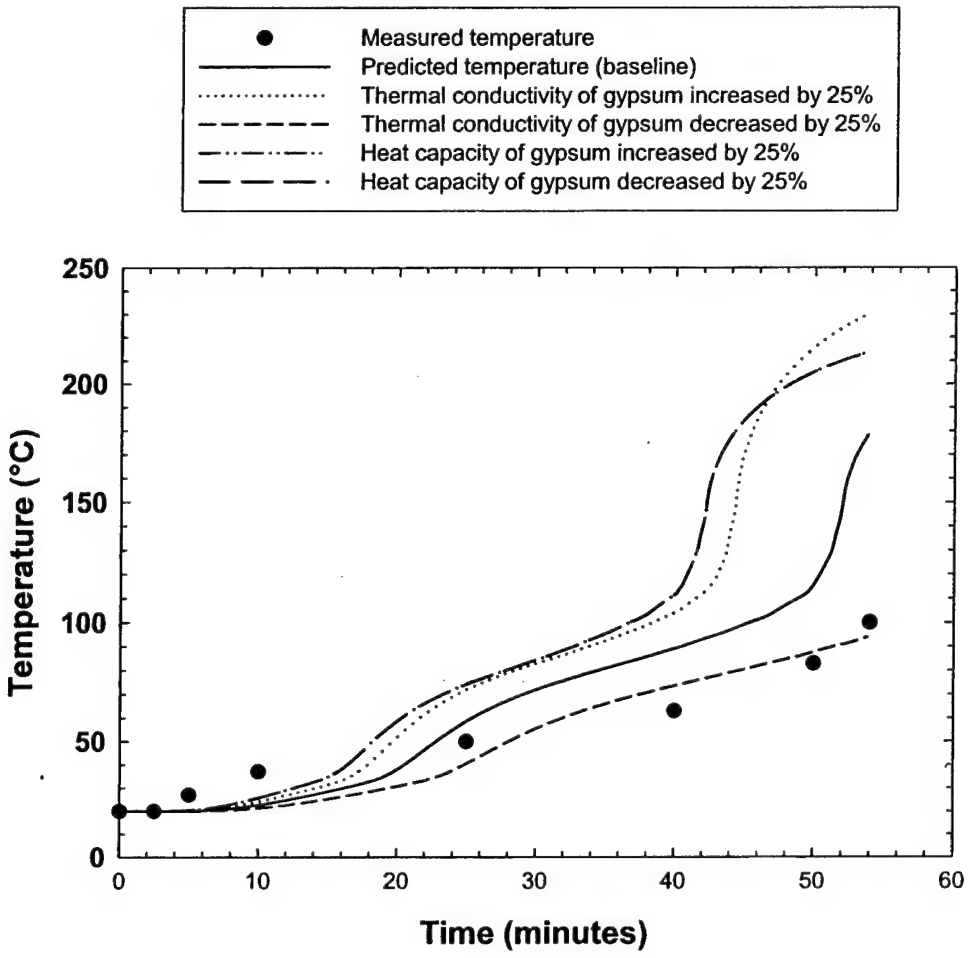

Fig. D-43 — Sensitivity of Location #3 (Bare Thermocouple) Temperature Predictions to Material Property Uncertainty

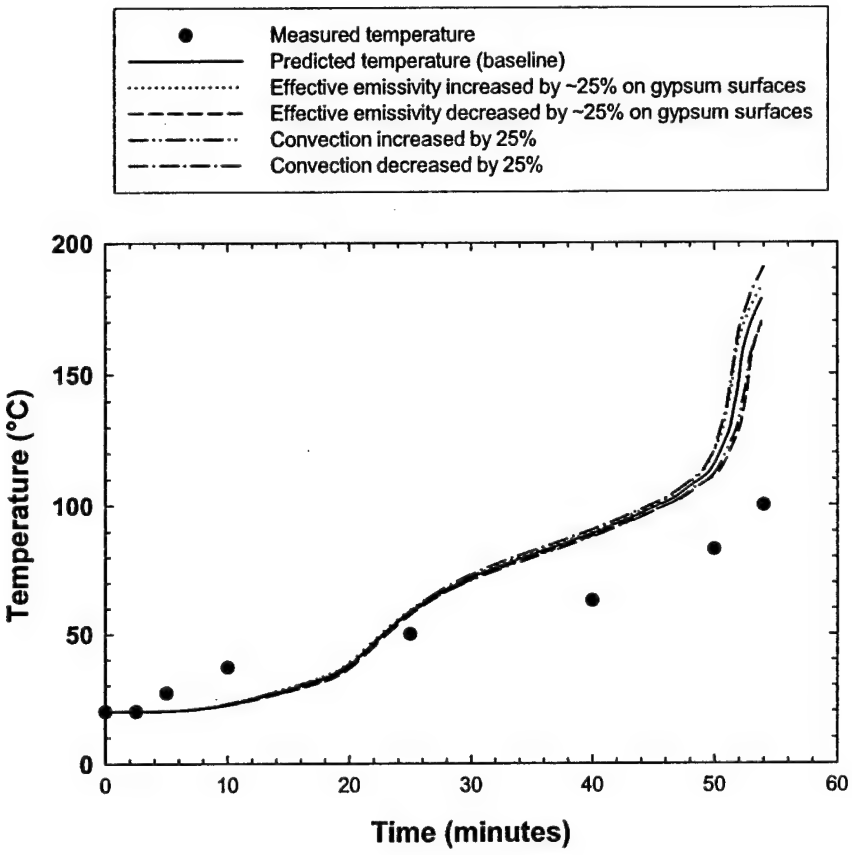

Fig. D-44 — Sensitivity of Location #3 (Bare Thermocouple) Temperature Predictions to Boundary Condition Parameter Uncertainty

Table D-10 indicates that the calculated fire resistance rating for gypsum wall assembly is somewhat sensitive to uncertainty in the material properties of the gypsum material. A twenty five percent increase or decrease in the material property values could result in a 10 – 25 percent increase or decrease in the predicted fire resistance rating using the CAN/ULC-S101-M89 [1989] criteria for wall assemblies.

Table D-10 — Sensitivity of the Calculated Fire Resistance of a Gypsum Wall Assembly to Uncertainty in the Material Property Data and Boundary Condition Parameters

Modified Parameter	Average temperature of 140°C		Peak Temperature of 180°C	
	Time (min)	Difference (min)	Time (min)	Difference (min)
Predicted (unmodified baseline)	48.5	–	49.3	–
Gypsum conductivity increased by 25%	42.0	- 6.5 (- 13.4%)	42.5	- 6.8 (- 13.8%)
Gypsum conductivity decreased by 25%	59.1	+ 10.6 (+ 21.9%)	60.2	+ 10.9 (+ 22.1%)
Gypsum heat capacity increased by 25%	57.2	+ 8.7 (+ 17.9%)	57.8	+ 8.5 (+ 17.2%)
Gypsum heat capacity increased by 25%	39.5	- 9.0 (- 18.6%)	40.5	- 8.8 (+ 17.8%)
Effective emissivity increased by ~25% on all gypsum surfaces	47.8	+ 0.3 (+ 0.6%)	49.5	+0.2[1] (+ 0.4%)
Effective emissivity decreased by ~25% on all gypsum surfaces	49.8	+ 0.8 (+ 1.6%)	50.8	+ 1.5[1] (+ 3.0%)
Convection increased by 25%	48.5	– (–)	49.0	- 0.3 (- 0.6%)
Convection decreased by 25%	48.7	+ 0.2 (+ 0.4%)	49.7	+ 0.4 (+ 0.8%)

[1]Note that an increase in the predicted fire resistance rating is observed when the effective emissivity is increased *and* decreased. The reason this occurs is because the emissivity of the thermocouple pad remains constant.

4.0 CONCLUSIONS

HEATING has compared successfully with eight validation cases of increasing complexity. Validation cases were selected based on the availability of test data and material properties for the configurations tested. The validation basis varied from case to case depending on the particular test available, and included fire resistance ratings, temperatures at fixed locations at fixed times, and transient temperatures at fixed locations. Convergence was demonstrated in each case by increasing the number of nodes, reducing the time step, reducing the tolerance, and using alternative solution methods.

The sensitivity of each validation case to the input parameters was also investigated because of the inherent uncertainty in the specific material properties, especially at elevated temperatures, as well as the boundary condition parameters. An uncertainty of plus or minus 25 percent was assumed where applicable. It was found that the validation cases generally separated into three categories: those sensitive to boundary condition parameters, namely the effective emissivity of the exposed surface; those sensitive to the material properties, in particular the thermal conductivity of the dominant material, and those that were insensitive to uncertainty in either parameter group.

5.0 REFERENCES

1. Abrams, M. S. (1979), "Behavior of Inorganic Materials in Fire," *Design of Buildings for Fire Safety*, ASTM STP 685, E. E. Smith and T. Z. Harmathy, Eds., American Society of Testing and Materials, Philadelphia, PA, 1979.

2. Abrams, M. S. and Gustaferro, A. H. (1968), "Fire Endurance of Concrete Slabs as Influenced by Thickness, Aggregate Type, and Moisture," Research Department Bulletin 223, Portland Cement Association, Skokie, IL, 1968.

3. Alfawakhiri, F. (2000), "Computer Program TRACE User Manual," Canadian Steel Construction Council and National Research Council Canada, Ottawa, August, 2000.

4. Alfawakhiri, F., Sultan, M. A., and Kodur, V. K. R. (2000), "Loadbearing LSF Walls Exposed to Standard Fire," Proceedings of the 3rd Structural Specialty Conference of the Canadian Society for Civil Engineering, London, Ontario, June, 2000.

5. Arpaci, V. S. (1966), *Conduction Heat Transfer*, Reading, MA: Addison-Wesley, 1966.

6. ASCE 29-99 (1998), "Standard Calculation Methods for Structural Fire Protection," ASCE Standard ASCE/SFPE 29-99, American Society of Civil Engineers, Structural Engineering Institute, Reston, VA, 1998.

7. ASTM E119-98 (1999), "Standard Test Methods for Fire Tests of Building Construction Materials," American Society of Testing and Materials, West Conshohocken, PA, 1999.

8. Barnett, J. R. (1989), "The Development of an Analytical Methodology for the Design of Steel Framed Structures Exposed to Fires," Ph. D. Dissertation, Worcester Polytechnic Institutes, Worcester, MA, 1989.

9. Becker, B. R. (1977), "A Direct Solution Technique for Solving Steady-State Problems Using the HEATING6 Heat Transfer Code," Technical Report K/CSD/TM-15, Union Carbide Corp., Nuclear Div., Gaseous Diffusion Plant, Oak Ridge, Tennessee, 1977.

10. Bird, R. B., Stewart, W. E., and Lightfoot, E. N. (1960), *Transport Phenomena*, John Wiley & Sons, New York, New York, 1960.

11. Bryan, C. B., Childs, K. W., and Giles, G. E. (1986), "HEATING6 Verification," Technical Report K/CSD/TM-61, Oak Ridge National Laboratory, Oak Ridge, Tennessee, 1986.

12. CAN/ULC-S101-M89 (1989), "Standard Methods of Fire Endurance Tests of Building Construction and materials, Underwriters' Laboratories of Canada, Scarborough, Ontario, 1989.

13. Carslaw, H. S., and Jaeger, J. C. (1959), *Conduction of Heat in Solids*, 2nd ed., Oxford, England, Clarendon, 1959.

14. Carlson, C. C., Benjamin, I. A., Sheridan, R. R., and Troxell, G. E. (1961), "Symposium on Fire Resistance of Concrete," Special Publication SP-5, American Concrete Institute, 1961.

15. Childs, K. W. (1990), HEATING 7.0 User's Manual, Technical Report K/CSD/INF/90-32, Martin Marietta Energy Systems, Inc., Gaseous Diffusion Plant, Oak Ridge, Tennessee, 1990.

16. Childs, K. W. (1991), "HEATING 7.1 User's Manual," Technical Report K/CSD/TM-96, Martin Marietta Energy Systems, Inc., Gaseous Diffusion Plant, Oak Ridge, Tennessee, 1991.

17. Childs, K. W. (1998), "HEATING 7: Multidimensional, Finite-Difference Heat Conduction Analysis Code System, Versions 7.2i and 7.3," RSICC Report PSR-199, Oak Ridge, Tennessee: Oak Ridge National Laboratory, 1998.

18. Childs, K. W., Giles, G. E., Bryan, C. B., and Cobb, C. K. (1990), "HEATING: A Computer Program for Multidimensional Heat Transfer Analysis (Version 6.1), Sect. F10 of SCALE: A Modular Code System for Performing Standardized Computer Analysis for Licensing Evaluation," Technical Report ORNL/NUREG/CSD-2/V2/R3, Martin Marietta Energy Systems, Inc., Oak Ridge National Laboratory, Oak Ridge, Tennessee, 1990.

19. Chu, W. (1989), "HEATCHEK: A Computer Program to Automate Verification of New Versions of HEATING," Technical Report K/CSD/INF-89/4, Union Carbide Corp., Nuclear Div., Gaseous Diffusion Plant, Oak Ridge, Tennessee, 1989.

20. Danish Institute of Fire and Security Technology (DIFST) (2002a), "Class A-60 Bulkhead," File No. PG110022, February 22, 2002.

21. Danish Institute of Fire and Security Technology (DIFST) (2002b), "Class A-60 Deck," File No. G10685 February 22, 2002.

22. Danish Institute of Fire and Security Technology (DIFST) (2002c), "Class A-30 Bulkhead," File No. PG11043, July 17, 2002.

23. Danish Institute of Fire and Security Technology (DIFST) (2002d), "Class A-30 Deck," File No. PG11052, July 22, 2002.

24. Elrod, D. C., Giles, G. E., and Turner, W. D. (1984), "HEATING6: A Multidimensional Heat Conduction Analysis with the Finite-Difference Formulation, Sect. F10 of SCALE: A Modular Code System for Performing Standardized Computer Analysis for Licensing Evaluation," Technical Report NUREG/CR-0200, Rev. 2, U.S. Nuclear Regulatory Commission, Washington, D.C, 1984.

25. Fleischmann, C. (1995), "Analytical Methods for Determining Fire Resistance of Concrete Members," Chapter 4-10, The SFPE Handbook of Fire Protection Engineering, Second Edition, National Fire Protection Association, Quincy, MA, 1995.

26. Flynn, D. R. (1999), "Response of High Performance Concrete to Fire Conditions: Review of Thermal Property Data and Measurement Techniques," NIST GCR 99-767, National Institute of Standards and Technology, Gaithersburg, MD, 1999.

27. Fowler, T. B. and Volk, E. R. (1959), "Generalized Heat Conduction Code for the IBM-704 Computer," Technical Report ORNL-2734, Union Carbide Corp., Nuclear Div., Oak Ridge National Laboratory, Oak Ridge, Tennessee, 1959.

28. Harmathy, T. Z. (1983), "Properties of Building Materials at Elevated Temperatures," DBR Paper No. 1080, Division of Building Research, National Research Council of Canada, Ottawa, March, 1983.

29. Holman, J. P. (1990), *Heat Transfer*, Seventh Edition, McGraw-Hill Publishing Company, New York, New York, 1990.

30. Howell, J. R. (1982), *A Catalog of Radiation Configuration Factors*, McGraw-Hill Book Company, New York, New York, 1982.

31. Incropera, F. P. and De Witt, D. P. (1985), *Fundamentals of Heat and Mass Transfer*, Second Edition, John Wiley & Sons, New York, New York, 1985.

32. International Maritime Organization (IMO) A.754(18) (1993), "Fire Test Procedures, Resolution A.754(18), Recommendations on Fire Resistance Tests for 'A','B', and 'F' Class Divisions," London, England, November 4, 1993.

33. International Standards Organization (ISO) 834 (1999), "Fire Resistance Tests – Elements of Building Construction – Part 1 – General Requirements," International Organizations for Standardization, Geneva, Switzerland, 1999.

34. Issen, L. A. (1974), "An Analytical Model for Calculating the Fire Resistance of Simply Supported Prestressed and Reinforced Concrete Beams," National Bureau of Standards Special Publication 411, Fire Safety Research, Gaithersburg, MD, 1974.

35. Jaluria, Y. and Torrance, K. E. (1986), *Computational Heat Transfer*, Washington, DC: Hemisphere, 1986.

36. Jones, J. B. and Hawkins, G. A. (1986), *Engineering Thermodynamics*, John Wiley & Sons, 1986.

37. Leonard, J. T., Fulper, C. R., Darwin, R. L., Back, G. G., Ouellette, R. J., Scheffey, J. L., and Willard, R. L. (1991), Post-Flashover Fires in Simulated Shipboard Compartments:

Phase II-Cooling of Fire Compartment Boundaries," NRL Memorandum Report 6896, Naval Research Laboratory, Washington, D. C., September 19, 1991.

38. Leonard, J. T., Scheffey, J. L., and Beitel, J. J. (1993), "Fire Resistance Tests of Insulation Subjected to UL-1709 Fire Exposure," NRL Letter Report Series 6180/312, Naval Research Laboratory, Washington, D. C., August, 1993.

39. Levy, S. (1968), "Use of 'Explicit Method' in Heat Transfer Calculations with an Arbitrary Time Step, 68-C-282, General Electric, Schenectady, NY, August, 1968.

40. Lie, T. T. (1972), *Fire and Buildings*, Applied Science Publishers, LTD, London, 1972.

41. Lie, T. T. (1995), "Fire Temperature-Time Relations," Chapter 4-8, The SFPE Handbook of Fire Protection Engineering, Second Edition, National Fire Protection Association, Quincy, MA, 1995.

42. Liguori, T. B. and Stephenson, J. W. (1961), "The HEATING Program," Technical Report ASTRA 417-5.0, ASTRA Inc., Raleigh, NC, 1961.

43. Patankar, S. V. (1980), *Numerical Heat Transfer and Fluid Flow*, Washington, DC: Hemisphere, 1980.

44. Pettersson, O., Magnusson, S. E., and Thor, J. (1976), Fire Engineering Design of Structures, Swedish Institute of Steel Construction, Publication 50, Lund, Sweden, 1976.

45. Smith, G. D. (1987), *Numerical Solution of Partial Differential Equations: Finite Difference Methods*, 3rd (corrected) ed., Oxford, England, Clarendon, 1987.

46. Soriathia, U., Lugar, J., and Beck, C. (1998), "UL-1709 Fire Testing of Glass/Vinyl Ester Composite Panels," NSWCCD-64-RE-1998/07, U. S. Navy, Carderock Division, West Bethesda, MD, Maryland, 1998.

47. Sparrow, E. M. and Cess, R. D. (1978), *Radiation Heat Transfer*, Augmented Edition, McGraw-Hill Book Company, New York, New York, 1978.

48. Sultan, M. A. (1996), "A Model for Predicting Heat Transfer Through Noninsulated Unloaded Steel-Stud Gypsum Board Wall Assemblies Exposed to Fire," *Fire Technology*, Third Quarter, 1996.

49. Thermal Ceramics (2000), "Thermal Conductivity, Specific Heat Capacity, and Density of Structo-Gard," 2000.

50. Trelles, J., Hunt, S. P., and Williams, F. W. (2003), "Verifying HEATING 7.3 Against the Swedish National Testing and Research Institute's Suite of Fire Resistance Examples," NRL Memorandum Report in Publication, Naval Research Laboratory, Naval Technology Center for Safety and Survivability, Washington, D. C., April 10, 2003.

51. Turner, W. D. and Crowell, J. S. (1969), "Notes on HEATING - An IBM 360 Heat Conduction Program," Technical Report CTC/INF-980, Union Carbide Corp., Nuclear Div., Oak Ridge National Laboratory, Oak Ridge, Tennessee, 1969.

52. Turner, W. D., Elrod, D. C., and Siman-Tov, I. I. (1977), "HEATING5 - An IBM 360 Heat Conduction Program," Technical Report ORNL/CSD/TM-15, Union Carbide Corp., Nuclear Div., Oak Ridge National Laboratory, Oak Ridge, Tennessee, 1977.

53. Turner, W. D. and Siman-Tov, I. I. (1971), HEATING3 – "An IBM 360 Heat Conduction Program," Technical Report ORNL/TM-3208, Union Carbide Corp., Nuclear Div., Oak Ridge National Laboratory, Oak Ridge, Tennessee, 1971.

54. Underwriters Laboratories (1919), "Fire Tests of Building Columns," Underwriters Laboratories, Chicago, IL, 1919.

55. Underwriters Laboratories (UL) 1709 (1998), "Rapid Rise Fire Tests of Protection Materials for Structural Steel," Underwriters Laboratories Inc., Northbrook, IL, 1998.

56. Underwriters Laboratories (2003), "Fire Resistance Directory," Volume 1, Underwriters Laboratories, Inc., Northbrook, IL, 2003.

6.0 NOMENCLATURE

Roman

c	Thermal heat capacity (J/kg-°C or J/kg-m-K)
f	A generic function (units vary)
F	Radiation configuration factor
h	Convection coefficient (W/m-°C or W/m-K), length of inner web (m)
k	Thermal conductivity (W/m-°C or W/m-K)
n	Normal coordinate (m)
q	Heat, energy (J or kJ)
t	Time (s, min, or hr)
x	The first Cartesian coordinate (m)
$\mathbf{x}$	The Cartesian position vector, equal to x, y, z (m,m,m)
T	Temperature (°C or K)
w	width of inner flange (m)
y	The second Cartesian coordinate (m)

Greek

δ	Thickness (m)
ε	Emissivity of a surface
ρ	Density (kg/m^3)
σ	Stefan-Boltzmann constant (5.669E-8 $W/m^2\text{-}K^4$)

Superscript

h_e	Denotes natural convection exponent
n	Natural convection exponent (same as h_e)
$\bullet$	Quantity per unit time (s^{-1})
$''$	Quantity per unit area (m^{-2})
$'''$	Quantity per unit volume (m^{-3})

Subscript

1, 2, etc.	Denotes distinct location or quantity
A	Denotes ambient (exposed or unexposed)
B	Denotes boundary
c	Denotes convection
C	Denotes concrete surface
E	Denotes effective or resultant quantity
f	Denotes forced convection, furnace
I	Denotes insulation surface
n	Denotes natural convection
r	Denotes thermal radiation
s	Denotes surface
S	Denotes steel surface, general surface
∞	Denotes an ambient quantity